The Institution of Engineers Pakistan
Karachi Centre
&
NED University of Engineering & Technology, Karachi

Jointly Organizing

13th International Mechanical Engineering Conference

6th & 7th March, 2024 - Karachi - Pakistan

IMEC 2024

Theme: Industry 4.0 and Allied Digital Trends - Current Perspective and Future Direction

Conference Proceedings

GetInnovative 4Impact

Co-funded by the European Union

In Collaboration With

Federation of Engineering institutions of Islamic Countries (FEIIC)

FEISCA
Federation of Engineering institutions of South & Central Asia (FEISCA)

NED International Alumni Network (NEDIAN) Association, Pakistan

ASHRAE Pakistan Chapter
The American Society of Heating, Refrigeration and Air-Conditioning Engineers

PSPP
Pakistan Society of Plumbing Professionals Karachi

Media Partner
ENGINEERING REVIEW

Advisory Board

Engr. Sohail Bashir
Chairman
IEP, Karachi Centre
Engr. Asim Murtaza Khan
President, NED International
Alumni Network
(NEDIAN) Association-Pakistan
Engr. Abdul Rahim
Vice-Chairman (Mechanical &
Allied) IEP, KC & Chief Organizer
13th IMEC-2024
Engr. Ayaz Mirza
Vice-President (Mechanical &
Allied),IEP Karachi Centre

Engr. Prof. Dr. Sarosh Hashmat Lodi
Vice-Chancellor
NED University of Engg.& Tech., Karachi
Engr. Prof. Dr. Muhammad Tufail
Pro Vice-Chancellor
NED University of Engg. & Tech. Karachi
& Convener 13th IMEC-2024
Engr. Prof. Dr. Amir Iqbal
Dean, Department of Mechanical Engg.,
NEDUET & Co-Convener, 13th IMEC-2024
Engr. Prof. Dr. Mubashir Ali Siddiqui
Chairperson, Department of Mechanical
Engg.,NEDUET & Co-Convener, 13th
IMEC-2024

Engr. Muhammad Abbas Sajid
Ex. President
ASHRAE Pakistan Chapter
Engr. Prof. Dr. Mirza Jahanzaib
Dean, Faculty of Industrial Engg.,
University of Engg. & Tech., Taxila
Engr. Dr. Abdullah Mengal
Chairman, Mechanical Engineering
Department, BUET-Khuzdar

Technical Review Committee

Engr. Dr Inam Ul Ahad
Dublin City University, Ireland
Dr. Marialaura TOCCI
University of Brecia, Italy
Assoc. Prof. Dr. Noorhafiza Muhammad
University of Malaysia, Perlis
Engr. Dr. Asnul Hadi Ahmad
Universiti Malaysia Pahang, Malaysia
Engr. Dr. M. Kashif Khan
Coventry University, UK
Engr. Dr. Sohaib Zia Khan
Islamic University of Madinah, Saudi Arabia

Engr. Prof. Dr. Wasim Ahmad
UET, Taxila
Engr. Dr. Salman Hussain
UET, Taxila
Engr. Dr. Anis Fatima
NEDUET, Karachi
Engr. Prof. Dr. Murtuza
NEDUET, Karachi
Engr. Dr. Muhammad Shakaib
NEDUET, Karachi
Engr. Dr. Muhammad Uzair
NEDUET, Karachi
Engr. Dr. Ing. Usman Allauddin
NEDUET, Karachi

Engr. Dr. Haider Ali
NEDUET, Karachi
Engr. Dr. M. Ehteshamul Haque
NEDUET, Karachi
Engr. Dr. Mumtaz Hussain Qureshi
NEDUET, Karachi
Engr. Dr. Syed Ahmad Raza
NEDUET, Karachi
Engr. Dr. Muhammad Muzamil
NEDUET, Karachi
Engr. Dr. M. Uzair Yousuf
NEDUET, Karachi
Engr Dr. Kashif Noor
NEDUET, Karachi

IEP Headquarter Committee

Engr. Farhat Adil
President, IEP
Engr. Masood Ali Khan
Chairman, IEP Lahore Centre
Engr. Abdur Rab
Chairman, IEP Islamabad Centre

Engr. Amir Zamir Ahmed Khan
Secretary General, IEP
Engr. Syed Raghib Abbas Shah
Chairman, IEP Hyderabad Centre
Engr. Dr. Zaka Ullah Khan
Chairman, IEP Peshawar Centre

Engr. Muhammad Waseem Asghar
Chairman IEP Quetta Centre
Engr. Muhammad Kashif Kaleem
Chairman, IEP Faisalabad Centre
Engr. Muhammad Murtaza Khursid
Chairman, IEP Multan Centre

IEP Management Committee

Engr. M.Aijaz ul Haque
Member Central Council, IEP
Engr. Mustafa Hussain Khan
Member Central Council, IEP
Engr. Ghulam Farooq Maniar
Member Central Council, IEP

Engr. Muhammad Farooq
Member Central Council, IEP
Engr. Syed Ali Hasnain Naqvi
Member Local Council, IEP, KC
Engr. Ifrah Asif
Member Local Council, IEP, KC

Engr. Abdul Wahab Tajwani
Member Local Council,
IEP, Karachi Centre
Engr. Muhammad Kanzul Qavi
Member Local Council,
IEP, Karachi Centre

Organizing Committee

Engr. Dr. Tariq Jamil
Secretary, IMEC-2024
NEDUET, Karachi
Engr. M. Farooq Arbi
Secretary, IEP, Karachi Centre
Engr. Dr. Ali Raza Jafri
Chairperson, Dept. of Automotive
& Marine Engg, NEDUET
Engr. Dr. Maqsood Ahmed Khan
Chairperson, Dept. of Industrial
& Manufacturing Engg., NEDUET

Prof. Engr. Dr. Zahoor-ul-Hussain Awan
Chairperson, Dept. of Food Engg., NEDUET
Engr. Dr. Muhammad Wasif
NEDUET, Karachi
Engr. Dr. Shehroz Tahir Khan
NEDUET, Karachi
Engr. Dr. S.M Asad Akhtar
NEDUET, Karachi
Engr. Dr. Aun Ali
NEDUET, Karachi

Engr. Bushra Fatima
NEDUET, Karachi
Engr. Talha Bin Nadeem
NEDUET, Karachi
Engr. Zain Shahid
NEDUET, Karachi
Engr. Shehzaib Yousuf
NEDUET, Karachi
Engr. Muhammad Bilal
Project Manager - Erasmus+ CBHE
Project (GetInnovative4Impact)

Preface

The 13ᵗʰ International Mechanical Engineering Conference was held on 6ᵗʰ & 7ᵗʰ March 2024, an annual conference collaboratively organized by Institution of Engineers Pakistan (IEP), NED University of Engineering & Technology, Karachi and Project GetInnovative4Impact. It aims to bring together people who are working on the Industry 4.0 and related domains.

This year, the IMEC conference was structured around 8 tracks on various thematic topics, including

- Implementation of Digital/Smart Manufacturing Systems
- Applications of Artificial Intelligence and AR/VR and MR
- Advancements in Additive and other Manufacturing Processes
- Role of Cloud Computing in Mechanical and Manufacturing Engineering
- Adoption of Big Data Analytics, Visualisation and Dashboards
- Advanced Robotics and Material Handling System
- Energy 4.0, Advancements in Power Generation and Transmissions
- Advancements in Material Science and Technology.

IMEC-24 received 30 papers from all over the world. All submissions were peer-reviewed and also evaluated during the presentation of authors on conference days. We are very pleased to report that the quality of the submissions this year turned out to be very high. A total of 21 papers were accepted as full papers which is around 70% full paper acceptance rate.

We acknowledge the invaluable assistance of the track chairs and the technical review committee members. A complete list of all committee members can be found on the previous page. Most reviewers provided detailed and constructive comments which were valuable for the authors to continue improving their papers, even if their submissions were not selected for the conference.

Given the high-quality works done by authors, reviewers, and track chairs, we are confident that the IMEC 2024 proceedings capture the current state-of-the-art research in the learning technology field and will have a significant impact on the research community in the longer term.

Dr. Tariq Jamil
Conference Secretary, IMEC-24
Assistant Professor,
NED University of Engineering & Technology, Karachi.

Conference Proceedings International Mechanical Engineering Conference 2024

Table of Contents

DESIGN AND SIMULATION OF PHOTOVOLTAIC POWER PARK FOR EVACUATING SINDH SOLAR POTENTIAL USING HVDC TRANSMISSION SYSTEM

M.M. Khan[1, *], B. Akram[2], M.A. Shafi[3], S. Jabbar[1], J. Faiz[1], and R. Nazeer[4]

[1]Department of Electrical Engineering and Technology, Institute of southern Punjab, 6000, Multan, Pakistan.

[2]Department of Electrical Engineering, Glasgow Caledonian University, G40BA, Glasgow Scotland, UK

[3]Department of Electrical & Computer Engineering, COMSATS University Islamabad, 45550, Pakistan.

[4]Department of Electrical Engineering, NFC Institute of Engineering and Technology Multan, Pakistan.

[*]*Corresponding author E-mail address:* muneebkhan@isp.edu.pk (M.M. Khan)

ABSTRACT

Mega-sized power plants that use both conventional and unconventional energy sources and are situated in remote locations are producing electricity. The electricity industry in Pakistan has several issues due to outdated and inadequate domestic power plants as well as unstable, costly, and insecure power generation. While finding adequate land to establish a Photovoltaic power Park (PPP) is challenging, on-grid solar photovoltaic power parks (OGSPPPs) are a key step towards addressing the energy shortfall in urban load centers. Despite this, PPPs are the most simple and straightforward technology to deploy. The strategic challenge, though, is in determining the solar energy potential of Pakistan's Sindh and Punjab Provinces. Sindh province is perfect for large-scale solar installation because of its high solar irradiance and lack of fog throughout the year, the yearly average global horizontal solar potential of Sindh is 1978.9 kWh/m^2 and diffuse solar irradiation of 871.7 kWh/m^2, greater than Punjab. The $\pm$660 KV HVDC transmission line in Sindh is designed to transfer large amounts of power from the various Sindhi areas, which generate from various power plants, to the load centers located in North Punjab. The findings indicate that the PVSyst software records an annual average performance ratio of 84.8% for the Jamshoro area of Sindh. The paper's findings show that the execution of this PPP project involves adding more energy to load centers in order to combat energy shortages and increases in per-unit costs. This can lead to both energy security and national economic stability.

Keywords: Photovoltaic Power Park (PPP); Solar irradiation; Power Evacuating; Sindh solar Potential; Solar irradiance; Power Generation; On grid Solar Photovoltaic Power Park (OGSPPP); Load centers

1. INTRODUCTION

The need for energy is growing daily as time goes on. Nearly all homes and businesses require electricity, which puts a heavy company. The use of traditional fossil fuels for energy production, such as coal, natural gas, and oil, results in rising greenhouse gas emissions that have a negative effect on the environment and drive global warming [1,2].

Cleaner energy sources including sun, wind, biomass, magneto hydrodynamics (MHD), and hydropower must be used in order to replace traditional power generating methods with new ones. These resources are renewable since nature replenishes them constantly [3]. Solar energy is among the most practical answers to the global energy crisis. Due to the expensive impossibility of connecting power lines to remote and rural areas, PPP systems have emerged as a dependable global energy generating source [4].
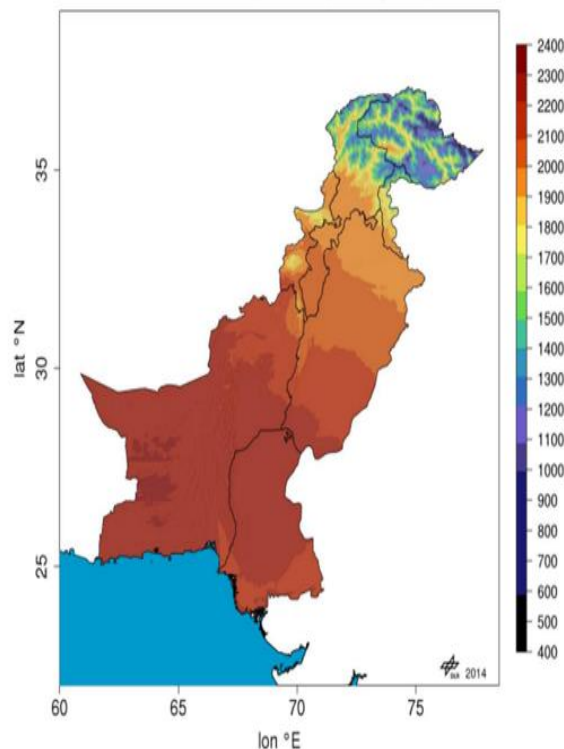
Figure 1. Pakistan's yearly global horizontal irradiance (GHI) in kWh/m2.

In Pakistan's Sindh and Baluchistan, where horizontal surface global irradiations are highest, direct solar radiation presents an enormous opportunity for clean, green electrical energy production. In Pakistan's northern and northeastern areas, global horizontal irradiance is decreasing and peaks in the Himalayas. While other portions of Pakistan also have significant solar potential, with about 1500 kWh/m^2 per year, encompassing more than 90% of Pakistan's total area, Figure 1 [5] shows that the maximum solar radiation in Sindh as a whole is slightly over 2300 kWh/m^2 per year. This energy can be captured efficiently enough to meet all of the country's energy requirements. With Pakistan's population expanding at an exponential rate and conventional energy supplies like gas, furnace oil, and coal running out quickly, photovoltaic energy is the only dependable substitute for traditional energy sources. In this context, a number of actions have already been taken. To maximize the benefit of the solar resource, system parameters must be sized and simulated for an efficient energy production. The energy production and necessary PV system size may be assessed using the modeling tool PVSyst [6,7]. Numerous studies have used PVSyst to assess the system's performance. The efficacy of a grid-connected, 190kW$_p$ solar power plant was investigated by the authors [9]. PVSyst was used to analyze the electrical power produced by solar arrays and photovoltaic systems in grid-tied systems in Berlin and Kathmandu, together with all conversion losses and losses from the inverter system. Regarding PVSyst simulator usage PV system-based power generating. The authors used PVSyst to model a grid tie system in order to determine if building a 1 MW solar photovoltaic (PV) power station would be feasible. They achieved this by simulating the southern Tamandua area of India and comparing performance analyses from various geographic locations [8-11].

The objective of this research is to utilize PVSyst simulation to build and model a grid-connected PV system for a specific geographic area in Jamshoro, Sindh, and its potential transmitted through the already

8

existing HVDC system depicted in Figure 2. Due to this reason installation of PPP near the HVDC transmission line to evacuate maximum Sindh solar potential and export this power to Punjab and other area of Pakistan. Meteonorm-8.1 is the source of meteorological data used in the design of photovoltaic systems and their performance research over a period of many months and a year.
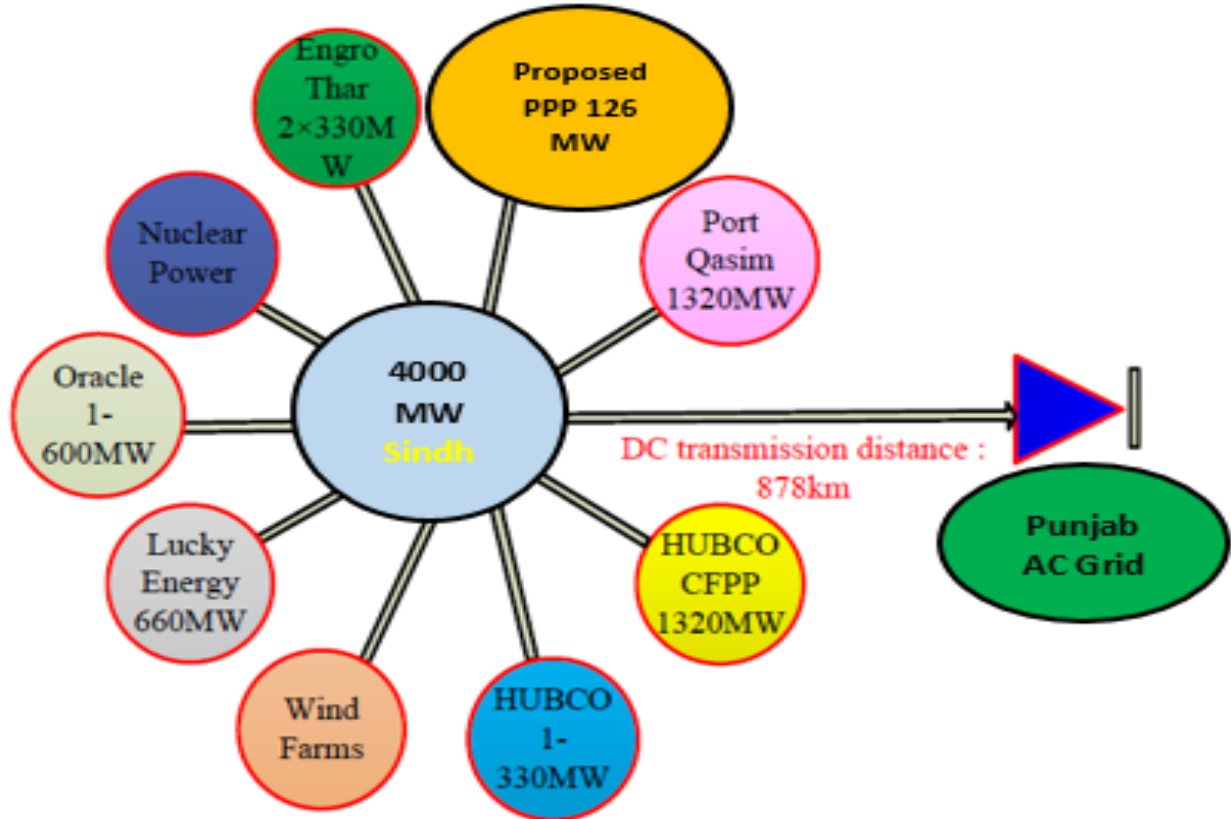
Figure 2. Proposed PPP interconnection with the HVDC line

For the suggested site, a suitable tilt angle has been calculated, which greatly increases the solar energy generation capability. Design and simulation of a PPP at Jamshoro, Sindh, with the goal of exporting electricity to Punjab via an HVDC transmission line with a 4000MW evacuating capacity. The power plants are located 878 Km away from load centers. Due to Sindh's greater solar potential than Punjab and the availability of an HVDC transmission line with a 4000 MW energy evacuation capacity from Sindh to Punjab, the primary load center that experiences a severe year-round energy shortage, a PPP simulation design has been proposed for Jamshoro, Sindh. As a result, this study will assist the government in making use of Pakistan's Sindh province's OGPPPGS.

2. METHODOLOGY

For the purpose of building and scaling solar systems, Meteonorm-8.1 is used to calculate temperature, wind speed information, and photovoltaic irradiance for the Jamshoro location, which is located at latitude 25.43°N, 68.53°E, and an altitude of 23 meters. This section explains how to use PVsyst Simulator to estimate the design and create a 126 MW_p DC/103 MW_p AC photovoltaic system for the Proposed site in Sindh. The planned solar system's size and performance analysis are estimated for a

9

given geographic area using simulation-based software called PVSyst. Researchers, designers, and engineers utilize it as a simulator and fundamental design for solar energy systems. PVSyst is more efficient in the design and development of solar systems when selecting the right cell model and inverter for the intended system's intended output. Data may be manually added to PVSyst from several locations, a massive global database, and its meteorological data. Tables and graphs are used to display the software's results.

2.1 Proposed Location:

Figure 3. is the location of proposed site for the installation of PPP near Manjhand, Jamshoro Sindh. Vast area for the solar park with ideal sun irradiance to generate maximum clean and green power generation.
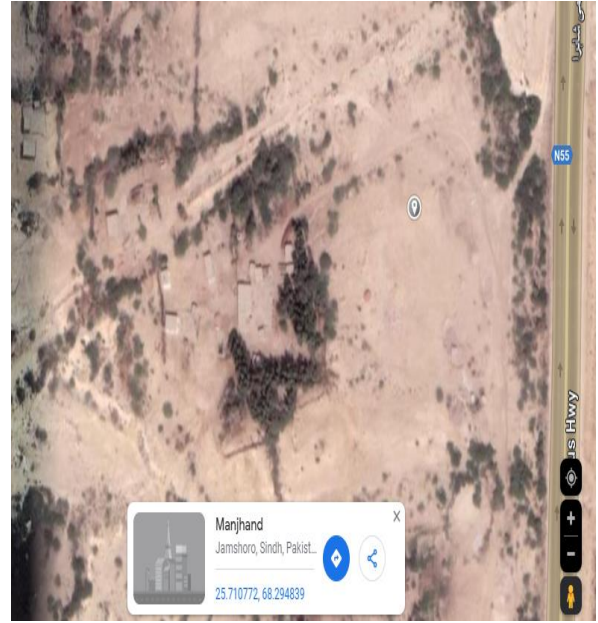
Figure 3: Proposed location of PPP

Month	Direct irradiation (kWh/m^2/day)	Diffuse irradiation (kWh/m^2/day)	Direct irradiation (kWh/m^2/month)	Diffuse irradiation (kWh/m^2/month)	Temperature (°C)	Wind Velocity (m/sec)	Relative Humidity (%)
January	4.08	1.27	126.4	39.4	14.6	1.90	58.5
February	4.67	1.91	130.9	53.5	18.5	2.20	54.4
March	5.73	2.23	177.7	69.1	24.7	2.19	47.9
April	6.11	2.80	183.4	84.1	29.2	2.70	43.2
May	6.50	3.21	201.4	99.5	33.7	3.70	43.5
June	6.89	3.33	206.7	99.8	33.6	4.40	51.0
July	6.11	3.38	191.0	104.8	32.3	4.60	60.0
August	5.66	3.23	175.4	100.3	30.9	4.09	63.7
September	5.92	2.47	177.7	74.2	30.0	3.40	61.1
October	5.11	2.04	158.3	63.4	27.4	2.11	53.2
November	4.53	1.28	136.0	38.4	21.3	1.50	55.0
December	3.68	1.46	114.1	45.2	16.3	1.80	59.4
Yearly	5.42	2.39	1978.9	871.7	26.0	2.9	54.2

Table 1. Input Data for The Proposed Location of PPP

The PVSyst program receives the following inputs: the Meteonorm-8.1 data, radiations from solar panels, appropriate design for photovoltaic (PV) cells and arrays, positioning of the photovoltaic field, Losses in the inverter system operational circumstances, efficiency and utilization of energy, index of normalized performance.

The placement of photovoltaic (PV) systems is crucial for solar energy generation since different parts of the planet receive different quantities of solar radiation on solar cells. A unique collection of location-specific metrics, such as latitude, longitude, and altitude, may be used to describe this positional difference. The proposed location

10

of Jamshoro in southern Pakistan is situated at an elevation of 242 meters, with latitude 25.71°N, longitude 68.29° E, and both. Total 126 MW$_p$ DC solar system with 229086 unit of Si-mono based Longi solar cell model LR5-72 HPH 550 M and 15 unit of Sungrow inverter 6874 kW$_p$.
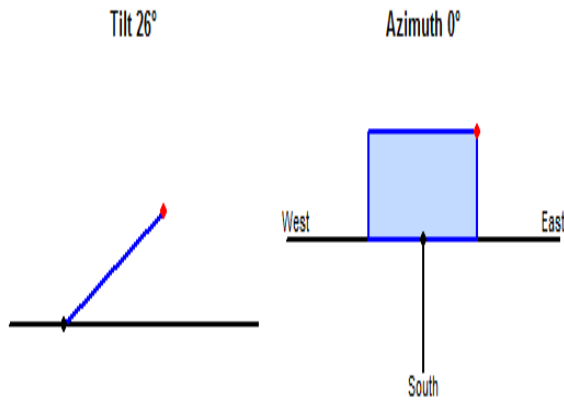
Figure 4.Tilt angle and Azimuth angle for PPP

Tilt angle is important to maximize solar radiation in the sun's path. Photovoltaic cells are positioned at a certain angle to maximize solar energy capture, especially around sunrise and sunset as depicted in Figure 4. Tilt angle is selected for the PPP is 26° and azimuth angle 0° is selected to minimize conversion losses 0.0% on this particular angle. Overall arrangement of system model is depicted in Figure 5. PV array is connected to inverter and converted all DC power into AC and injected into grid. A photovoltaic system's overall performance and efficiency can be increased by precisely angling the solar cells so that they face the sun the most.
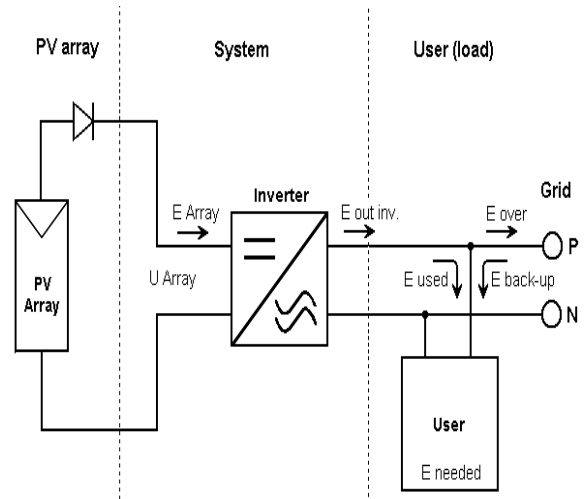
Figure 5. PPP system

The tilt angle that is considered is typically equal to or near the latitude value of the geographic location where the collector plane's global irradiance is at its maximum and the loss with respect to the ideal condition is zero. The tilt angle is 26°, the loss with respect to optimal is 0.0% for the global collector plane, and other input data are displayed in Table 1. An azimuth angle is essentially a measure of how the sun is oriented around the planet. It is zero when facing the sun, therefore a solar cell should be oriented southward to capture the lightest. Given the azimuth angle of 0°, seven solar pathways are found that change the major sun direction shown for the proposed site. In Table 02 Annual average worldwide direct horizontal irradiance of 1978.9 kWh/m^2 suggests a high potential for solar power production. The monthly diffuse irradiance, temperature, wind speed, and global horizontal irradiance are displayed in Table 1 for the proposed site. The maximum global monthly average of horizontal irradiance is 206.7 kWh/m^2 is recorded in June and minimum in the month of December 114.1 kWh/m^2.

Months	GlobHor (kWh/m²)	DiffHor (kWh/m²)	TAmb (°C)	GlobInc (kWh/m²)	GlobEff (kWh/m²)	E-Array (MWh)	E-Grid (MWh)	Performance Ratio (%)
January	126.4	39.4	14.62	174.7	172.8	19845	19617	0.891
February	130.9	53.5	18.52	161.9	159.8	18067	17869	0.876
March	177.7	69.1	24.66	199.2	196.3	21462	21231	0.846
April	183.4	84.1	29.16	185.9	182.8	19692	19463	0.831
May	201.4	99.5	33.74	189.4	185.9	19796	19574	0.820
June	206.7	99.8	33.60	188.1	184.7	19768	19549	0.825
July	191.0	104.8	32.34	176.9	173.6	18866	18652	0.837
August	175.4	100.3	30.86	171.8	168.8	18403	18186	0.840
September	177.7	74.2	30.00	191.1	188.2	20303	20072	0.833
October	158.3	63.4	27.44	189.0	186.5	20256	20035	0.841
November	136.0	38.4	21.27	184.3	182.2	20243	20029	0.862
December	114.1	45.2	16.26	157.3	155.4	17882	17680	0.892
Year	1978.9	871.7	26.07	2169.8	2137.0	234581	231957	0.848

Table 2. PR And Injected Energy into Grid

3. RESULTS AND DISCUSSION

The output power is obtained after all necessary efficiency adjustments have been made. The results of the system simulation are shown in Table 2. 1978.9 kWh/m² is the yearly incidence global horizontal radiation on the collector plane of the solar cell when the solar plate is positioned at a 26° tilt angle to get the best incident irradiation on the plane. In Figure 6 incident energy on surface area of solar plane is one of the crucial parameters for calculating the power production throughout the year, maximum 6.5 kWh/m²/kW$_p$ in the month of March and September which are the best month with moderate temperature. Minimum per day power production 5.1 kWh/m²/kW$_p$ overall annual average incident energy 5.945 kWh/m²/day. The proposed PPP has a high potential for solar energy, and using an existing 878-kilometer HVDC transmission line to simulate the design of a park in Sindh and then transmit power to Punjab is one of the best ways to optimize load demand. Clean and green energy will be affordable and controlled at the unit cost of electricity.
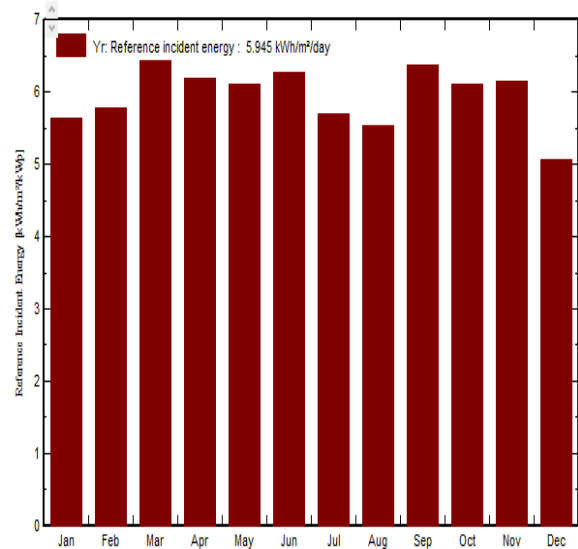
Figure 6. Reference incident energy of PPP

The system operates at peak efficiency and performance ratio recorded for more than 89% of the time due to low temperatures 14.62° and 16.26° in the month of January and December, respectively, even though incident sun irradiance is reduced in these months by approximately 114.1–126.4 kWh/m². This is because high temperatures also have an impact on solar cell efficiency and increase conversion losses that decrease the (PR) of solar cell in the month of May and

12

June is recorded 82%. Longi solar cell efficiency is recorded 21.56% and converted 1982 kWh/m² irradiance into 269803 MWh with the help of 585555m² surface area of PV array collector. PV arrays and solar cell modules suffer from a range of losses. Included are the following losses: The photovoltaic loss resulting from incident irradiance is 1.5%, while the inverter loss during operation is 1.1%. PV losses due to high temperature 10.7%, The wiring loss is 1.1%, the module quality loss is 0.2%, and the module array mismatch loss is 2.1%. The remaining energy at the inverter's output, 231957 MWh, is supplied to the grid system's infinite load after all energy losses have been subtracted is depicted in Figure 9. Provide losses and leftover energy to the solar system linked to the grid. The entire energy generated by solar cells, the energy lost during photovoltaic conversion, mismatched and wiring losses, and the total energy available at the inverter output for grid feeding are all shown in the proposed system. The performance ratio (PR) is used to evaluate the PV plant's performance. The link between energy output and radiation incidence on a specific location is measured by the system's PR with incorporating all losses. Because it remains at 84.8% for most of the year, it is reasonable for a system of size as depicted in Table 02 and Figure 7. Figure 8 shows the daily production of energy injected into the grid (kWh/day) and the daily intake of solar irradiance (kWh/m2/day). The PPP can inject more energy per day than 700 MWh/day, as seen by the maximum dotted concentration, which is over that amount.
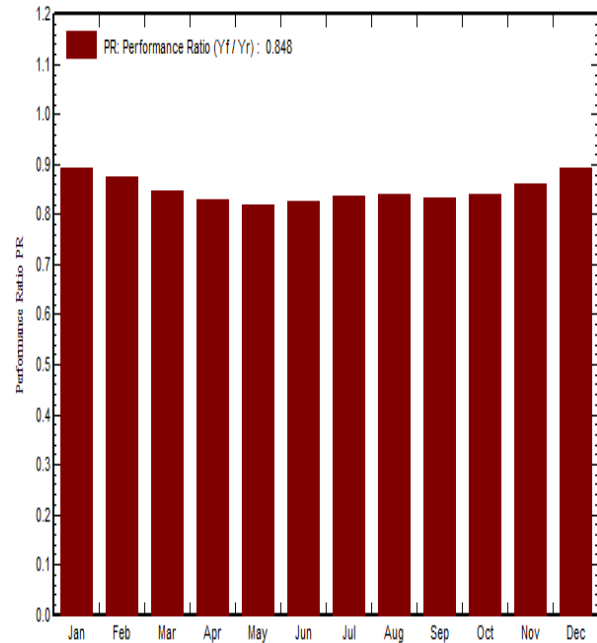
Figure 7. Performance ratio of PPP
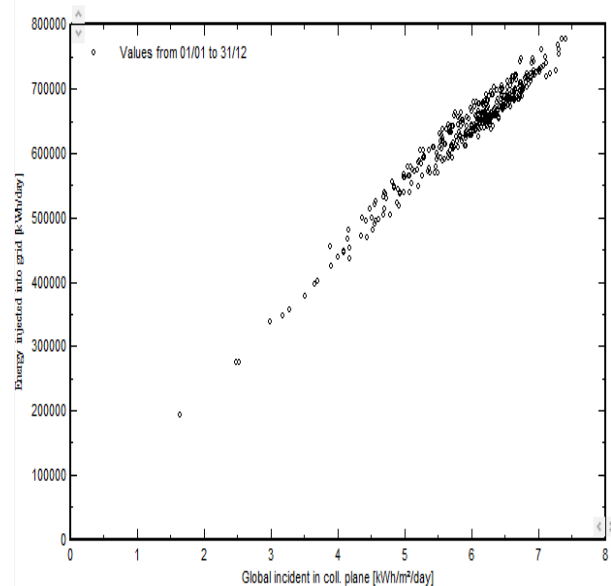
Figure 8. Daily input and output Analysis of PPP

13
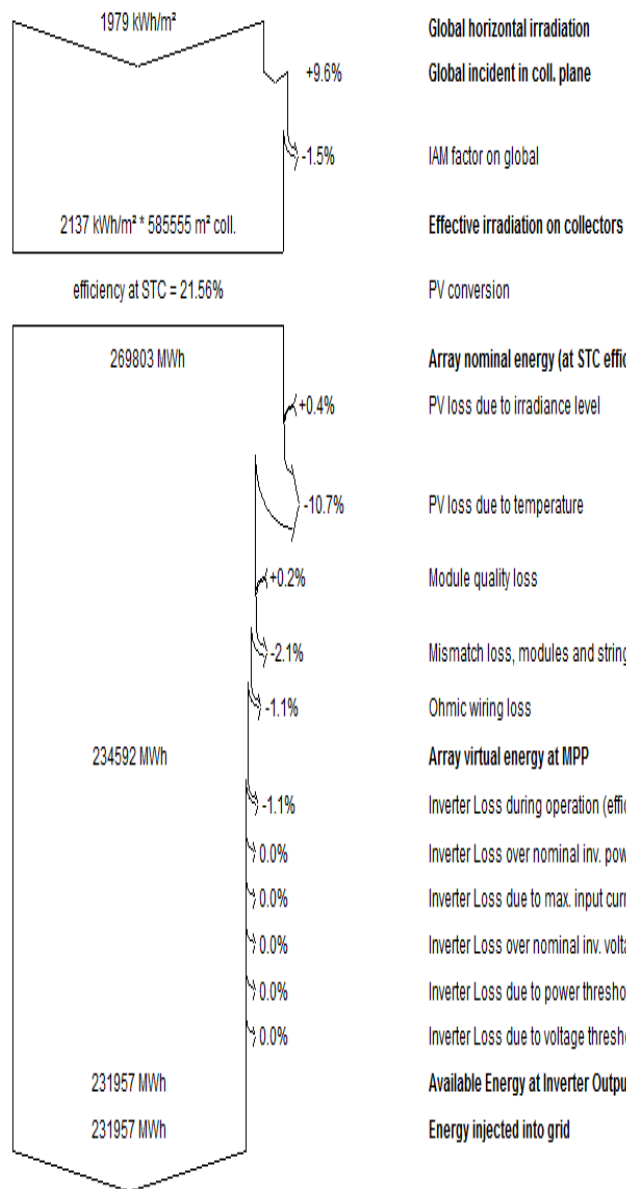
Figure 9: Loss diagram of PPP

4. CONCLUSION

In this current research, a complete design and simulation technique for solar systems utilizing PVsyst simulation is described. The globally horizontal irradiation data of the suggested location is used to get more accurate results. It is found that a Photovoltaic (PV) system's design is totally reliant on its geographical location.

Performance ratio is a crucial factor to consider when assessing system performance. The system's performance ratio for the entire year is calculated to be 84.8%, which is highest in Pakistan's Sindh province and exhibits a strong potential for solar energy production. It demonstrates that Jamshoro should consider using a Photovoltaic system to generate electrical power and fulfil the load demand in local level. Based on this study and performance ratio, large capacity systems may be developed for this location as well as the whole Sindh province. Power can then be sent by HVDC transmission lines to distant regions of the nation like Punjab and KPK in order to address the country's power crisis and provide a less expensive energy alternative.

REFERENCES

[1] M. M. Khan, M. A. Shafi and B. M. Soucase, Financial Analysis of PV-Wind Cogeneration for a Remote Village in Gwadar-Pakistan, *Southern Journal of Research*, 2(2), 145–152, 2022.

[2] M. M. Khan, M. A. Shafi and M. S. K. Khosa, An Analysis of Stochastic Wind Power Approach for Economic Load Dispatch Optimization Using Genetic Algorithm, *Southern Journal of Engineering & Technology,* 1(2), 30-41, 2023.

[3] M. M. Khan, M. A. Shafi and Z. Riaz, Magneto Hydro Dynamic Generation, *International Journal of Scientific & Engineering Research,* 7(2), 281—289, 2016.

[4] M. M. Khan, M. A. Shafi and N. Khan, Development of Prototype of Grid Tie Inverter (Grid Synchronization and Load Sharing, *International Journal of engineering and advanced technology*, 5(5), 245–255, 2016.

[5] Solar modeling report, *The World bank Solar resource mapping in Pakistan,* https://documents.worldbank.org/pt/publication/documentsreports/documentdetail/200771468096863184/solar-resource-mapping-in-pakistan-solar-modeling-report. 2015.

[6] M. Asim, S. Kamran, M. Farooq, M. Amjad, A. Qamar, Modelling of optimized standalone PV system for basic domestic energy use in Pakistan, *Journal of Faculty of Engineering & Technology,* 22(2) 61-68, 2022.

[7] M. A. Shafi, S. Bibi, M. M. Khan, B. M. Soucase, A numerical simulation for efficiency enhancement of CZTS based thin film solar cell using SCAPS-1D, *East European Journal of Physics,* 5(1), 52–63, 2022.

[8] M. A. Shafi, M. M. Khan and B. M. Soucase, Effect of parasitic parameters and environmental conditions on IV and PV characteristics of 1D5P model solar pv cell using LTSPICE-IV, *East European journal of Physics,* 5(1), 2022.

[9] Y. Sharma, and S. S. Chandel, Performance analysis of a 190 kWp grid interactive solar photovoltaic power plant in India, *Energy,* 55(1), 476-485, 2013.

[10]
. M. Khan, S. Ahmad, S. Jabbar, S. Baloch, M. A. Shafi, R. Nazeer and J. Faiz, Simulation design of Grid Tied Photovoltaic (PV) system of a 1.05 kWp DC for a geographical location of Tandojam, Sindh, *1st International Conference on Women Development in Engineering, Science & Technology (WD-EST'23)*, Pakistan 2023.

[11]
. M. Khan, S. Ahmad, H. Sikandar, B. Akram, A. Raza, R. G. Hassan, M. Hussain, Designing and Performance analysis of Photovoltaic system using PVSyst Software: A geographical location of Pakistan, *TechXchange International Conference, QUEST Nawabshah (TechXchange 2024)*, Pakistan 2024.

IMPACT OF HEAT EXCHANGER, OIL BATH CLEANING UNIT AND EXHAUST GAS RECIRCULATION ON PERFORMANCE AND EMISSIONS OF A DIESEL ENGINE FUELED BY DIESEL MIXTURES WITH CARBON NANOTUBES

Muhammad Sarfraz Ali[1]*, Sadia Saleem[2], Rozeena Aslam[1], Muhammad Imran[1], Hamza Akhtar[1], Muhammad Ali[1], Muhammad Faheem Nazar[1], Muhammad Hashaam Kamal[1], Abdul Sattar[1], Muhammad Babar Hurr[1]

[1]Mechanical Engineering Department, Swedish College of Engineering & Technology, Rahim Yar Khan, Pakistan

[2]Institute of Computer Science and Information Technology, The Women University, Multan, Pakistan

*Corresponding author E-mail address: sarfrazali@piet.edu.pk (Muhammad Sarfraz Ali)

ABSTRACT

Adverse atmospheric conditions and health hazards originating due to the discharge of unburned hydrocarbons (UHC), nitrogen oxides (NOx) and carbon monoxide (CO) are the fundamental challenges to researchers working on diesel engines. The solution is to develop cleaner technologies to abate emissions from diesel engine exhaust. In this paper, a novel hybrid emission control unit composed of a counter-flow heat exchanger (HE), oil bath cleaning unit (OBCU) and exhaust gas recirculation (EGR), the combination abbreviated as HE-OBCU-EGR unit, was designed, fabricated and implemented on the exhaust manifold of Massey Ferguson (MF-260) tractor engine to reduce the regulated gaseous emissions. An experimental study was conducted to investigate the effects of the HE-OBCU-EGR unit on the emissions of a four-stroke, three-cylinder diesel engine equipped with an eddy-current dynamometer. The tests were conducted on engine speed of 1200 to 2200 rpm with an interval of 200 rpm at full load. The AVL DiTEST and AVL smoke meter were used to analyse the emissions of CO, UHC and NOx. To analyse the performance parameters data acquisition system was used and values were stored in a computer. The BSCF of the diesel engine decreased by 3.56% when the carbon nanotubes were added to pure diesel in a concentration of 30 and 60 ppm. With these concentrations, there was an increase of 10.62% in torque when compared to pure diesel. The results obtained with the HE-OBCU-EGR unit revealed 26.3% and 24.8% reduction in UHC and NOx emissions respectively, whereas CO emissions were increased by 14.3% due to a limited supply of oxygen from EGR. Results revealed that the HE-OBCU-EGR unit may help to minimize the emissions of UHC and NOx but is not suitable to control CO emissions. To minimize the emissions of CO, this technology can be superposed with a turbocharger or supercharger to enhance the availability of O2 in the combustion chamber.

Keywords: Diesel engine; HE-OBCU-EGR; Nanoparticles; Carbon nanotubes; Emissions; Performance

1. INTRODUCTION

Diesel engines produce their amazing performance and exceptional fuel economy by first compressing air to extremely high pressures and then spraying a small amount of fuel into this highly compressed air. Diesel engines are still plagued by excessive emissions of nitrogen oxides (NO$_X$) and particulate matter (PM) [1,2]. New technologies, like fuel post-combustion emission control devices, will aid future pollution restrictions. It was more economical to use fuel additives to lower the number of particles smaller than 2.5μm. strategy. The freezing point of organic manganese was shown to decrease most at 15 °C, and 700 ppm was found to be the optimal dosing rate [3].

When the metal dosage was administered, notable patterns in the freezing point fall were seen. Diesel was mixed with different metal additions to enhance fuel quality, resulting in more thorough combustion and fewer pollutants from the exhaust. The influence of a catalyst on the burning of unburned hydrocarbons is the fundamental idea behind this additive action [4]. The addition of noble or transitional metals to fuel lowers the soot ignition temperature.

Diesel additives can also be categorized into three groups based on the purpose for which they were designed: (i) pre-flame additives; (ii) flame additives; and (iii) post-flame additives[5].

Particles begin to form above a predefined threshold when the amount of additive increases. The only factors influencing the additive dose limit were the type of engine and the soot emissions (normally aspirated and turbocharged engines behave identically). Higher additive concentrations demonstrated a more concentrated benefit, even if lesser additive dosages were still beneficial [6].
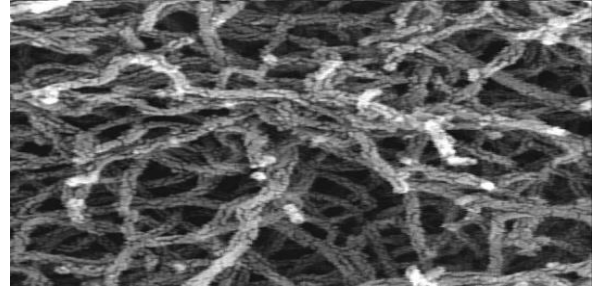
Figure 1. (a) SEM CNTs

Rather than in the gaseous phase, the nano additive was largely released in the particle phase. The main component of all the additions is metal, which is discharged as oxide in the exhaust. Additives were beneficial for trap renewal but had little effect on suppressing soot. Fuel additives including catalytic compounds were among the most tempting approaches to reduce PM. Additives are added to fuel to improve engine performance and reduce emissions. Nearly every technique for lowering diesel engine emissions at the source compromises the levels of NOX, particulates, and UHC [7]. The engine maker has several options at their disposal to precisely manage the emissions of any given contaminant during the combustion and injection stages. The following facts and trends were noteworthy: (i) the increased injection speed led to a reduction in particulate emissions and improved air-fuel mixing; (ii) the injection pressure increase was advantageous as well; and (iii) using an injector with pintles as flat lowers residuals and emissions of particulate matter and unburned hydrocarbons [8].

The additive method calls for a constant addition of diesel fuel to all vehicles, excluding those equipped with filters. Metal-organic compounds that were completely dissolved in diesel fuel made up the bulk of fuel additives. To decrease the ignition delay, stabilize and function as an anti-oxidant, and operate as a surface-active agent, diesel fuel is treated with a metal addition [9].

Metal-based additives effectively decreased diesel emissions in two ways. The metals first

17

work with the soot's carbon molecules in a straight line to reduce the oxidation temperature, or they work with water to process hydroxyl radicals, which quickens the soot's oxidation [10]. The nanoparticles act as the soot's oxidation nucleus if the additives are used in the diesel engine after combustion.

Engine exhaust particles are always under suspicion, even in small amounts, due to their propensity to penetrate and simply dwell in the respiratory alveoli, with severe health repercussions. Diesel particulates have been demonstrated to match the size of particles that were most readily maintained for the longest amount of time in the respiratory system among all the types of dust that may be found in the atmosphere [11].

Previous research demonstrates the significant impact of nanoparticle additions on the efficiency and emissions of diesel engines. In this investigation, a four-stroke, single-cylinder diesel engine was used for the experimental work. 30 and 60 parts per million of each carbon nanotubes were combined with pure diesel. At engine speeds of 1200, 1400, 1600, 1800, 2000, and 2200 rpm, the performance and emission characteristics were measured. When nanoparticles were added to diesel fuel, the fuel's performance significantly improved. When pure diesel and carbon nanotubes are combined, the number of unburned hydrocarbons decreases by a maximum of 8.43%. Emissions of carbon monoxide were decreased by 20.34% using carbon nanotubes at 1600 rpm engine speed. When both manganese oxide and carbon nanotubes were utilized at a concentration of 30 and 60 ppm each, there was a 6.2% decrease in NOx emissions.

2. FUEL PREPARATION

In the current study, pure diesel (D) and carbon nanotubes were utilized in a diesel engine. With and without a heat exchanger oil bath cleaning unit, carbon nanotubes were combined with pure diesel (D) at concentrations of 30 and 60 parts per million. Table 1 displays the experiment's design. A magnetic stirrer was used for 30 minutes to mix the CNTs added to pure diesel to produce a homogenous emulsion fuel. Pure diesel can be made better by adding carbon nanotubes (CNTs). Carbon nanotubes (CNTs) bearing Amido groups were extremely reactive and could interact with a wide range of materials.

Name	Diesel (%)	CNTs (ppm)	HE-OBCU-EGR
D	100	0	No
DC30	100	30	No
DC60	100	60	No
DHOE	100	0	Yes
DC30HOE	100	30	Yes
DC60HOE	100	60	Yes

Table 1. Design of experiment

3. EXPERIMENTAL SETUP

Fig. 2 displays the diesel engine test bench's schematic diagram. A diesel engine with three cylinders and water cooling, operating on four strokes, was connected to an eddy current dynamometer. Engine speed ranges of 1200 to 2200 rpm at 100 rpm intervals under full load were tested. The AVL DiTEST emission analyser was used to measure the emissions of CO and NOx, while the AVL smoke meter was used to measure the emissions of BSFC and UHC.
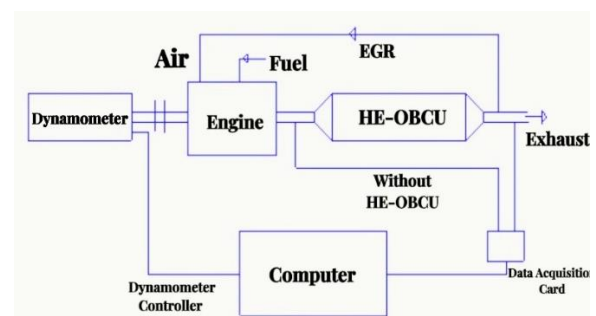
Figure 2. Schematic diagram of the experimental setup

18

The tests were conducted using manganese oxide and multi-walled carbon nanotube fuel blends with pure diesel. In the first test, pure diesel was used in the engine and performance and emission characteristics were recorded for reference. After that manganese oxide and multiwalled carbon nanotubes were blended separately with the pure diesel at a concentration of 90 ppm and the result was recorded. After that, both manganese oxide and multiwalled carbon nanotubes in a concentration of 90 ppm were blended with the pure diesel and results were recorded. Before every next test, the engine was run with pure diesel for at least 10 minutes so that the residuals of the previous fuel blend could be cleaned from the fuel line. Every test was repeated three times and the average value was used for comparison. Performance parameters i.e., BTE and emission characteristics i.e., NO_X, UHC, and CO were assessed. An exhaust gas analyzer was used to measure the exhaust emissions.

4. RESULTS & DISCUSSIONS

4.1 Torque

Figure 3 shows the fluctuation in the engine's torque at different speeds. By shortening the ignition delay, the addition of CNTs to the pure diesel improves combustion efficiency. At an engine speed of 2200 rpm, the best maximum torque was found since it rises as the engine speed rises. Additionally, the torque increased by mixing nanoparticles with pure diesel. More complete combustion caused by the presence of too much oxygen in the engine cylinder increases torque [12]. The maximum increase in torque was achieved when carbon nanotubes were used at a concentration of 30 and 60 ppm each with pure diesel. With this combination, there was an increase of 10.62% in torque when compared to pure diesel.
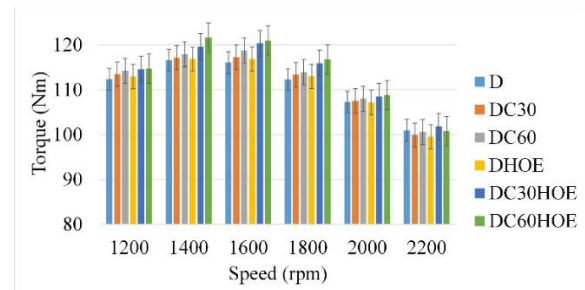
Figure 3. Variation of Torque with speed

4.2 Brake-specific fuel consumption

Brake Specific Fuel Consumption (BSFC) is a measure of the fuel efficiency of an internal combustion engine, typically expressed in terms of fuel consumption per unit of power produced. It is commonly used to evaluate the performance of engines, including diesel compression ignition engines. The engine's fuel consumption to power generated ratio, or BSFC, is calculated over a certain period. Because the engine uses more gasoline to accomplish the same performance, a lower BSFC number is expected. Since BSFC often decreases as load increases, comparing load to engine load is a crucial factor. The BSFC is governed by four performance characteristics: calorific value, volumetric fuel injection, density, and viscosity. The studies on different Nano-additives are examined in this section. Figure 4 shows the Variation brake specific fuel consumption with speed.
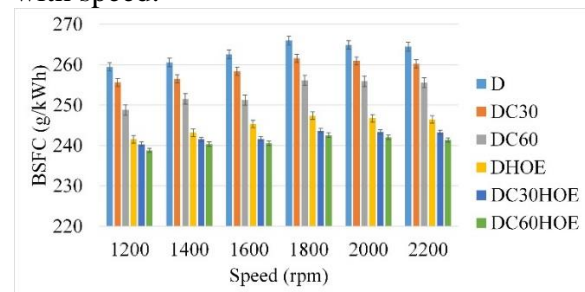
Figure 4. Variation brake brake-specific fuel consumption with speed.

Published Date: 08/07/2024 Version: 00

4.3 CO emissions

Carbon monoxide is produced as a result of incomplete combustion and is exacerbated by the lack of oxidants, low temperature, and extended residence time. Figure 5 displays the carbon monoxide emissions from the engine. When metal oxide additives were catalytically oxidized in an oxygen-rich environment, carbon monoxide emissions were trending lower [14]. The graph shows that at 1600 rpm, the use of carbon nanotubes with the heat exchanger oil bath cleaning unit decreased carbon monoxide emissions by
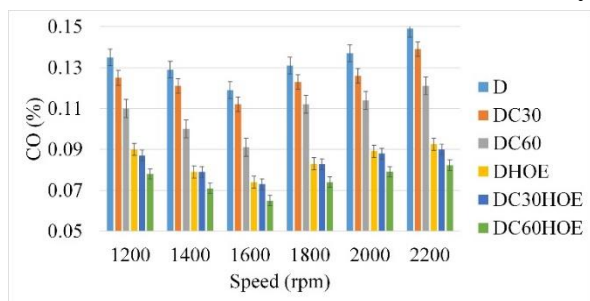
0.06%.

Figure 5. Variation of carbon monoxide with speed

4.4 NOₓ emissions

It has been discovered that NO_x emissions were on the decline when diesel fuel contains nanoparticle additives. There was a change of 1-1.4% in the cetane number of diesel fuel due to nanoparticles which has an impact on emissions. Compared to fuels with lower cetane numbers, those with higher cetane numbers have lesser premixed fuel fractions and fewer NO_x emissions [6]. Figure 6 illustrates the engine's nitrogen oxide (NO_X) emission. The data indicates a 6.2% reduction in NO_x emissions when carbon nanotubes were used at a concentration of 30 and 60 ppm each.
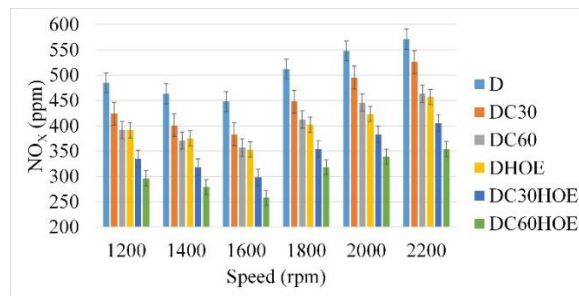
Figure 6. Variation of nitrogen oxide emissions with speed.

4.5 UHC emissions

At 1200 rpm, the DI diesel engine's emissions of unburned hydrocarbons were reduced. Up to 1600 rpm, it rises as engine speed increases. The highest rate of unburned hydrocarbon emissions was 1600rpm. Subsequently, a decrease in unburned hydrocarbon at faster rates becomes apparent. As a result, unburned hydrocarbon emissions from idling engines have received attention. The engine's unburned hydrocarbon exhaust pattern is shown in Figure 7. When pure diesel fuel is mixed with nanoparticles, the number of unburned hydrocarbons decreases [13]. The highest reduction in unburned hydrocarbons was observed when 90 parts per million of carbon nanotubes were combined with pure diesel.
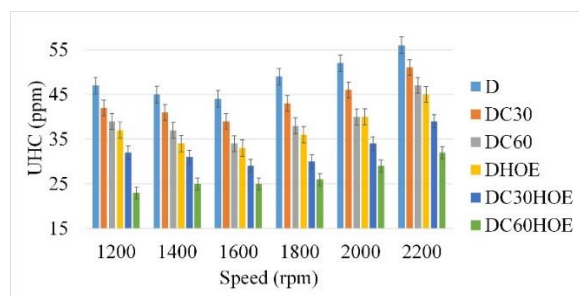
Figure 7. Variation of unburned hydrocarbon with speed

5. CONCLUSIONS

From the results of the experimental study, carbon nanotubes additive somewhat improves an engine's performance. The BSCF of the diesel engine decreased by 3.56% when the carbon nanotubes were

20

added to pure diesel in a concentration of 30 and 60 ppm. With this concentration, there was an increase of 10.62% in torque when compared to pure diesel.

Measurements of the exhaust emissions for the fuel with the carbon nanotube additives show a significant decrease. The unburned hydrocarbons decreased maximum by 8.43% when carbon nanotubes were blended with pure diesel. Carbon monoxide emissions were reduced by 20.34% with carbon nanotubes at the engine speed of 1600 rpm. There was a 6.2% reduction in NO_x emissions when carbon nanotubes were used at a concentration of 30 and 60 ppm with, HE-Oil Bath cleaning Unit and Exhaust Gas Recirculation System.

If additives were used, they must be kept from venturing into the surrounding air by suitable traps.

A novel hybrid emission control unit having a combination of a counter flow shell and tube type heat exchanger (HE), oil bath cleaning unit (OBCU) and exhaust gas recirculation (EGR) was designed and fabricated followed by its installation on the exhaust manifold of MF-260 tractor diesel engine. The unit, being a combination of three techniques, was called as HE-OBCU-EGR unit. An experimental study was conducted to investigate the effects of this emission control unit on the exhaust emissions of a four-stroke three-cylinder water-cooled CI engine coupled to an eddy-current dynamometer. The testing standard BS-AU-141 was used for smoke emissions from heavy-duty diesel engines. The tests were performed on a speed range of 1200 to 2200 rpm with an interval of 100 rpm under full load to examine the effects of the HE-OBCU-EGR unit on BSFC, CO, NOx, and UHC emissions. The emission analyses were performed on AVL DiTEST and AVL smoke meter. Fig. 13 briefly describes the effects of the HE-OBCU-EGR unit on engine emissions. The results showed that with the

implementation of the HE-OBCU-EGR unit on the engine, BSCF emissions were reduced by 42.9%, the UHC was decreased by 26.3%, NOx emissions were diminished up to 24.8%, and CO emissions were increased by 14.3%. Finally, it is concluded that the HE-OBCU-EGR unit may help to minimize the emissions of BSCF, UHC, and NO_X but is not suitable to control CO emissions.
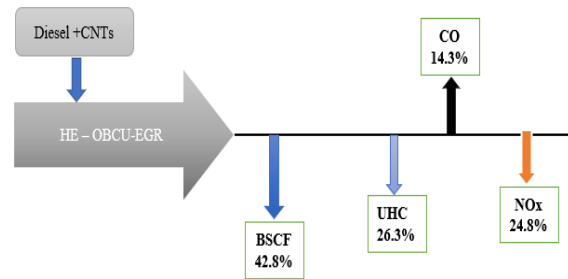
Figure 8. Comparison of altered fuel with base fuel

ACKNOWLEDGEMENT

REFERENCES

[1] H. Solmaz, S. M. S. Ardebili, A. Calam, E. Yılmaz, and D. İpci, "Prediction of performance and exhaust emissions of a CI engine fueled with multi-wall carbon nanotube doped biodiesel-diesel blends using response surface method," *Energy*, vol. 227, 2021, doi: 10.1016/j.energy.2021.120518.

[2] M. Mirzajanzadeh *et al.*, "A novel soluble nano-catalysts in diesel-biodiesel fuel blends to improve diesel engines performance and reduce exhaust emissions," *Fuel*, vol. 139, no. x, pp. 374–382, 2015, doi: 10.1016/j.fuel.2014.09.008.

[3] M. Ghanbari, G. Najafi, B. Ghobadian, T. Yusaf, A. P. Carlucci, and M. Kiani Deh Kiani, "Performance and emission characteristics of a CI engine using nanoparticles additives in biodiesel-diesel

21

blends and modelling with GP approach," *Fuel*, vol. 202, pp. 699–716, 2017, doi: 10.1016/j.fuel.2017.04.117.

[4] G. R. Kannan, R. Karvembu, and R. Anand, "Effect of metal-based additive on performance emission and combustion characteristics of diesel engine fuelled with biodiesel," *Appl. Energy*, vol. 88, no. 11, pp. 3694–3703, 2011, doi: 10.1016/j.apenergy.2011.04.043.

[5] A. F. Chen, M. Akmal Adzmi, A. Adam, M. F. Othman, M. K. Kamaruzzaman, and A. G. Mrwan, "Combustion characteristics, engine performances and emissions of a diesel engine using nanoparticle-diesel fuel blends with aluminium oxide, carbon nanotubes and silicon oxide," *Energy Convers. Manag.*, vol. 171, no. June, pp. 461–477, 2018, doi: 10.1016/j.enconman.2018.06.004.

[6] A. Heidari-Maleni, T. M. Gundoshmian, B. Karimi, A. Jahanbakhshi, and B. Ghobadian, "A novel fuel based on biocompatible nanoparticles and ethanol-biodiesel blends to improve diesel engines performance and reduce exhaust emissions," *Fuel*, vol. 276, no. April, p. 118079, 2020, doi: 10.1016/j.fuel.2020.118079.

[7] V. Arul Mozhi Selvan, R. B. Anand, and M. Udayakumar, "Effect of cerium oxide nanoparticles and carbon nanotubes as fuel-borne additives in diesterol blends on the performance, combustion and emission characteristics of a variable compression ratio engine," *Fuel*, vol. 130, pp. 160–167, 2014, doi: 10.1016/j.fuel.2014.04.034.

[8] A. I. EL-Seesy and H. Hassan, "Investigation of the effect of adding graphene oxide, graphene nanoplatelet, and multiwalled carbon nanotube additives with n-butanol-Jatropha methyl ester on a diesel engine performance," *Renew. Energy*, vol. 132, pp. 558–574, 2019, doi: 10.1016/j.renene.2018.08.026.

[9] D. Balasubramanian, A. T. Hoang, I. Papla Venugopal, A. Shanmugam, J. Gao, and T. Wongwuttanasatian, "Numerical and experimental evaluation on the pooled effect of waste cooking oil biodiesel/diesel blends and exhaust gas recirculation in a twin-cylinder diesel engine," *Fuel*, vol. 287, no. August 2020, p. 119815, 2021, doi: 10.1016/j.fuel.2020.119815.

[10] A. Taghizadeh-Alisaraei and A. Rezaei-Asl, "The effect of added ethanol to diesel fuel on performance, vibration, combustion and knocking of a CI engine," *Fuel*, vol. 185, pp. 718–733, 2016, doi: 10.1016/j.fuel.2016.08.041.

[11] M. Kapetanović, A. Núñez, N. van Oort, and R. M. P. Goverde, "Reducing fuel consumption and related emissions through optimal sizing of energy storage systems for diesel-electric trains," *Appl. Energy*, vol. 294, no. November 2020, 2021, doi: 10.1016/j.apenergy.2021.117018.

[12] O. M. I. Nwafor, G. Rice, and A. I. Ogbonna, "Effect of advanced injection timing on the performance of rapeseed oil in diesel engines," *Renew. energy*, vol. 21, no. 3, pp. 433–444, 2000, doi: 10.1016/S0960-1481(00)00037-9.

[13] A. Pourahmadiyan, P. Ahmadi, and E. Kjeang, "Dynamic simulation and life cycle greenhouse gas impact assessment of CNG, LNG, and diesel-powered transit buses in British Columbia, Canada," *Transp. Res. Part D Transp. Environ.*, vol. 92, no. February, p. 102724, 2021, doi: 10.1016/j.trd.2021.102724.

[14] S. H. Hosseini, A. Taghizadeh-Alisaraei, B. Ghobadian, and A. Abbaszadeh-Mayvan, "Performance and emission characteristics of a CI engine fuelled with carbon nanotubes and diesel-biodiesel blends," *Renew. Energy*, vol. 111, pp. 201–213, 2017, doi: 10.1016/j.renene.2017.04.013.

ENERGY, EXERGY AND ECONOMIC ANALYSIS OF AN INDUSTRIAL BOILER: A CASE STUDY OF KAPCO POWER PLANT

Muhammad Sarfraz Ali[1]*, Sadia Saleem[2], Rozeena Aslam[1], Muhammad Imran[1], Hamza Akhtar[1], Muhammad Ali[1], Saleem Nawaz[1], Muhammad Hassan Nawaz[1]

[1]Mechanical Engineering Department, Swedish College of Engineering & Technology, Rahim Yar Khan, Pakistan
[2]Institute of Computer Science and Information Technology, The Women University, Multan, Pakistan

*Corresponding author E-mail address: sarfrazali@piet.edu.pk (Muhammad Sarfraz Ali)

ABSTRACT

A boiler is the main component of a power plant. A boiler performs mainly two tasks; it converts the energy of fuel to heat. Secondly, it has a water and steam system which converts water into steam by using heat. This case study was done at unit-3 KAPCO power plant which is located at Kot Addu, Punjab, Pakistan with location coordinates 30.445066443158 latitude and 70.981078147888 longitude. The boiler system in the present paper makes use of the concepts of energy and exertion. This case study's primary goal is to evaluate the boiler's parameters and pinpoint the system's primary energy and exhaustion losses. Energy and exhaustion flows have also been displayed. Numerous energy-saving strategies have been developed, and energy and energy efficiencies have also been calculated. It has also been established that employing variable-speed drives and recovering heat from exhaust gases can save energy. This case study concludes that exergy analysis gives more accurate performance of different devices. Boiler efficiency is increased by further use of exhaust gases in heat recovery steam generator (HRSG) by decreasing the temperature of flue gases from 160°C to 150°C and shortening the length of pipes which carry heat by using variable speed drive.

Keywords: Energy; Exergy; Flue gases; HRSG; Boiler

1. INTRODUCTION AND LITERATURE REVIEW

Coal accounts for over 40% of global electricity production, with nuclear and natural gas producing only 15% and 20% of it, respectively. As a result, boiler turbine steam systems are typically used by these energy sources to convert their chemical energy potential into the production of electricity. It is conceivable to envision how steam boiler efficiency could be slightly increased. Boiler efficiency has a significant impact on heat-related energy savings, according to Saidur [1]. Thus, it is important to minimize heat loss in the boiler and optimize heat transfer to the water. Gupta and Rosen [2, 3] found that a variety of methods, such as hot exhaust gas loss and radiation losses, can result in energy loss from boilers. Blower failure losses in the steam boiler scenario. Finding the most likely places for energy usage is crucial for boiler process optimization in plants. Since all of the heat created by the fire fuel cannot be converted into water or steam in a boiler, a significant quantity of energy is lost through flue gases. The boiler temperature typically varies between 160°C and 250°C when the flue gas exits the stack. It suggests that by lowering its

losses, there is a great deal of potential for energy savings. Cai [4] suggested that although the first rule of thermodynamics is frequently used to compare energy use, it is unable to analyze the quality of energy in the future. I.e., the point at which an evaluation of energy becomes relevant. Dunbar [5] established that the 2nd law of thermodynamics, which tells us how to calculate the efficient use of a particular amount of energy at a certain condition, equates to exergy. The best performance is achieved when exergy loss in a process is the least.Kanoglu et.al, [6] suggested a greater awareness of energy and energy efficiency for power plant energy management. where the power cycle is analyzed using different energy and energy-base efficiency. Examined are the cogeneration, geothermal, and vapour and gas power cycles; several cycle designs were taken into consideration. Som [7] determined that the energy balance and thermodynamic irreversibility in combustion processes, which are present in practically all circumstances, are significant. The internal energy exchange connected to high-temperature gradients brought on by the release of heat in combustion reactions was the main cause of irreversibility. Reducing the irreversibility of the conduction of heat was the main strategy for keeping the energy dissipation in the burning process within an acceptable bound. Saidur [1] suggested a framework of industrial boiler energy, energy, and economic analysis. 72.46% and 24.89%, respectively, were found for energy and energy efficiency. The primary source of energy destruction was the combustion chamber, which was supported by the flue gases. Boiler fan motors were equipped with variable-speed drives to reduce energy consumption. Regulagadda [8] It is suggested that based on the thermodynamic study of a subcritical boiler-turbine generator of a 32 MW coal-fired electric power plant, the irreversibility of the boiler and turbine

produces the greatest energy decreases in the power plant as compared to the condenser, which results in the lowest energy losses. Since consumption of water and water rejected from the electric power plant have decreased, the plant's air cool condenser proved to be environmentally beneficial. Patel [9] compared various coal types, including imported, Indian, and a combination of both (40 percent Indian, 60 percent imported), as well as L.S.H.S. oil, and concluded that the boiler's energy efficiencies were 37%, 37.7%, 37.8%, and 40.1%, respectively, based on the first principle of efficiencies. Ohijeagbon [10] concluded that, at conventional reference state temperatures of 250°C and an evaporating ratio of 12, the energy & exergy efficiency attained for the complete boiler was 69.56% & 38.57%. The analytical method served as the foundation for all calculations. Gulhane [11]] determined that the boiler's exergy destruction at a residential load of 1.1 MW was around 83.35%, and that figure increased to 76.33% as the load grew to 5.6 MW. As a result, the first and second laws' efficiency rose with load; therefore, to lessen irreversibility, we must focus on peak load. Kanoglu [12] found a diesel engine power plant's performance characteristics. Energy conversion & management concluded that energy appeared to be a key idea. It establishes a link between the engineering and physical worlds and the surrounding environment and demonstrates the true effectiveness of engineering systems, making it an invaluable concept to identify areas for development. Energy calculations, the opposite of the current material & energy balances, can provide deeper and more insightful insights into the process. It can be emphasized that energy analysis has a great deal of potential usefulness concerning energy usage and that energy plays a crucial role in the process of developing energy policies. Kanoglu [6] To study, increase, and

24

improve energy systems through appropriate strategy and policy, both energy and energy efficiency analyses are required. Regular actions may assist increase the performance of industrial boilers if such regulations were in place. Som [7] employed the hot-gas recovery systems to enhance the boiler's existing specifications and reported that a heat recovery system might save as much as 55% of the cost. The energy, energy efficiency, energy losses, and energy damage associated with boilers are identified in this study, and strategies for enhancing effective heat transfer by reducing boiler energy consumption through the use of variable speed drives are suggested. Analysis has also been done on the benefits related to energy and the economy. Many other techniques, such as managing excess air, increasing consumption efficiency, using environmentally friendly fuel, recovering excess heat, recovering condensate, improving the blowdown process, preventing escape, and offering appropriate protection, can all help reduce the amount of energy used by boilers.

This paper's primary goal is to examine the boiler's parameters and pinpoint the main energy and exergy losses in the boiler system. Energy & exergy flows have also been demonstrated. Numerous energy-saving strategies have been developed, and energy and energy efficiencies have also been calculated. It has also been established that employing variable-speed drives & recovering heat from flue gases can save energy. The case study concludes that energy analysis provides a more precise performance for various devices.

2. METHODOLOGY AND DATA COLLECTION

The methods used to calculate the energy & exergy efficiency and the destruction of a boiler, as well as the energy & exergy

efficiency for a boiler, are described in the section that follows. Cost-benefit analyses of energy-saving measures to lower the temperature of exhaust gases at the HRSG output and employ VSD to lower boiler fan energy consumption are covered.

Block Schematic:
The KAPCO power plant unit 3 block schematic is displayed in Figure 1.
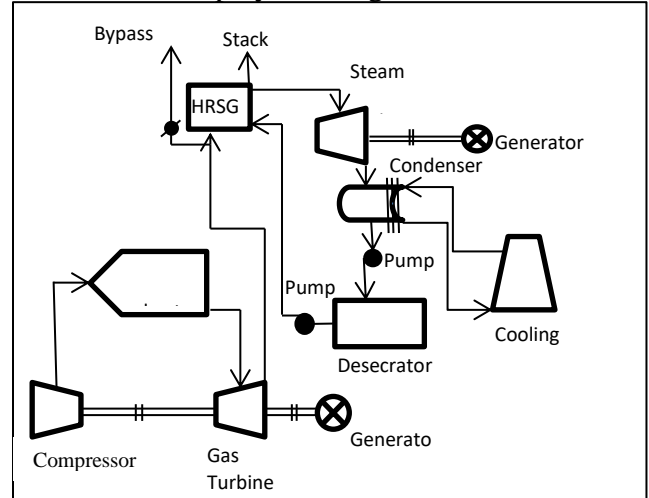
Figure 1. Block schematic

2.1. The equation for energy analysis
The heat exchange system and the combustor are the two components that make up a boiler. Below is a discussion of these two components' energy and exergy analyses. Because a boiler's combustion is usually well-insulated, very little heat is lost to the environment. The loss of energy will become equal with the difference between the enthalpies of the reactants and products, according to the 1st law of thermodynamics. The combustor's energy balance is provided by:

$$E_{in} - E_{out} = \frac{dE_{system}}{dt}$$
$$= 0 =\gg steady \qquad (1)$$
$$E_{in} = E_{out}$$
$$E_{loss} = \dot{m}_1 h_1 + \dot{m}_2 h_2 - \dot{m}_3 h_3 \qquad (2)$$

Where,

E_{in} = enrgy in

E_{loss} = enrgy loss

E_{out} = enrgy out
h_1 = fuel's specific enthalpy (KJ/kg)
h_2 = air's specific enthalpy (KJ/kg)
h_3 = Particular enthalpy of heated combustion products
$\dot{m}_1$ = mass fuel flow rate
$\dot{m}_2$ = air mass flow rate
$\dot{m}_3$ = thermal products of combustion's mass flow rate

For each fluid stream, a heat exchanger typically experiences negligible potential and kinetic energy changes as well as no work interactions (w=0). In general, the heat exchanger's outer shell is well-insulated to stop heat loss into the surrounding medium. A tiny quantity of heat will, nevertheless, disappear.

The energy balance for a heat exchanger is determined by the first law of thermodynamics, as shown in Figure 2.
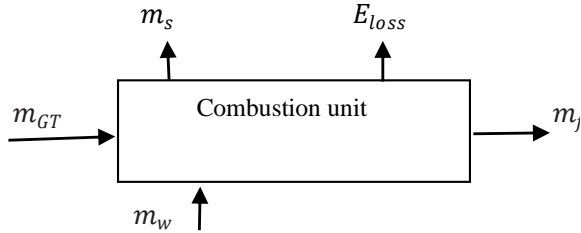
Figure 2. Energy balance for heat exchanger

Assuming that there will be no mixing in a heat exchanger and using the following mass flow rates: m_p for hot products, m_g for flue gases, m_l for water, and m_s for steam, it will be understood that:

$$\dot{m}_p = \dot{m}_{GT} = \dot{m}_{fg} \tag{3}$$

And,

$$\dot{m}_l = \dot{m}_s$$

The energy balance under these assumptions can be written as follows:

$$E_{in} - E_{out} = \frac{dE_{system}}{dt} = 0 \tag{4}$$

$$(\dot{m}_4 h_4 + \dot{m}_5 h_5) - (\dot{m}_6 h_6 + \dot{m}_7 h_7) = E_{loss} \tag{5}$$

A heat exchanger's efficiency can be represented using the first law as follows:

$$\eta_c = \frac{E_{out}}{E_{in}} \tag{6}$$

Where,

$$\eta_c = \text{efficiency of a HRSG}$$

2.2. The exergy analysis equation

By assuming a zero rate of change in exergy within the boiler's system and applying an exergy balance to the boiler, the maximum power output, or reversible power, can be calculated. This is done while keeping in mind the boundary temperature of 25 °C. According to the second rule of thermodynamics:

$$X_{in} - X_{out} - X_{destroyed} = \frac{dX_{system}}{dt} = 0 ==> steady \tag{7}$$

$$(\dot{m}_1 \epsilon_1 + \dot{m}_2 \epsilon_2) - (\dot{m}_3 \epsilon_3 + l_c) = 0c \tag{8}$$

$$l_c = (\dot{m}_1 \epsilon_1 + \dot{m}_2 \epsilon_2) - (\dot{m}_3 \epsilon_3) \tag{9}$$

The energy efficiency of the combustor determines the appropriate second law efficiency, which is expressed as follows:

$$\psi_c = 1 - \frac{X_{destroyed}}{X_{in}} \tag{10}$$

For each fluid stream, a heat exchanger typically experiences negligible potential and kinetic energy changes as well as no work interactions (w=0). In general, the heat exchanger's outer shell is well-insulated to stop heat loss into the surrounding medium. A tiny quantity of heat will, nevertheless, disappear. Assuming that there has been no mixing in a heat exchanger and using the following mass flow rates: m_p for hot products, m_g for flue gases, m_l for water, and m_s for steam, it will be understood that:

$$\dot{m}_p = \dot{m}_{GT} = \dot{m}_{fg} \tag{11}$$

$$\dot{m}_w = \dot{m}_s$$

Energy balance is determined by the second rule of thermodynamics, which is:

$$X_{in} - X_{out} - X_{destroyed} = 0 \tag{12}$$

$$l_H = (\dot{m}_4 \epsilon_4 + \dot{m}_5 \epsilon_5) - (\dot{m}_6 \epsilon_6 + \dot{m}_7 \epsilon_7) \tag{13}$$

26

Exergy efficiency is determined using the second rule of thermodynamics as follows:

$$\psi_H = 1 - \frac{X_{destroyed}}{X_{in}} \qquad (14)$$

For analysis of energy, the exergy data we took from the plant is given in Table 1.

Flow rate (KJ/s)	Temperature (°C)	Enthalpy (KJ/Kg)	Entropy (KJ/Kg.K)
426	340.9	621.64	2.430
9.72	110	43.890	1.97
435.72	1050	1424	3.29
435.72	506	1002	2.710
52.19	472.4	4013	7.72
52.19	120	554.92	1.70
435	160	432.42	2.07

Table 1. Exergy data from power plant

Boiler energy loss can be minimized in a boiler by employing various techniques. However, this thesis has taken into consideration energy saving through the recovery of heat from exhaust gases in a boiler as well as energy saving through the use of variable speed drives to lower the speed of the boiler fan.

2.3. Concept of variable speed drive

One of the best-organized control strategies is VSD. Under specific conditions, it provides only the necessary power to overcome system resistance. In contemporary industrial and commercial boilers, variable-speed drives are typically employed. When regular low-load times are required due to work conditions, it works well. If you lower the fan speed, you can improve combustion efficiency at low fire. A crucial factor affecting all kinds of combustion apparatus is the ambient air temperature. Boiler efficiency may be significantly impacted by this.

A device called a variable frequency drive modifies the power supply's frequency to control the motor's speed. The frequency and the driven equipment's speed are proportionate. Energy savings are substantial even with little speed reductions since the power required to run pumps & motors varies with a cube of the speed. By directly increasing motor voltage with frequency, the percentage of applied motor voltages to deliver frequency remains constant, allowing for the achievement of maximum constant torque. Constantly volts per Hertz is the common word used to describe this kind of control.

Electrical energy is saved when an alternating current (AC) motor is slowed down by the use of an inverter in a variable-speed drive. In addition to reducing stack losses through the limited extra air rate and the addition of a driver to that system, these measures also save electrical energy. Because of this, running the motor at a variable speed will save electrical energy in addition to increasing boiler efficiency. Oxygen prolongs the duration of the plant's boiler and saves fuel and emissions. Although this is an objective modification to the motor, a motor's speed can also be altered by changing the number of poles. Rewinding it would be necessary, causing the speed to alter step by step. Therefore, the ideal answer is to change the frequency for convenience, economy, and accuracy. It is necessary to adjust the volts per Hz ratio to alter the motor torque. An output of numerous frequencies is provided by a drive. The use of variable speed drives can be summed up as follows: lower electricity usage, less need for a separate motor starter, better fan control, and longer equipment lifespan. By regulating the surplus air, a VSD keeps fuel efficiency high under part load settings.

For a boiler with VSD, the annual energy savings are provided by:

$$AES_{boiler-VSD} = (AEC_{without-VSD} - AEC_{with-VSD}) \qquad (15)$$

2.4. Heat recovery from flue gases

Since not all of the heat produced by burning fuel can be transferred to water or steam in the boiler, a significant amount of heat energy is lost through flue gas; approximately 10 to 30 percent of the heat energy lost through flue gas is in the 120°C to 160°C range. As a result, recovering some of the heat from the flue gases can help to increase the boiler's efficiency. Heat can be recovered from flue gases by moving it through the heat exchanger that is installed after the boiler; flue gases are typically at high temperatures to guarantee that they are sufficient to pre-heat the fluid. The process of recovering heat from flue gas can be expressed as follows:

$$Q_r = \dot{m}_{fg} \times cp \times \Delta T_{fg} \qquad (16)$$

Savings related to energy conservation are expressed as:

$$Cost\ saved = annual\ energy\ saved \times unit\ price\ of\ energy \qquad (17)$$

The KAPCO power plant unit 3's TS diagram is displayed in Figure 3.
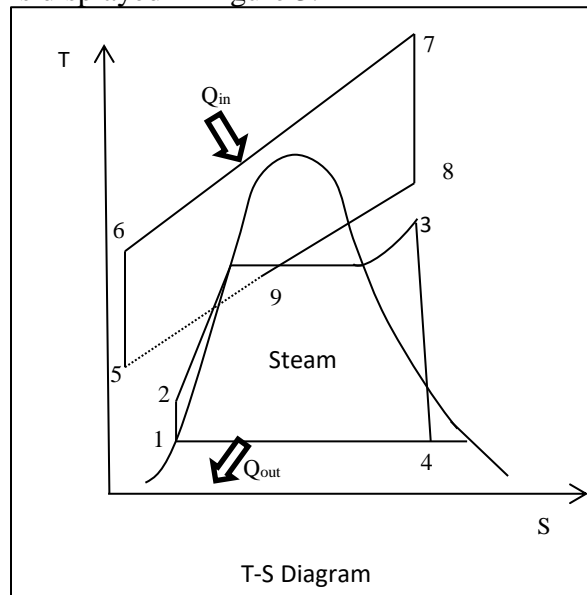
Figure 3. TS diagram

2.5. Rules of thumb

- Reducing surplus air by five percent results in a one percent gain in boiler efficiency (or reducing the remaining oxygen in stack gas by one percent boosts boiler efficiency by one percent).

- A 22°C drop in the flue gas temperature results in a 1% gain in boiler efficiency.

- An increase in feed water temperature of 6°C resulted in economizer/condensate recovery and a 1% reduction in boiler fuel usage.

- One percent (%) of fuel savings occurs from a 20°C rise in the combustion temperature of the air that is preheated through waste heat recovery.

- A 3 mm hole with a steam pressure of 7 kg/cm^2 would lose 32,650 litres of fuel annually.

- A 150 mm-diameter bare steam pipe that carried saturated steam at a rate of 8 kg/cm^2 would waste 25,000 litres of furnace oil annually.70 percent of heat losses can be reduced by floating a layer of 45 mm diameter polypropylene balls on the surface of a 90°C hot liquid/condensate.

- The barrier to heat transfer provided by a 0.25 mm thick air film is equivalent to that of a 330-millimeter thick copper wall. A 3mm thick soot deposit on a heat transfer surface can cause a 2.5 percent increase in fuel consumption.

- A scale deposit over the waterside that is 1 mm thick could result in a 5–8% increase in fuel usage.

3. RESULTS AND DISCUSSIONS

The boiler's component-by-component heat loss is calculated, beginning with the combustor. Using the information from the

28

table and the assumptions outlined in the previous subject, the energy input may be computed as follows:

$$E_{loss} = \dot{m}_f h_f + \dot{m}_a h_a - \dot{m}_p h_p \qquad (18)$$

$$E_{loss} = 70964.16 KW$$

The combustion chamber's energy efficiency can be determined as follows:

$$\eta_c = \frac{Actual\ Heat\ Release}{Theoratical\ Heat\ Release} \times 100 \qquad (19)$$

$$\eta_c = 77.2293\%$$

Regarding HRSG, the full exchanger is taken into account as the control volume, and the following formula is used to determine the system's heat loss:

$$(\dot{m}_{GT} h_{GT} + \dot{m}_w h_w) - (\dot{m}_s h_s + \dot{m}_{fg} h_{fg}) = E_{H,loss} \qquad (20)$$

$$E_{H,loss} = 171239.232\ KW$$

Table 2 provides the energy efficiency of heat exchangers based on first law efficiency.

$$\eta_c = \frac{E_{out}}{E_{in}} = 55\% \qquad (21)$$

Components	Energy Loss(KW)	Energy Efficiency (%)
Combustor	70964.16	77.2293
Heat Exchanger	171239.232	55
Total	242203.392	

Table 2. Energy loss & energy efficiency

Components exergy destruction and exergy efficiency of the boiler are given, starting from the combustor. The exergy destruction of the combustor can be found by using the equation. The combustor is thought to run on a steady flow procedure. Therefore, the control volume of the combustor has zero mass and energy change. Furthermore, since

the potential and kinetic energies are minimal and there is no assumption of a work interaction, the information from the energy destruction table will be evaluated as follows:

$$l_c = (\dot{m}_1 \epsilon_1 + \dot{m}_2 \epsilon_2) - (\dot{m}_3 \epsilon_3) \qquad (22)$$

$$= \dot{m}_1(h_1 - T_0 S_1) + \dot{m}_2(h_2 - T_0 S_2) - \dot{m}_3(h_3 - T_0 S_3)$$

$$l_c = 98535 KW$$

A formula and information from the table are used to compute the combustor's exergy efficiency via second law efficiency:

$$\psi_C = 1 - \frac{l_c}{X_{c,in}} \qquad (23)$$

$$\psi_C = 75.73\%$$

Using the process outlined in the preceding section, HRSG anticipates that the heat exchanger will exergy destroyed. The following formula is used to determine the energy destruction:

$$l_H = (\dot{m}_4 \epsilon_4 + \dot{m}_5 \epsilon_5) - (\dot{m}_6 \epsilon_6 + \dot{m}_7 \epsilon_7) \quad (24)$$

$$l_H = 224150 KW$$

Equation and information from Table 3 are used to compute the appropriate 2nd law efficiency for the heat exchanger energy efficiency.

$$\psi_H = 1 - \frac{l_H}{X_{H,in}} = 45\% \qquad (25)$$

Components	Energy Destruction (Kw)	Energy Efficiency (%)
Combustor	989535	75.73
Heat	224150	45

Table 3. Energy destruction and energy efficiency

These days, most boilers are built with the VSD concept in mind. The power-saving data is displayed in Table 4.

Load (%)	Time (hr)	Power Load (without VSD) (Kw)	Energy Use (Kwh/yr)	Power Load (with VSD) (Kw)	Energy use (Kwh/yr)	Saving (Kwh/yr)
100	400	2.9	1160	2.9	1160	0
80	900	2.9	2610	2.2	1980	630
70	800	2.9	2320	1.9	1520	800
60	820	2.9	2378	1.4	1148	1230
Total	2920		8668		5808	2660

Table 4. Power saving by using VSD

Using VSD, an annual total energy savings of 2660 kWh can be attained, assuming a per-KWh charge of Rs. 29.78 Pkr. This equates to Rs. 79,214.8 Pkr annually.

4. CONCLUSION

Component-wise energy and exergy analysis was done for the boiler at unit 3 KAPCO power plant. According to the first law, HRSG experiences the highest heat losses, which total 171.2 MW. Exergy analysis represents the more accurate performance of thermodynamic devices. Exergy calculation shows that maximum exergy destruction occurred in HRSG whereas destruction was calculated at 224.15MW.

ACKNOWLEDGEMENT

REFERENCES

[1] Saidur, Ahamed, and Masjuki, "Energy, exergy and economic analysis of industrial boilers," Energy Policy, vol. 38, pp. 2188-2197, 2010.

[2] Gupta, Ghai, and Jain, "Energy efficiency improvement strategies for industrial boilers: a case study," Journal of Engineering and Technology, vol. 1, p. 52, 2011.

[3] Rosen,"The relation between thermodynamic losses and capital costs for a modern coal-fired electrical generating station," in Proceedings of computer-aided energy systems analysis, ed, 1990.

[4] Cai and Kim, "First law of thermodynamics and Friedmann equations of Friedmann-Robertson-Walker universe," Journal of High Energy Physics, vol. 2005, p. 050, 2005.

[5] Dunbar, Lior, and Gaggioli, "The component equations of energy and exergy," Journal of Energy Resources Technology, vol. 114, pp. 75-83, 1992.

[6] Kanoglu, Dincer, and Rosen, "Understanding energy and exergy efficiencies for improved energy management in power plants," Energy Policy, vol. 35, pp. 3967-3978, 2007.

[7] Som and Datta, "Thermodynamic irreversibility's and exergy balance in combustion processes," Progress in energy and combustion science, vol. 34, pp. 351-376, 2008.

[8] Regulagadda, Dincer, and Naterer, "Exergy analysis of a thermal power plant with measured boiler and turbine losses," Applied Thermal Engineering, vol. 30, pp. 970-976, 2010.

[9] Ankit Patel "Energy and exergy analysis of a boiler with different fuels like Indian coal, imported coal and L.S.H.S oil," IJERT, vol. 1, 2012.

[10] Ohijeagbon, Waheed, and Jekayinfa, "Methodology for the physical and chemical exergetic analysis of steam boilers," Energy, vol. 53, pp. 153-164, 2013.

30

[11]   Gulhane and Thakur, "Exergy analysis of boiler in cogeneration thermal power plant," Am J Eng Res, vol. 2, pp. 385-392, 2013.

[12]   Kanoglu, Işık, and Abuşogˇlu, "Performance characteristics of a diesel engine power plant," Energy Conversion and Management, vol. 46, pp. 1692-1702,

A CFD ANALYSIS FOR THERMAL PERFORMANCE ENHANCEMENT OF SOLAR PARABOLIC DISH CAVITY SYSTEM USING SPHERICAL AND ELLIPTICAL CAVITIES

Shehzaib Yousuf Khan[1]*, Muhammad Uzair[1]

[1]Department of Mechanical Engineering, NED University of Engineering & Technology, Karachi, Pakistan

*Corresponding author E-mail address: shehzaib@neduet.edu.pk (S. Y. Khan)

ABSTRACT

The objective of this work is to compare the thermal performance of spherical and elliptical cavity receivers with a conical-shaped cavity for a solar dish cavity system. The Monte-Carlo ray-tracing method is used to determine the radiation flux distribution and solar flux uniformity of the receiver. The radiation flux is found to be more uniform in the spherical and elliptical cavities, and cavities that are positioned far away from the focal plane of the solar concentrator. The result from optical analysis is used as a boundary condition for the computational model. CFD analysis is performed to determine thermal performance using ANSYS Fluent where convective heat loss in the cavity receiver is calculated. Convective heat loss of the receiver with different wind speeds varying from 1 – 10 m/s is investigated in different shapes of cavity receivers. The computational results show that the convective heat loss in spherical and elliptical cavity receivers is significantly reduced due to the swirling action of turbulent flow inside the cavity receiver.

Keywords: Cavity receiver; Convection heat loss; CFD; Parabolic dish system; Optical analysis

1. INTRODUCTION

A concave dish reflector is used in the Solar Cavity Dish System to direct sunlight onto a receiver positioned at the focal point of the system. The receiver, which is usually situated above the dish, contains a solar energy conversion device, like a Stirling engine or a cavity receiver transferring heat through heat transfer fluid through conductive tubes. Sunlight is converted into useful energy as it converges into the receiver, which may take the form of heat, electricity, or both. Because the system can reach better energy conversion rates than typical flat plate collectors or photovoltaic panels due to concentrated solar power (CSP) technology, it is especially well-suited for applications where space efficiency is crucial. Clausing [1] used an analytical model for estimating convective losses from cavity solar central receivers. The study highlighted the effect of geometry and environmental conditions on thermal losses with emphasis on wind direction and orientation. Stine and McDonald [2] extended the understanding of convective heat loss in cavity receiver with the effect of wind speed and orientation. McDonald [3] studied open cavity receiver and obtained correlations for natural and forced convection loss in the receivers. The established correlations by these early researchers were limited to fixed operating conditions in cavity receivers until the investigations by Paitoonsurikarn and Lovegrove [4] where their findings were important for optimizing dish design and minimizing the adverse wind effects. Paitoonsurikarn et al. [4] and Uzair et al. [5-7] examined the influence of wind patterns

32

around cavity receivers coupled with parabolic dish structure. Roux et al. [8] studied a small scale solar thermal Brayton cycle coupled with solar parabolic dish system at the focal point of the system. The study involved the investigation of geometry parameter of dish such as concentrator shape, diameter, rim angle, reflectivity, optical errors, and solar tracing errors which effect the efficiency of the receiver. Daabo et al. [9] studied different shapes of cavity receiver to determine its effect on the optical and thermal performance of the solar cavity dish system. Liu et al. [10] investigated the design parameters of heater tube arrays in cavity receivers to maximize the heat absorption and minimizing thermal losses. Li et al. [11] investigated cavity receivers by adding transparent aerogel at receiver opening which improved the efficiency of the receiver and minimizing the convection loss significantly.

The optical performance mainly depends on the cavity shape and opening of the receiver. Thermal shocks are caused by non-uniformity of solar flux inside the cavity receiver which deteriorate thermal performance of cavity dish system. Furthermore, the convection loss is affected significantly by wind patterns, orientation and opening of the cavity receiver. The effect of cavity shapes has already been investigated by Daboo et al. [9] but the optimum cavity shape was selected based on maximum solar flux instead of uniform flux distribution. Xiao et al. [12] modified the receiver opening by adding quartz window to cylindrical cavity which resulted in lower convection loss. Rajan and Reddy [15] performed optical analysis on corrugation cavity receiver with dish concentrator and varied aperture diameter to obtain optimum opening of cavity receiver.

There is a need to determine such cavity shapes that allow capturing uniform distribution of solar radiation flux inside the cavity as well as lowering the chances of convection loss. The improvement can be done by modifying the opening with backward facing step in cavity receiver and positioning the cavity with offset distance. The main focus of this paper is to investigate the effect of the spherical and elliptical shaped cavities with modified receiver opening on the convection heat loss. The numerical analysis is performed using $k - \omega$ SST turbulence model inside fluid domain of parabolic dish cavity system. The Monte-Carlo ray tracing (MCRT) method is useful to determine the solar flux on cavity surface which can be set as wall boundary condition. The spherical and elliptical cavity receivers are selected to improve the performance of the system by reducing convection heat loss.

2. SIMULATION FRAMEWORK

The computer simulation of the cavity receiver system was set up in two steps: (1) optical analysis, (2) CFD analysis. The optical modeling was carried out for a 3.8 m diameter parabolic dish with focal length of 2.2 m where the cavity receiver was placed. The optical analysis was performed using Monte-Carlo ray-tracing method in COMSOL Multiphysics software. The ray tracing flux map was validated through the experiments of Shuai et al. [14]. The CFD analysis was performed using ANSYS Fluent solver where a computer-generated three-dimensional model was discretized into finite number of volume cells and governing equations were applied with finite volume approach. Grid convergence was also performed following validation through the experiments of Uzair et al. [6], so that further CFD analysis could be performed by tweaking the design parameters of the cavity receiver. The optical performance of the cavity receiver was characterized by concentration ratio and solar radiation flux uniformity index. The cavity receiver was

33

selected based on the highest uniformity index from optical analysis and then the radiation flux profile was used as boundary conditions for the CFD analysis of cavity receiver.

The concentration ratio (C_r) is estimated by taking ratio of solar concentrated flux on the receiver (q) and the ambient flux from the sun (G_{bn}) as represented in Eq. (1).

$$C_r = \frac{q}{G_{bn}} \qquad (1)$$

The solar flux uniformity index is determined from the ratio of average solar flux to the maximum solar flux concentrated on the cavity surface as represented in Eq. (2).

$$\mu = \frac{\sum q}{n \cdot \max(q)} \qquad (2)$$

2.1 Computational Domain

The design specifications of solar parabolic dish cavity receiver system used in the experiment of Uzair et al. [6] are provided in Table 1.

Geometric Parameter	Dimension
Aperture area of collector	11.34 m²
Aperture diameter of dish	3.8 m
Focal distance of dish	2.2 m
Surface area of receiver	0.72 m²
Aperture diameter of receiver	0.2 m
Rim angle	45°

Table 1: Geometric Parameters

The three-dimensional computer model is shown in Figure. 1 (a) which consists of a parabolic dish coupled with a cavity receiver. Fig. 1 (b) shows the design specifications of six different types of cavity receivers. First cavity is conical shape with frustum shape at

the aperture which is considered for the validation of CFD model. Second cavity is spherical shape with same frustum opening. Third cavity is the same spherical shape without any modification at receiver aperture. Fourth cavity is the same spherical shape with a backward facing step inside the cavity. Fifth and sixth cavities are the elliptical shape of eccentricity 0.3 and 0.7 respectively whereas having similar opening of fourth cavity.
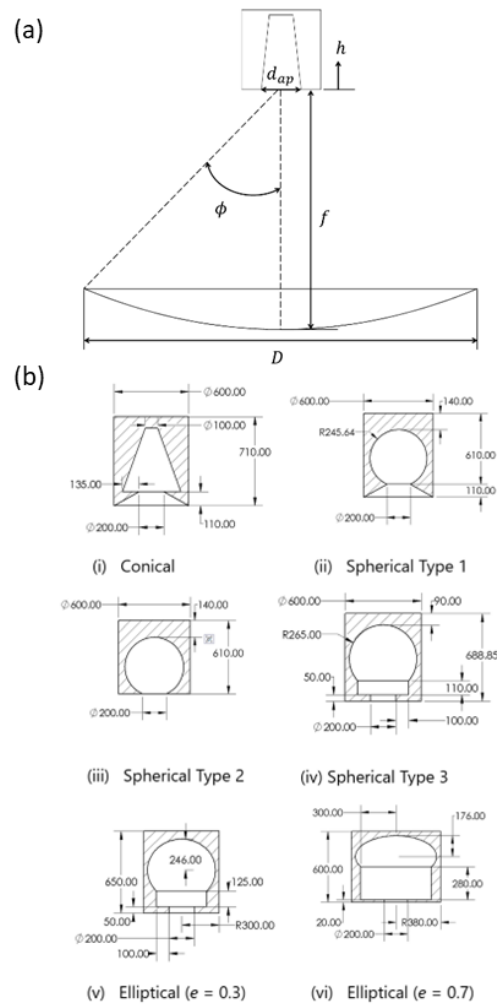
Figure 1. Computer-Aided Drawing with Dimensions of (a) Solar Parabolic Dish Cavity System and (b) Selected Cavities.

The three-dimensional computational domain for CFD analysis was extended 4 m

upstream, 6 m downstream positioning the cavity receiver in between the width and height of 4 m. The boundary conditions were velocity inlet and pressure outlet at inlet and outlet of the fluid domain, respectively, as shown in Fig. 2 (a).

The walls of the domain were considered completely adiabatic and no-slip condition was assumed while the cavity walls were at constant temperature. The operating pressure was set to 101325 Pa, turbulent intensity of 5% and turbulent viscosity ratio of 10. The boundary conditions were set according to the published experimental data.

- Inlet Temperature: 300 K
- Inlet Velocity: 1, 3, 5, 10 m/s
- Outlet Pressure: 0 Pa
- Cavity wall temperature: 873 K
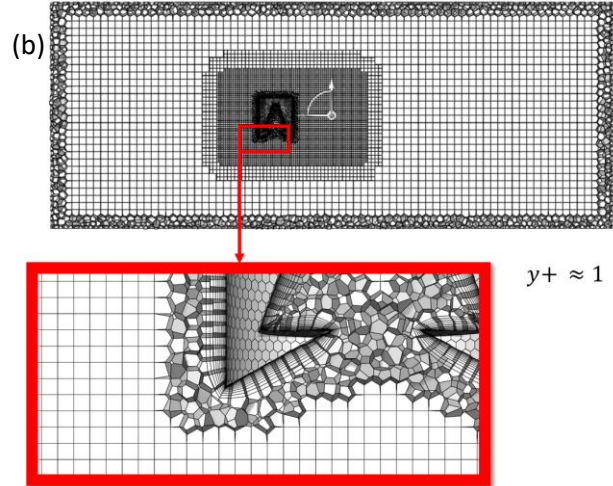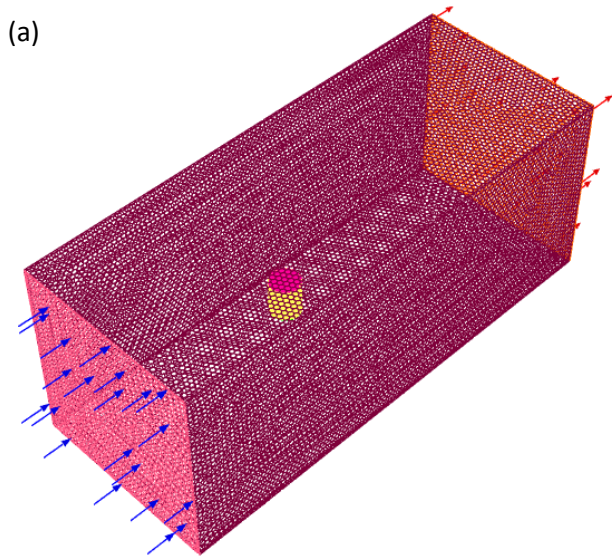
Figure 2. Computational grid with y+ layers near to the wall of the cavity receiver.

The computational grid is shown in Fig. 2(b). The computational model for the fluid domain of the cavity receiver was discretized into combination of polyhedral and hexahedral cells known as poly-hexcore mesh with 12 inflation layers near the walls of cavity receiver inside and outside. The refinement region was formed in the domain near the cavity receiver and the near-wall y+ spacing was selected carefully to achieve the value of $y+ \leq 1$.

2.2 Governing Equations

The flow inside the computational domain involves turbulence as well as heat transfer which can be approximated with steady-state assumptions. Therefore, it is required to model the fluid domain using the continuity, the momentum, and the energy equations, given by Eqs. (3), (4), and (5), respectively. The working fluid inside the domain is air and the thermophysical properties are kept constant.

$$\frac{\partial(\rho v_i)}{\partial x_i} = 0 \tag{3}$$

$$\frac{\partial(\rho v_i v_j)}{\partial x_i} = \frac{\partial}{\partial x_j}\left[\mu\left(\frac{\partial v_i}{\partial x_j} + \frac{\partial v_j}{\partial x_i} - \frac{2}{3}\delta_{ij}\frac{\partial v_k}{\partial x_k}\right)\right] - \frac{\partial P}{\partial x_j}$$

$$+ \frac{\partial}{\partial x_j}(-\rho\overline{v_i' v_j'})$$

$$\frac{\partial}{\partial x_i}\left[\rho v_i\left(h + \frac{1}{2}v_i v_j\right)\right] = \frac{\partial}{\partial x_j}\left[k_{eff}\frac{\partial \bar{T}}{\partial x_j} + v_i(\tau_{ij})_{eff}\right]$$

$$k_{eff} = K + \frac{c_p \mu_t}{Pr_t} \tag{5}$$

The term involving $-\rho\overline{v_i' v_j'}$ in Eq. (9) is known as Reynolds Stress, which is the cause of turbulence, and for its closure turbulence equation is required. Therefore, the $k - \omega$ SST model is applied to solve the non-linearity in the RANS equations applied to the fluid domain. The turbulent kinetic energy (k) and the specific dissipation rate (ε) are represented by Eqs. (6) and (7) respectively:

$$\frac{\partial(\rho v_i k)}{\partial x_i} = \frac{\partial}{\partial x_j}\left[\Gamma_k \frac{\partial k}{\partial x_j}\right] + \bar{G}_k + Y_k + S_k \tag{6}$$

where $\bar{G}_k = \min\left(-\rho\overline{v_i' v_j'}\frac{\partial v_j}{\partial x_i}, 10\rho\beta^* k\omega\right)$

$$Y_k = \rho\beta^* k\omega$$
where $\beta^* = \beta_i^*(1 + \xi^* F(M_t))$
$$F(M_t) = f(x) = \begin{cases} 0, M_t < M_{to} \\ M_t^2 - M_{to}^2, M_t > M_{to} \end{cases}'$$
$$M_t = \frac{2k}{\gamma RT}$$

$$\frac{\partial(\rho v_i \omega)}{\partial x_i} = \frac{\partial}{\partial x_j}\left[\Gamma_k \frac{\partial \omega}{\partial x_j}\right] + G_\omega - Y_\omega + D_\omega + S_\omega \tag{7}$$

where $G_\omega = \frac{\alpha}{v_t}\left(-\rho\overline{v_i' v_j'}\frac{\partial v_j}{\partial x_i}, 10\rho\beta^* k\omega\right)$

$$Y_\omega = \rho\beta'\omega^2$$

$$D_\omega = 2(1 - F_1)\rho\sigma_{\omega,2}\frac{1}{\omega}\frac{\partial k}{\partial x_j}\frac{\partial \omega}{\partial x_j}$$

In above, F_1 is termed as blending function and is defined as:

$$F_1 = \tanh(\varphi_1^4)$$

where $\varphi_1 = \min\left(\max\left(\frac{\sqrt{k}}{\beta^*\omega y}, \frac{500v}{\omega y^2}\right), \frac{4\rho k}{D_{k\omega}\sigma_{\omega 2}y^2}\right)$

and $D_{k\omega} = \max\left(2\rho\frac{1}{\sigma_{\omega,2}\omega}\frac{\partial k}{\partial x_j}\frac{\partial \omega}{\partial x_j}, 1.0 \times 10^{-10}\right)$

The default values of the model constants are: $M_{to} = 0.25$, $\xi^* = 1.5$, $\beta^* = 0.09$, $\beta_{i,1} = 0.075$, $\beta_{i,2} = 0.0828$, $\sigma_{k1} = 1.176$, $\sigma_{k2} = 2$, $\sigma_{\omega 1} = 1$, $\sigma_{\omega 2} = 1.168$, $\alpha_\infty^* = 1$, $\alpha_\infty = 0.52$.

The RANS equations also include pressure-velocity coupling, and this can be resolved using Semi-Implicit Method for Pressure-Linked Equations (SIMPLE) [16]. The second-order upwind scheme is used for this finite volume solver and the discretized RANS equations are limited to default residuals for their convergence. Also, the under-relaxation factors are set to default for all variables in the governing equations.

2.3 Grid Independence Test

The simulation data is obtained after iterative convergence in three different grid sizes: (1) coarse, (2) medium and (3) fine. The technique based on Richardson extrapolation [17, 18] as prescribed by Roache [19, 20] is used for minimizing the discretization errors which is known as Grid Convergence Index (GCI) study. Celik et al. [21] suggested that the solution should be converged at a certain iteration number and the structured mesh of hexahedral cells are suitable to calculate GCI. The GCI study consists of several steps, which include calculations of grid refinement ratio (r), apparent order (p), relative error (e) and convergence index (GCI).

The coarse, medium, fine grids are described in Table 2 with the number of elements and grid size (h). The selection of grids is made in a sequential manner with constant grid refinement ratio of 1.60. Eqs. (8) and (9) provide formulae used for grid size and grid refinement ratio respectively.

$$h = \left[N\sum_{i=1}^{N}(\Delta V_i)\right]^{1/3} \tag{8}$$

$$r_{12} = \frac{h_1}{h_2} \tag{9}$$

36

where N is the total number of elements and ΔV_i is the volume of the ith cell for a certain grid. The grid refinement ratio is similar found between medium and fine mesh by taking ratio of medium grid size to fine grid size.

Grid	Elements	h (mm)	r
(1) Coarse	342,346	9.10	-
(2) Medium	1,402,355	5.74	1.60
(3) Fine	5,925539	3.55	1.61

Table 2: Multiple Grid Specifications

The relative error is calculated from the extrapolated values for coarse to medium and medium to fine grids where it is assumed that the grid size is approaching zero. However, it is easy to calculate approximate relative errors and apparent order by neglecting $q(p)$ to find GCI, which are formulated as shown in Eqs. (10) and (11) respectively.

$$e_{12} = \left|1 - \frac{f_2}{f_1}\right| \tag{10}$$

$$p = \frac{1}{\ln(r_{12})}\left|\ln\left|\frac{f_2 - f_3}{f_1 - f_2}\right| + q(p)\right| \tag{11}$$

where f_1, f_2, f_3 are the values obtained from simulation result in coarse, medium, and fine grid respectively.

The GCIs are calculated for coarse to medium and medium to fine using the formula as provided in Eq. (12). All the parameters required to calculate GCI as shown in Table 3.

$$GCI = \frac{1.25\,e}{r^p - 1} \tag{12}$$

v	p	e_{12}	e_{23}	GCI_{12}	GCI_{23}
1	2.97	0.04460	0.01094	1.828%	0.431%
3	2.82	0.07743	0.02100	3.509%	0.915%
5	1.47	0.01586	0.00077	1.993%	0.948%
10	2.70	0.06133	0.01736	3.000%	0.817%

Table 3: Grid Convergence Index Calculations

The GCI is determined from the simulation results of convection loss for conical shape cavity receiver with frustum opening. The GCI value is found to be 0.778% and the expression for asymptotic convergence is achieved. The computational results of convection loss in the domain are plotted with three selected grid sizes varying wind velocity from 1 – 10 m/s as shown in Fig. 3.
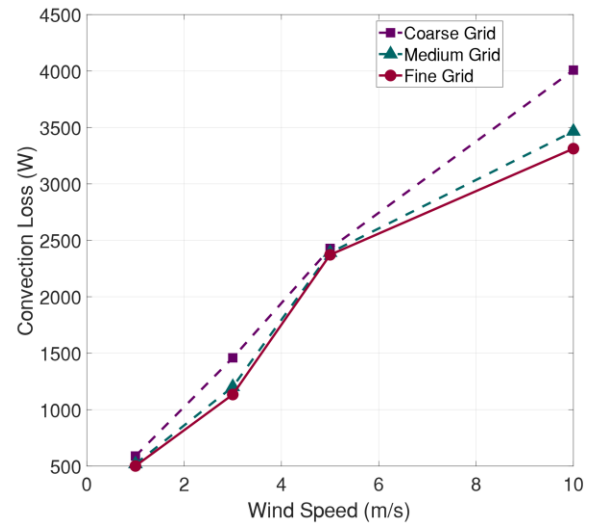
Figure 3. Grid convergence plot for convection loss as a function of wind speed.

The error band is formulated with the range of extrapolated values with the simulation results. Fig. 4 show a plot of error band based on GCI for convection loss as a function of wind speed. The extrapolated value and the

37

range of error band can be calculated from Eqs. (13) and (14) respectively.

$$f_{h \to 0} \cong f_1 + \frac{f_2 - f_1}{r^p - 1} \quad (13)$$

$$R = f_{h \to 0}(1 \pm GCI) \quad (14)$$
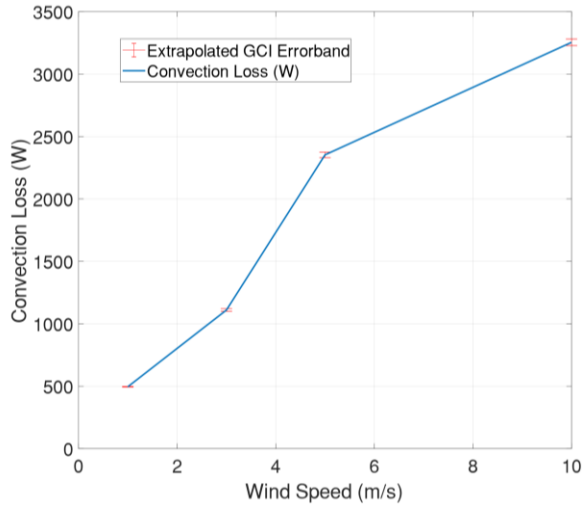
Figure 4. GCI error band plot for convection loss as a function of wind speed.

The asymptotic convergence is achieved through a criterion provided in Equation. (15).

$$\frac{1}{r^p} \times \left(\frac{GCI_{23}}{GCI_{12}} \right) \cong 1 \quad (15)$$

where subscript 23 represents coarse to medium and 12 represents medium to fine.

2.4 Model Validation

The optical model of the parabolic dish cavity system is validated with the experimental data as published by Shuai et al. [14]. Shuai et al. used a limb darkening model in order to achieve better accuracy of solar flux simulations in such solar receiver system. Limb darkening provides a more detailed solar flux distribution on curved surfaces like solar parabolic dish in which variation of angular diameter and intensity are considered. A more simplified model by Jeter [13] can also be used for validating the

optical model but it can not predict hot spots and area of potential thermal stress within the receiver. The computer simulation result of concentration ratio calculated from MCRT technique is compared with the experimental data as shown in Figure 4. The CFD results are also in good agreement with the experiments of Uzair et al. [6] as shown in Fig. 5, and therefore the model can be used for predicting the performance of selected cavity receivers.
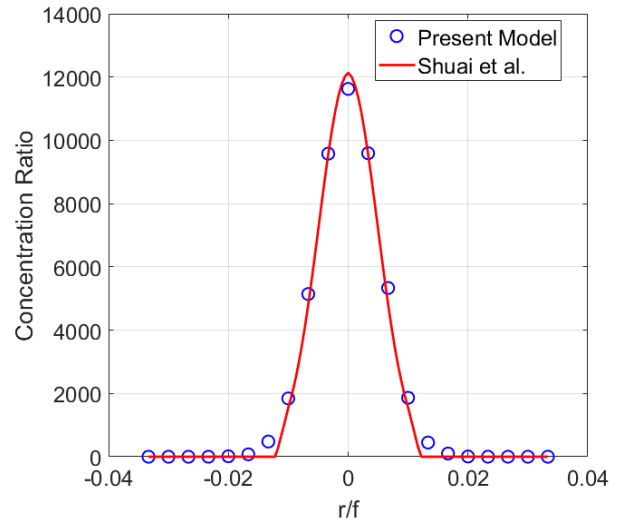
Figure 5. Optical model validation with experimental data [14].
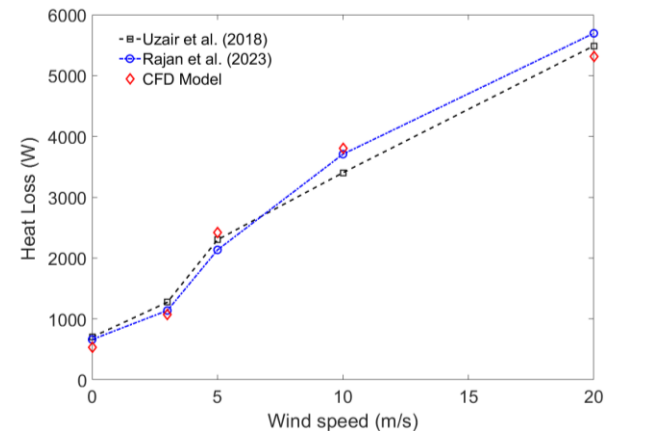
Figure 6. CFD model validation with experimental data [6].

3. RESULTS AND DISCUSSION

The simulation results are obtained with the boundary conditions same as performed for the validation but with different cavity shapes. The solar flux in spherical and elliptical cavities is uniformly distributed as compared to the conical cavity receiver. The highest solar flux is obtained in conical receiver with the value of $16\,\mathrm{kW/m^2}$ as shown in Figure 7(a). The cavity opening should be cautiously designed to capture maximum solar radiation and it is found that the cavities with backward facing step inside the cavity can provide more space to distribute solar flux. Whereas the optical performance of cavities reduces with frustrum opening as shown in Figure 7(a). Conical, spherical type 1 and type 2 cavities receive lower solar radiation flux as compared to the cavities with backward facing step opening.

The solar flux distribution in the conical shaped cavity receiver with frustum opening is found to be non-uniform compared to spherical and elliptical shaped cavity receiver. The non-uniformity of solar flux inside the cavity could lead to higher thermal stresses resulting in thermal shocks. The spherical shaped cavity of type 1 and type 2 with frustum opening and simple opening respectively provided poor capturing of solar flux inside the receiver. The reason is due to the positioning of the cavity receiver and as the offset distance is increased relative to focal point in backward facing step opening, the flux distribution becomes uniform.
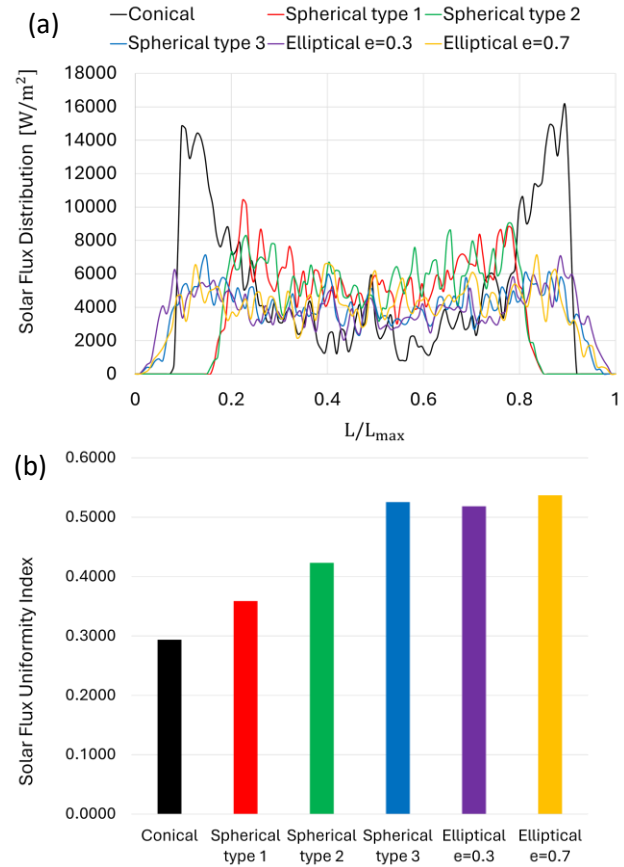
Figure 7. Comparisons of different cavity shapes for (a) solar flux distribution and (b) solar flux uniformity index.

Figure 7(b) shows that higher solar flux uniformity index in spherical and elliptical cavities with backward facing step opening. The highest solar flux uniformity is obtained in elliptical cavity of 0.7 eccentricity with the value of 0.5365 and the lowest in conical cavity with frustum opening with the value of 0.2955. The thermal performance is determined from the convection loss using CFD analysis in spherical and elliptical cavity receivers. Figure 8 shows the comparison of convection loss in 3 different spherical cavity receivers with validated conical cavity. The convection loss increases as the wind speed is increased and it is found higher in the frustrum opening type cavity receivers. The lower convection loss is found in the elliptical cavity of 0.7 eccentricity with

39

backward facing step opening. There is a 68.6% reduction in the spherical cavity with backward facing step opening as compared to the conical cavity receiver and 70.5% reduction in the elliptical cavity of 0.7 eccentricity as shown in Figure 9.

The significant reduction of convection loss is caused by the vortices formation inside the spherical and elliptical cavities which is found near the corners of backward facing step opening as shown in Figure 10. The frustum type opening exhibits wider circulation region formed outside the opening which increases the convection loss. Whereas the backward facing step inside the spherical and elliptical cavities introduces a secondary circulation region which reduces the convection loss greatly.
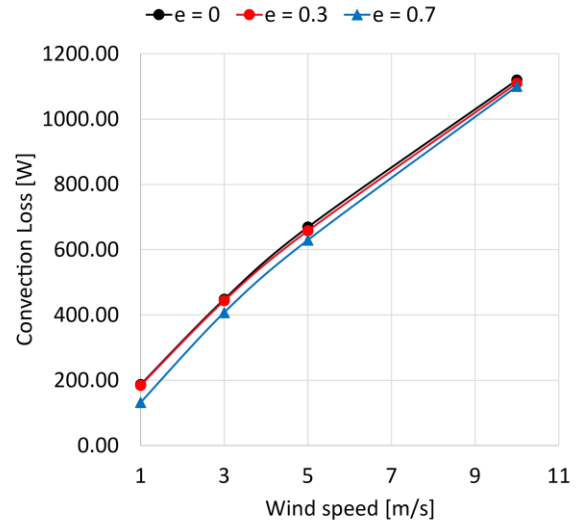
Figure 9. Comparison of convection loss in different elliptical cavity shapes varying wind speed
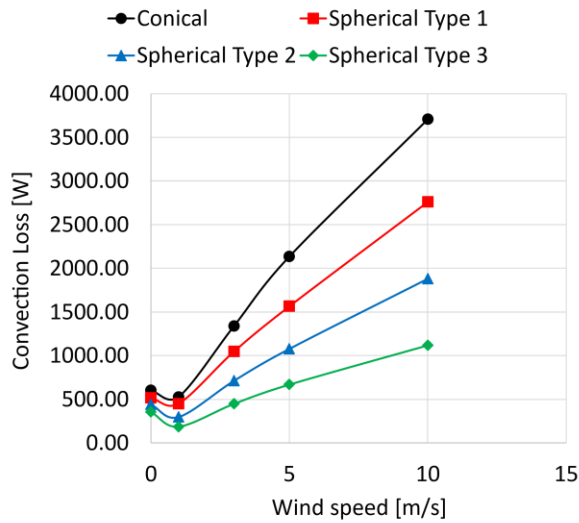
Figure 8. Comparison of convection loss in different cavity types varying wind speed.

also resulted in higher uniformly of solar flux inside the cavity receiver. The convection loss in frustum type opening in both conical and spherical

cavity is higher as compared with the backward facing step opening. The elliptical cavity receiver was further examined to investigate the effect of eccentricity. With higher eccentricity, the solar flux uniformity was found to be slightly higher and convection loss is slightly reduced in this type. Therefore, it is recommended to use elliptical shaped cavity receiver with backward facing step opening.

Figure 10. A comparison of velocity streamlines for six different type of cavity receivers.

4. CONCLUSIONS

This research paper focused to study the effect of spherical and elliptical shapes of cavity receiver on optical and thermal performance of parabolic dish cavity system. The study involved investigation on solar flux uniformity index and convection loss in different cavity receivers which determine the optical and thermal performance, respectively. The results showed that the backward facing step opening provided higher efficiency in both optical and thermal performance. The spherical and elliptical cavities elevated from focal point of the dish

REFERENCES

[1] A.M. Clausing, "An Analysis of Convective Losses from Cavity Solar Central Receivers," 1981.

[2] Stine WB and McDonald CG, "Cavity receiver convective heat loss," in Proceedings of the International Solar Energy Society (ISES) solar world conference, Kobe, Japan, 1989.

[3] C. G. Mcdonald, Heat Loss from an Open Cavity. 1995.

[4] S. Paitoonsurikarn and K. Lovegrove, "Effect of Paraboloidal Dish Structure on the Wind near a Cavity Receiver," 2006.

[5] M. Uzair, T. Anderson, R. Nates, and E. Jouin, "A validated simulation of wind flow around a parabolic dish," in 2015 Asia-Pacific Solar Research Conference, 2015.

[6] M. Uzair, T. N. Anderson, and R. J. Nates, "Modeling of convective heat loss from a cavity receiver coupled to a dish concentrator," Solar Energy, vol. 176, pp. 496–505, Dec. 2018, doi: 10.1016/j.solener.2018.10.060.

[7] M. Uzair, T. N. Anderson, and R. J. Nates, "The impact of the parabolic dish

41

concentrator on the wind induced heat loss from its receiver," Solar Energy, vol. 151, pp. 95–101, 2017, doi: 10.1016/j.solener.2017.05.022.

[8] W. G. Le Roux, T. Bello-Ochende, and J. P. Meyer, "The efficiency of an open-cavity tubular solar receiver for a small-scale solar thermal Brayton cycle," Energy Convers Manag, vol. 84, pp. 457–470, Aug. 2014, doi: 10.1016/j.enconman.2014.04.048.

[9] A.M. Daabo, S. Mahmoud, and R. K. Al-Dadah, "The effect of receiver geometry on the optical performance of a small-scale solar cavity receiver for parabolic dish applications," Energy, vol. 114, pp. 513–525, Nov. 2016, doi: 10.1016/j.energy.2016.08.025.

[10] F. Liu, K. Wu, Z. Rao, and Y. Peng, "Spatial layouts and absorbing surface design of heater tube arrays of direct-illumination receiver used in high power dish/stirling system," Energy, vol. 188, p. 116026, Dec. 2019, doi: 10.1016/j.energy.2019.116026.

[11] X. Li, R. Li, H. Chang, L. Zeng, Z. Xi, and Y. Li, "Numerical simulation of a cavity receiver enhanced with transparent aerogel for parabolic dish solar power generation," Energy, vol. 246, May 2022, doi: 10.1016/j.energy.2022.123358.

[12] L. Xiao, X. D. Cai, and S. Y. Wu, "Experimental investigation on natural convective heat loss of cylindrical cavity with/without a quartz window," International Journal of Thermal Sciences, vol. 150, Apr. 2020, doi: 10.1016/j.ijthermalsci.2019.106220.

[13] S. M. Jeter, "The Distribution of Concentrated Solar Radiation in Paraboloidal Collectors," 1986. [Online]. Available: http://solarenergyengineering.asmedigitalcollection.asme.org/

[14] Y. Shuai, X. L. Xia, and H. P. Tan, "Radiation performance of dish solar concentrator/cavity receiver systems," Solar Energy, vol. 82, no. 1, pp. 13–21, Jan. 2008, doi: 10.1016/j.solener.2007.06.005.

[15] A.Rajan and K. S. Reddy, "Optical modeling of corrugation cavity receiver for large-aperture solar parabolic dish collector," Energy Sources, Part A: Recovery, Utilization, and Environmental Effects, vol. 44, no. 2, pp. 3330–3348, Jun. 2022, doi: 10.1080/15567036.2022.2063458.

[16] B.E. Launder and D.B. Spalding, The Numerical Computation of Turbulent Flows, Computer Methods in Applied Mechanics and Engineering 3, 269-289 (1974).

[17] Richardson LF. The approximate arithmetical solution by finite differences of physical problems involving differential equations, with an application to the stresses in a masonry Dam. Trans Roy Soc Lond, Ser. A 1910;210:307–57.

[18] Richardson LF, Gaunt JA. The deferred approach to the limit. Trans Roy Soc Lond, Ser A 1927;226:299–361.

[19] Roache, P.J., "Quantification of Uncertainty in Computational Fluid Dynamics." Annual Review of Fluid Mechanics, 29, 123-60, 1997.

[20] Roache, P.J., Verification and Validation in Computational Science and Engineering, Hermosa Publishers, Albuquerque, NM, 1998.

[21] Celik IB, Ghia U, Roache PJ, Freitas CJ, Coleman H, Raad PE. Procedure for estimation and reporting of uncertainty due to discretization in CFD applications. J Fluids Eng, ASME 2008;130:078001-1–4. doi:10.1115/1.2960953.

A CONSTRAINT HEURISTIC FOR INTELLIGENT PLANNING AND SCHEDULING OF OPERATING ROOMS IN INDUSTRY 4.0 PERSPECTIVES

Aisha Tayyab[1] and Saif Ullah[1,*]

[1]Department of Industrial Engineering, University of Engineering & Technology, Taxila, Pakistan

[*]*Corresponding author E-mail address*: saif.ullah@uettaxila.edu.pk, (Saif Ullah)

ABSTRACT

Operating rooms are considered as critical resource in hospitals as they involve maximum investment in hospitals. Inefficient planning of patients on operating rooms underutilized their capacity and may not generate revenue as per their investment. In recent years, Industry 4.0 has increased the trend of industries towards intelligent and efficient decision making which has also attracted researchers for its implementation in healthcare industry. Therefore, current research investigates planning and scheduling problem of patients on operating rooms in context of industry 4.0 keeping in view resource constraints. A mixed integer programming model of the considered problem is made, and a resource constraint heuristic is introduced for intelligent planning and scheduling of patients in operating rooms to maximize the utilization of operating rooms using theory of constraints. Experiments are performed to validate the performance proposed heuristic as compared to the standard scheduling rules used in literature and a case problem taken from Case Hospital is solved. Results indicate that the proposed heuristic outperforms other scheduling heuristics.

Keywords: Operating rooms; Planning and scheduling; Industry 4.0; Heuristic

1. INTRODUCTION

Industry 4.0 is causing significant changes in industrial sectors [1]. According to Dilberoglu et al. [2] and Mosterman and Zander [3] industry 4.0 is an integrated set of intelligent production systems and advanced information technologies that are based on set of integrated software systems. Drath and Horch [4] stated that industry 4.0 is a path with no return and will become a competitive challenge for companies interested in long term survival. Therefore companies must be prepared for this competitive challenge [5]. Industry 4.0 is an established reality that seems to fulfil various requirements of medical field as well. Industry 4.0 seems to be an essential part of tomorrow's medical field and smart factories. It can provide a type of digital hospital and a complete monitoring system that fulfils the individual requirements of the patient/medical industry with optimized time and cost.

Industry 4.0 is an innovative approach to generate new concept and undertake development in the medical field through the integration of technologies, smart machines and different software. It creates connectivity and data exchange with the help of new technologies, software, sensors, robots and other advanced information technologies. It uses artificial intelligence (AI) to share information digitally in hospitals and enables to create full visibility in operation that provides a higher level of information about quality, inventory, raw material, waste, output, assets and customer demand visibilities, help industries to save

43

time and money and improve customer satisfaction [6,7].

Industry 4.0 concepts has been used in planning of resources. As an example, Pham and Klinkert [8] considered scheduling of surgical cases and decided on the time to perform surgeries to efficiently use hospital resources and to increase quality of service for patients. They proposed a mixed integer linear programming model with an objective to minimize the makespan and minimizing sum of all starting times. They solved the model on CPLEX with small set of generated instances and larger instances were not solved.

In their study Gartner and Kolisch [9] addressed the problem of planning the patient flow in hospitals subject to scarce medical resources with an objective to maximize the contribution margin. Patients were classified on their diagnosis related group based on their clinical pathway and decision was made on which day each procedure of clinical pathway should be done. Clinical pathway defines the procedures such as different types of diagnostic tests and surgery as well as the sequence in which they must be applied to the patients. Two mixed integer programs were developed and embedded in a static and rolling horizon approach to cope with stochastic data. Efficient planning and scheduling of patients is significant for the performance of healthcare facilities. Therefore, lot of research is available in literature focusing on planning and scheduling of operating rooms [10-22]. In literature, planning and scheduling of patients in operating rooms have been studied at three levels of decision making, including strategic level, tactical level and operational level planning problems. At strategic level, the operating room capacity is divided among different type of patients and different blocks are created for each type of surgeries. While

at the tactical level, master surgery schedule is made and at the operational level, patients are scheduled in each surgery block. These three levels of plans are interrelated to each other, and they are interdependent. Therefore, some researches have integrating higher level planning with medium level planning while integration of all three levels of planning are scarce [13, 21]. The hierarchical level integration of different decision levels can give local optimal results of schedule as there is no feedback information which can update the respective higher level of plan. Without integration and feedback mechanism, the decision made at different levels are not coherent and result in local optimal solutions. Planning decisions made at higher levels cannot incorporate the day by day changes and particularly, seasonal changes. Therefore, an integrated approach combining all levels of decision making is highly needed in healthcare and present study serves the purpose of developing a method for integration of higher, medium and lower level planning and making the planning and scheduling decisions more realistic and reflective of day by day dynamic situations in hospitals.

Moreover, Some of the studies used the planning decisions which have been made at higher planning levels such as case mix , type and capacity of clinical resources as well as tactical decisions on master surgery schedule [9]. The studies conducted on operational level use the data from tactical level planning which is done far ahead of time. On medium level planning most of researches use a cyclic master surgery schedule [8,11,12,23,24] to ensure stability of schedules for surgeons and nurses. These schedules remain the same until decided by the managers based on changing demand. These cyclic schedules lead to some of the capacity overutilized and

long waiting lists and some of the capacity is underutilized due to fixed blocks or rooms for surgical specialties. Such a situation cannot lead to optimum utilization of critical resources like operating rooms, ICU and recovery wards and also waiting lists keep on increasing in such a situation. To tackle this problem, present study proposes a reconfiguration method for master surgery schedule, where schedules are reconfigured based on demand. Present study investigates master surgery schedule and allocation of operating rooms to the specialty groups and reconfigured at operational level which is rarely discussed in literature [23]. Further current research first identify the bottleneck operating room based on the patient data and flow. Later, the respective model of operating room planning and scheduling is solved using optimization algorithm. Current research proposed a heuristic method to schedule patients in operating rooms with an aim to maximize the utilization of operating rooms keeping in view the patient constraints related to their treatment requirements.

2. PROBLEM DESCRIPTION

A scenario of hospital is assumed in order to explain the nature of problem in this section. Figure 1 shows the flow of surgical patients in a hospital. A surgical patient is one who needs surgical procedures to be performed in his/her flow through the hospital. Patients visiting the hospital are either elective patients or non-elective patients. Elective patients are those patients who are known beforehand and can be scheduled in surgery lists. They include both inpatients and outpatients. Inpatients are those patients who spend at least one night at hospital and outpatients visit the hospital for a few hours and are not admitted to hospital. Non-elective patients, on the other hand are urgent or emergency patients who can visit the hospital any time depending upon level of urgency. Depending upon the treatment requirements

the patients can visit the relevant departments and leave the hospital after the completion of treatment process as explained in below Figure 1.
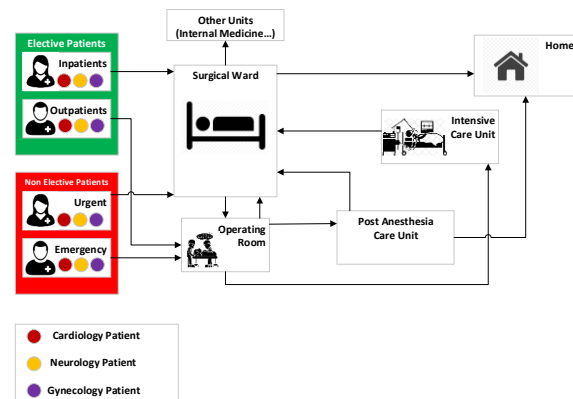
Figure 1. Flow of surgical patients in a hospital

When the patients of different categories and different specialties visit the hospital, the patient treatment time or workload on various units of hospital is different and the department which have highest load as compared to the other departments becomes bottleneck according to theory of constraints. In proposed method, three planning levels, Higher level planning, medium level planning and lower-level planning are integrated. Planning and scheduling of three critical departments which have highest operational costs, including operating room (OT) Intensive care units (ICU), and recovery wards are considered.

For example, considering the flow of different patients from different departments as shown in the below Figure 2. Patients flow from three departments; cardiology, neurology and gynecology are shown in the Figure 2. All three patients need the surgical procedures to be performed as a part of their treatment as shown. In the Figure 2 for example neurology patient visits the neurology department, then radiology department and operating room and intensive care unit. Similarly, at the same time patients from other departments also need surgeries in

45

operating rooms. Operating rooms are dedicated for different specialties by master surgery schedule at medium level planning as shown in the Figure 2 through different colours. Due to load of patients, operating room may become bottleneck.

Patients flow from three departments; cardiology, neurology and gynaecology is shown in Figure 2.

Figure 2. Patients flow from three departments; cardiology, neurology and gynecology

2.1 Assumptions:
- List of patients obtained from forecast is available.
- Only elective patients are considered for scheduling.
- An open scheduling policy is adopted for OR.
- Operating room staff are available.
- All operating rooms are considered as identical.

2.2 Mathematical Model:
A mixed integer programming model for scheduling of patients in operating rooms and their allocation in different planning horizons is presented in this section. The objective function for scheduling of patients is aimed to minimize the makespan of all operating rooms in a planning horizon, as shown in Equation (1). The detail of makepsan is shown in Equation (2). While Equation (3) shows the completion time of a surgery of a patient. Equation (4) and (5) represents the earliest and latest start time of surgeries of patients. Equation (6) indicates the planned start time of a patient. Equation (7) shows the constraints on available capacity of any operating room and ensures that the workload of an operating rooms should not exceed the workload of patients on the operating room. Constraint shown in Equation (8) guarantees that a patient can only be treated once in the schedule. Equation (9) shows binary variables and Equation (10) shows non-negativity constraints.

$$(Obj)_b = \min(makespan)_{ob\tau} \quad o \in O \,\forall\, 0 < b \le B, \forall\, \tau \tag{1}$$

$$(makespan)_{ob\tau} = t_q^{pre} + \sum \max\left\{t_q^{comp}, t_{q+1}^{pre}\right\} + \sum t_{qq'}^{SDS} \times Y_{qq'ob\tau}^{x,(x+1)} + \sum t_q^{s} \times Z_{qq'ob\tau}^{x,(x+1)} \tag{2}$$

$$\forall q, q' \in Q, o \in O \,\forall\, 0 < b \le B, \forall\, \tau$$

$$t_q^{comp} = \sum t_q^{set} + t_q^{sur} + t_q^{clr} \times X_{qob\tau} \,\forall q \in Q, o \in O \,\forall\, 0 < b \le B, \forall\, \tau \tag{3}$$

$$LPST_q = D_q - \left(t_q^{pre} + t_q^{set} + t_q^{sur}\right) \forall q \in Q \tag{4}$$

$$EPST_q = A_q + \max\left\{t_q^{pre}, t_q^{st}\right\} \forall q \in Q, o \in O \tag{5}$$

$$PST_q = avg\left\{EPST_q, LPST_q\right\} \forall q \in Q \tag{6}$$

$$WL_{ob\tau} \le At_{ob\tau} \,\forall\, o \in O, \, 0 < b \le B, \forall\, \tau \tag{7}$$

$$\sum X_{oqb\tau} \leq 1 \quad \forall q \in Q, 0 < b \leq B, \forall \tau \tag{8}$$

$$X_{qob\tau}, Y_{qq',ob\tau}^{x,(x+1)}, Z_{qq',ob\tau}^{x,(x+1)}, U_{sqob}^{\tau}, W_{qob\tau}, V_{qob\tau} \in \{0,1\} \quad \forall q \in Q, s \in S, o \in O, 0 < b \leq B, \forall \tau \tag{9}$$

$$ST_q, makespan_{ob\tau} \geq 0 \tag{10}$$

3. CONSTRAINT HEURISTICS FOR INTELLIGENT PLANING AND SCHEDULING

An overview of the procedure adopted for multi-level intelligent planning and scheduling of patients is shown in Figure 3. It can be seen from Figure 3 that case mix planning, master surgery schedule and patient scheduling are integrated. Further, flow of information during multi-level planning is indicated in Figure 3.
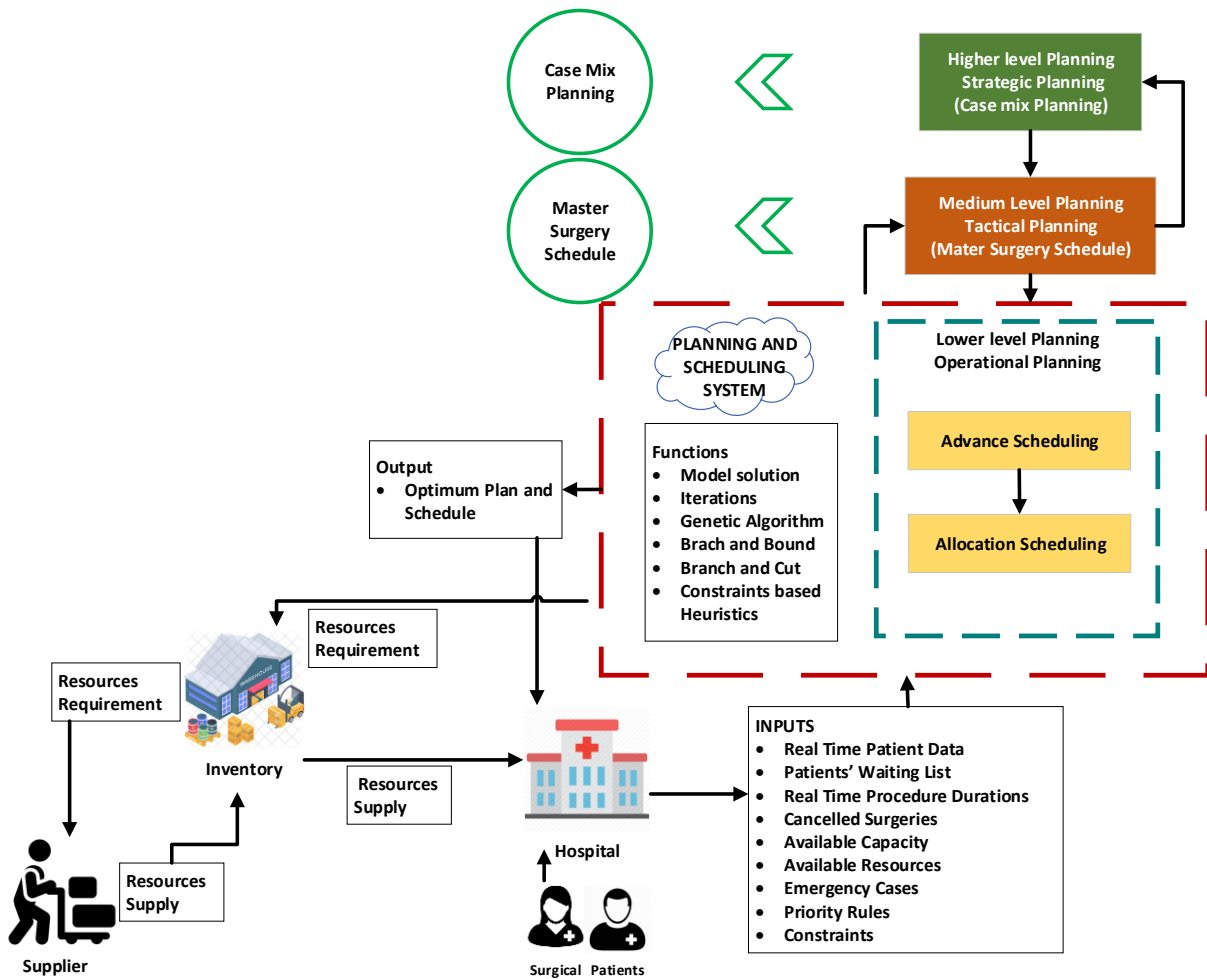
Figure 3. An overview of the procedure adopted for multi-level planning and scheduling

The procedure of the proposed resource constraint heuristic for multi-level intelligent planning and scheduling of patients on operating rooms based on theory of constraint is presented in this section. At higher level planning, infinite capacity plan of patients is made and patients are allocated to planning horizons based on their planned

47

start time. A medium level, operating room resources are configured based on the patient workload on operating rooms. Similarly, plan is based on the capacity of operating rooms and lower level schedule is made based on the real capacity available in each operating rooms room and a feedback information is going back towards medium level planning horizons and higher level planning horizons.

Step 3: Compute the workload of each operating room with their available capacity in each planning horizon to search for best finite capacity plan.

Step 4: Schedule patients in planning horizon in each operating room and identify the bottleneck operating room.

Step 5: Reconfigurable operating rooms based on the push, pull and offload strategies as shown in Figure 4. While pulling, pushing and offloading the constraints such as priorities of patients, surgeons, supporting staff and material availability, start date and due date of patients are considered. An operating room can only offload to other operating room, if the capacity on the other operating room is available in same time period. An operating room can pull a patient from later time periods only if it has the available capacity and all constraints are fulfilled by the pull. Similarly, an operating room can push the patients to later time period if the constraints are fulfilled and capacity is available in later time periods.

Step 6: Once, load balancing on all the operation rooms is performed, sequence the patients considering precedence constraints and other special constraints of patients and optimum schedule of the surgeries for next day is produced and released.

Step 7: Feedback the optimal schedule to medium level planning horizon to update the patients in medium level planning horizon.

Step 8: check, if the medium level planning horizon is completed, send the feedback

medium level plan to higher level planning horizon to update the higher level plan.

Figure 4. Allocations of operating rooms reconfigurable based on the push, pull and offload strategies

4. COMPUTATIONAL EXPERIMENTS AND RESULTS

In this section, performance of proposed resource constraint heuristic is compared with the other scheduling rules used in literature. The data used for experimentation is obtained from a Case Hospital in Pakistan. The data obtained from the case hospital includes the information of arrival date, patient preparation time, setup time of operating room, actual surgery duration and due date of the surgery patients.

To check the performance of proposed method on generalized data, the obtained data from case hospital is modified to create more instances. Randomly 15 instances of problem are created. The algorithm was coded in standard C# and compiled in Visual Studio version 2019. All tests were performed on a 2.60 GHz Intel core i7 processor, with 16 GB of RAM running under Windows 10.

No. of Operating rooms	No. of patients	No. of Surgeons	No. of Specialties	No. of Instances
3-4	75-100	3-4	6-7	15

Table 3. Problem data for 15 instances

48

The performance of the proposed method is compared with sequencing rules including (1) increasing duration (ID) i.e., patients are arranged in order of increasing surgery duration and (2) Decreasing duration (DD), i.e., patients are scheduled in decreasing order of their surgery duration.

Comparison of results obtained by proposed method is made for 15 problems for a planning horizon of One Week. The regular capacity of operating rooms is considered as 8 hours per day and seven days a week. Lower-level scheduling period is taken as one day and lookahead period is taken as one day. Cleaning time after surgery of patient of different specialty groups is taken as variable. It is assumed that sequence dependent setup time occurs when patients of different specialty groups are operated in the same operating room consecutively. The same input data of surgery patients for one week is used to evaluate all the methods.

At first, initial allocation of patients to planning period is based on Planned Start Time for all methods. Once the operating rooms and surgeons are allocated to the patients, schedule of allocated patients is made with proposed and other methods.

The objective function, i.e., Makespan of the patients for operating rooms using proposed method is calculated with same number of patients as well as with increased number of patients as a result of push pull strategies proposed in present method. In the RCBH method, patients are pulled to fully utilize the capacity of operating rooms once the optimal schedule for the operating rooms is made. Following comparison metrics are used to compare the proposed RCBH method with other scheduling methods.

4.1 Number of Patients Operated

During making higher level plan, patients are inserted to their most suitable planning periods based on their planned start time (PST). All the patients with same PST are inserted to same planning period as the capacity of all resources on higher level is considered infinite. Table 2 shows the average number of patients inserted on higher level planning periods for all instances of experiments.

While making medium level plan, patients are allocated to operating rooms and workload of operating rooms is balanced, and patients are pulled to next planning horizons if the workload of operating rooms exceeds available capacity of operating rooms. Operating room allocation is optimized and same specialty patients are inserted to same operating room to reduce sequence dependent setups.

On the lower level planning horizon, the patients are sequenced in the allocated operating rooms. The optimal sequence results in release of capacity of operating rooms and more patients are pulled from next lower level planning period to fully utilize the capacity of operating rooms. Average number of patients on all planning levels are represented in Table 2.

Number of patients in different planning horizons			
Higher Level	Medium Level	Lower Level (Other methods)	Lower Level (RCBH)
21	14	14	18

Table 2. Average number of patients in all planning horizons per day

It can be seen from the results shown in Table 2 that average number of patients operated in the schedule produced by proposed method is higher than the number of patients operated as per schedule generated by the other methods. This increased the average number of patients in the schedule which is produced by proposed method i.e., from 14 to 18. More patients are inserted to operating rooms using push pull strategies of proposed method.

4.2 Makespan

Table 3 represents the comparison of makespan values for all problems. It can be seen that proposed method shows less value of makespan as compared to the other methods when the number of patients is considered same for all methods. This shows that the proposed method generates schedule of patients a can treat patients in less time as compared to the other methods. However, as per proposed method, there is push and pull strategy used to insert more patients from the next planning horizons, if there is available capacity in the operating rooms, therefore, three are 4 more patients inserted and the total number of patients served in the planning horizon increased to 18 from 14. In this situation, the makespan value of proposed method increased as compared to the other methods but at the same time, schedule generated by proposed method increased the utilization of the operating rooms.

Method	Proposed				When more Patients are scheduled using push pull strategy	
		ID	DD	No. of Patients	Proposed	No. of Patients
Makespan	2839	2887	2858	14	3024	18

Table 3. Comparison of Average makespan values for all Problem categories

5. CONCLUSION

In the current research, a constraint heuristic method is proposed for intelligent planning and scheduling of patients in operating rooms. The proposed method used theory of constraint and integrates strategic level, tactical level and operational level planning and scheduling of patients in rolling horizon planning periods. The proposed method optimized the schedule of patients day by day and used a feedback method to update the patient list in medium level planning horizon. If there is capacity available, the patients are pushed or pull between the planning horizons and the update patient list is created. Due to this feedback mechanism, surgeries which were not performed in any day are added in the list based upon their priority and rescheduled again. The developed method is intelligent due to incorporation of postponed and cancelled surgeries in the unscheduled patients list and scheduling them again before their due date is passed. The proposed method integrates different level of decision making and increase the utilization of operating rooms in each planning horizon based on the available capacity. Various experiments are performed to evaluate the performance of the proposed method as compared to scheduling rules used in literature based on the data taken from Case Hospital in Pakistan. The scheduling results obtained from proposed method are compared with scheduling rules such as ID and DD. Comparison of results shows that proposed method performs better in terms of number of patients and capacity utilization. Future work can be extended to include real time data of resources and patients using cloud and IOT technology to estimate the values of variables using intelligent deep learning algorithms and make intelligent plan of patients on expected critical resources.

ACKNOWLEDGEMENTS

REFERENCES

[1] Pacchini, A.P.T., et al., The degree of readiness for the implementation of

Industry 4.0. *Computers in Industry*, 113, 103-125, 2019.

[2] Dilberoglu, U.M., et al., The role of additive manufacturing in the era of industry 4.0. *Procedia Manufacturing*, 11, 545-554, 2017.

[3] Mosterman, P.J. and J. Zander, Industry 4.0 as a cyber-physical system study. *Software & Systems Modeling*, 15(1), 17-29, 2016.

[4] Drath, R. and A. Horch, Industrie 4.0: Hit or hype?[industry forum]. *IEEE industrial electronics magazine*, 8(2), 56-58, 2014.

[5] Lee, J., H.-A. Kao, and S. Yang, Service innovation and smart analytics for industry 4.0 and big data environment, *Procedia Cirp*, 16, 3-8, 2014.

[6] Javaid, M. and A. Haleem, Industry 4.0 applications in medical field: A brief review. *Current Medicine Research and Practice*, 9(3), 102-109. 2019.

[7] Haleem, A., M. Javaid, and R. Vaishya, *Industry 5.0 and its applications in orthopaedics.* J Clin Orthop Trauma, 10(4), 807. 2019.

[8] Pham, D.-N. and A. Klinkert, Surgical case scheduling as a generalized job shop scheduling problem, *European Journal of Operational Research*, 185(3), 1011-1025, 2008.

[9] Gartner, D. and R. Kolisch, Scheduling the hospital-wide flow of elective patients, *European Journal of Operational Research*, 233(3), 689-699, 2014.

[10] Burdett, R.L. and E. Kozan, An integrated approach for scheduling health care activities in a hospital, *European Journal of Operational Research*, 264(2), 756-773, 2018.

[11] Oliveira, M., et al., Assessing the impact of patient prioritization on operating room schedules, *Operations Research for Health Care*, 24: p. 100232, 2020.

[12] Schneider, A. T., van Essen, J. T., Carlier, M., & Hans, E. W, Scheduling surgery groups considering multiple downstream resources, *European journal of operational research*, 282(2), 741-752, 2020.

[13] Roshanaei, V., Booth, K. E., Aleman, D. M., Urbach, D. R., & Beck, J. C., Branch-and-check methods for multi-level operating room planning and scheduling, *International Journal of Production Economics*, 220, 107433, 2020.

[14] Younespour, M., et al., Using mixed integer programming and constraint programming for operating rooms scheduling with modified block strategy. *Operations Research for Health Care*, 23, 100220, 2020.

[15] Vijayakumar, B., et al., A dual bin-packing approach to scheduling surgical cases at a publicly-funded hospital, *European Journal of Operational Research*,. 224(3), 583-591, 2013.

[16] Moreno, M.S. and A.M. Blanco, A fuzzy programming approach for the multi-objective patient appointment scheduling problem under uncertainty in a large hospital. *Computers & Industrial Engineering*, 123, 33-41, 2018.

[17] Chen, X., et al., Patient flow scheduling and capacity planning in a smart hospital environment. *IEEE Access*, 4,135-148, 2015.

[18] Vancroonenburg, W., P. Smet, and G.V. Berghe, A two-phase heuristic approach to multi-day surgical case scheduling considering generalized resource constraints, *Operations Research for Health Care*, 7, 27-39, 2015..

[19] Marques, I. and M.E. Captivo, Different stakeholders' perspectives for a surgical case assignment problem: Deterministic and robust approaches. *European Journal of Operational Research*, 261(1), 260-278, 2017.

[20] Marques, I., M.E. Captivo, and M.V. Pato, Scheduling elective surgeries in a Portuguese hospital using a genetic heuristic, *Operations Research for Health Care,* 3(2), 59-72, 2014..

[21] Ma, G. and E. Demeulemeester, A multilevel integrative approach to hospital case mix and capacity planning, *Computers & Operations Research*, 40(9), 2198-2207, 2013.

[22] Vancroonenburg, W., P. De Causmaecker, and G.V. Berghe, Chance-constrained admission scheduling of elective surgical patients in a dynamic, uncertain setting. *Operations Research for Health Care*, 22,100196, 2019.

[23] Kamran, M.A., et al., Adaptive operating rooms planning and scheduling: A rolling horizon approach. *Operations Research for Health Care*, 22,100200, 2019.

[24] Freeman, N., M. Zhao, and S. Melouk, An iterative approach for case mix planning under uncertainty, *Omega*, 76,160-173, 2018.

IOT IN INDUSTRY 4.0: CHALLENGES AND OPPORTUNITIES

Muhammad Danish Saleem[1*], Muhammad Mubashir Khan[2] and Anis Fatima[1]

[1] Department of Industrial and Manufacturing Engineering, NED University of Engineering & Technology, Karachi, Pakistan

[2] Department of Computer Science & Information Technology, NED University of Engineering & Technology, Karachi, Pakistan

[*]*Corresponding author E-mail address*: mdanishsaleem@neduet.edu.pk

ABSTRACT

Due to successive technological advancements, developments and innovations, the global industrial landscape has drastically transformed over the last years. Industry 4.0 aims at transforming traditional industries into intelligent ones by incorporating innovative technologies. Industry 4.0 enables physical assets to be integrated into intertwined digital and physical processes thus creating smart factories and intelligent manufacturing environments. Internet of Things (IoT) is a rapidly growing technology that has drastically contributed to the Industry 4.0 realization. IoT pursues to pervade our everyday environment and its objects, linking the physical world to the digital world and allowing people and "things" to be connected anytime, anywhere, with anything and anyone ideally using any network and service. This study scrutinizes literature review on IoT in the Industry 4.0 context. More specifically, it describes the IoT concept, its security and privacy challenges and explores numerous IoT application domains. Moreover, it presents and analyses the concept of Industry 4.0 and the benefits it offers as well as the relevant key technologies (e.g. industrial internet of things (IIoT), cyber-physical systems (CPSs), cloud computing, big data and advanced data analytics). Furthermore, it describes the emerging application of IoT in Industry 4.0 and highlights the IoT and Industry 4.0 research gaps. Finally, the need for innovation in the industrial domain and the impact and benefits that IoT and Industry 4.0 provide to everyday life and industries are described.

Keywords: Internet of Things (IoT), Industry 4.0, IoT applications

1. INTRODUCTION

Nowadays, due to the rapidly evolving technological advancements, smart devices are able to interconnect, communicate and interact over the Internet. Moreover, over the years, the size of these devices has been reduced whereas their processing power and storage capabilities have significantly increased. Contemporary, smart devices are equipped with advanced embedded systems and have the capabilities of communication, sensing, actuation as well as real-time data retrieval, collection, storage and processing.

Internet of Things (IoT) is a rapidly growing innovative technology with various applications, functions and services in everyday life and in a wide variety of domains. IoT aims at pervading our everyday environment and its objects, linking the physical world to the digital world and allowing "people and devices to be connected anytime, anywhere, with anything and with anyone" [1], [2]. IoT and more specifically, Industrial Internet of Things (IIoT) along with the digitalization and automation of industrial manufacturing

53

are thought to be what truly have initiated the fourth industrial revolution (Industry 4.0). Industry 4.0 combines traditional manufacturing and industrial practices with innovative technologies, such as large-scale machine-to-machine (M2M) communications, IoT, cyber-physical systems (CPSs), etc. Moreover, it aims at fundamentally transforming traditional industries into intelligent ones by introducing self-maintainability, self-optimization, self-cognition, and self-customization into the industry. There is no doubt that by utilizing the advanced and dynamic network of interconnected devices, IoT can offer a magnitude of solutions to industries as well as multitude of contemporary and advanced applications and services that cannot only enhance life quality, but can also lead to personal, professional and economic opportunities and benefits [3].

2. IOT AND ITS APPLICATIONS

As an off-promising technology, IoT provides solutions to transform the operation of many existing industrial systems. IoT allows all the prevailing systems to connect to a network, using which they can communicate among themselves and with the surroundings such that some actions to take place. Connecting all the devices to a network can be done by using a unique ID called IP address. IP address helps to identify and locate a device on the network and routes the information. Today commonly accepted definition for IoT is *"A network of physical objects or 'things' that can interact with each other to share information and take action."* or: *"The Internet of Things (IoT) is the interconnection of uniquely identifiable embedded computing devices within the existing Internet infrastructure"* [4].

Initially IoT used radio-frequency identification (RFID) technology for identifying the connected devices. Later on, IoT locate devices by using sensors, actuators, and mobile devices. Specifically, integrating sensors, RFID tags and communication protocols serves as the foundation for IoT [5]. Research shows that there is tremendous growth in the area of IoT. Most of the industries are trying to work on more projects related to IoT in the fields of health care, agriculture, aqua-forms, transportation and others.

2.1 Background

During initial days of IoT, RFID served as the foundation technology, which allows user to send or receive information using radio-frequency signals. The connected device should be attached with RFID tags, which contains reader and transmitter. With the help of RFID reader, people can locate and monitor the devices [6]. Main application of RFID is transportation. Later on, wireless sensor networks (WSN) served as a building block for IoT. Here sensors / actuators will be attached to the devices with in the network. Sensors are used to sense the data and using actuators data will be transmitted. The main application of WSN includes health-care. With the advancement of RFID and WSN, there is a significant growth in the development of IoT [5]. IoT finds its main applications in the fields of tracking & monitoring, health-care, home automation, environment monitoring, smart building, agriculture, aqua-culture and others. With the advancement of smart phones, communication protocols, sensor networks technologies; it is possible to connect more objects in a network. IoT application contains both hardware and software. IoT hardware is broadly classified in to wearable devices and embedded system

54

boards. Wearable devices will come with preassembled hardware application [7]. The scope of wearable devices is limited to a particular application. For example, a smart watch may be designed for call receiving and fitness monitoring only. The advantage with wearable device is handy to use. The examples of wearable devices are: Samsung gear, google glass, digitsole smart shoe and others. On the other hand, embedded system boards are open for the user. That is, a user can program these boards depending on the application he want. In present day market, there are so many embedded system boards are available. Examples include Arduino boards, raspberry pi boards, Samsung artik board, cloudbit, ESP8866 Wi-Fi module and others. After selecting a particular embedded system board, the user has to choose application software. There are wide range of programming languages like C, C++, python etc. IoT deals with connecting the devices to a network and sharing the information, in this point of view one has to ensure security and reliability. Also, IoT deals with various kinds of devices, so in order to perform the task properly, standardization is required.

Standardization provides interoperability and compatibility on a global scale [8]. Many professional bodies are working on creating standards for IoT. At present organizations like IEEE, International Electro-technical Standardization, China Electronics Standardization Institute, American National Standards Institute are working on the development of standards for IoT [9]. By designing IoT applications on accepted standards, one can achieve reliability and interoperability, which in-turn will reduce maintenance costs in the long run [10]. The main aspects of the smart city project are waste management, intelligent

transportation, smart urban lightening, tele-care and others. IoT applications aims at improving the life quality for the end-user community and supporting infrastructure and general-purpose operations. A survey has also been conducted in which IoT applications has categorized into the following domains [11], [12]:

- Transportation and logistics domain: Applications of this domain involve logistics, assisted driving, mobile ticketing, environment monitoring, augmented maps etc.
- Healthcare domain: Applications of this domain involve tracking, identification, authentication, data collection, sensing etc.
- Smart environment domain: Applications of this domain involve comfortable homes/offices, industrial plants, smart museum and gym etc.
- Personal and social domain: Applications of this domain involve social networking, historical queries, losses and thefts etc.
- Futuristic domain: Applications of this domain involve robot taxi, city information model, enhanced game rooms etc.

2.2 IoT Applications

A number of IoT applications are presented below [12], [13], [14], [15], [16], [17], [18], [19], [20], [210]:

1) Healthcare and sanitary

The medical domain is one of the first industries which adopted IoT and was heavily influenced. IoT technologies can create new opportunities, services and applications to improve the healthcare and sanitary domain. Moreover, IoT platforms and services enhance current living solutions and facilitate the realization of

55

Ubiquitous healthcare vision that is "healthcare to anyone, anytime, and anywhere by removing location, time and other restraints while increasing both the coverage and quality of healthcare" [22]. Furthermore, in the context of IoT, all objects in the healthcare industry will be equipped with sensors and patients will carry mobile medical sensors. Moreover, it optimizes and enhance workflow, operations and drug management while simultaneously decrease operational costs. It also provides more effective methods for medical records and data analysis as well as ad- hoc diagnosis by taking advantage of rapidly automated decisions and continuous advanced remote patient state monitoring. Therefore, IoT has an enormous impact on independent living and provides smart solutions for ameliorating life quality and supporting the aging population.

2) Smart cities

The rapid urban growth is already placing a considerable strain on the existing infrastructure and utilities and highlighting the need for more sustainable urban planning and public services. IoT applications and services are being exploited in order for these new requirements to be satisfied and the societal changes commensurate with this rapid growth to be responded to. Moreover, autonomic city and home networks will be intelligent and capable of sensing, monitoring and adapting to environmental changes as well as reacting to human activities. More specifically, through IoT, smart technologies and devices are interconnected and as a result, they are able to improve and enhance the quality and lifestyle for city dwellers as well as ensure that their essential services are provided. Some of the few benefits of utilizing IoT applications and services in smart cities involve:

- Energy efficient utilities, buildings and facilities that will reduce the long-term costs and waste.
- Novel and effective systems of consuming, managing, distributing and renewing resources.
- Advanced traffic control and monitoring systems as well as more reliable public transportation means and pedestrian support.

Advanced monitoring and security surveillance systems so as to improve public safety and security.

3) Smart environments

By utilizing fully interconnected technological devices and embedded systems, IoT aims at pervading our everyday environment and its objects and creating new ways to interact with these smart environments. The concept of smart environments evolves from ubiquitous computing and promotes the idea of "a physical world that is richly and invisibly interwoven with sensors, actuators, displays, and computational elements, embedded seamlessly in the everyday objects of our lives, and connected through a continuous network" [23]. Through using IoT in combination with automated software agents for real time tracking and monitoring, smart environments become a technological ecosystem of various interconnected devices. These smart devices can securely communicate and interact as well as retrieve, process, store and exchange data in real time. By integrating these heterogeneous data into applications, the adaptation process to dwellers and environmental continuously changing needs are facilitated. As a result, their requirements are being promptly and satisfactorily met. Moreover, IoT applications in this domain aim at improving

56

the current environmental safety by reducing and mitigating the potential impact of damage and disaster. IoT technologies allow the development of innovative real-time monitoring and decision-making support systems and applications regarding environmental issues, such as early prediction and detection of natural disasters, weather conditions etc.

4) Transportation and Logistics

Nowadays, vehicles as well as roads and transported goods, are equipped with more sophisticated technological devices such as on near field communication (NFC) tags, radiofrequency identification (RFID) tags, actuators, sensors etc. IoT technologies can be used to enhance the potential of these systems and optimize their use in the domains of transportation, logistics and suppliers, which are regarded as essential components in the productivity of many industries. Intelligent transportation systems (ITS) are able to communicate, share and exchange mission-critical information and data promptly, timely and accurately. Hence, they are used to ensure that the transportation network is efficiently monitored and controlled. IoT offers several contemporary applications and services and in combination with the ubiquitous 5G mobile networks can provide industries with intelligent transportation and logistics systems. These systems provide solutions which are designed specifically for certain needs and goals, thus accelerating productivity, profitability and operations. Moreover, they offer real-time monitoring and tracking throughout the entire supply chain, thus helping enterprises increase end-to-end visibility as well as maintain efficient transportation control and cost-effective management. In addition, they conduct more effective route planning and optimization,

allow for better energy efficiency and reduce the overall system downtime.

3. SECURITY AND PRIVACY ISSUES IN IOT

IoT has four main layers which are perception layer, network layer, transport layer (Middle-ware Layer) and application layer. All IoT layers have their own privacy and security concerns as conferred in Fig. 1.

3.1 IoT Perception Layer Security and Privacy

Perception layer contains groups of information. It is classified in to two main sections which are perception node and perception network.

Perception node is responsible for collecting data and perception network handles the instructions of sending and managing data [24].

Perception layer is composed of many different sensor technologies like Radio Frequency Identification (RFID) [25]. RFID systems are exposed to privacy and security problems. The perception layer checks collect and process data then transmits the information to the next layer which is the network layer. Perception layer is responsible for controlling data sources where IoT nodes are the main source of data. The IoT nodes are widely vulnerable to attacks due to which a security and privacy node in the perception layer scheme (SNPL) is developed [26]. Some security and privacy issues of perception layer are discussed below:
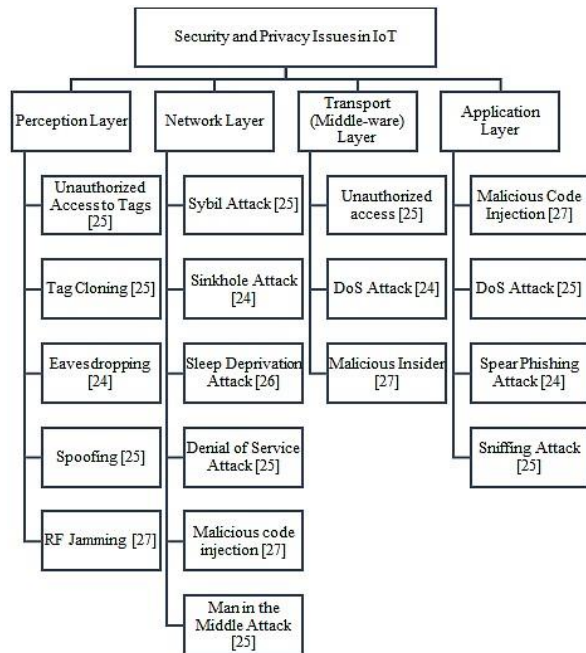
Figure 1. Security and Privacy Issues in IoT

1) Unauthorized Access to Tags:

Systems that have a large number of RFID face security issues because of the lack of proper authentication. Unauthorized users or hackers can access tags without authorization, delete and even can modify tags [25].

2) Tag Cloning:

Tags are distributed on different objects. Objects data can be viewed to be read and modified with the help of some hacking techniques. This leads to tag cloning which occurs when tags can be captured by criminals with ease who easily can make a replica of tags and compromise it. [25]

3) Eavesdropping:

Eavesdropping is an interception of information between two nodes or communication devices [24]. The wireless characteristic of the RFID makes it easier for hackers to sniff out the confidential information flow from tag-to-reader or from reader-to-tag [25].

4) Spoofing:

Spoofing occurs when an attacker transmits false and incorrect information to the RFID system and try to make its originality falsely and making it appear from the authenticated and original source.

With the help of this, attackers get full access to the system and make it vulnerable [25].

5) RF Jamming:

Radio Frequency (RF) Jamming tries to not comply with lower-level protocols to be able to interfere with the ongoing legitimate communication. This attack occurs when RFID tags are compromised by DoS attack that makes communication through RF signals distributed with noise signals. The source that initiates jamming attacks could be very powerful to damage the network or it could have less power to only damage small parts of the network [25].

All IoT layers are prone to security attacks and threats. There are three main security issues that are related to the perception layer. First issue, is wireless signals strength [27]. In Perception layer, signals are sent and received to and from the sensors with the help of wireless technologies whose efficiency can be compromised by disturbing waves. Second issue in IoT devices is that the sensor nodes can be stopped by the owner and the attackers due to the reason of the external and outdoor nature of IoT system could lead to physical attacks upon the IoT nodes and the IoT system. The third issue is the nature of network topology. IoT nodes usually move around many different places which means the network topology is dynamic. The

58

Perception layer consists of RFID and sensors. RFID and sensors storage, power consumptions, capacity and computation capability are limited and this led to making them prone to attacks. Perception layer security problems can be easily addressed with the help of pint-to-point or end-to-end encryption. Perception Layer can provide various security features and it supplies four purposes which are privacy of data and sensitive information, authentication and risk assessment. Authentication is one of the security goals that must be satisfied in systems in order to protect systems against hackers and attackers. Cryptography can be used to apply authentication to systems. Cryptography has some algorithms that can be used to provide a digital signature that could protect against attackers. Data need to be protected and secured while collecting and forwarding to the next layer. Symmetric and asymmetric encryption algorithms can also be used to apply privacy to data.

Encryption algorithms are easy to be implemented in sensors due to their benefit which is low power consumption. Location anonymity and identity anonymity are must to hide and secure sensitive information. This can be achieved by KAnonymity approach that protects information like identity, location and sensitive data of users. Risk assessment has an important role in IoT security because of its help in discovering new threats of systems. Also, it helps in defining security strategies that could be classified to be the best. Also, it prevents security breaches [25].

3.2 IoT Network Layer Security and Privacy

The next layer after the perception layer is the network layer. The network layer is the layer that is responsible for providing security of information and enabling the network transmission [24]. It includes mobile devices, internet and cloud computing. The network layer consists of Wireless Sensors Networks (WSN). This layer takes care of transmitting data from the sensors to their destinations with reliability [25]. The network layer is responsible for transmitting data to and from IoT devices and hubs and to serve data routing. In this layer, technologies like Wi-Fi, Bluetooth, 3G, LTE and Zigbee are used to operate the Internet, switching, routing and gateways [27]. Network layer is composed of protocols, communication technologies with corresponding hardware and network [28]. The network layer does an important job of connecting the IoT nodes and IoT applications together. The main threat that threatens the network layer is the DoS attack where the attackers make the service unavailable for the legitimate users. Network layer security and privacy issues are listed below [25]:

1) *Sybil Attack:*
In a Sybil attack, the attacker works on attacking the system by manipulating the node to have the single node more than one identity. This results in false information [25].

2) *Sinkhole Attack:*
Sinkhole attack works on trying to present compromised nodes attractive to other close nodes. So, all data will flow from nodes to compromised nodes which result in packets drop.
The system believes that the data have been transmitted to the other side while system traffic is silenced. Sinkhole attack can cause DoS attack due to more energy consumption. Sinkhole attack process seems to be unknown to the network where attackers deceive the system to make it

59

believe that all transmitted data is received to the receiver [25].

3) *Sleep Deprivation Attack:*

Sleep Deprivation Attack works on the point of keeping sensor nodes awake for a portion of time which leads to batteries consumption which in turns minimize batteries life time which results in causing the sensor nodes to shut down. This attack can keep the sensor node awake for some time. Energy constrained devices are prone to this attack.

4) *Denial of Service (DoS) Attack:*

DoS attack occurs when an attacker works on enforcing the network to flood with a lot of useless traffic which results in resources exhausting of the system. So, the network of the system becomes unavailable to the users [25].

5) *Malicious code injection:*

Malicious code injection attack occurs when an attacker tries to make a sensor node to insert some code that is malicious into the system which in turns cause the network to shut down. Then, the attacker gets full control over the network [25].

6) *Man-in-the-Middle Attack:*

Man-in-the-middle attack is like a form of eavesdropping attack. In Man-in-the-middle attack the target is the communication channel where unauthorized user can monitor and control the communication between other two parties. Also, the unauthorized user can impersonate the identity of the victim and then communicates through the channel to gain information [25].

IoT introduces machine-to-machine communication which has compatibility security issue. In machine-to-machine communication network components are heterogeneous which makes it impossible to use network protocols as it is. Protecting the network's objects has equal importance of protecting the network itself. The objects should be able to have some actions to be taken to from a guard to protect themselves from attacks initiated against the network by having the ability to know the network state. In order to achieve this, there must be good protocols and software in the network that help the objects to respond the situations and behaviours that are abnormal or affect the objects and the network security. Security of Network layer is divided to three types which are authentication, routing security and data privacy. Implementing authentication and encryption could stop illegal accesses to nodes and this, in turn, prevents spreading fake information. Routing algorithms must be used to ensure data privacy of data transmitted between the sensors and the system. To improve the ability of the system to figure out errors and protect the system against any kind of failure, the system has to provide multiple paths for data routine. To monitor the system and protect it against any kind of intrusion, safety control mechanisms must be implemented. To check whether data received on an end is the same as the original data sent from the other end, data integrity methods must be implemented [25].

3.3 IoT Transport (Middle-ware) Layer Security and Privacy

The next layer after the network layer in IoT systems is the Transport (Middle-ware) Layer. Transport (Middle-ware) Layer consists of data storage technologies like cloud computing. It is split into three layers which are local area, core network and access network. The security problems of the transport layer are classified as follows [25]:

1) Unauthorized Access

Unauthorized system access can occur when an attacker deletes data or forbid IoT services access to cause damage to the IoT system. Attackers can have unethical access to intrude into the network with misconfiguration access control rights [25].

2) DoS Attack

DoS attack generates a lot of useless traffic to shut down the system. Attackers can shut down the service of the network to make the system unavailable for a portion of time. A big number of DoS attacks can be started to attack the IoT system.

3) Malicious Insider

Malicious Insider attack occurs when an insider tampers data for personal benefits or third parties' benefits. One of the possible ways to protect IoT systems against malicious insider attack is Isabelle insider framework that detect any violation occurs in the policy.

3.4 IoT Application Layer Security

The last layer in IoT after Transport (Middleware) Layer is the application layer. Services offered by the application layer in several ways have the role of structuring the application layer. It is visible to the end user and it is the uppermost layer [24]. This layer ensures authenticity, integrity and confidentiality. The lack of standards that work on managing the applications development process and their interactions can cause many issues in the security of the application layer. It is difficult to confirm data privacy and authentication for applications that work with different authentication mechanisms. Application layer is composed of different service domains like connected cars and healthcare. Each application should consider its own security threats and prepare countermeasures for security threats [28]. Application Layer provides access to the users for IoT applications. Security can be applied into the application layer by adding security into the functional architecture in a form of policies of access control. Application layer's security issues can be eliminated and solved by using firewalls, anti-virus and intrusion detection systems. The security problems of application layer can be classified as follows:

1) Malicious Code Injection

Malicious code injection occurs when an attacker inserts a code that is malicious into the system and steal user's data. Hackers influence the attack on the system from end users [25]. Malicious code injection cannot be prevented using anti-virus tools. Also, it can automatically activate itself or need the attacker to take action to start attacking the system.

2) DoS Attack

DoS attacks offer a smokescreen that carry out attacks to violate the defence of the system. It tricks the users about where the attack is happening. It makes the user believe that the attack is occurring in another part of the system. DoS put user un-encrypted sensitive information into the hands of hackers. DoS attackers has the ability to destroy the availability of the service or the application.

3) Spear-Phishing Attack

Spear-Phishing attack initiates when an attacker try to start an attack on users by an email to victims and try to lure victims to open the email to get more sensitive data from victims. SpearPhishing is a multistage process where an attacker collects

information on a target or a group of targets [25].

4) *Sniffing Attack*

Sniffing attack occurs when an attacker introduces sniffing into the system in a form of a sniffing application that in turn gain information of the network which results in corrupting the system. Sniffing can be categorized into DNS poisoning, ARP poisoning, DHCP attack, MAC flooding and password sniffing [25].

There are several IoT applications security issues. IoT applications have different mechanisms for authentication which in turns makes data privacy, identity authentication and integration of all of IoT applications very difficult. When designing IoT application, these following three points must be taken in consideration how users interact with the application, the amount of data and who will manage the system. IoT applications users must have tools that enable them to control, manage and decide upon which data they want to disclose. Users must be knowing how their data is being used, when and by whom. Transport (Middleware) layer and application layer security is partitioned into four categories which are risk assessment, authentication data security and intrusion detection. Authentication prevents malicious users from accessing the system by integrated identity identification. Middle-ware layer uses some major technologies like cloud technologies which are easily compromised and also vulnerable to the insider threat. Virtualization is another technology that is used in this layer which is exposed to data threat and DoS attack. Intrusion detection technologies start an alarm on the presence of any abnormal event in the system. This can be done by the continuous keeping of a log and monitoring of intruder's activities.

There are various types of intrusion detection technologies, two of them are data mining approach and anomaly detection. Risk Assessment is required in giving justifications for the security strategies and improving security structure. Encryption technologies can be used in order to prevent data from being stolen or abused. Encryption can be a way to ensure the security of data. Encryption also can be a way to prevent malicious activities from attackers and malicious users [25].

4. INDUSTRY 4.0

With growing advancements in manufacturing processes, the concept of Industry 4.0 has emerged, becoming an increasingly relevant global topic in the last few years. This term was first presented in 2011, in an article published by German government regarding an initiative about high-tech strategy for 2020 [29].

Industry 4.0 is the fourth industrial revolution and can be compared with the last three industrial revolutions that have emerged over the last centuries, that have brought relevant changes in manufacturing due to disruptive technological advances [30]. The first industrial revolution, in the middle of the 18th century, was enabled by the use of steam and waterpower, while the second industrial revolution that emerged during the second half of 19th century was characterized by mass production and the replacement of steam power by electricity. In the last years of 20th century, the use of computers, electronics and Information Technology have triggered the third industrial revolution [31], [32]. However, the emerging fourth industrial revolution is being shaped by the integration of Cyber-Physical Systems (CPS) and Internet of Things (IoT) in industrial processes [29]. This new industrial paradigm will bring together the digital and physical worlds

62

through the use of technologies, allowing the improvement of productivity and efficiency among the companies that are adopting this new manufacturing paradigm. This concept is an umbrella term that embraces a set of future technological developments regarding CPS, IoT, Big Data, Cloud Manufacturing, Augmented Reality (AR) and Robotics [30]. The adoption of these technologies is crucial to the development of intelligent manufacturing processes, including smart devices, machines and product that are able to autonomously exchange information, trigger actions and control each other.

Industry 4.0 is a complex technological system that has been widely discussed and researched by academics and companies in recent years, holding a huge potential to greatly influence the industrial sector and bringing several economic and social opportunities through the paradigm shift regarding to work organization, business models and production technology [33]. Furthermore, this emerging industrial revolution, besides the transformation in manufacturing, will have a great impact in many other areas, such as, products and services, new business models and markets, economy, work environment and skills development [30]. Industry 4.0 can be regarded as a highly integrated, digitalized, automated and autonomous, and efficient manufacturing environment. Industry 4.0 may also be defined as the "digitization of the manufacturing sector, with embedded sensors in virtually all product components and equipment, ubiquitous cyberphysical systems, and analysis of all relevant data" [35]. In addition, Industry 4.0 is driven by the following four technological clusters; data, computational power and connectivity, analytics and intelligence, human-machine

interaction and digital-to-physical conversion.

Industry 4.0 focuses on the end-to-end digitalization of all physical assets and their integration into digital ecosystems, while enabling them to seamlessly generate, analyse and communicate data including the digitalization and integration of vertical and horizontal value chains, the digitalization of product and service offerings and the digital business models and customer access [36]. The following eight planning objectives are the prerequisites for achieving Industry 4.0 are; standardization of systems, efficient management, establishment of a comprehensive and reliable industrial broadband infrastructure, safety and security, organization and design of work, staff training and continuing professional development, establishing a regulatory framework and improving the efficiency of resource use [37].

A crucial new aspect of the manufacturing and production process is the dynamic interaction between the real and virtual worlds in which the industrial production machinery is no longer simply processes the products, but it also communicates with them. As a result, industry production value chains and business models are radically transformed into intelligent ones, thus leading to the development of smart factories. Moreover, this new manufacturing paradigm lays high emphasis on creating smart products and developing smart processes by utilizing smart machines and transforming conventional manufacturing systems in smart factories. Smart factories allow the development of intelligent manufacturing environments throughout the entire value chain and they are the outcome of integration through digitalization, usage of flexible and adaptive structures and

63

strategies as well as of artificial intelligence methods [38].

4.1 Industry 4.0 Technologies

Industry 4.0 aims at enhancing and upgrading the current manufacturing facilities, management, maintenance systems and technologies to an intelligent level by utilizing the key technologies such as IoT, Internet of Services (IoS), CPS, autonomous, flexible and cooperative robotics, simulations that leverage real-time data and mirror real world into a virtual model, big data analytics, augmented reality (AR), additive manufacturing, information and communication technologies (ICT) and advanced networking technologies e.g. cloud computing etc. [39], [40]. Moreover, it seeks to address the dynamic global market and the competitive nature of today's industries in line with the continuously changing customers and market needs. Horizontal and vertical system integration will also allow the capabilities, functions, departments and enterprises to be evolved in an interconnected network that enables an automated value chain. Intelligent manufacturing will pave the way for the advancement of modern industry and economy as it will apply cutting-edge technologies to various traditional products and systems [40]. In an Industry 4.0 context, data collection, analysis and comprehension from many diverse sources, including production systems and equipment, as well as customer management enterprise systems will become the norm to support decision making in real time. Some of the key technologies involved in Industry 4.0 are briefly described and analysed below:

1) *Industrial internet of things*

Industrial Internet of Things (IIoT) is a specific category of IoT which focuses on its applications in modern industries and intelligent manufacturing. IIoT, which is used in the context of Industry 4.0, can be considered to be a complex system of diverse systems and devices. More specifically, with a view of producing a system which functions more efficiently than the sum of its parts, IIoT combines several contemporary key technologies [41]. Through the use of appropriate services, networking technologies, applications, sensors, software's, middleware and storage systems, IIoT provides solutions and functions to develop insight and improve the potential and capability of monitoring and controlling enterprises processes and assets. IIoT services and applications provide vital solutions for more effective scheduling, planning and controlling of manufacturing operations and systems.

Additionally, through the various interconnected devices that are able to communicate and interact both with each other and with more centralized controllers, IIoT will decentralize analytics and decision-making, thus rendering real-time responses and reactions feasible. As a result, the overall availability and maintainability of enterprises is enhanced, their operational efficiency is improved, productivity is accelerated, their product time-to-market is decreased by reducing unplanned downtime and their overall operational efficiency is optimized. Thus, it increases the enormous potential for unprecedented levels of economic growth and productivity efficiency [42].

2) *Cyber-physical systems*

Cyber-physical technologies and frameworks, also known as cyber-physical systems (CPSs), have been increasingly adopted in industry due to the significant technological advancements in the domains of computer science, ICT and manufacturing [43]. Unlike traditional embedded systems,

64

CPS-enabled systems contain "cyber twined services such as control algorithms and computational capacities" [40] along with specialized computational capabilities, physical assets and networked interactions and involve a large number of trans disciplinary methodologies. The CPSs concept facilitate an ecosystem of cyber manufacturing, where smart machines process production data through a wireless embedded network system. Moreover, CPSs are defined as transformative technologies that can seamlessly link the physical with the virtual world through their advanced and novel systems [44]. Hence, they are designed and developed to have both physical inputs and outputs so as to enable and enhance the interaction with humans using innovative modalities [45].

3) *Cloud computing*
Cloud computing or simply "Cloud" plays a leading role in enhancing and transforming the current industry as it is a kind of outsourcing that combines large numbers of computer servers and resources with a view to offering computer programs, high-level services and resources on an on-demand or pay per-cycle basis in real time.

Cloud computing is "a set of networks enabled services, providing scalable, guaranteed, normally personalized, inexpensive computing infrastructure on demand, which could be accessed in a simple and pervasive way" [46]. Cloud computing is divided into three levels of service offerings, namely Software as a Service (SaaS), Platform as a Service (PaaS) and Infrastructure as a Service (IaaS) which support different levels of virtualization and management of the solution stack [47]. The use of advanced applications and services that dynamically scale with the increased number of users is considered to be one of the main benefits of cloud computing. Moreover, users and enterprises have prompt access to applications, programs and services which are rapidly provisioned with minimal management effort and are hosted in the "Cloud" at any time and from any place. Hence, enterprises in the industrial domain use various cloud-based applications widely in order to enhance the crucial for their effective function systems such as Customer Relationship Management (CRM), Human Resource Management (HRM) etc. Furthermore, enterprises that utilize cloud computing can avoid the complexity of owning and maintaining their own Information

Technology (IT) infrastructure and the up-front costs which can be accomplished by a "pay-asyou-go" method allowing the enterprises to start small and invest into more resources if there is more service demand [48]. Some further benefits and significant advantages include high availability and maintainability, consistent accessibility to data and services from any connected device as well as reduced development cost and product time-to-market. Taking into consideration the continuously evolving nature, the numerous application domains and multiple benefits of cloud computing, a lot of profits can be yielded in the industrial domain, thus, more and more enterprises of different sizes and types are rapidly adopting this advanced technology with the aim of enhancing their capabilities and capacity at a minimum cost [49].

4) *Big data*
The digitalization of everyday life through the adoption of smart devices and advanced technologies (e.g. IoT, Artificial Intelligence (AI), Social Networks (SNS)

65

etc.) has led to the increase of data sources and the diversity of digital content as well as data types, forms and structures [50]. Consequently, an enormous volume of heterogeneous data, named big data, is generated and increases exponentially on a daily basis. Volume, variety, veracity, velocity and value are the key factors which characterize and differentiate big data from traditional data. Big data plays a key role in industries and intelligent manufacturing as it can provide enterprises with numerous advantages, merits and benefits through various predictive and prescriptive insights. Hence, enterprises, which want to remain competitive, should give priority to the implementation and utilization of contemporary advanced analytical tools, techniques, methods and applications with the aim of processing big data, gleaning intelligence and retrieving the value of the vital data in each case. These tools are named big data analytics (BDA) and use parallel and analytic techniques to analyse huge volume of diverse, rapidly transforming data enabling, thus, the collection, the process and the management of vital information and statistics [51]. By far, the most effective way for enterprises to gain immense benefits over their competitors, optimize operations, enhance productivity, quality and efficiency and reduce operational costs is to use all the newly gained knowledge in order to generate invaluable insights and improve equipment service and maintainability.

Nonetheless, in order to fully utilize big data and exploit all of its benefits, enterprises must change their decision-making culture and take into consideration that no matter how much the potential of big data and analytic tools increase, the need for human insight should not be overlooked [52].

5. EMERGING APPLICATION OF IOT IN INDUSTRY 4.0

Manufacturing comprises of a core industrial component which has a vital impact on people's livelihood and a nation's economy. Additionally, it is one of the largest and highly interconnected IoT markets and it involves a wide variety of operations, processes, services, products etc. With the aim of enhancing the overall production, productivity and product quality management (PQM) throughout the various stages of the lifecycle of products, IoT offers applications and services under the umbrella of Industry 4.0 which includes advanced monitoring and tracking, performance and maintainability optimization and human machine interaction. Hence, it stands for a reason that IoT can provide a lot of solutions for Industry 4.0 in the manufacturing domain which is characterized by its complexity and breadth of applications with its diverse CPSs and its manufacturing operation management (MOM) methodologies [49]. Internet of things (IoT) is a pervasive technology and now it has numerous applications in every technology sector. The fourth industrial revolution has also been evolved through the connected technologies enabled by the IoT. In fact, IoT provide a connected framework for large scale manufacturing and production which is very efficient, fast, cost effective, and free from the traditional manufacturing faults. In Industry 4.0, IoT apprehends the basic concept of intelligent manufacturing 4.0, also known as smart manufacturing that transform the overall dilemma of every sector, it uses Service-Oriented Architecture (SOA) and is considered to be a novel manufacturing model that takes advantage of and fully utilizes various advanced information and manufacturing techniques, methodologies and technologies using IoT [49]. It aims at fundamentally transforming

66

traditional enterprises into intelligent ones so as to effectively respond to demand-dynamic economies keyed on "customers, partners and the public; enterprise performance and variability management; realtime integrated computational materials engineering and rapid qualification, demanddriven supply chain services; and broad-based workforce involvement" [53]. IoT enabled intelligent manufacturing 4.0 uses the combined intelligence of people, processes and machines so as to increase production, product quality and productivity efficiency. It offers smart solutions for the detection and monitoring of potential damage, malfunctions and breakdowns.

Moreover, it enhances control and management, improves maintainability and availability and optimizes resource management and sharing. Additionally, it applies cutting-edge technologies to various traditional systems, services and products. As a result, it is obvious that IoT enables intelligent manufacturing 4.0 has a drastic impact on the overall function and economics state of enterprises and will pave the way for the advancement of modern industries. It aims at developing real-time, autonomous and human like intelligent decision-making systems that reduce the need for human involvement and intervention. In order for this to be accomplished, artificial intelligence, machine learning, genetic algorithms and other advanced technologies, methodologies and techniques are also used. This fact comprises a major distinguishing factor between IoT enabled intelligent manufacturing 4.0 and traditional manufacturing. Nonetheless, the goal of both manufacturing domains remains the same, that is, to satisfy customers requirements and market needs as well as maximize profits while simultaneously minimizing possible cost and waste.

6. RESEARCH GAPS

It is obvious that in the context of Industry 4.0, IoT can enhance and transform the current industries and yield a lot of benefits due to its advanced technologies, applications and services. It is also vital to point out that IoT not only aims at transforming industries and increasing their productivity but also adding value to the core purpose of enterprises and mitigating the weaknesses caused by legacy systems. Hence, it should be compatible with existing devices, systems and infrastructure and be able to embed intelligence into them. As a result, enterprises that are undergoing digital transformation will be facilitated to adopt and implement IoT and exploit its numerous benefits and solutions without having to directly invest in totally brand-new equipment as cost might far outweigh the immediate benefits. Nonetheless, in order for Industry 4.0 to be fully implemented and for IoT to be adopted and fully utilized by industries and enterprises, a lot of challenges and research gaps are addressed as shown in Table 1.

S.No.	Summary of Gap Analysis			
	Gap	*Category*	*Domain*	*Reference*
8	·Development of smart devices, ·Construction of network environments, ·Lack of digital strategy in line with resource scarcity as well as the lack of standards and poor data security	Smart digital manufactu-ring	Producti on Enginee ring	[35], [36], [37], [38].

67

Many elaborate studies, which analyse vital IoT challenges, integration and implementation problems and research gaps involving standardization activities, addressing and networking as well as security and privacy were analysed [12].

Key IoT challenges involves interoperability and standardization, data and information confidentiality, encryption and privacy, naming and identity management, IoT greening as well as object and network security [15], communication and identification technologies, distributed system technologies, intelligence and emphasized security issues such as data confidentiality and privacy and trust [16]. In addition to these, secure reprogrammable networks and privacy, energy efficient sensing, architecture and protocols, Geographic Information System (GIS) based visualization, data mining and cloud computing [17], object mobility, M2M communications, data management, network architecture and system design, addressing, naming and traffic characterization and security [18], privacy and data analytics, interoperability on products and services as well as resources and energy management are the most common open issues to be investigated [20]. The management of fault tolerance, functional safety, latency and scalability of data, mixed criticality and scalable as well as secure real-time collaboration, data management and mining, security and privacy are also regarded as the main challenges which enterprises face in IoT development [22]. To sum up, based on the above-mentioned studies, the most significant and common IoT challenges and open research gaps which industries and enterprises should be aware of are:

- Availability, reliability, mobility and other QoS criteria
- Security, privacy and confidentiality of data
- Interoperability and scalability
- Fault tolerance and functionality safety
- Management of operations, resources, energy and data
- Networking addressing and identification
- Architecture, protocols and standardization activities

In addition to these, there are also many intricate studies, regarding vital challenges, integration and implementation problems and open research issues of Industry 4.0. Several challenges and fundamental issues in various sections that occur throughout the implementation of Industry 4.0 are intelligent decision making and negotiation mechanism, high speed industrial wireless network (IWN) protocols, manufacturing specific big data and its analytics, system modelling and analysis, cyber and property security, modularized and flexible physical artefacts and investment issues [46]. Moreover, some of science and technology challenges concerning the implementation of Industry 4.0 involves the development of smart devices, the construction of network environments, big data analysis, processing and digital production, lack of digital strategy in line with resource scarcity as well as the lack of standards and poor data security are regarded as the main obstacles for the technological implementation of Industry 4.0 due of which some manufacturers and enterprises hesitate to implement Industry 4.0 due to these concerns [37]. These barriers instigate uncertainties about financial benefits, lack of strategies of coordinating across different organizational units, missing talent, skills and capabilities, hesitation to go through

68

radical transformation and concerns regarding the thirdparty providers security. Some of the main concluded challenges in the implementation of Industry 4.0 are found to be [31]:

- Lack of courage to push through the radical change needed for introducing Industry 4.0
- Lack of necessary talents for making Industry 4.0 happen
- Lack of a clear business case justifying investments in Industry 4.0 IT architecture
- Difficulty in coordinating actions across different organizational units, such as research & development (R&D), IT, manufacturing, sales, and finance departments, due to poor interaction between them
- Uncertainty about insourcing versus outsourcing and lack of knowledge about service providers
- Concerns about cyber security when involving third-party technology/software and implementation providers
- Concerns about data ownership when working with third-party providers
- Challenges with integrating data from disparate sources to enable Industry 4.0 applications.

7. DISCUSSION

Technological advances and digitalization of everyday life have led to the increase of rapidly changing customers' needs and requirements. Simultaneously, the fierce competition which prevails in global markets has drastically risen. As a consequence, the need for flexibility and real time response to these changes is becoming vital. Therefore, with a view to fulfilling and satisfying these new demands, staying ahead of their competitors, enhancing their product and service quality and raising their profits, enterprises opt to implement new technological means, practices and methodologies and seek for new innovative approaches to increase their productivity.

The four broad types of innovation that enterprises mostly target at are; product innovation, process innovation, position innovation and paradigm innovation. Generally, innovations result in more changes such as manufacturing paradigm shifts, progress in technologies, create new opportunities and bring about new challenges. In order for enterprises to sustain in the context of globalization, there is a need to create new values and drive innovation to achieve more competitive success in their business, also the digital transformation and the virtualization process needs to be adapted. Moreover, innovations in the manufacturing process should be incorporated and integrate technological and managerial approaches so as to strengthen overall competence. Industry 4.0 is a response to the newly created challenges in a fastchanging and evolving environment. It is regarded as a highly integrated, digitalized, automated, autonomous and efficient intelligent manufacturing environment and it constitutes a new level of organization and control throughout the entire value chains. More specifically, it puts emphasis on the development of smart factories and intelligent manufacturing and aims to deal with customers and market changing needs and transform conventional industries into intelligent ones. Industry 4.0 combines the powers of traditional industries with cutting edge technologies e.g. IIoT, CPSs, cloud computing, big data and advanced data analytics etc. enabling physical assets to be integrated into intertwined digital and physical processes. The main contribution to the realization of Industry 4.0 was made by

69

IoT. It allows people and "things" to be connected anytime, anywhere, with anything and anyone ideally using any network and service. Additionally, IoT pursues to pervade our everyday environment and its objects, linking the physical to the digital world. IoT which is regarded as a dynamic and global network of uniquely addressable interconnected "things" aims at implementing autonomous, robust and secure connections. Moreover, IoT provides various applications, functions and services in everyday life and in a wide range of markets and industries. By implementing and adapting to Industry 4.0 and IoT technologies, unprecedented levels of economic growth and productivity efficiency can be achieved by enterprises, such as:

- Development of production systems which are characterized by interoperability, flexibility, adaptability, agility and proactivity
- Optimization and improvement of efficiency, speed and quality particularly in engineering, operation, administration and decision-making
- Enhancement of overall application, services and system availability and maintainability
- Acceleration of productivity and reduction of lead time resulting in decreasing timeto-market
- Facilitation of the adaptation to individualized customer requirements and market demands

IoT in Industry 4.0 can provide a multitude of contemporary solutions, applications and services and can yield significant personal, professional and economic opportunities. Hence, enterprises and industries that are able to fully implement and adapt to Industry 4.0 and IoT will reap many benefits and profits and will be able to stay ahead of market competition. Nonetheless, IoT in Industy 4.0 are still at an early stage of development, adoption and implementation, therefore there are still various open issues and challenges that need to be addressed.

8. CONCLUSION

IoT is an innovative and rapidly growing technology which offers various novel applications, services and solutions and links the physical to the digital world. It also allows people and "things" to be connected anytime, anywhere, with anything and with anyone ideally using any path/network and any service. Moreover, it improves the quality for the end-user community and our lives in general and supports infrastructure and general-purpose operations. In addition, it aims at transforming the current industries into intelligent ones utilizing the dynamic network of interconnected devices. Enhancing their operation and functionality, increasing their productivity and reducing their costs and waste are some of the many benefits and profits that enterprises can gain by using IoT. Moreover, enterprises that fully adopt IoT in Industry 4.0 will be ahead of their competitors, become more agile, adapt to the continuously changing market, create products of higher quality that satisfy customers' needs and requirements. Moreover, in the context of Industry 4.0, IoT can be utilized in combination with other innovative technologies such as big data, cloud computing, CPSs etc. in order to enhance and transform the current manufacturing systems into intelligent ones. Industry 4.0 allows for machines to become independent entities that are able to collect and analyse data and give advice upon it without requiring any human intervention as it introduces self-maintainability, self-

70

optimization, selfcognition, and self-customization as well as intelligence to the industry. It seeks to cope successfully with the global competitive nature of today's markets and industries in line with the ever-changing customers' needs and requirements. Although IoT offers a magnitude of solutions to industries as well as multitude of contemporary and advanced applications and services, it is still at an early stage of development, adoption and implementation. Thus, in order for the various current challenges and open issues to be encountered and solved, further research should be carried out. The complete implementation and prompt adoption of IoT in Industry 4.0 along with appropriate utilization of its novel technologies, applications and services cannot only improve life quality, but can also yield significant personal, professional and economic opportunities and benefits in the near future.

REFERENCES

[1] Vermesan, O., Friess, P., Guillemin, P., Gusmeroli, S., Sundmaeker, H., Bassi, A & Doody, P. (2011). Internet of things strategic research roadmap. Internet of things-global technological and societal trends, 1(2011), 952.

[2] Perera, C., Zaslavsky, A., Christen, P., & Georgakopoulos, D. (2013). Context aware computing for the internet of things: A survey. IEEE communications surveys & tutorials, 16(1), 414-454.

[3] Li, J., Huang, Z., & Wang, X. (2011). Notice of Retraction Countermeasure research about developing Internet of Things economy: A case of Hangzhou city. In 2011 International Conference on E-Business and E-Government (ICEE) (pp. 1-5). IEEE.

[4] S Mandal (2015) , "Internet of Things (part 1)," Introduction ,[Online], source:http://www.csharpcorner.com/up loadfil e/f88748/internet-of-things-iotanintroduction/.

[5] Da Xu, Li & He, Wu & Li, Shancang. (2014), "Internet of Things in Industries: A Survey," IEEE Transactions on Industrial Informatics, Vol 10, pp 2233-2243.

[6] X. Jia, O. Feng, T. Fan, and Q. Lei (2012), "RFID technology and its applications in Internet of Things (IoT)," Proceedings of the 2nd IEEE International Conference on Consumer Electronics, Communications and Networks (CECNet), April 21-23, pp.12821285.

[7] Kiran Jot Singh (2017) , "A Survey of IoT platforms. Create your own Internet of Things," IEEE consumer electronics magazine.

[8] D. Bandyopadhyay, and J. Sen (2011), "Internet of things: applications and challenges in technology and standardization," Wireless Personal Communications, vol.58, no.1, pp.49-69.

[9] ITU NGN-GSI Rapporteur Group (2010), "Requirements for support of USN applications and services in NGN –environment," Geneva: International Telecommunication Union (ITU).

[10] D. Miorandi, S. Sicari, F. De Pellegrini, and I. Chlamtac (2012), "Internet of things: vision, applications and research challenges," Ad Hoc Networks, vol.10, no.7, pp.1497-1516.

[11] Akpakwu, G. A., Silva, B. J., Hancke, G. P., & Abu-Mahfouz, A. M. (2017). A survey on 5G networks for the Internet of Things: Communication

technologies and challenges. IEEE Access, 6, 3619- 3647

[12] Atzori, L., Iera, A., & Morabito, G. (2010). The internet of things: A survey. Computer networks, 54(15), 2787-2805.

[13] Sundmaeker, H., Guillemin, P., Friess, P., & Woelfflé, S. (2010). Vision and challenges for realising the Internet of Things. Cluster of European Research Projects on the Internet of Things, European Commision, 3(3), 34-36.

[14] Vermesan, O., Friess, P., Guillemin, P., Gusmeroli, S., Sundmaeker, H., Bassi, A. & Doody, P. (2011). Internet of things strategic research roadmap. Internet of things-global technological and societal trends, 1(2011), 952.

[15] Khan, R., Khan, S. U., Zaheer, R., & Khan, S. (2012), Future internet: the internet of things architecture, possible applications and key challenges. In 2012 10th international conference on frontiers of information technology (pp. 257-260). IEEE.

[16] Miorandi, D., Sicari, S., De Pellegrini, F., & Chlamtac, I. (2012). Internet of things: Vision, applications and research challenges. Ad hoc networks, 10(7), 1497-1516.

[17] Gubbi, J., Buyya, R., Marusic, S., & Palaniswami, M. (2013). Internet of Things (IoT): A vision, architectural elements, and future directions. Future generation computer systems, 29(7), 1645-1660.

[18] Borgia, E. (2014). The Internet of Things vision: Key features, applications and open issues. Computer Communications, 54, 1-31.

[19] Zanella, A., Bui, N., Castellani, A., Vangelista, L., & Zorzi, M. (2014). Internet of things for smart cities. IEEE Internet of Things journal, 1(1), 22-32.

[20] Perera, C., Liu, C. H., & Jayawardena, S. (2015). The emerging internet of things marketplace from an industrial perspective: A survey. IEEE Transactions on Emerging Topics in Computing, 3(4), 585-598.

[21] Gilchrist, A. (2016). Industry 4.0: the industrial internet of things. New York, NY: Apress., ISBN: 1484220463.

[22] Lee, C. P., & Shim, J. P. (2009). Ubiquitous healthcare: Radio frequency identification (RFID) in hospitals. In Handbook of research on distributed medical informatics and ehealth (pp. 273-281). IGI Global.

[23] Weiser, M., Gold, R., & Brown, J. S. (1999). The origins of ubiquitous computing research at PARC in the late 1980s. IBM systems journal, 38(4), 693-696.

[24] F. A. Alabaa, M. Othmana, I. A. T. Hashema, and F. Alotaibi (2017), "Internet of Things security: A survey," Journal of Network and Computer Applications, vol. 88, pp. 10–28.

[25] M.U. Farooq, M. Waseem, A. Khairi, and S. Mazhar (2015), "A Critical Analysis on the Security Concerns of Internet of Things (IoT)," International Journal of Computer Applications (0975 8887), vol. 111, no. 7, pp. 1-6.

[26] Y. Fan, G. Zhao, K. Li, B. Zhang, G. Tan, X. Sun, and F. Xia (2020), "SNPL: One Scheme of Securing Nodes in IoT Perception Layer," Sensors, ol. 20, no. 4.

[27] R. Mahmoud, T. Yousuf, F. Aloul, and I. Zualkernan (2015), "Internet of Things (IoT) Security: Current Status, Challenges and Prospective Measures," 10th International Conference for Internet

72

Technology and Secured Transactions (ICITST), pp. 336-341.

[28] H. Shin, H. K. Lee, H. Cha, S. W. Heo, and
H. Kim (2019), "IoT Security Issues and Light Weight Block Cipher", International Conference on Artificial Intelligence in Information and Communication (ICAIIC), pp. 381-384.

[29] K. Zhou, T. Liu, L. Zhou (2016), Industry 4.0: Towards Future Industrial Opportunities and Challenges, International Conference on Fuzzy Systems and Knowledge Discovery: 2147–2152.

[30] Schmidt R, et al (2015), Industry 4.0 - Potentials for Creating Smart Products: Empirical Research Results, International Conference on Business Information Systems, pp. 16–27.

[31] Acemoglu D (2002), Technical Change, Inequality, and the Labor Market, J. Econ. Lit., 40(1): 7–72.

[32] Von Tunzelmann N (2003), Historical Coevolution of Governance and Technology in the Industrial Revolutions, Struct. Chang. Econ. Dyn., 14(4): 365–384.

[33] Kagermann H, Wahlster W, Helbig J (2013) Recommendations for Implementing the Strategic Initiative, INDUSTRIE 4.0, München.

[34] Pereira A, Romero F (2017), A review of the meanings and the implications of the Industry 4.0 concept, Procedia Manuf. 13(S): 1206– 1214.

[35] Wee, D., Kelly, R., Cattel, J., & Breunig, M. (2015). Industry 4.0-how to navigate digitization of the manufacturing sector. McKinsey & Company, 58.

[36] Geissbauer, R., Vedso, J., & Schrauf, S. (2016). Industry 4.0: Building the digital enterprise. Retrieved from: https://www.pwc.com/gx/en/industries/industr ies-4.0/landing-page/industry-4.0-buildingyour-digitalenterprise-april-2016.pdf.

[37] Zhou, K., Liu, T., & Zhou, L. (2015). Industry 4.0: Towards future industrial opportunities and challenges. In 2015 12th International Conference on Fuzzy Systems and Knowledge Discovery (FSKD) (pp. 2147-2152). IEEE

[38] Hajrizi, E. (2016). Smart solution for smart factory. IFAC-PapersOnLine, 49(29), 1-5.

[39] Lasi, H., Fettke, P., Kemper, H. G., Feld, T., & Hoffmann, M. (2014). Industry 4.0. Business & information systems engineering, 6(4), 239-242.

[40] Zhong, R. Y., Xu, X., Klotz, E., & Newman, S. T. (2017). Intelligent manufacturing in the context of industry 4.0: a review. Engineering, 3(5), 616-630.

[41] Lampropoulos, G., Siakas, K., & Anastasiadis, T. (2018). Internet of Things (IoT) in Industry: Contemporary Application Domains, Innovative Technologies and
Intelligent Manufacturing. International Journal of Advances in Scientific Research and Engineering, 4(10), 109-118.

[42] Bi, Z., Da Xu, L., & Wang, C. (2014). Internet of things for enterprise systems of modern manufacturing. IEEE Transactions on industrial informatics, 10(2), 1537-1546.

[43] Monostori, L. (2014). Cyber-physical production systems: Roots,

expectations and R&D challenges. Procedia Cirp, 17, 9-13.

[44] Mourtzis, D., Vlachou, E., & Milas, N. (2016). Industrial Big Data as a result of IoT adoption in manufacturing. Procedia Cirp, 55, 290-295.

[45] Baheti, R., & Gill, H. (2011). Cyber-physical systems. The Impact of Control Technology, T. Samad and AM Annaswamy. IEEE Control Systems Society, 1.

[46] Wang, L., Von Laszewski, G., Younge, A., He, X., Kunze, M., Tao, J., & Fu, C. (2010). Cloud computing: a perspective study. New Generation Computing, 28(2), 137-146.

[47] Bhardwaj, S., Jain, L., & Jain, S. (2010). Cloud computing: A study of infrastructure as a service (IAAS). International Journal of engineering and information Technology, 2(1), 60-63.

[48] Zhang, Q., Cheng, L., & Boutaba, R. (2010). Cloud computing: state-of-the-art and research challenges. Journal of internet services and applications, 1(1), 7-18.

[49] Zhong, R. Y., Xu, X., Klotz, E., & Newman, S. T. (2017). Intelligent manufacturing in the context of industry 4.0: a review. Engineering, 3(5), 616-630.

[50] Gahi, Y., Guennoun, M., & Mouftah, H. T. (2016, June). Big data analytics: Security and privacy challenges. In 2016 IEEE Symposium on Computers and Communication (ISCC) (pp. 952-957). IEEE.

[51] Parwez, M. S., Rawat, D. B., & Garuba, M. (2017). Big data analytics for user-activity analysis and useranomaly detection in mobile wireless network. IEEE Transactions on Industrial Informatics, 13(4), 2058-2065.

[52] McAfee, A., Brynjolfsson, E., Davenport, T. H., Patil, D. J., & Barton, D. (2012). Big data: the management revolution. Harvard business review, 90(10), 60-68.

[53] Davis, J., Edgar, T., Porter, J., Bernaden, J., & Sarli, M. (2012). Smart manufacturing, manufacturing intelligence and demanddynamic performance. Computers & Chemical

INVESTIGATION OF DEVIATIONS IN THIN-WALLS MACHINED BY THE MILLING PROCESS IN THE AEROSPACE GRADE ALUMINUM

Muhammad Wasif[1], Syed Amir Iqbal[1], Naseem Ahmed[1]

[1]Department of Industrial and Manufacturing Engineering, NED University of Engineering and Technology, Karachi. Pakistan.

*Corresponding author E-mail address: wasif@neduet.edu.pk

ABSTRACT

A research has been conducted to figure out the impact of cutting speed over the deviation in the thin-walls machined in the aerospace grade Aluminum 6061-T6. In this research, an experimental setup has been designed to machine the thin-walls (ribs) of thickness ranging from 1 mm to 3 mm. CNC milling machine is used to machine the thin-walls precisely using a constant tool path, including both roughing and finishing operations. Two workpieces of Aluminum 6061-T6 have been prepared upon which milling operation has been applied with the different cutting speeds. It has been found that the thinner walls exhibit higher deviation as the cutting speed is increased, whereas, the thicker walls have lower deviation, if the cutting speed is increased. It contradicts the hypothesis in the previous research that the deviation in the thin walls can be decreased by using the high-speed machining in the metals. Hence this research outlines a unique characteristic of the Aluminum 6061-T6 grade, which exhibits a different pattern of deviation in the thin-walls cut through the milling process.

Keywords: milling, aerospace grade Aluminum, T6061-T6, thin-walls, deviation.

1. INTRODUCTION

To reduce the mass of vehicle's components, thin-walled Aluminum alloy components are used in wide variety of applications in various industries, most notably in the aviation/aerospace sector. The ratio of the height to the thickness of the milling wall is a typical characteristic in thin-walled structures, which is 15:1 [1] Thin-walled parts of aerospace grade Aluminum 6061-T6 and 7071 series are being used in industry. During the machining of thin-walled alloys, most of the material is removed, due to which excessive heat is generated, resulting in large deformations in the thin-walls. This is one of the major concerns of machining of such class of materials, that is its vulnerability to deform because of nature of convoluted structure. The machining of intricate geometries will be intended to perform at high cutting speeds due to advantages of having high materials removal rates and good surface finish.

Rejection of parts and rework may result in high cost and delayed time of response to the strategic and defense-based projects, such as rockets, satellites and other products.

In this research, various factors would be explored which leads to high distortion potential of thin-walled structures and address a few measures which may perhaps lead to reduction in the predisposition of the thin-walled parts to deform. A limited literature review is available regarding the machining of thin-walled parts; however, the research articles were reviewed critically and hence presented below.

Due to ongoing advancements in the field of High-speed milling (HSM), currently available machine tools can accurately and precisely process hard metals, difficult-to-cut materials, complicated 3D geometry, and micro/nano-features [2]. Schultz and Moriwaki define the cutting speed for HSM of aluminum alloys in the range from 2500 to 10,000 m/min [3]. Izamshah et al. developed Finite Element Model to specifically predict the distortions or displacements for machining thin-wall component made of Titanium [4]. Izamshah et al. experience the magnitude of wall deflection decreases as the value of tool's helix angle increase [5]. Ding et al. conclude that higher cutting speed, smaller feed rates, and positive rack angles results in thinner deformation layers in machined surface [6]. Using the carbide tool, Yang et al. accurately predict chattering and stability for peripheral milling of thin-walled Al 6061-T6 plate and workpiece with a curved surface. [7]. Sun et al. indicate that force-induced deformation has a significant effect on chatter stability in milling thin-wall parts [8]. Due to the low stiffness value, Bolar and Joshi noticed increased deflection at the free end during machining thin-wall Al-7075-T6 as they expected during their simulation [9]. Kuczmaszewski et al. found that Surface quality was low in the transverse rolling direction. In addition, the carbide tool produced higher roughness values than the PCD tool. They also noticed that the maximum deflection was seen in the center of the workpiece, and high deflection was noted in the transverse rolling direction [10]. Czyzycki et al. demonstrated that a high-speed camera may be used to evaluate thin wall deflections during milling, as evidenced by comparisons to displacement measurements using a laser sensor with an accuracy of up to 11% and modeling using the finite element approach with a 22 percent error [11].

Based on the above literature review, it can be stated that the major challenge encountered when machining of above components is distortion / bending, dimensional error, surface finish, flatness, parallelism, perpendicularity and clamping. To investigate the effects of controllables parameters of high-speed milling and the thin-wall thickness, comprehensive research has been conducted to explore the deflection in the thin-walls and the surface roughness. By varying the controllable parameters, it has been found that the deflection and the roughness can be overcome.

Hence the research article comprises of six sections, the first section presents the introduction, literature review and the problem statement of the work. The second section defines the design of research, the third section discusses the tool path planning for the machining, whereas the fourth section outlines the measurement methodology of the sample workpieces through the CMM. The fifth section presents the discussion over the measurements and analysis, and the final section concludes the research work.

2. DESIGN OF EXPERIMENT

There are three major controllable parameters used for the machining, which are; spindle speed, feedrate and depth of cut, among which spindle speed are considered to be varied, whereas, the feedrate and depth of cut are kept constant for the machining in Aluminum 6061-T6 alloy workpiece. The deflection in the thin-wall was measured after the machining. The following table presents the parameters to be set for the two pieces to be cut with the levels.

The other parameters which remained unchanged during the experiments are diameter of the tool, tool geometry, cutting condition (dry) and workpiece material (Al 6061-T6).

Table 1. Controllable process parameters

Parameter	Levels	
	Workpiece 1	Workpiece 2
Feed Rate (mm/min)	1,000	1,000
Spindle Speed (r/min)	2000	4000
Depth of Cut (mm)	0.1	0.1

Using the controllable parameters, seven types of ribs are machines on the Al 6061-T6 workpiece of thickness 1mm, 1.25mm, 1.5mm, 1.75mm, 2mm, 2.5mm and 3mm. The machining was performed in sequential manner by applying roughing and finishing. Fig. 1 shows the final geometry of the Al 6061-T6 workpiece.
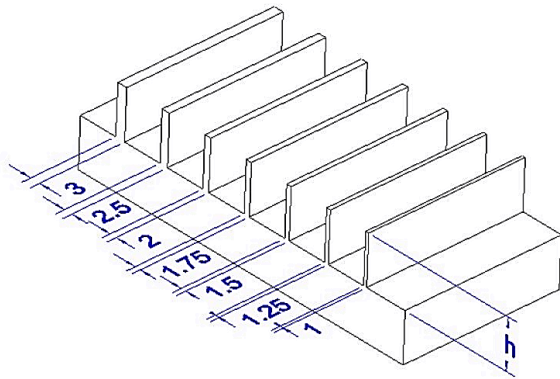
Figure 1. Geometry of the workpiece

3. TOOL PATH AND MACHINING
The milling of the workpiece of Al 6061-T6 was applied on the roughing and finishing of the thin walls. For roughing, step over is considered 70 percent of tool diameters, scan type is spiral, cut type is zig-zag. For finishing operation, type of cut is "climb" is selected. Geometric and machining codes for roughing and finishing for all 27 samples were generated using the CAM software. About 1000 mins were required to machine the two workpieces of Al 6061-T6 with the

seven ribs on the CNC milling machine. Input parameters and their levels are already shown in the 2. For the said experiments 3-Axis Vertical CNC Machining Center was used. The machining of the workpiece of Al 6061-T6 is conducted using the generated tool path and is shown in Fig. 2. Two workpieces were machined.

Figure 2. Machining of thin walls

4. MEASUREMENTS AND ANALYSIS
To measure the deflection in the thin walls cut by the milling process, the rib sections are cut into the pieces through the lines shown in Fig. 2. Each piece is precisely labelled and using a marker, a grid of 3 x 3 has been developed as shown in Fig. 3. A Messprotokoll ZEISS Calypso coordinate measuring machine (CMM) has been used to measure the deflection of the thin wall with respect to the base of the ribs. Here the location of points 1 to 9 are measured through the CMM. For each column of the grid the base points are taken as the reference, such as 7 in the first columns, and

77

the locations of 1 and 4 are deducted from it. It provides the deviation of point 1 and 4 with respect to the 7. Hence the same method is applied on each of the three grids of the rib. The procedure is applied to all the seven ribs on both the workpieces of the Aluminum. Hence a total of 144 points are measured through the CMM. The deviation of the six points with respect to the three base points are presented in Table 2 and 3 for both the Al 6061-T6 workpieces. The deviations of the upper part of the rib (points 1-2-3) and the medium part of the rib (points 4-5-6) are also plotted against the thicknesses of each rib for the two workpieces are shown in Fig. 4 and Fig. 5.

Figure 3. Sample Machined Thin Walls

Points	Thicknesses of Thin Walls						
	1.00	1.25	1.50	1.75	2.00	2.50	3.00
1	0.080	0.002	0.485	0.138	0.178	0.123	0.037
2	0.143	0.038	0.218	0.056	0.156	0.190	0.033
3	0.110	0.063	0.080	0.112	0.173	0.146	0.035
4	0.094	0.015	0.276	0.164	0.167	0.216	0.026
5	0.090	0.049	0.175	0.084	0.145	0.139	0.031
6	0.088	0.068	0.127	0.104	0.162	0.152	0.030
Mean Deviation	0.091	0.044	0.193	0.117	0.158	0.169	0.029

Table 2. Deviation of Point 1 – 6 for Workpiece 1

Points	Thicknesses of Thin Walls						
	1.00	1.25	1.50	1.75	2.00	2.50	3.00
1	0.125	0.128	0.096	0.061	0.062	0.079	0.011
2	0.110	0.127	0.085	0.061	0.059	0.085	0.012
3	0.076	0.101	0.101	0.078	0.060	0.076	0.008
4	0.198	0.317	0.214	0.173	0.169	0.184	0.018
5	0.222	0.356	0.182	0.144	0.052	0.181	0.017
6	0.235	0.255	0.248	0.188	0.143	0.189	0.017
Mean Deviation	0.161	0.214	0.154	0.118	0.091	0.132	0.014

Table 3. Deviation of Point 1 – 6 for Workpiece 2
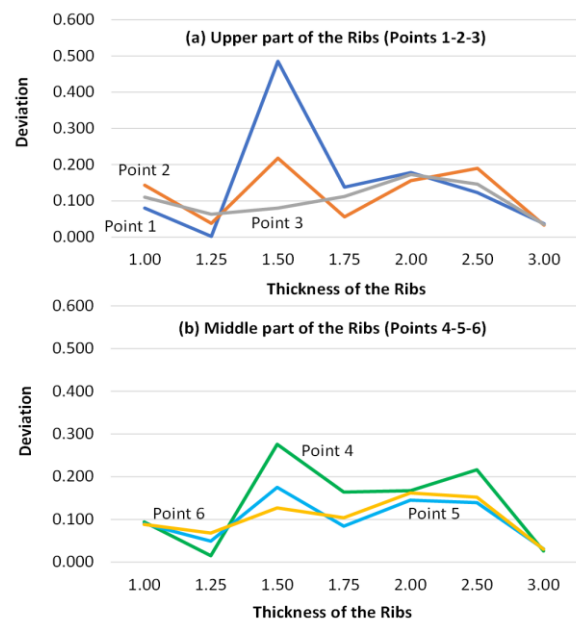
Figure 4. Deviation in Grid Points in Workpiece 1
(a) Upper part of the Rib, (b) Middle Part of the Rib

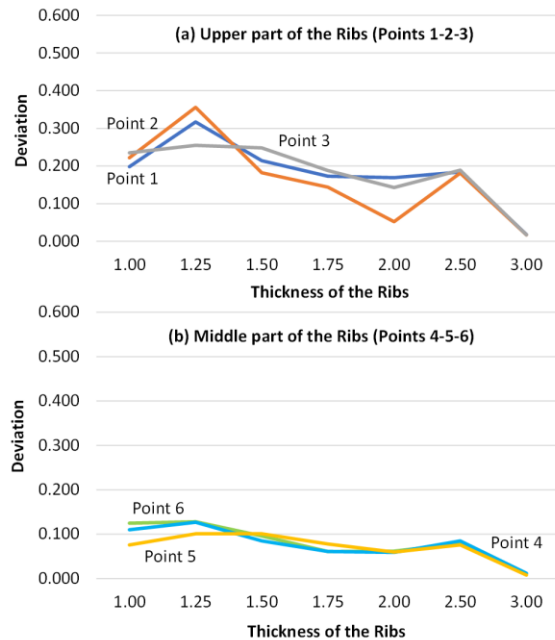Published Date: 08/07/2024 Version: 00

Figure 5. Deviation in Grid Points in Workpiece 2
(a) Upper part of the Rib, (b) Middle Part of the Rib

5. DISCUSSION

In the previous research, it has been stated that the deflection in the thin walls can be reduced by applying the higher cutting speed, in contrast to this, higher deflection in the thin walls of thicknesses 1 mm and 1.25 mm have been observed in the workpiece no. 2, which was machined with the higher spindle speed. In workpiece no. 2, at points 1, 2, 3, 5 and 6, the deflection was between 0.1 mm and 0.2 mm, whereas it was slightly less in the point 5 (see Fig. 5a and 5b). Whereas in Fig. 4a and 4b, it can be seen that for the same thicknesses, the deflection was between 0.05 mm to 0.15 mm for the points 1 to 6. Hence it can be inferred that for the thin-walls of aerospace Aluminum grade Al 6061-T6, the thin walls shows a different characteristics.

For the other thicknesses (1.5 mm to 3.0 mm), the statement of the previous research might be true, where the devotion in the workpieces 1 (cut with lower cutting speed) is between 0.1 mm to 0.2 mm, and the deviation in the workpiece 2 (cut with the higher cutting speed) is within the 0.1 mm range.

The factors which influence the deviation in the thin walls are usually the temperature generated during the machining, tool path strategy, use of coolant and other ambient factors. Whereas, in this research a unique characteristics of the material Al 6061-T6 has been seen which totally changes the hypothesis assumed by the previous research for the metal machining. Hence, it can be considered that the aerospace aluminum grade Al 6061-T6, exhibits entirely different characteristics as compared to the other metals.

6. CONCLUSION

An experimental setup has been developed to investigate the unique characteristics of an aerospace grade Aluminum Al 6061-T6, which shows the deviation in the thin-walls do not reduce with the increase in the cutting speed. Rather it is observed less in the workpieces, machined with the lower cutting speed. Though for the slightly thick walls ranging from 1.75 mm to 3.00 mm, they show the same characteristics of lower deviations with the higher cutting speed. During this research, several other parameters are kept constant to solely observe the influence of the cutting speed over the deviation of the thin walls.

6. REFERENCES

[1] Balon, P., et al., *High speed machining of the thin-walled aircraft constructions.* Mechanik, 2017. **90**(8-9): p. 726-729.
[2] M. Rahman, W.Z.-G.W.Y.-S., *A review on high-speed machining of titanium alloys.* JSME International Journal, 2006. **49**(1).

[3] Schulz, H. and T. Moriwaki, *High-speed machining.* CIRP annals, 1992. **41**(2): p. 637-643.

[4] R. Izamshah R.A, J.P.T.M., Songlin Ding, *Finite Element Analysis of Machining Thin-Wall Parts.* Key Engineering Materials, 2011. **458**: p. 283-288.

[5] R. Izamshah, Y.M.Y., M. Hadzley, *Effects of End Mill Helix Angle on Accuracy for Machining Thin-Rib Aerospace Component* Applied Mechanics and Materials, 2013. **315**: p. 773-777.

[6] Liqiang Ding, X.Z., C. Richard Liu, *Dislocation Density and Grain Size Evolution in the Machining of AI6061-T6 Alloys.* Journal of Manufacturing Science and Engineering, 2014. **136**: p. 041020-1 to 041020-10.

[7] Yun Yang, W.-H.Z., Ying-Chao Ma, Min Wan, *Chatter Prediction for the Peripheral Milling of Thin-walled Workpieces with Curved Surfaces.* International Journal of Machine Tools and Manufacture, 2016.

[8] Yuwen Sun, S.J., *Predictive modeling of chatter stability considering force-induced deformation effect in milling thin-walled parts.* International Journal of Machine Tools and Manufacture, 2018.

[9] Bolar, G. and S. Joshi. *3D finite element modeling of thin-wall machining of aluminum 7075-T6 alloy.* in *5th International & 26th All India Manufacturing Technology, Design and Research Conference.* 2014.

[10] Kuczmaszewski, J., et al., *Assessment of the accuracy of high-speed machining of thin-walled EN AW-2024 aluminium alloy elements using carbide milling cutter and with PCD blades*, in *Advances in Manufacturing.* 2018, Springer. p. 671-680.

[11] Czyzycki, J., P. Twardowski, and N. Znojkiewicz, *Analysis of the Displacement of Thin-Walled Workpiece Using a High-Speed Camera during Peripheral Milling of Aluminum Alloys.* Materials, 2021. **14**(16): p. 4771.

DESIGN OF SOLAR WATER DESALINATION MACHINE WITH RO AND UV PURIFIER

Muhammad Sarfraz Ali[1]*, Sadia Saleem[2], Rozeena Aslam[1], Muhammad Imran[1], Hamza Akhtar[1], Muhammad Ali[1], Danyal Anwar[1], Muhammad Saad[1]

[1]Mechanical Engineering Department, Swedish College of Engineering & Technology, Rahim Yar Khan, Pakistan
[2]Institute of Computer Science and Information Technology, The Women University, Multan, Pakistan

*Corresponding author. Tel.: +92-3458329528
E-mail address: sarfrazali@piet.edu.pk (Muhammad Sarfraz Ali)

ABSTRACT

In all ages of human beings, water performs a very vital function for everyone. As is well known, contaminated water can lead to several potentially fatal diseases. Water-related problems plague many nations worldwide, the majority of which lack access to potable water. We have seen that many villages are experiencing power outages, and middle-class people and tiny communities are unable to purchase a water filter. Conventional energy has a finite supply and negatively impacts the environment. In this study work, we use an unconventional approach that uses a solar-powered water purifier. We need to take the purifying process to the next level so that everyone can afford it. Direct current is produced by the solar panel and is kept in a battery. The filtration mechanism that this purifier uses to remove undesirable germs and debris from water is powered entirely by solar energy. By driving a pump that pushes water through a purifier's network of filters, pumps, and hoses, the motor's rotation aids in the removal of pollutants. The method we employed in this purifier was using solar panels to power the motor that lifted the water.

Keywords: RO membrane, Pre filters, Purifier, Solar panel, Small scale

1. INTRODUCTION

One of the most important resources in the world is water. Thirty percent of Earth is land and seventy percent is water. Water is necessary for both human survival and animal well-being. The process of purifying water involves taking out unwanted chemicals, biological pollutants, suspended particles, and gases. According to a survey conducted by physicians, an average male and female should drink around 3.7 litres and 2.7 litres of water respectively each day to maintain a healthy lifestyle [1]. In Pakistan, water-borne illnesses including cholera, diarrhoea, and typhoid caused roughly 2439 deaths and over 1.5 million cases of the disease.

A water resource must be both reasonably priced and trustworthy. Many parts of the nation have brackish, saline, or polluted water supplies. In the Rahim Yar Khan district and the coastal regions of Karachi, salinity is a serious issue. The method for purifying water that is already accessible is called RO, and one of the conventional energy sources that may be used to power our

81

system is sunshine [2]. The most reliable way to purify polluted water is RO filtration. The RO system's semi-permeable membrane removes excess minerals as well as other soluble particles including bacteria, fungi, viruses, and algae. The device efficiently removes particles as small as 0.0001 microns while turning the motor. In Pakistan, access to clean drinking water is a big issue in both rural and urban areas [3]. There are several conventional techniques for purifying drinking water, including the use of chlorine pills, pots for good chlorination, slow and quicksand filters, and fluoride removal. However, these techniques are more complex to use and yield lower purity levels than RO. In this study, we present a concept that uses a solar panel to raise the water level in a tank and supply power to a RO system for purification [4]. In the event of an environmental issue or power outage, such as a flood or other disaster, the solar purifier's battery stores energy, enabling the process to continue using solar power. It is a simple-to-assemble portable purifier that may be used in remote locations without electricity. This purifier operates without producing any pollutants [5].

Rural communities across the world have embraced basic, low-tech healing methods, with the specific goal of removing obvious pollutants from water obtained from adjacent resources. These conventional techniques are quick and effective in eliminating some types of particles from the water, but they don't provide enough water to meet current standards for drinking quality. This is a great method for rural areas, and with a simple disinfection step, they can often provide water free of germs. There are several approaches.

1.1 Filtration along Winnowing Sieve

When the water source is contaminated by airborne contaminants such as dried leaves,

stalks, and coarse particles, this kind of filtering is employed. A winnowing sieve is used to filter the contaminants out of the raw water. Since the sieve cannot filter small suspended particles in raw water, this approach cannot be employed in extremely turbid or muddy conditions.

1.2 Filtration through cloth:

In the villages, the filter medium is made of white, thin cotton fabric or old, abandoned clothing. Uncooked water including particles of dust, germs, insects, plants, or mud detritus can be removed using this filter. Only a limited amount of the suspended particles in the water may be removed by this cleaning method. In Pakistani communities, the technique of cloth filtering is rather widespread.

1.3 Filtration through Clay Vessels (Earthen Pot):

Occasionally, rather turbid water is filtered using clay jars with the proper particle size. Muddy water is collected in a large clay pot or jar and let sit on the pot's lower surface, allowing the water to drip through the jar's porous clay wall. The trickling water is combined in a clay pot by lowering it to the bottom of the porous clay container.

Y. Zhang et al. [6] uses solar energy, which is a free energy source, and stores it in batteries. After that, the water is heated to a predetermined temperature (below boiling points) using cheap heating coils. The filtering chalk allows the cold water to be further purified once it has condensed. At this point, the water returns to ambient temperature by condensation. We can acquire pure drinking water using this procedure. We experienced nearly every phase of the product development process, from obtaining client requirements to completing the design.

M. Rizwan et al. [7] suggested that solar-powered water filtration devices could be considered a significant way to generate

82

clean water. Solar energy is now a stable energy source that produces no pollution. A solar-powered water purification system's design is entirely based on the thermal technique, which harnesses the sun's heat-converting energy to create heat. The process of absorbing heat to cause water to evaporate is the most important component. According to research, liquids are often heated using flat plate collectors, which generate heat at comparatively modest temperatures (27°C to 60°C). A solar-powered water purification system is made up of a filter that eliminates impurities and a solar collector that collects sunlight to guarantee vaporization, the initial stage of purification. There are now four distinct concepts in development.

R. K. Kumawat et al. [8] revealed from their study that reverse osmosis affected water purification. Reverse osmosis technology using raw water has advanced significantly in the creation of high-yielding, energy-efficient systems. The main objectives for this field of study turned out to be a decrease in energy consumption, an extension of membrane life, and an increase in energy recovery. The main goal of the study is to optimize the variables in the pre-treatment process of various water sources (ponds, canals, and surface waters) for reverse osmosis plants. This will extend the membrane life of the raw water by lowering its solids content. To guarantee the greatest possible decrease in total solids as well as in several chemical parameters (BOD, TDS, and bacteria), experiments were conducted. These characteristics were determined to be ideal for feeding the pretreatment effluent into the reverse osmosis section of the plant, producing RO water that is safe for human consumption.

R. M. Garud et al. [9] identified a purifying method including reverse osmosis. The three primary circuits in this system are the control, purification, and power supply circuits. The solar panel, charge controller, battery, and inverter make up the power supply. A booster pump, a reverse osmosis system, and a control circuit with a sensor, microcontroller, and relays make up the purification unit. A booster pump generates high pressure to complete the reverse osmosis process. The microprocessor monitors the water tank's level and stops it from overflowing. We may get pure water in the water tank by employing this method.

The fundamental idea of reverse osmosis. Solar panels are used to capture solar radiation. A battery is then used to store this energy. A relay that operates on electromagnetic principles connects the battery to the purifying unit. The reverse osmosis system, water tank, and high-pressure motor make up the purification unit. Reverse osmosis may be performed because of the pressure created by the high pressure. The 8051 microprocessor monitors the water level in the tank and stops it from overflowing. We can receive clean water from the water tank through this technique.

2. METHODOLOGY

As indicated in Fig. 1. Filters, solar panels, booster pumps, solar charge controllers, reverse osmosis membranes, and other components are the main parts of this purifier. This purifier's operation is entirely reliant on solar panel electricity. Batteries are used to store energy, which is obtained from solar power.
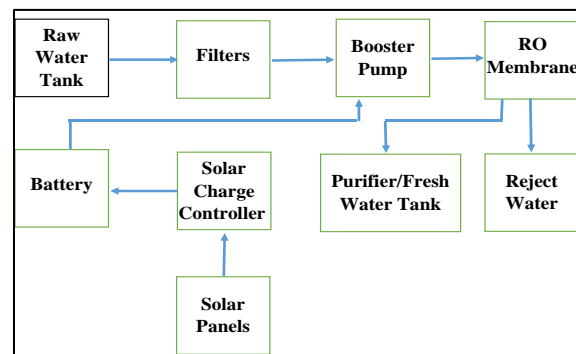
Figure 1. Block Diagram of System

The solar panel is composed of photovoltaic cells, which convert solar radiation into electrical energy. The energy from the panel is stored in batteries, and a solar charger controller controls the voltage and amperage the panel delivers to keep the batteries' load from being overcharged. The power supply then activates the filters and motor rotor, which in turn causes the eccentric swing wheel to move eccentrically. The diaphragm is driven by the water scaffold assembly, which is made up of three cameras attached to the eccentric tread wheel, turning in reverse. The diaphragm of the RO booster pump can continue to reproduce due to the engine's continual spinning, which serves to pump and increase the water once it enters. The RO membrane can eliminate the bulk of pollutants by forcing the water through a semi-permeable membrane, which eliminates all water impurities. There are three layers in the membrane. The first layer is composed of a 0.2-micron-thick polyamide sheet that excludes all other types of particles. The polysulfide layer can eliminate any nutrients, bacteria, chemicals, or viruses that are present in the water. The polyester foundation, through which the cleaned water passes, is the final. Both the clean and the filthy water are separated after the purification procedure. Figure 2 shows the design of the model.
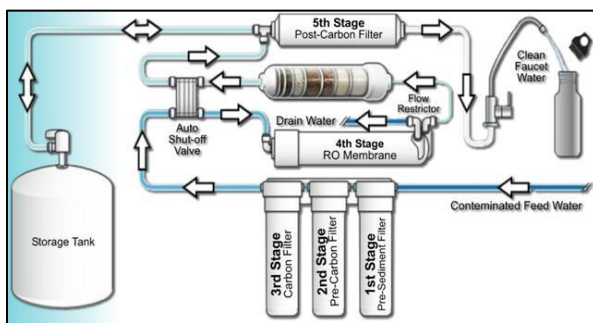
Figure 2. Design of the Model

3. COMPONENTS SPECIFICATIONS

3.1 Reverse Osmosis Membrane

The membrane is composed of three layers. All other kinds of particles are blocked from entering the first layer by a polyamide sheet that is 0.2 microns thick. Any nutrients, bacteria, chemicals, or viruses that are present in the water can be removed by the polysulfide layer. The cleansed water travels through the polyester foundation, which is the last. Following the purification process, the clean and dirty water are separated. Table 1 shows the technical specifications of the RO plant.

Characteristics	Values
Voltage and Frequency	110V~220V
Wattage	23W - 36W
Inlet TDS	< 500 ppm
Chlorine Level	< 0.2 ppm
Pressure Tank	3.0G Plastic Tank
Flush Type	Manual

Table 1. Technical Specifications of RO Plant

The membrane is composed of three layers. All other kinds of particles are blocked from entering the first layer by a polyamide sheet that is 0.2 microns thick. Any nutrients, bacteria, chemicals, or viruses that are present in the water can be removed by the polysulfide layer. The cleansed water travels through the polyester foundation, which is the last. Following the purification process, the clean and dirty water are separated.

Figure 3. Reverse Osmosis Process

A typical three-stage reverse osmosis system consists of three different kinds of filters. A sediment filter is designed to capture bigger particles floating in water, such as rust and mud. The carbon filter purges water of VOCs, chlorine, and other minor impurities. Reverse osmosis membrane that is semi-permeable and effectively eliminates almost all leftover impurities.
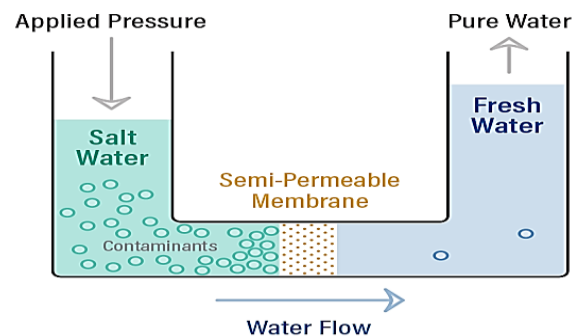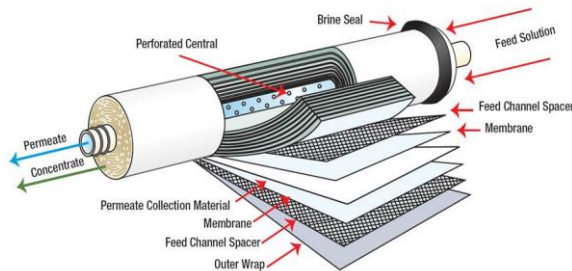

Figure 4. Inside of an RO Membrane Filter

3.2 Booster Pump

Booster pumps are used to increase water pressure. Usually, the osmotic pressure is higher. Purification requires that water flow from a high concentration to a low concentration. Therefore, to perform the reverse osmosis process, the high-concentration lateral pressure must be higher than the osmotic pressure.

3.3 Solar Panel

In this concept, solar energy is captured using a solar panel. Photovoltaic cells are used to make solar panels. The power output is entirely dependent on the light's intensity. We are utilizing a 20-watt miniature solar panel to charge a 12-volt battery that is exposed to sunlight. This portable solar panel is lightweight and has a wide range of uses. The panel is specifically made to charge tiny batteries with a maximum capacity of 10,000 mAh or 10 Ah. The dimensions of little solar panels vary from 0.6 x 2.55 inches to 14×18 inches, or 1.7 square feet, which is similar to a standard medium-sized house mirror.

3.4 Solar Charger Controller

An electrical gadget called a solar charge controller regulates the amount of electricity that the solar panel supplies to the battery. This makes sure that energy is not replenished during the day and that the solar panel receives electricity during the night to prevent the deep cycle battery from being depleted. While some charge controllers come with other capabilities like load control and illumination, power management is the primary objective.

3.5 Storage Battery

It is a crucial component of the setup. Seasonal variations in atmospheric conditions result in variations in the intensity of solar radiation. The impurity pump is shielded from overvoltage by the constant 12V voltage. It features a 12-volt output voltage and a 5-amp output current.

3.6 Sediment Filter

Sand, grit, precipitated mineral particles, insoluble iron oxide, and other debris are removed by the sediment cartridge, which prevents them from clogging the reverse osmosis film surface or plugging the drain flow restrictor, which reduces the amount of water produced. Sediment filters rated to remove particles as small as 5 microns are used in the majority of RO systems. We advise changing this filter at least once every six months. It is necessary to change TINY RO sediment filters every three months.

3.7 Carbon Filter

City utilities disinfect drinking water to stop the growth of dangerous bacteria, viruses, and other microbes that can cause life-threatening diseases or even death. Nevertheless, over time, TFC films may degrade in these chlorinated water sources. A basic chlorine level of 1.0 mg/L (1.0 ppm) is required for water going through the plant

85

by the majority of city water utilities. Extended TDS passage (less impurity rejection) may be allowed by the RO membranes after 1000 ppm-long regions of free chlorine openness. In addition to eliminating chlorine, the carbon filter shields the membrane underneath it.

3.8 UV Lamp

UV lamp: A UV lamp is typically used in Ultra Violet disinfection. To create clean, safe drinking water, a UV light is employed. A strong UV light known as UV-C, or germicidal UV, is employed in this procedure. UV-C rays enter the body of the pathogens and assault them. The harmful organisms' DNA has been modified to prevent growth and disease-causing properties. UV treatment only adds energy to the water; it makes no chemical changes. There is no removal of the sterilised bacteria from the water. These rays can render 99.9% of the bacteria inactive. Unlike chemical disinfection, UV radiation does not cause live things to build an immune system.

3.9 Flow Restrictor

As the name suggests, a flow restrictor limits the flow of RO reject water. The flow restrictor not only regulates the purifier's recovery ratio but also generates back pressure on the RO membrane to maintain high pressure within it, which is a prerequisite for RO purification. The high-pressure water entering from the booster pump will flow freely from the RO membrane's reject exit if the flow restrictor is not employed. Low pressure inside the RO membrane and increased water waste are the results of this. If the pressure inside the RO membrane is not high, the membrane will not function.

3.10 Water Tank

The primary purpose of a water tank is to hold water. Another name for it is the storage tank. Water is stored in a tank on the building's roof, and gravity distributes the water to the lower stories. Basement pumps feed the tank with water from the mains system, and when the tank is empty, the pumps start up again. In this sense, the tower serves as a reservoir and a supply of water.

4. DESIGN CALCULATIONS

4.1 Design solar parameters

The following are the primary panel designs that have an impact on collector panel performance.

- **Power for Application:** The manifold panel is directly impacted by the power needed for a certain application. In terms of cost and received power, bigger panels have larger areas. This panel has an 18W maximum power output. The angle of Latitude: To maximize solar energy absorption, the panel should be kept at the angle of latitude. The angle between the earth's equator plane and the line connecting a specific place on its surface to the equatorial centre is known as the latitude of a certain location.

- Using the following method, the latitude angle is determined.

  ➢ Check off all three points. i.e.
  ➢ The Equatorial plane lines.
  ➢ The Earth's centre.
  ➢ The location on a globe map where the panel is to be created.

- Join the location point with the earth point.

- Determine the angle formed by the earth's centre point and the equatorial plane line.

- **Average Power Intensity:** The average power intensity for any locality is the unit of power collected per day.

$$Average\ global\ radiation = 6.1\ KWh/m^2.day \quad (1)$$

But,

$$1\ KWh/m^2 = 3.6\ MJ/m^2$$

86

$$Avg.\,global\,radiation = 6.1 \times 3.6$$
$$= 211.96\,MJ/m^2$$

i.e,

$$(21.96 \times 10^6)/24 \times 60$$
$$= 15250\,J/m^2.min$$

$$15250/60 = 254\,J/m^2.sec$$
$$U/sec = 1W$$

$$Therefore\,avg.\,global\,radiation$$
$$= 254\,W/m^2$$

- **The angle of Incidence:** It depends upon the time of day also the angle of sunrays makes the horizontal Surface measured w.r.t,

As the sun travels the angular distance of 180° for 12 hrs. it travels at an angular speed of 180/12 = 15°/hr.

Sr. #	Water quality parameter	Units	Permissible limits	Results
1	Total Dissolved Solids (TDS)	(mg/L)	1000	55.0
2	pH	-	6.5-8.5	7.44
3	Alkalinity	(mg/J)	NGVS	2.4
4	Total Hardness	(mg/L)	500	36.0
5	Chloride	(mg/L)	250	5.7
6	Calcium	(mg/L)	NGVS	11.2
7	Magnesium	(mg/L)	NGVS	1.9
8	Sodium	(mg/L)	NGVS	7.0

Table 2. Purified Water Properties

The ideal angle of incidence is the angle which makes the sun at an angle of Latitude (Q) & incidence = 90°

$$As\,angle\,of\,latitude = Q = 20^o$$
$$Ideal\,angle\,of\,incident = 90^o - 20^o$$
$$= 70^o$$

4.2 Area of Collector

The collector's area mostly affects the power that the collector produces. The following protocol is adhered to during the design process.

$$in = ibn \times A \times \cos\emptyset$$
(2)

Where,

$$in = power\,developed$$

$$A = area\,of\,collector.$$

$$Ibn = Average\,solar\,intensity$$

As the ideal angle of incidence is 70°

$$In = Ibn \times A \times \cos\emptyset$$

$$6 = 254 \times A \times \cos 70$$

$$Therefore\,A = 0.069066\,m$$

Consider it a rectangular panel having a side ratio of 1:3

$$I^2 = 0.069066$$

$$= 0.325m = 32.5$$

$$B = 3 \times I = 47\,cm$$

$$Panel\,area = 32.5 \times 47$$
$$= 1527.5cm^2$$

4.3 Discharge of water

The discharge of water can be calculated from the continuity equation.

$$Q = Arae \times Velocity$$
(3)

Now,

87

$$Area = 0.01 \times 0.01 = 0.0001 mm^2$$
(4)

Now find the velocity of water through the pipe,

$$Hf = (4 \times f \times L \times V^2)/ Area\ of\ c/s \times 2g$$
(5)

Where,

$$Hf = difference\ of\ pressure\ head = 4m$$

$$F = cofficient\ of\ friction = 0.009$$

$$L = total\ length\ of\ pipe = 10.0584m$$

$$V = velocity\ of\ water$$

So,

$$4 = 4 \times 0.009 \times 10.058 \times V^2/0.00001 \times 2 \times 9.8$$

$$V = 1.4721\ m/s$$

$$Q = 0.0001 \times 1.4721$$

$$Q = 0.000014721\ m^3/s$$

$$Q = 0.01472\ litre/s$$

5. RESULTS

The most readily available energy source—sunlight—was used to build the water purification system. Sunlight is simply absorbed and stored using solar panels, requiring no additional energy or power. However, the remaining components are working to move the process along via the motor and further filtering through several RO membranes and filter pumps, eliminating not just undesired bacteria, viruses, and other materials but also dirt, algae, and minerals. It is more cost-effective and efficient to utilize due to its design and simplicity of usage. Properties of the purified water are shown in Table 2.

6. CONCLUSIONS

In situations when power supplies and water purification methods are not mapped, this equipment is the most accessible and practical for disinfecting water. Potable water is produced by the straightforward mechanism and integrated structure, which turns solar energy into a motor that runs on a schedule and helps filter out undesired viruses, minerals, bacteria, and other particles. It may be used somewhere there is no power because it is cheap and uses solar energy to purify copious water. In this day and age, this may be a topic for further study. There aren't any water purifiers of this kind available right now. Therefore, we think that if solar water purifiers are deployed successfully and barriers are removed, they would be able to draw in customers from all sectors of the metropolitan population.

ACKNOWLEDGEMENT

REFERENCES

[1] B. Benelam and L. Wyness, "Hydration and health : a review," pp. 3–25, 2010, doi: 10.1111/j.1467-3010.2009.01795.x.

[2] S. G. Salinas-rodriguez, G. L. Amy, J. C. Schippers, and M. D. Kennedy, "The Modi fi ed Fouling Index Ultra fi ltration constant fl ux for assessing particulate / colloidal fouling of RO systems," vol. 365, pp. 79–91, 2015, doi: 10.1016/j.desal.2015.02.018.

[3] S. Khalil and I. Introduction, "RESEARCH NOTES DRINKING WATER QUALITY CHALLENGES OF PAKISTAN Samina KHALIL* I. Introduction," vol. 23, no. 1, 2013.

[4] M. S. Atab, A. J. Smallbone, and A. P. Roskilly, "A hybrid reverse osmosis /

adsorption desalination plant for irrigation and drinking water," *Desalination*, vol. 444, no. May, pp. 44–52, 2018, doi: 10.1016/j.desal.2018.07.008.

[5] I. E. Imiete, N. V. Alekseeva, I. E. Imiete, and N. V. Alekseeva, "Reverse osmosis purification : A case study of the Niger Delta region Reverse osmosis purification : A case study of the Niger Delta region," *TITLE=Water Sci.*, vol. 32, no. 1, pp. 129–137, 2019, doi: 10.1016/j.wsj.2018.04.001.

[6] Y. Zhang, M. Sivakumar, S. Yang, and K. Enever, "Application of solar energy in water treatment processes : A review," *Desalination*, vol. 428, no. October 2017, pp. 116–145, 2018, doi: 10.1016/j.desal.2017.11.020.

[7] M. Rizwan, S. Shaikh, and S. Labade, "A Review Paper on Electricity Generation from," no. September 2017, 2018, doi: 10.22214/ijraset.2017.9272.

[8] R. K. Kumawat, S. Agrawal, S. Chourasiya, and D. K. Palwalia, "A Comparative Study of Power Inverter Topology and Control Structures for Renewable Energy Recourses," pp. 350–354, 2015, doi: 10.17148/IARJSET.

[9] R. M. Garud, S. V Kore, V. S. Kore, and G. S. Kulkarni, "A Short Review on Process and Applications of Reverse Osmosis Abstract : 1 . 3 Reverse Osmosis Process Description : 1 . 2 Treatment options for Reverse Osmosis :," vol. 1, no. 3, pp. 233–238, 2011.

AUTONOMOUS AND EFFECTIVE SOLUTION FOR CLEANING OF AIR CONDITIONING DUCT

Syed Saad Farooq[1],* Muhammad Abdur Rafay[1], Muhammad Faizan Shah[1]

[1]Institute of Mechanical and Manufacturing Engineering

Khwaja Fareed University of Engineering and Information Technology (KFUEIT) Rahim Yar Khan Pakistan

Corresponding author E-mail address: syedsaad34@gmail.com

ABSTRACT

Closed and long air ventilation ducts (HVAC systems) become polluted by different contaminants and particulate matters while functioning for larger period of time. Ventilation duct cleaning process is difficult and expensive with manpower and usually takes a longer time. It can also cause respiratory and other health problems for labor in cleaning and investigation. This paper aims to propose an air duct cleaning robot (ADCR) for a duct which is low powered Arduino operated and sensory based robust controlled system. It is an upgradation of some cleaning and brushing mechanisms in terms of design. Further proposed design is being evaluated in terms of effective suction and time taken analysis by robot is also done as validation for sustainable solution. The work highlights mechanism as light, inexpensive and easily works in a closed environment.

Keywords: Autonomous Vehicle, Dry Duct Cleaning, Arduino controlled Cleaning Robot

1. INTRODUCTION

The purpose of an air duct ventilation system is to provide fresh air into confined spaces used in industries, subway stations, and offices where people do work and spend most of their time [1]. This air duct system controls various air flows, i.e., exhaust air, outlet air, return air, and supply air. It consists of mechanical parts like dampers, filters, and air terminals [2]. Filters have been installed which will trap some dust particles initially, but they cannot filter out all particulate matter at the outlet of the air duct [3]. Therefore, these dust particles accumulated at the inner surface of ventilation system [4]. To provide clean and fresh air through these air ventilation duct, it is mandatory to remove these accumulated particles. Ventilation duct cleaning process is difficult and sometimes need to replace with new duct which is expensive [5]. In the study of duct cleaning process, this paper suggests an autonomous duct cleaning robot that is capable of fulfilling the purpose of duct cleaning using appropriate dry-cleaning method and required less manpower and cost effective [6]. This method includes vacuum fans and filters which suck the small particles from the duct. Mechanical brush is used to displace sticky particles. Sensor controlled movement which senses the path of the duct and performing turning action within the duct [7]. Arduino based circuit and two gear motors used for the low RPM movement. Only horizontal surfaces can be cleaned from the duct. It can be made for vertical, round and other wall pressed cleaning robot. This type of robot used in industrial HVAC system and domestic level duct cleaning system to provide healthy and fresh air to the environment [8]

The characterization of cleaning methods involves dry method and wet method. Both

90

dry and wet method used for purpose of duct cleaning. Dry cleaning method is mostly used including mechanical brushing, compressed air cleaning and vacuuming, while wet cleaning method includes water jet and chemical sterilizing which is less used because air duct is watertight. In order to clean

accumulated dust particles, vacuum cleaning and brushing is most effective and rapid and convenient method as compared to wet cleaning. [9].

Annual accumulation for dust particles found to be approximately 1 g/m^2. It is noted that in less than a year the average accumulation rate was 5.1g/m^2 as compared to newly constructed duct in which the dust level was maximum to 4.9 g/m^2 [10], Normally if dust level increases from 2-5 g/m^2 in the duct system then the cleaning is inevitable. Many other factors that interrupt the air flow in ventilation systems besides dust concentration are e.g., humidity, surface roughness, vortex of air flow [11]. The problem lies as the duct is manually cleaned by labour which is both the wastage of time and money. Corollary resulting in health concerns for the labour. The current work endeavours to tackle the issue by establishing a cleaning robot to clean dry ducts for complex shapes and sizes.
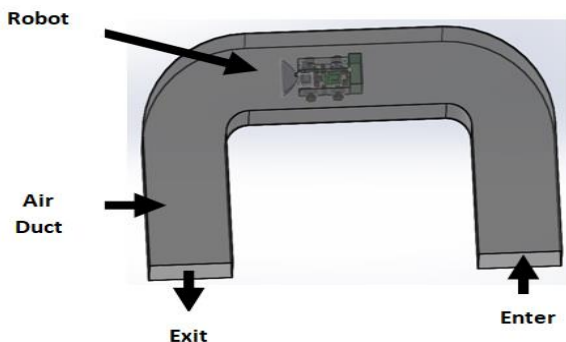
2. CONSTRUCTION

The proposed design is based on dry cleaning methods with vacuum cleaner and brushing system [12]. This work focuses on the capacity of the air duct cleaning robot for efficiently cleaning inside the duct in the absence of labour [13]. Some newly advanced cleaning robots can be fitted with directional air nozzles, sampling devices, spinning brushes, and whips, and spraying sanitizing solutions for several coatings [4].

The mobile robot consists of acrylic base body, two rubber wheels and one 3-D wheel for free motion, two DC gear motors are used to take motion back two wheels at specific RPM [14]and provide required torque and two DC motors inside suction fans [15]. The design of each component of the robot was developed in SolidWorks Design Software as shown in figure 2 and 3. This duct cleaning robot design is unique in its working and usability. This robot is upgraded in its vacuum cleaning, brushing, working mechanism and cleaning power capabilities as compared to other cleaning methods as described in [16] and it had now been observed on the basis of performance evaluation criteria like dust collection and time analysis in this work. Powerful suction fans and a filter is used in vacuum cleaner to make effective surface cleaning [17].

Figure 1. ADCR path

Figure 2. ADCR Isometric view

Figure 3. ADCR Top View

The duct is 5x2x1 fts and 4 fts in length after the turn [18]. The duct is made of wood with its starting and closing paths open. Duct is designed according to ASTM F1005 – 91 Standard Rectangular Air Duct Sizes [19]. For the chassis of robot, poly-methyl-methacrylate (PMMA), commonly known as acrylic, was used, owing to its lightweight and high strength characteristics [20]. The size of the frame is 12 inch wide and 16 inch long. The surface clearance of the frame is 5 mm.

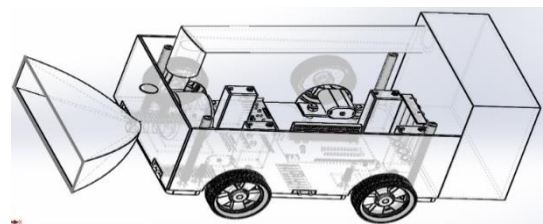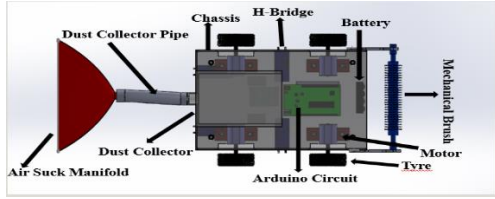Robot dimensions are 12 x 16 x 12 inch and has a maximum speed of 281 rpms and a mass of 3.5 kg. This vacuum cleaner consists of two suction fans, a dust collector, two pipes and a strainer. A 12 V, 3 cell, 5200 mAh Li-Po battery which is being used as an voltage source that supplies electrical energy to components such as sensors, vacuum blowers, and motors. Air suction fan having 3000 rpm are installed on the rooftop of the robot which suck the dust particles during brushing the duct [21]. The conduit is connected to the tube and the vent collector's door. In the suction mechanism, filters are installed to collect the dust particles and to protect from fan's choking. After one-time cleaning, the filter is cleaned for repeated use[14]. One fan being operated on 12 volts and draws 2.3 A of current [22]. Duct collector with two single-inch pipes connected to two fans independently. The scale of the suction fans is 90x90 mm and each fan has a suction capacity of 30 cfm. A brush is attached on its front and its rotation is followed by motion of robot. The purpose of brush is to remove the sticky dust (if any) for effective cleaning.

3. CONTROLLER AND WORKING

This ADCR is being operated by Arduino Mega 2560.The requirement for the ADCR controller is that it must contain at least 54 I / O pins. Other specifications are shown in appendix A. Six HC-SR04 Ultrasonic distance measurement sensors, as shown in the figure 4, are used to detect and avoid obstacles in the pathway. Four of them are mounted on the front and four on the back. Other specifications are mentioned in appendix B. The Motor driver consists of the H-Bridge circuit. The H-Bridge circuit is a circuit used to control the rotation direction of the engine. It consists of four switching components and a central motor. The switching element can be transistors or MOSFETs (metal-oxide-semiconductor field-effect transistor) are H-like configurations, hence the name. Two switches stay ON at a time to complete the circuit while two others remain OFF. If the course is to be changed, the other two are set to ON and the previous two are set to OFF. In this way, the path of the current from the motor is changed in order to reverse the motion of the piston.

The robot is a four-wheel drive vehicle. Each of the four wheels is powered independently by a DC gear motor. The independent engine is powered by the H-Bridge connection. The purpose of driving the wheel independently is to make it easier and efficient for the robot to operate the programmed circuit functioned on Arduino. There are four proximity sensors on the periphery of the base that have been installed to detect the clearance distance between the walls and the robot during movement.Other hardware calculations will be presented in its sub section ahead.

92
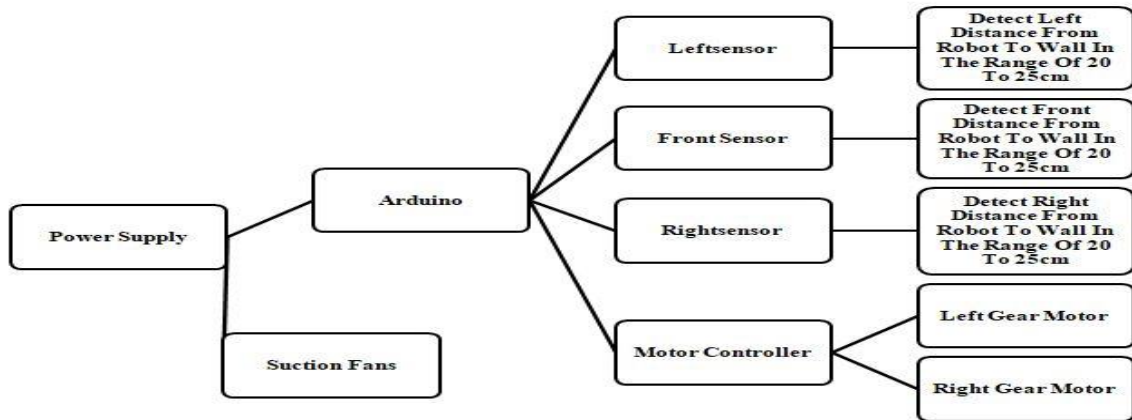
Figure 4. Process Methodology

3.1 Formulation of Suction Required

Suction of fans is determined using mathematical equations as shown in table 1 [23].While volume air
flow can be formulated from [21]. It is found that the suction of one fan is 30.30 cfm and hence accumulative will be 60.60 cfm for two suction fans.

Design Parameters	Formulation
Force	$m.a = 3.5 \times 0.375 = 1.31 N$
Radius of wheel	$r = 0.102$ m
Torque	$r \times F = 0.102 \times 1.31 = 0.1336 Nm$
Velocity	$\dfrac{d}{t} = \dfrac{1.5}{4} = 0.375 m/s$
RPM	$N = \dfrac{v \times 60}{r \times \pi} = \dfrac{0.375 \times 60}{0.102 \times 3.14} = 70.25$
Angular Velocity	$\dfrac{2\pi N}{60} = \dfrac{2 \times 3.14 \times 70.25}{60} = 7.35$
Power required	Angular Velocity$\times$Torque $= 7.35 \times 0.1336 = 0.981$watt

Table 1. Calculation of air flow of fan

3.2 Power Required

Weight was found to be 3.5kg (Maximum with Gear). The power required to rotate the wheels at a specific speed is found [21]. Other necessary formulations are given below.

Design Parameters	Formulation
Length	0.1476 ft
RPM	3000
Average air speed	$L \times RPM = 0.1476 \times 3000 = 442.8$ ft/min
Diameter of fan	$d = 0.2952$ft
Area of fan	$\dfrac{\pi d^2}{4} = \dfrac{3.14 \times 0.2952^2}{4}$
Air flow of fan	Area x Average air speed= 0.068 x 442.8 = 30.30 cfm

Table 2. Calculations of gear motor

To meet these above requirements, the selection of JGA25-370 DC Gear motor was done and its specifications are represented in appendix C at the end of paper.

93

3.3 ADCR Speed Control Calculations

In speed analysis, finding the theoretical speed of robot on duct using following equations. As power can be found as [24]

$$P = T(\omega)\omega \qquad (1)$$

Then acceleration will be

$$a = \frac{T(\omega)\omega}{mv} \qquad (2)$$

The time taken to reach the speed 'v' is

$$t = \int_0^v \frac{1}{a} dv \qquad (3)$$

$$t = \int_0^v \frac{mv}{T(1 - \frac{v}{\omega r})\frac{v}{r}} \qquad (4)$$

$$v(t) = v(1 - e^{\frac{-T \times t}{r \times m \times v}}) \qquad (5)$$

Where v=ω * r ,

Given data, t=1 sec, ω= 15.7rad/s, motor torque=T= 0.04 Nm, Radius of tire= r = 0.045 m, Mass of robot = 3.5 kg, inserting values in equation (5), the speed of robot V (theoretical) was found to be 0.213 m/s. It is meant that robot cover 0.213-meter distance in 1 sec. Experimentally V(actual) was found to be 0.186 m/s, hence efficiency of robot speed will be [25]

$$\eta = \frac{\text{Actual Speed}}{\text{Theoretical speed}} \times 100 \qquad (6)$$

$$\eta = \frac{0.186}{0.213} \times 100$$

$$\eta = 87.32\%$$

This is efficiency of air duct cleaning robot and it is appropriate speed for dust collection. For a 1-radian step reference, following controlled states are given below [26]

- Settling time smaller than 0.040 seconds
- Overshoot smaller than 16%
- Steady-state error is zero.

The open loop response of the system is shown below in the figure. This response is generated in MATLAB®.

$$\frac{0.044}{9.45e^{-5}s^2 + 6.5e^{-2}s} \qquad (7)$$

The required response of the system is that the distance covered by the Air Ventilation Duct's Cleaning Robot increases as the current increases.
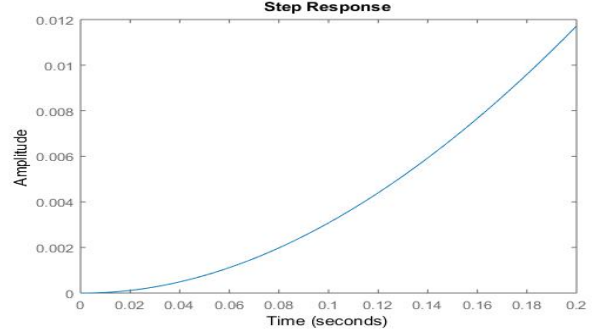
Figure 5. Graph of Step Response of DC Gear Motor

The closed-loop response yields a more precise and accurate simulation when compared with the open-loop response. The transfer function in case of the closed-loop is given as:

$$\frac{0.044}{9.45e^{-5}s^2 + 6.5e^{-2}s + 0.1319} \qquad (8)$$

4. RESULTS AND DISCUSSIONS

4.1 Performance Evaluation On The Basis Of Dust Collection

Suction is tested on duct prototype of (8 *1 * 2) feet (length * height * width) in dimension. Table 1 summarized the results before and after cleaning. A common vacuum cleaner operate at the range of 50-100 cfm and this ADCR has vacuum suction of 60 cfm [22]. It is in the range of other vacuum cleaner and it can clean all dust particles inside the duct in one forward movement [18]. Performance of this suction was also verified by dust collection evaluation which concludes the

better suction for the sampled atmosphere. It can be seen from the figure 6 ,7, the duct collection process.

Figure 6. ADCR before Cleaning

Figure 7. ADCR after Cleaning

Test No.1			Test No.2			
Dust Weight (g) before operation	Dust Weight (g) After in duct	Percentage Dust Reduction (%)	Before in duct	After in duct	Percentage Dust Reduction (%)	Overall dust removed (%)
4.11	0.7	82.9	0.7	0.6	14.28	85.40

The purpose was to get maximum cleaned surface. Two tests were carried out simultaneously. Dust particles collected has net approximate weight of 4.11g which then undergoes cleaning operation. Finally in comparison of percentage dust reduction of dust particles was found to be 82.9%. ADCR is put again in duct for second test. Dust collection is reduced, it was due to some sticky particles. It is evident that percentage dust collection will be further reduced for further tests and it may become steady. Overall efficiency from the beginning of operation is 85.40 % hence suction is proven appropriate and sufficient for the sampled duct. In that way, the system may be enhanced to more complex duct and dimensions.

The environmental benefit of Air Ventilation Duct's Cleaning Robot is that it creates a cleaner living environment by reducing allergies and irritants which help everyone to breathe easier and improve air flow efficiency [27].

It was addressed and claimed in [28] that average one-time duct cleaning cost by applying labour is $200 which is very expensive while air duct cleaning robot (ADCR) manufacturing cost is $180 only and this is one time cost and the cleaning function can be performed multiple times.

4.2 Time Consumption Analysis

ADCR moves with different velocities at different points. By using standard deviation of all working velocities of robot. At these optimum velocities, the time taken by robot for one operation/test is calculated below.

Initial speed = v1= 0.213 m/s

Speed while dust collection in process = v2 = 0.186 m/s

Speed at turn = v3 =0.160 m/s

Speed where dust will maximum = v4 = 0.174 m/s

$$\text{Standard deviation} = S.D = \sqrt{\frac{(v-\mu)^2}{N}} \quad (9)$$

$$\text{Mean} = \mu = \frac{v_1 + v_2 + v_3 + v_4}{4} \tag{10}$$

$$\text{Mean} = \mu = 0.1832 \, m/s$$

$$\text{Standard deviation} = S.D = 0.0194$$

Vmini = 0.1636 m/s, Vmax = 0.202 m/s and size of duct prototype = 2.74 m

At minimum velocity:

$$t_{mini} = 16.7 \, s$$

At maximum velocity:

$$t_{max} = 13.5 \, s$$

As velocities in the duct is varying throughout the duct. The time has been calculated and can have any value between the ranges of 13.5 to 16.7 seconds.

5. CONCLUSION AND RECOMMENDATIONS

If a duct is being cleaned by labour, the dust contaminants like asbestos can produce health hazards like lung scarring and fibrosis which in later stages can cause cancer. Most of the cases, irritating particles can produce disfunctioning of mucous membranes of the nose and throat. Though covering of face by mask can reduce the risk but still the particles can attach to PPE if safety measures had not taken during cleaning. It also can cause chronic pulmonary disease like emphysema and bronchitis. In order to facilitate the cleaning of duct, an autonomous air duct cleaning robot (ADCR) is designed, which consists of sensory based integration of parts. This autonomous strategy can reduce human effort. The ADCR dust collection and time taken analysis of mechanism is the necessary performance evaluation criteria which is an additional ingredient to the previous work. Amount of dust is significantly reduced to 85 percent in second test. Multiple tests can be performed in order to increase the percentage dust collected. It has been noticed that one operation/test can take up to approximately 16.7 seconds. Time taken by mechanism to complete one operation/test was performed.

These performance criteria's lead the way towards the effective and reliable design solution. The consideration of environment and social benefits in second paragraph of section 4.1 has enhanced its advantages to local community and has concluded the strategy to be viable in future.

ACKNOWLEDGEMENT

Appendix A

Operating Voltage	5V
Input Voltage (recommended):	7-12V
Input Voltage (limit)	6-20V
Digital I/O Pins	54 (of which 15 provide PWM output)
Analog Input Pins	16
DC Current per I/O Pin	20 mA
DC Current for 3.3V Pin	50 mA
Flash Memory	256 KB of which 8 KB used by bootloader
SRAM	8 KB
EEPROM	4 KB
Clock Speed	16 MHz
LED_BUILTIN	13
Length	101.52 mm
Width	53.3 mm
Weight	37 g

Table 4. Microcontroller ATmega2560 Specifications

Appendix B

Voltage	DC 5V
Static current	Less than 2mA
Level output	High-5V
Level output	The end of 0V
Sensor angle	15 degrees
Detection distance	2cm-450cm
High precision	Up to 0.3 cm
Connection	VCC, trig(control side), echo(receiving end), GND

Table 5. Specification of Ultrasonic Sensor

Appendix C

Operating voltage	Between 3 V and 9 V
Nominal voltage	6 V
The free-run speed at 6 V	281 RPM
Free-run current at 6 V	80 mA
Stall current at 6V	900 mA
Stall torque at 6V	4 kg.cm
Gear ratio	1:21
Weight	84 g

Table 6. Specifications of JGA25-370 DC Gear motor

REFERENCES

[1] W. Wu, H. Skye, and P. Domanski, "Selecting HVAC Systems to Achieve Comfortable and Cost-effective Residential Net-Zero Energy Buildings," Appl. Energy, vol. 212, pp. 577–591, Feb. 2018.

[2] J. Shim and R. C. Arkin, "Robot Deception and Squirrel Behavior: A Case Study in Bio-inspired Robotics," 2014.

[3] CDC, "Appendix B : HVAC Systems and Indoor Air Quality," Cdc, 2014.

[4] W. Jeong and S. Researcher, "Performance Analysis of a Mobile Duct Cleaning Robot 1," vol. 7, pp. 26–32, 2014.

[5] P. Gloriani, N. Rahman, and D. Caldwell, "ScienceDirect ScienceDirect ScienceDirect models for capacity in Industry Novel Integrated Robotic System for Tiny Duct Inspection," Procedia Manuf., vol. 17, pp. 342–349, 2018.

[6] S. G. Faal, "Design and Analysis of a Robotic Duct Cleaning System," 2011.

[7] R. Seals, "Mobile robotics," Electron. Power, vol. 30, no. 7, p. 543, 2010.

[8] A. Bulgakov and D. Sayfeddine, "Air Conditioning Ducts Inspection and Cleaning Using Telerobotics," Procedia Eng., vol. 164, no. June, pp. 121–126, 2016.

[9] W. Jeong, S. W. Jeon, D. Park, and S. B. Kwon, "Force control of a duct cleaning robot brush using a compliance device," ICINCO 2012 - Proc. 9th Int. Conf. Informatics Control. Autom. Robot., vol. 2, pp. 372–376, 2012.

[10] I. Survey and I. Survey, "CHAPTER 2," no. 1992, pp. 9–21, 1997.

[11] D. Version, "Removal of Particles from the Supply Air of Ventilation Systems Avoiding the Formation of Sensory Pollution Source Delivery of Clean Air to Building Occupants D o c t o r a l d i s s e r t a t i o n," 2008.

[12] M. A. Koledoye, "Design of a Mobile Robot for Air Duct Exploration," 2017.

[13] P. Shukla, "Design of Inspection and Cleaning Robot," Int. J. Sci. Res. Eng. Technol., vol. 3, no. 6, pp. 2278–882, 2014.

[14] W. Ya and Z. Jianhua, "Autonomous Air Duct Cleaning Robot System,"

undefined, vol. 1, pp. 510–513, 2006.

[15] G. Mester, "Applications of Mobile Robots Unmanned Autonomous Systems View project Self-Driving Cars View project," 2006.

[16] W. Jeong, S. W. Jeon, and D. Park, "Operational effects of a mobile robot system for cleaning ventilation ducts," ACM Int. Conf. Proceeding Ser., 2013.

[17] S. Pedre, M. Nitsche, and F. Pessacg, "Design of a Multi-purpose Low-Cost Mobile Robot for Research and Education Design of a multi-purpose low-cost mobile robot for research and education," no. September, 2014.

[18] Z. Bhuiyan, Design analysis of Dust collection system. 2020.

[19] "ASTM F1005 - 91(2013) Standard Practice for HVAC Duct Shapes; Identification and Description of Design Configuration." .

[20] E. Pawar, "A Review Article on Acrylic PMMA Eshwar Pawar," ISOR J. Mech. Civ. Eng., vol. 13, no. 2, pp. 1–4, 2016.

[21] V. Gajbhiye, N. Ahmad, and M. S. Tufail, "Design and Application of D.C. Vacuum Cleaner using Axial Flow Fan," Int. J. Eng. Tech., vol. 4, no. 1, 2018.

[22] A. Viegand Maagøe and B. V. Van Holsteijn en Kemna, "Review study on vacuum cleaners - Final report," no. June, 2019.

[23] D. Karayel, Z. B. Barut, and A. Özmerzi, "Mathematical modelling of vacuum pressure on a precision seeder," Biosyst. Eng., vol. 87, no. 4, pp. 437–444, 2004.

[24] X. Jiang, L. Chen, X. Xu, Y. Cai, Y. Li, and W. Wang, "Analysis and optimization of energy efficiency for an electric vehicle with four independent drive in-wheel motors,"

Adv. Mech. Eng., vol. 10, no. 3, pp. 1–9, 2018.

[25] M. S. Essers and T. H. J. Vaneker, "Developing concepts for improved efficiency of robot work preparation," Procedia CIRP, vol. 7, pp. 515–520, 2013.

[26] A. S. Semenov, V. M. Khubieva, and Y. S. Kharitonov, "Mathematical modeling of static and dynamic modes DC motors in software package MATLAB," 2018 Int. Russ. Autom. Conf. RusAutoCon 2018, pp. 1–5, 2018.

[27] "DOHS Fact Sheet on HVAC Duct Cleaning DOHS Fact Sheet on HVAC Duct Cleaning," vol. 04, no. 301, pp. 4–6, 2015.

[28] "2020 Air Duct Cleaning Costs | Clean AC, Furnace, HVAC Vents - HomeAdvisor." .

PREDICTION & COMPARISON OF OPTIMAL MACHINING PARAMETERS OF ALUMINIUM ALLOY Al5454 BY WIRECUT ELECTRICAL DISCHARGE MACHINE USING STATISTICAL METHOD AND MACHINE LEARNING ALGORITHM

Maria Iruj[1], Anis Fatima[1], Muhammad Wasif[1], Muhammad Tufail[1]

[1]Department of Industrial and Manufacturing Engineering, NED University of Engineering and Technology, Karachi. Pakistan.

[*]*Corresponding author E-mail address:* <u>wasif@neduet.edu.pk</u>

ABSTRACT

Aluminum and its alloys are widely adopted material in industries like aviation and avionics because of its durability and strength as compared to their inherited lightness. These industries require extreme precision for which nontraditional machining processes are employed. Wirecut electrical discharge machining (WEDM) is one of the commonly used technique which gives satisfactory results of required accuracy and precision. It is a complex process for optimization, because of the involvement of multiple input and output variables. This research aims to optimize the WEDM for aluminum targeting four major output variables, i.e. material removal rate (MMR), surface roughness (SR), wire wear rate (WW) and kerf width (KW) on different sets of input variables, namely cutting angle, pulse on-time (POT) and current. By using actual experimental machining data, Response Surface Methodology (RSM) and Artificial Neural network (ANN) are employed and compared, based on root mean square error, and coefficient of determination. The results declare that both RSM & ANN give accurate results and can be used as a reliable means for predictions, but ANN gives a little improved prediction than RSM.

Keywords: Wirecut Electric Discharge Machining (WEDM), Artificial Neural Network (ANN), Response Surface Methodology (RSM), Root Mean Square Error (RMSE), Regression Value (R2).

1. INTRODUCTION

In recent years, aluminum and aluminum alloys have been widely used in the automotive industry. Their prominent properties include low density, have good formability and formability, high resistance to corrosion, and high electrical and thermal conductivity. Due to their excellent combination of mechanical, physical and tribological properties compared to base alloys, aluminum alloys are of enormous industrial importance. These properties include high specific strength, high resistance to wear and seizure, high stiffness, better resistance to high temperatures, a not least, a controlled coefficient of thermal expansion.[1]. For their precise machining, electrical discharge machining (EDM) and wire EDM are widely used methods worldwide. EDM, which is the most widely used non-traditional material exclusion processes, is a non-conventional, non-contact type machining processes, where the material is detached with the help of stimulated frequency sparks generated between the tool and work piece [2]. Due to the absence of physical contact of tool and

99

work piece, this process can be used for any type of material regardless of their hardness, provided the material is electrically conductive [3,4]. Its prominent feature is the use of thermal energy to machine electrically conductive parts irrespective of their hardness, which proves to be its typical advantage in the manufacturing of different dies & molds and specifically to bring innovation in the automotive, aerospace and surgical components. The process is interesting to study with having different variables to evaluate, which include a long list of electrical as well non-electrical parameters that have great potential for a substantial amount of research. The optimum selection of the EDM process parameters is critically important to obtain an energy and material efficient process design. Numerous researchers carried out several investigations for refining the process performance, and have been brining optimal solutions for many of the process parameters and variables [[5,6,7]

From the list of all parameters and variables EDM offers, machining parameters comes in first place by playing a crucial role in achieving high precision or high tolerance machining with the required quality of the other output responses[8] .The selection of machining parameters is critical, as altering one parameter may disturb the optimization model for this process.. Hence, there is an actual justification for the ongoing experimentation and research that is striving to support and generate a systematic mathematical approach supported by artificial intelligence to obtain the optimum combination of multiple inputs and output parameters for different work piece and wire materials, in order to get better overall optimum machining performance and process efficiency in WEDM process. On discussing the overall process efficiency, the parameters with highest level of importance in terms of performance trials in WEDM,

material removal rate (or sometimes the cutting speed), surface finish and kerf (cutting width), and wire wear are considered as the prime variables to start with. The same are being considered in this research.

The process to determine an optimum model for a sustainable WEDM process requires thorough knowledge of this process, empirical equations based on realistic constraints as well different mathematical based optimization techniques [9]. The selection of optimal combination of parameters for the process is the job of the process planner who incorporates his experience to the model to get the sustainable solution of the process. The experience is achieved by experimentation which is a costly, time consuming and tedious approach for sustainability [10]. When we talk about the real-life support for the EDM process in terms of sustainability, low energy consumption and better productivity, the manufacturer must be provided with workable mathematical models. The most common practice to get a sustainable working model for WEDM is to employ the theoretical or empirical based models, which are never up to the mark for obvious reasons [11]. The empirical models have been formulated on the basis of specific, limited experimental setups, for example the type of objective function, constraints (linear, nonlinear) number and nature of variables used (integer, continuous etc.), solution space size, solution space structure (convex, non-convex etc.), are too not predictive and supportive of the actual WEDM process [11,12,13,14] Hence, the latest trends in research goes with incorporating the concept of machine learning and artificial intelligence for the optimization modelling of WEDM.

Machine learning is becoming an increasingly popular concept in the modern world since its common goal is to optimize systems by allowing one to make smarter use

of products and services. In the manufacturing industry machine learning can lead to cost savings, time savings, increased quality, and waste reduction. [15] At the same time, it enables systems to be designed for managing human behavior. Machine learning is the concept of enabling the computer to take out decisions without being explicitly programmed. Here the systems are trained on some of the predefined algorithm, are trained to sparse from those algorithms, learn from them, and take decisions on the basis of inference and pattern of the data. The latest research trend is focused on the incorporation of machine learning with the existing manufacturing practices to achieve optimized production systems. [15]

Neural Network, more commonly termed as Artificial neuro network or ANN, is the extensively applied model for corelating the complex, non-linear behavior of many machining models, especially in WEDM [16]. an algorithm derived from the biological pattern of human brain, in which neurons are responsible for sending and receiving signals and eventually taking decisions as what to do when a particular event happens. In machine learning, a neural network is used where there is a non-linear relationship between the input and output layer. The layers are categorized as an input layer, a hidden layer, and an output layer. The layers are having their levels of weightage and biasness and utilize the basic mathematical functions, like linear activation function, sigmoid activation function, tangent hyperbolic activation function, hyperbolic tangent sigmoid activation function, logistic activation function etc. [17]. The sequence for development and application of ANN starts with training, then the algorithm validation and ending with the testing. There are various training algorithms like Conjugate Gradient Descent (CGD), Bayesian Inference (BI), Levenberg

Marquardt Algorithm. Various statistic based measures are used to check for the net error, among which Mean Absolute Percentage Error (MAPE), Mean square error (MSE), Regression values (R or R2), and maximum or average relative error are the commonly used ones [18]. To skip this phase of validation, the Bayesian regularization can be adopted during the training stage [19]. Different possible NNs are being used in machine learning, where feed-forward NN (FFNN) and back-propagation NN (BPNN) are the most frequently adopted ones [20]. Response surface methodology (RSM) is a statistical method for used for planning the experiments, constructing related models and assessing the inter relationship of input parameters on responses, and is a commonly used tool for optimization of processes (21) It generates experimental patterns by approaching the factual efficient association between the conditional variable(s), i.e. the response surface and a set of investigational factors which are provided to the system as input, or self-governing variables. Both ANN and RSM are the convenient techniques for prediction of different process parameters, and are commonly used in many non-traditional machining processes across the globe, including WEDM by researchers.

K. P. Somashekhar et. al [22] worked on optimizing the WEDM process by focusing on MRR and employed the feed forward artificial neuro network to model the machining process. He even proceeded the optimization by AI in micro WEDM and targeted the MRR as the response variable. The feed forward ANN with back propagation algorithm was used to obtain a higher MRR The theoretical models have been developed on the basis of the mandatory laws and have assumptions to avoid the complications, which obviously doesn't support the actual process. M.A.M. Zakaria et. al [23] also worked on WEDM

sustainability in terms of MRR and surface roughness. Their research employed ANN as the modeling tool and found the results satisfactory. To overcome the unpredictive support of WEDM optimization models, the latest trend of research goes into utilizing the artificial intelligence techniques because of their ability to overcome the non-linearity between the input parameters and output response, and to effectively handle the incomplete data and encountering the multiple variables. [24,25,26].

As discussed in the initial paragraphs above, the popular empirical optimization techniques have been employed are Response surface methodology (RSM) and Taguchi method, which are extensively used in modelling the process parameters with respect of optimization and sustainability [27,28,29,30]. All of these approaches target towards the optimization of the overall process but are unable to provide a generic approach for the optimization problem while having different sets of variables types, objectives and constraints. Research shows that employment of artificial intelligence-based models brings up to three times more accurate results than the one achieved by the statistical methods and hence are the ultimate options to work on the sustainability based parametric model for WEDM. Shandilya et al. [26] observed this support in making energy focused model by employing AI techniques while machining of composites with WEDM. Devarasiddappa et al. [27] supports the same idea as he observed the values of surface roughness while machining the aerospace alloys and employing AI techniques and getting the level of accuracy as high as 93.62%. He also urged the researchers to further develop an ONLINE SYSTEMS based on artificial intelligence by probably using ANN technique. Muthukrishnasen and Davim [28] states that ANN offers higher potential for predicting non experimental patterns. They carried their

research on WEDM focusing of MRR and surface roughness only, and used water based di electric which offers greater difficulty in understanding the cutting parameters of WEDM. Their results provided a good prediction when it produced the average relative error of 0.27% and 0.67% in MRR and surface roughness respectively.

D. Devarasiddappa et. al [31] developed an ANN based model by using Box Behnken experimental design for the prediction of surface roughness of aerospace alloy Inconel 825 against few of the input parameters and the developed model showed an accuracy of 93.62% with an average error of 6.38%. Girish Kant et. al [32] used SVR (support vector regression) model along with the ANN (artificial neuro network) to evaluate the WEDM process for the optimal prediction of energy consumed in the machining process An investigation on WEDM is also carried out by using neuro-fuzzy inference system to get sustainable model which supports higher productivity by focusing on the overall quality of the machined product and less heat-affected zone [33]. A Conde [34] declares that the prediction of the machined part accuracy of WEDM process is too, highly unpredictive in nature, and there have been very little efforts in getting it modelled due to many of the phenomena involved in the WEDM process which are not clear yet. He has presented an AI model based on Elman-based Layer Recurrent Neural Network which supports the accuracy of machined part by WEDM, based on the wear rate of tool wire. His model reduced the average deviation of the machined parts due to wire deformation by 80%. Sandeep Kumar et.[35] al experimented on WEDM by using the titanium super alloy Ti–6Al–4V and employed the ANFIS (adapted neuro fuzzy inference system) model and investigated the effect on MRR and surface roughness of the machined product. Deepak Kumar et. al [36]

102

also derived a model for higher MRR by the WEDM process by using the feed forward ANN method based on the Levenberg-Marquardt back propagation. The AI techniques namely SVM (support vector machines) along with GP (Gaussian process) and ANN to evaluate the WEDM characteristics while machining the Nimonic-90 super alloy, extensively used in aerospace industry, while focusing on the surface roughness values of the machined part [37]. Yen et. al [38] worked with Inconel 718 on WEDM and adopted ANN for multivariable optimization. Cascade forward back propagation neural network (CFNN) was employed and there was 5.16% error. They also worked on Ti–48Al intermetallic alloys with ANN supported by multi objective genetic algorithm (multi GA) [39]. The results yielded optimized solution for few of the input and output response variables of the WEDM system.

Numerous procedures are accessible to define the basics of a RSM model. RSM and design of experiments (DOE) technique is governed by the Box-Behnken design. For instances, CCD (central composite design) and full factorial design [40] are dominated to enforce trials in a fashion that the correlation impact between all the factors significantly be recognized with minimal number of tests. ANOVA is a kind of analysis applies to accomplish further to evaluate the range of impact among numerous factors as well as the connections between them [41]. There is Grey rational analysis (GRA) or weighted GRA which identifies the multiple responses and the inter relationship between them, where GR coefficients (or weight factors) are defined for multiple factors [42]. Further, the RSM model is confirmed by the ANOVA analysis [43] and the determined variation between the tested outcomes and the RSM model is noted.

2. EXPERIMENTAL DESIGN

For investigating the impact of the selected three process parameters for four of the output responses, we need a considerable number of experiments. Using the RSM methodology, however, we can significantly reduce the amount of experimentation required, while not compromising on the effects of factors as well as their interaction. The quantitative form by RSM is shown in equation 1, showing relationship between input and output variables [44].

$$y = f(x_1, x_2, \ldots, x_k) + \varepsilon \tag{1}$$

where "f" is the response function of controllable input parameters $x_1, x_2, \ldots x_k$, and "y" is the dependent output parameter and ε represents the statistical error.

$$Y = \beta_o + \sum_{i=1}^{n} \beta_1 X_{i+} \sum_{i=1}^{n} \beta_n Xi^2 + \sum_{i<j}^{n} \beta_{iJ} XijXiXj + \varepsilon \tag{2}$$

Equation (2) is a lower order polynomial equation for the true output-input relationship, where the unknown constants β's are estimated by regression analysis.

2.1 Experimental Setup

Fig 1 shows the CHMER CW-43CF CNC EDM wire cut resent at the department of industrial & manufacturing engineering, NED University, with a machining envelope of 500 mm × 350 mm × 200 mm along its x, y and z axis. The values of kerf width were calculated through microscopic photography and the MM 500-T MTI corporation microscope was used having an attached digital camera DCM 310. Four different distances, that were 3,5,7 and 10mm, were marked to capture the snapshots of the work piece. Two readings were taken at each distance and the average of the two was taken as the final reading.

ConturoMatic T2 Surface roughness meter

was used for the measurement of surface roughness (Ra). It has a range of measuring up to 250 mm × 320 mm of workpiece with a resolution of 0.033 μm. Surface roughness was measured on each slot of workpiece at three different places,10%, 50% and 100% of the height of work piece, for incorporating the studying the varying thickness impact. The mean of average surface roughness measured with the mentioned criteria was used as the final reading.

Wire wear (WW) was calculated by subtracting the weight of wire after the WEDM cutting from the initial wire weight (measured before machining). An electronic physical balance with the least count of 0.0001 was used for this measurement.

The metal removal rate was found out by employing the equation number 3.

$$MRR=\Delta m/\rho \cdot Tm \qquad (3)$$

Where Δm is the change in mass of the Al5454 work piece, ρ is its density, and Tm is the machining time for the same. The experimental design matrix is shown in table 1.

Figure 1.

Material	Angle	Current	POT	SR	MRR	WW	KW	SR(mm)	MRR(msec/mm³)	WW(mg)	KW(mm)
Aluminum	30	5	20	0.0245	16.8255	0.0732	0.430000	0.0265	17.0127	0.0732	0.4425
Aluminum	30	5	20	0.0285	17.1999	0.0732	0.455000				
Aluminum	45	5	20	0.0215	12.9876	0.0742	0.407500	0.0275	13.1399	0.0827	0.4100
Aluminum	45	5	20	0.0335	13.2922	0.0912	0.412500				
Aluminum	60	5	20	0.0325	8.7959	0.1483	0.362500	0.0308	9.0130	0.1221	0.3863
Aluminum	60	5	20	0.0290	9.2300	0.0958	0.410000				
Aluminum	30	10	20	0.0395	27.5929	0.0703	0.565000	0.0368	25.9529	0.0768	0.5650
Aluminum	30	10	20	0.0340	24.3128	0.0834	0.565000				
Aluminum	45	10	20	0.0530	18.1123	0.0872	0.382500	0.0525	18.0898	0.0910	0.3838
Aluminum	45	10	20	0.0520	18.0672	0.0947	0.385000				
Aluminum	60	10	20	0.0555	15.4982	0.1566	0.387500	0.0478	16.1988	0.0817	0.4050
Aluminum	60	10	20	0.0400	16.8994	0.0067	0.422500				
Aluminum	30	5	40	0.0250	19.4838	0.0900	0.430000	0.0188	14.9529	0.0898	0.4463
Aluminum	30	5	40	0.0125	10.4220	0.0897	0.462500				
Aluminum	45	5	40	0.0180	9.7765	0.1115	0.340000	0.0245	9.7179	0.1183	0.3539
Aluminum	45	5	40	0.0310	9.6593	0.1250	0.367700				
Aluminum	60	5	40	0.0375	7.0178	0.0667	0.347500	0.0365	7.4243	0.0555	0.3850
Aluminum	60	5	40	0.0355	7.8307	0.0444	0.422500				
Aluminum	30	10	40	0.0330	22.9988	0.0693	0.562500	0.0290	23.4521	0.0719	0.5525
Aluminum	30	10	40	0.0250	23.9054	0.0745	0.542500				

Material	Angle	Current	POT	SR	MRR	WW	KW	SR(mm)	MRR(msec/mm³)	WW(mg)	KW(mm)
Aluminum	45	10	40	0.0630	15.3509	0.1127	0.280000	0.0608	16.7091	0.1259	0.2988
Aluminum	45	10	40	0.0585	18.0672	0.1391	0.317500				
Aluminum	60	10	40	0.0548	10.5454	0.1258	0.412500	0.0439	11.0519	0.1074	0.3938
Aluminum	60	10	40	0.0330	11.5584	0.0890	0.375000				

Table 1.

3. RESULT
3.1 Response Surface Methodology Modeling Results

MINITAB software is used for RSM modeling. The predicted response equations for MRR, SR, WW and KW are listed respectively as Equations no. 4,5,6, & 7.

$$MRR = 23.3 - 0.314 \text{ Angle} + 1.34 \text{ Current} - 0.134 \text{ POT} \quad (4)$$

$$SR = -0.0061 + 0.000399 \text{ Angle} + 0.00354 \text{ Current} - 0.000070 \text{ POT} \quad (5)$$

$$WW = 0.0571 + 0.000457 \text{ Angle} + 0.00044 \text{ Current} + 0.000346 \text{ POT} \quad (6)$$

$$KW = 0.579 - 0.00364 \text{ Angle} + 0.00583 \text{ Current} - 0.00135 \text{ POT} \quad (7)$$

3.2 Artificial Neural Networks Modeling Results

In this study, Levenberg-Marquardt (LM) training method, a multilayer feed-forward artificial neural network (ANN), is trained, using the Neural Network Toolbox of MATLAB. This is the most effective feed forward network, with respect to the training precision. [44] Figure 2 shows the used ANN pattern, which consists of an input layer of three neutrons representing angle, current and POT, one hidden layer of 20 neutrons, and an output layer of four neutrons representing the MRR, SR. KW and WW.
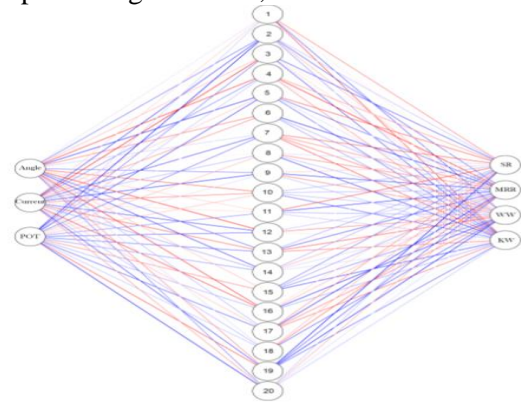

Figure 2

Material	Angle	Current	POT	SR	MRR	WW	KW	SR(mm)	MRR(msec/mm³)	WW(mg)	KW(mm)
Aluminum	30	5	20	0.0245	16.8255	0.0732	0.430000	0.0265	17.0127	0.0732	0.4425
Aluminum	30	5	20	0.0285	17.1999	0.0732	0.455000				
Aluminum	45	5	20	0.0215	12.9876	0.0742	0.407500	0.0275	13.1399	0.0827	0.4100
Aluminum	45	5	20	0.0335	13.2922	0.0912	0.412500				
Aluminum	60	5	20	0.0325	8.7959	0.1483	0.362500	0.0308	9.0130	0.1221	0.3863
Aluminum	60	5	20	0.0290	9.2300	0.0958	0.410000				
Aluminum	30	10	20	0.0395	27.5929	0.0703	0.565000	0.0368	25.9529	0.0768	0.5650
Aluminum	30	10	20	0.0340	24.3128	0.0834	0.565000				
Aluminum	45	10	20	0.0530	18.1123	0.0872	0.382500	0.0525	18.0898	0.0910	0.3838
Aluminum	45	10	20	0.0520	18.0672	0.0947	0.385000				
Aluminum	60	10	20	0.0555	15.4982	0.1566	0.387500	0.0478	16.1988	0.0817	0.4050
Aluminum	60	10	20	0.0400	16.8994	0.0067	0.422500				
Aluminum	30	5	40	0.0250	19.4838	0.0900	0.430000	0.0188	14.9529	0.0898	0.4463

105

Aluminum	30	5	40	0.0125	10.4220	0.0897	0.462500				
Aluminum	45	5	40	0.0180	9.7765	0.1115	0.340000	0.0245	9.7179	0.1183	0.3539
Aluminum	45	5	40	0.0310	9.6593	0.1250	0.367700				
Aluminum	60	5	40	0.0375	7.0178	0.0667	0.347500	0.0365	7.4243	0.0555	0.3850
Aluminum	60	5	40	0.0355	7.8307	0.0444	0.422500				
Aluminum	30	10	40	0.0330	22.9988	0.0693	0.562500	0.0290	23.4521	0.0719	0.5525
Aluminum	30	10	40	0.0250	23.9054	0.0745	0.542500				
Aluminum	45	10	40	0.0630	15.3509	0.1127	0.280000	0.0608	16.7091	0.1259	0.2988
Aluminum	45	10	40	0.0585	18.0672	0.1391	0.317500				
Aluminum	60	10	40	0.0548	10.5454	0.1258	0.412500	0.0439	11.0519	0.1074	0.3938
Aluminum	60	10	40	0.0330	11.5584	0.0890	0.375000				

Table 2. Experimental Data Input to the ANN

Material	Angle	Current	POT	SR	MRR	WW	KW
Aluminum	65	5	20	0.044527	13.15432	0.123374	0.353404
Aluminum	65	5	20	0.044527	13.15432	0.123374	0.353404
Aluminum	70	5	20	0.052071	16.80477	0.125314	0.322816
Aluminum	70	5	20	0.052071	16.80477	0.125314	0.322816
Aluminum	80	5	20	0.056926	22.4186	0.141862	0.308377
Aluminum	80	5	20	0.056926	22.4186	0.141862	0.308377
Aluminum	65	10	20	0.035456	15.12925	0.070847	0.397208
Aluminum	65	10	20	0.035456	15.12925	0.070847	0.397208
Aluminum	70	10	20	0.016	13.86752	0.064242	0.360217
Aluminum	70	10	20	0.016	13.86752	0.064242	0.360217
Aluminum	80	10	20	0.002683	9.990425	0.081416	0.369295
Aluminum	80	10	20	0.002683	9.990425	0.081416	0.369295
Aluminum	65	5	40	0.046396	5.189628	0.067924	0.449992
Aluminum	65	5	40	0.046396	5.189628	0.067924	0.449992
Aluminum	70	5	40	0.05317	3.769608	0.075708	0.489158
Aluminum	70	5	40	0.05317	3.769608	0.075708	0.489158
Aluminum	80	5	40	0.044492	0.378173	0.071855	0.481392
Aluminum	80	5	40	0.044492	0.378173	0.071855	0.481392
Aluminum	65	10	40	0.056883	12.00963	0.088767	0.34934
Aluminum	65	10	40	0.056883	12.00963	0.088767	0.34934
Aluminum	70	10	40	0.06709	14.74477	0.062524	0.298594
Aluminum	70	10	40	0.06709	14.74477	0.062524	0.298594
Aluminum	80	10	40	0.086439	21.23889	0.048611	0.267259
Aluminum	80	10	40	0.086439	21.23889	0.048611	0.267259

Table 3. Values predicted by ANN Model

3.3 Comparison of the performance of RSM and ANN modeling

The results of RSM and ANN are compared by calculating the coefficients of determination (R2) and the Root Mean Square Error (RMSE) for the four output parameters. The equations for these are listed below as equations 8 and 9 respectively.

$$R^2 = 1 - \frac{\sum_{i=1}^{n}(yi - y0i)^2}{\sum_{i=1}^{n}(y0i - ym)^2} \qquad (8)$$

106

$$RMSE = \frac{1}{n}\sum_{i=1}^{n}(yi - yai)^2 \qquad (9)$$

where "n" is the total no. of experiments, "yi" is the value predicted from the trained ANN model, "yai" is the actual value provided to the system as training data, and "ym" is the mean of the actual values obtained through the experimentation.

3.4 Results of ANOVA
General Linear Model: SR versus Angle, Current, POT

```
Factor   Type    Levels  Values
Angle    fixed      3    30, 45, 60
Current  fixed      2    5, 10
POT      fixed      2    20, 40
```

Analysis of Variance for SR, using Adjusted SS for Tests

```
Source   DF   Seq SS     Adj SS     Adj MS       F      P
Angle    2    0.0008796  0.0008796  0.0004398   5.95  0.010
Current  1    0.0018780  0.0018780  0.0018780  25.39  0.000
POT      1    0.0000116  0.0000116  0.0000116   0.16  0.696
Error    19   0.0014053  0.0014053  0.0000740
Total    23   0.0041745
```

S = 0.00860022   R-Sq = 66.34%   R-Sq(adj) = 59.25%

General Linear Model: MRR versus Angle, Current, POT

```
Factor   Type    Levels  Values
Angle    fixed      3    30, 45, 60
Current  fixed      2    5, 10
POT      fixed      2    20, 40
```

Analysis of Variance for MRR, using Adjusted SS for Tests

```
Source   DF  Seq SS  Adj SS  Adj MS      F      P
Angle    2   362.91  362.91  181.45  45.92  0.000
Current  1   269.26  269.26  269.26  68.14  0.000
POT      1    43.20   43.20   43.20  10.93  0.004
Error    19   75.08   75.08    3.95
Total    23  750.44
```

S = 1.98787   R-Sq = 90.00%   R-Sq(adj) = 87.89%

General Linear Model: WW versus Angle, Current, POT

```
Factor   Type    Levels  Values
Angle    fixed      3    30, 45, 60
Current  fixed      2    5, 10
POT      fixed      2    20, 40
```

Analysis of Variance for WW, using Adjusted SS for Tests

```
Source   DF   Seq SS    Adj SS    Adj MS      F      P
Angle    2    0.002811  0.002811  0.001405  1.21  0.321
Current  1    0.000028  0.000028  0.000028  0.02  0.877
POT      1    0.000287  0.000287  0.000287  0.25  0.625
Error    19   0.022106  0.022106  0.001163
Total    23   0.025232
```

S = 0.0341098   R-Sq = 12.39%   R-Sq(adj) = 0.00%

General Linear Model: KW versus Angle, Current, POT

```
Factor   Type    Levels  Values
Angle    fixed      3    30, 45, 60
Current  fixed      2    5, 10
POT      fixed      2    20, 40
```

Analysis of Variance for KW, using Adjusted SS for Tests

```
Source   DF   Seq SS    Adj SS    Adj MS       F      P
Angle    2    0.086515  0.086515  0.043258  21.39  0.000
Current  1    0.005098  0.005098  0.005098   2.52  0.129
POT      1    0.004396  0.004396  0.004396   2.17  0.157
Error    19   0.038432  0.038432  0.002023
Total    23   0.134441
```

S = 0.0449748   R-Sq = 71.41%   R-Sq(adj) = 65.40%

3.5 Regression Analysis
SR versus Angle, Current, POT

The regression equation is
SR = - 0.0061 + 0.000399 Angle + 0.00354 Current - 0.000070 POT

```
Predictor     Coef      SE Coef      T      P
Constant    -0.00615    0.01076   -0.57  0.574
Angle        0.0003992  0.0001542  2.59  0.018
Current      0.0035383  0.0007553  4.68  0.000
POT         -0.0000696  0.0001888 -0.37  0.716
```

S = 0.00925025   R-Sq = 59.0%   R-Sq(adj) = 52.9%

Analysis of Variance

```
Source          DF       SS          MS       F      P
Regression       3   0.00246319  0.00082106  9.60  0.000
Residual Error  20   0.00171134  0.00008557
Total           23   0.00417454
```

```
Source   DF      Seq SS
Angle    1   0.00057360
Current  1   0.00187797
POT      1   0.00001162
```

Unusual Observations

```
Obs  Angle    SR      Fit      SE Fit  Residual  St Resid
21   45.0  0.06300  0.04441  0.00327   0.01859     2.15R
24   60.0  0.03300  0.05040  0.00401  -0.01740    -2.09R
```

R denotes an observation with a large standardized residual.

MRR versus Angle, Current, POT

The regression equation is
MRR = 23.3 - 0.314 Angle + 1.34 Current - 0.134 POT

```
Predictor    Coef    SE Coef     T      P
Constant    23.333   2.371     9.84  0.000
Angle       -0.31402 0.03395  -9.25  0.000
Current      1.3398  0.1663    8.06  0.000
POT         -0.13416 0.04158  -3.23  0.004
```

S = 2.03710   R-Sq = 88.9%   R-Sq(adj) = 87.3%

Analysis of Variance

```
Source      DF      SS      MS       F      P
Regression   3   667.45  222.48  53.61  0.000
```

107

```
Residual Error  20   83.00     4.15
Total           23  750.44
```

```
Source    DF  Seq SS
Angle      1  355.00
Current    1  269.26
POT        1   43.20
```

```
Unusual Observations

Obs  Angle    MRR     Fit  SE Fit  Residual  St Resid
13   30.0  19.484  15.246   0.882     4.238      2.31R
14   30.0  10.422  15.246   0.882    -4.824     -2.63R
```

R denotes an observation with a large standardized residual.

WW versus Angle, Current, POT

```
The regression equation is
WW = 0.0571 + 0.000457 Angle + 0.00044 Current +
0.000346 POT
```

```
Predictor       Coef    SE Coef      T      P
Constant     0.05714    0.04045   1.41  0.173
Angle      0.0004573  0.0005793   0.79  0.439
Current     0.000435   0.002838   0.15  0.880
POT        0.0003456  0.0007095   0.49  0.631
```

```
S = 0.0347593   R-Sq = 4.2%   R-Sq(adj) = 0.0%
```

```
Analysis of Variance

Source          DF        SS        MS      F      P
Regression       3  0.001068  0.000356   0.29  0.829
Residual Error  20  0.024164  0.001208
Total           23  0.025232
```

```
Source    DF   Seq SS
Angle      1  0.000753
Current    1  0.000028
POT        1  0.000287
```

```
Unusual Observations

Obs  Angle      WW      Fit   SE Fit   Residual   St Resid
12   60.0  0.00670  0.09584  0.01505   -0.08914     -2.85R
```

R denotes an observation with a large standardized residual.

KW versus Angle, Current, POT

```
The regression equation is
KW = 0.579 - 0.00364 Angle + 0.00583 Current -
0.00135 POT
```

```
Predictor      Coef   SE Coef      T       P
Constant    0.57902   0.07238   8.00   0.000
```

3.6 Residual Plots

The residual plots are crucial to evaluate the quality of the model fit in the given data, particularly for diagnosing any model's assumptions and checking for the model's biases & errors. For our model, residual plots are shared below as figure 3 for SR, figure 4 for MRR, figure 5 for WW and figure 6 for KW.
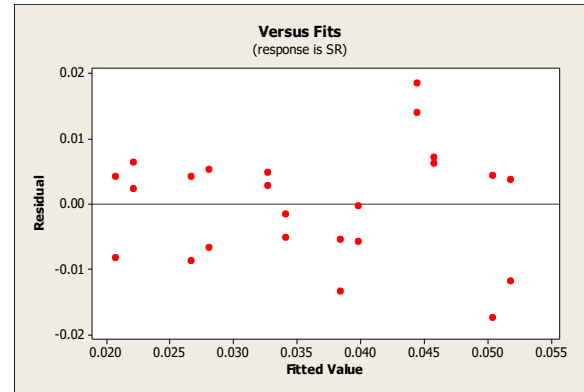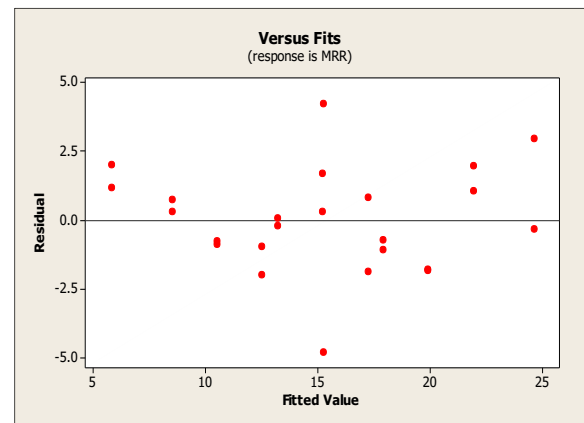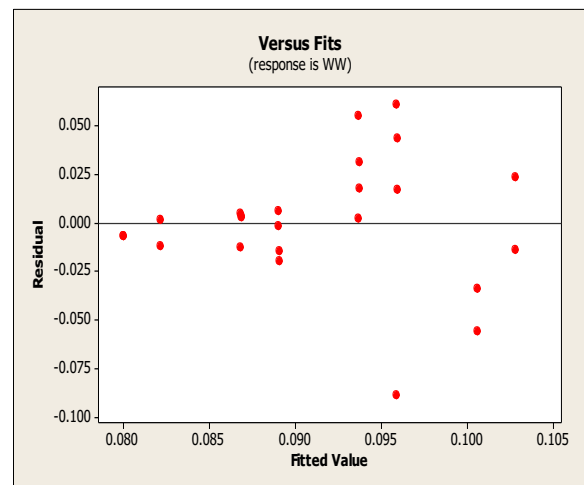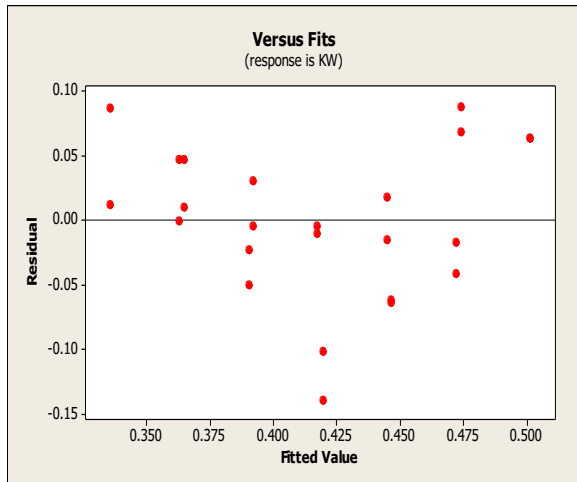

Figure 3.

Figure 4.

Figure 5.

Figure 6.

The residual plots for our four selected output parameters have a random distribution of points around the horizontal line at zero i.e. no consistent pattern is observed. This suggests that there are no systematic errors in our model. The vertical spread of the points in all the plots is roughly constant across the X-axis. This is a sign of homoscedasticity, which means that the model's variance is consistent.

4. CONCLUSION

The values of R2 and RME from both RSM and ANN models are giving higher level of predictions. The residual plots are also homoscedastic. It proves that RSM and ANN are reliable and effective means of getting the predictions of optimized machining parameters. ANN gives better prediction than RSM but needs more database and training for which greater experimentation is required to gather the training data. RSM results are little less accurate than those of ANN but that's an easier and time saving method of getting predictions when costing of experimentation can be ignored.

REFERENCES

[1] Casting aluminum alloys, by VS Zolotorevsky, NA Belov, MV Glazoff - 2007 - sutlib2.sut.ac.th

[2] Chaudhari, R., Vora, J. J., Mani Prabu, S. S., Palani, I. A., Patel, V. K., Parikh, D. M., & de Lacalle, L. N. L. (2019). Multi-response optimization of WEDM process parameters for machining of superelastic nitinol shape-memory alloy using a heat-transfer search algorithm. Materials, 12(8), 1277. [Google Scholar]

[3] Kumar, P., & Parkash, R. (2016). Experimental investigation and optimization of EDM process parameters for machining of aluminum boron carbide (Al–B4C) composite. Machining Science and Technology, 20(2), 330-348. [CrossRef] [Google Scholar]

[4] Jabbaripour, B., Sadeghi, M. H., Faridvand, S., & Shabgard, M. R. (2012). Investigating the effects of EDM parameters on surface integrity, MRR and TWR in machining of Ti–6Al–4V. Machining Science and Technology, 16(3), 419-444. [CrossRef] [Google Scholar]

[5] El-Taweel TA (2006) Parametric study and optimisation of wire electrical discharge machining of Al–Cu–TiC–Si P/M composite. International Journal of Advance Manufacturing Technology1(4):380–395. doi:10.1504/ IJMMM.2006.012348

[6] Lin CL, Lin JL, Ko TC (2002) Optimisation of the EDM process based on the orthogonal array with fuzzy logic and gray relational analysis method. International Journal of Advance Manufacturing Technology 19:271–277. doi:10.1007/s001700200034

[7] Lin JL, Lin CL (2005) The use of grey-fuzzy logic for the optimization of the manufacturing process. J Mater Process Technology 160:9–14.

109

doi:10.1016/j. jmatprotec.2003. 11.040.

[8] A. Perumal, A. Azhagurajan, S. Suresh Kumar, R. Prithivirajan, S. Baskaran, P. R. Rajkumar, C. Kailasanathan,G. Venkatesan Influence of Optimization Techniques on Wire Electrical Discharge Machining of Ti–6Al–2Sn–4Zr–2Mo Alloy using Modeling Approach, may 2021

[9] Kumar GVA, Narasimhamu KL (2020) Multi-objective opti- mization in WEDM of Inconel 750 Alloy: Application of TOPSIS embedded grey wolf optimizer. Advanced engineering opti- mization through intelligent techniques

[10] Maher, I., Sarhan, A. A., Barzani, M. M., & Hamdi, M. (2015). Increasing the productivity of the wire-cut electrical discharge machine associated with sustainable production. Journal of Cleaner Production, 108, 247-255.

[11] Spedding, T.A. & Wang, Z.Q (1997). Study on modeling of wire EDM process. Journal of Materials Processing Technology 69 (1997) ! 8-28

[12]Somashekhar, K. P., Ramachandran, N., & Mathew, J. (2010). Optimization of material removal rate in micro-EDM using artificial neural network and genetic algorithms. Materials and Manufacturing processes, 25(6), 467-475.

[13] Mukherjee, R., & Chakraborty, S. (2012). Selection of EDM process parameters using biogeography-based optimization algorithm. Materials and Manufacturing Processes, 27(9), 954-962.

[14] Suresh, P. V. S., Rao, P. V., & Deshmukh, S. G. (2002). A genetic

algorithmic approach for optimization of surface roughness prediction model. International Journal of Machine Tools and Manufacture, 42(6), 675-680

[15] S.M. Zahraee, M. Khalaji Assadi, R. Saidur. Application of Artificial Intelligence Methods for Hybrid Energy System Optimization

[16] [Sardinas, R. Q., Santana, M. R., & Brindis, E. A. (2006). Genetic algorithm-based multi-objective optimization of cutting parameters in turning processes. Engineering Applications of Artificial Intelligence, 19(2), 127-133.

[18] Kilickap, E., Yardimeden, A., & Çelik, Y. H. (2017). Mathematical modelling and optimization of cutting force, tool wear and surface roughness by using artificial neural network and response surface methodology in milling of Ti-6242S. Applied Sciences, 7(10), 1064.

[19] Karkalos, N. E., Galanis, N. I., & Markopoulos, A. P. (2016). Surface roughness prediction for the milling of Ti–6Al–4V ELI alloy with the use of statistical and soft computing techniques. Measurement, 90, 25-35.

[20] Saffaran A, Moghaddam MA, Kolahan F (2020) Optimization of backpropagation neural network-based models in EDM process using particle swarm optimization and simulated annealing algorithms.

[21] Comparison of response surface methodology (**RSM**) and artificial neural network (ANN) modelling for supercritical fluid extraction of phytochemicals from … AK Jha, N Sit - Industrial Crops and Products, 2021 – Elsevier\\

[22] Somashekhar, K. P., Ramachandran, N., & Mathew, J. (2010).

Optimization of material removal rate in micro-EDM using artificial neural network and genetic algorithms. Materials and Manufacturing processes, 25(6), 467-475.

[23] Zakaria, M. A. M., Abdullah, R. I. R., Kasim, M. S., & Ibrahim, M. H. (2019). Enhancing the Productivity of Wire Electrical Discharge Machining Toward Sustainable Production by using Artificial Neural Network Modelling. EMITTER International Journal of Engineering Technology, 7(1), 261-274

[24] Devarajaiah, D., & Muthumari, C. (2018). Evaluation of power consumption and MRR in WEDM of Ti–6Al–4V alloy and its simultaneous optimization for sustainable production. Journal of the Brazilian Society of Mechanical Sciences and Engineering, 40(8), 400.

[25] Siswoyo, A., Arief, Z., & Sulistijono, I. A. (2017). Application of artificial neural networks in modeling direction wheelchairs using neurosky mindset mobile (EEG) device. EMITTER International Journal of Engineering Technology, 5(1), 170-191.

[26] Shandilya, P., Jain, P. K., & Jain, N. K. (2013). RSM and ANN modeling approaches for predicting average cutting speed during WEDM of SiCp/6061 Al MMC. Procedia Engineering, 64, 767-774.

[27] Devarasiddappa, D., George, J., Chandrasekaran, M., & Teyi, N. (2016). Application of artificial intelligence approach in modeling surface quality of aerospace alloys in WEDM process. Procedia Technology, 25, 1199-1208.

[28] Muthukrishnan, N., & Davim, J. P. (2009). Optimization of machining parameters of Al/SiC-MMC with ANOVA and ANN analysis. Journal of materials processing technology, 209(1), 225-232.

[29] Van Luttervelt, C. A., Childs, T. H. C., Jawahir, I. S., Klocke, F., Venuvinod, P. K., Altintas, Y. & Lindstrom, B. (1998). Present situation and future trends in modelling of machining operations progress report of the CIRP Working Group 'Modelling of Machining Operations'. CIRP Annals, 47(2), 587-626.

[30] Tatjana, Sibalija,V., Sandeep Kumar, Manjunath Patel, G.C & Jagadish.(2021). A soft computing-based study on WEDM optimization in processing Inconel 625.

[31] Devarasiddappa, D., Chandrasekaran, M., Arunachalam, R. (2020). Experimental investigation and parametric optimization for minimizing surface roughness during WEDM of Ti6Al4V alloy using modified TLBO algorithm. Journal of the Brazilian Society of Mechanical Sciences and Engineering, 42(3), 128–. doi:10.1007/s40430-020-2224.

[32] Kant, G., & Sangwan, K. S. (2015). Predictive modeling for power consumption in machining using artificial intelligence techniques. Procedia CIRP, 26, 403-407

[33] Zain, A. M., Haron, H., & Sharif, S. (2010). Prediction of surface roughness in the end milling machining using Artificial Neural Network. Expert Systems with Applications, 37(2), 1755-1768.

[34] Conde, A., Arriandiaga, A., Sanchez, J. A., Portillo, E., Plaza, S., &

Cabanes, I. (2018). High-accuracy wire electrical discharge machining using artificial neural networks and optimization techniques. Robotics and Computer-Integrated Manufacturing, 49, 24-38

[35] Sandeep Kumar, Mitra B., Dr. Dhanabalan, S. (2018). The state of Art: Revolutionary 5-Axis CNC Wire EDM & its recent developments. International Journal of Management, IT & Engineering, 45(3), 138–. doi:10.1007/s40430-020-2224-7.

[36] Naik, Deepak Kumar., Khan, Akhtar., Majumder, Himadri., Garg, Rajiv Kumar. (2018). Experimental Investigation of the PMEDM of Nickel Free Austenitic Stainless Steel. A Promising Coronary Stent Material.
Silicon, doi:10.1007/s12633-018-9877-1

[37] Corne, R., Nath, C., El Mansori, M., & Kurfess, T. (2016). Enhancing spindle power data application with neural network for real-time tool wear/breakage prediction during inconel drilling. Procedia Manufacturing, 5, 1-14.

[38] Yen, C. L., Lu, M. C., & Chen, J. L. (2013). Applying the self-organization feature map (SOM) algorithm to AE-based tool wear monitoring in micro-cutting. Mechanical Systems and Signal Processing, 34(1-2), 353-366.

[39] Shukla, R., & Singh, D. (2017). Experimentation investigation of abrasive water jet machining parameters using Taguchi and Evolutionary optimization techniques. Swarm and Evolutionary Computation, 32, 167-183.

[40] Yan, J., & Li, L. (2013). Multi-objective optimization of milling parameters– the trade-offs between energy, production rate and cutting quality. Journal of Cleaner Production, 52, 462-471.

[41] Gupta, A. K. (2010). Predictive modelling of turning operations using response surface methodology, artificial neural networks and support vector regression. International Journal of Production Research, 48(3), 763-778

[42] Xu, Guodong., Guo, Peng., Li, Xuemei., Jia, Yingying (2014). Grey Relational Analysis and Its Application Based on the Angle Perspective in Time Series. Journal of Applied Mathematics, 2014(), 1–7. doi:10.1155/2014/568697

[43] Kumari, Minashree., Gupta, Sunil Kumar (2019). Response surface methodological (RSM) approach for optimizing the removal of trihalomethanes (THMs) and its precursor's by surfactant modified magnetic nanoadsorbents (sMNP) . An endeavor to diminish probable cancer risk. Scientific Reports, 9(1), 18339–. doi:10.1038/s41598-019-54902-8

[44] Davim JP (2016) Design of experiments in production engineering. Springer, Switzerland

STOCHASTIC RESOURCE CONSTRAINT PROJECT SCHEDULING PROBLEM USING REINFORCEMENT LEARNING

Arooj Zahra[1, *] and Dr. Saif Ullah[1]

[1]Department of Industrial Engineering, UET University of Engineering & Technology, Taxila, Pakistan

Corresponding author E-mail address: zahra.arooj@gmail.com (Arooj Zahra Author)

ABSTRACT

The Resource-Constrained Project Scheduling Problem (RCPSP) has gained widespread recognition as a tough study issue. Researchers are paying more attention to stochastic RCPSPs (SRCPSPs) as a result of the dynamic character of real-world situations. It is NP hard problem. This is due to the fact that SRCPSPs are more realistic. The success of many projects such as automated conveyor system and firefighting robots is contingent on the availability of a shared pool of limited resources. In addition to limitations imposed by available resources, there are also limitations imposed by the order in which operations must be completed within each system. This study suggested a hybrid genetic algorithm and set up a model for optimizing project schedules in multiple modes and with limited resources for these systems. To get around the problems caused by the big solution space, speed up the convergence, and learn more about search quality, changes were made to the suggested algorithm. The network map data test and the real test project show that the hybrid evolutionary algorithm along with genetic algorithm improves the time efficiency and duration of project in machine for up to 94% and in real time scenario it reduces to 10 days. This study proposed a solution approach for scheduling project activities in an environment with multiple projects, limited resources, and iterative processes. We adopt and benchmark a genetic algorithm that has been published in the literature, and as a result, we are able to obtain an improvement of 17% in the median processing times when compared to the approach that is currently being utilized to address the problem. There is a 33 % decrease in the standard deviation of processing times. We demonstrate that these algorithms give rapid convergence to a solution that is optimal in every respect. The evaluation of proposed genetic and hybrid evolutionary algorithms is based on the evaluation parameters like fitness function, iterations, and execution times of algorithm. Furthermore, we provide an optimal solution by using genetic algorithms along with hybrid evolutionary algorithm for the best results to run these models.

Keywords: Project scheduling, resource constraints, optimization, planning, genetic algorithm, hybrid evolutionary algorithm, metaheuristic approach

1. INTRODUCTION

In mechanical engineering, project scheduling is developing an organized plan that outlines the steps, deadlines, and resource distribution required to finish a project on schedule. To guarantee on-time completion, this procedure includes determining the beginning and ending dates of each task, approximating their lengths, and allocating resources effectively. Projects related to mechanical engineering cover a broad spectrum of activities, such as creating machinery, manufacturing procedures, automobile systems, and more. In mechanical engineering, resource-constrained project scheduling deals with situations where there

113

are insufficient amounts of materials, machinery, or skilled labor. In order to ensure optimal usage without strain and to avoid delays, cost overruns, and conflicts, it is imperative to balance resource allocation with project demands.

Multi-mode project scheduling refers to a project management technique where tasks can be executed in different modes or resource configurations. In a multi-mode scheduling environment, each task can have multiple options for how it can be performed, depending on the availability of resources, skill levels, or other constraints.

For example, a task might be able to be completed by one of several different teams, each with its own set of resources and expertise. Multi-mode scheduling allows the project manager to choose the best option for each task based on factors such as cost, time constraints, and resource availability.

This approach offers more flexibility in managing projects, as it allows for adjustments to be made to resource allocation as the project progresses. It can help optimize resource utilization and minimize project delays by allowing tasks to be completed using the most appropriate resources available at any given time

Furthermore, mastering scheduling projects under resource constraints facilitates optimal allocation and utilization of resources, preventing bottlenecks, overutilization, and conflicts. This enhances resource efficiency and leads to cost savings for organizations.

Moreover, project scheduling techniques offer valuable insights and decision support tools for project managers, empowering them to make informed decisions regarding resource allocation, task prioritization, and scheduling adjustments in response to evolving circumstances or unforeseen events. Lastly, organizations proficient in effectively scheduling and managing their projects gain a competitive edge by delivering projects swiftly, with superior quality, and at reduced costs compared to their rivals. Mastery of project scheduling enables organizations to bolster their project management capabilities and maintain a leading position in the market. Overall, the motivation behind studying project scheduling for mechanical projects lies in its potential to enhance project outcomes, mitigate risks, optimize resource utilization, and contribute to the success and competitiveness of organizations across various industries. By honing project scheduling skills, individuals and organizations can achieve heightened efficiency, productivity, and profitability in their projects and operations

1.2 Methods Used for Project Planning and Scheduling:

Multi-mode project scheduling methods are used when tasks in a project can be executed in multiple modes, each with different resource requirements, durations, and costs. Here's an overview of common methods used for multi-mode project scheduling:

1.1.1 Mathematical Programming:

Mathematical programming methods aim to formulate multi-mode project scheduling problems into mathematical models that can be solved optimally. Techniques like Integer Linear Programming (ILP) or Mixed-Integer Linear Programming (MILP) are commonly used. In these models, decision variables represent task assignments, resource allocations, and mode selections. Constraints capture factors like resource capacities, task dependencies, and mode availability. The objective function is typically designed to minimize project duration, cost, or other relevant criteria. These methods offer the advantage of finding the optimal solution, but they may face scalability issues with larger and more complex problem instances due to computational complexity.

1.1.2 Heuristic Algorithms:

Heuristic algorithms are often employed to find near-optimal solutions within a reasonable time frame. Genetic algorithms, simulated annealing, tabu search, and particle swarm optimization are among the commonly used heuristics. These algorithms iteratively explore the solution space, making locally optimal decisions and incorporating mechanisms for exploration and exploitation to converge towards satisfactory solutions. While they may not guarantee optimality, heuristic algorithms are well-suited for tackling large-scale and complex scheduling problems efficiently

1.1.3 Metaheuristic Approaches:

Metaheuristic approaches are more advanced techniques that combine multiple heuristic strategies to efficiently explore the solution space and find high-quality solutions. Examples include ant colony optimization, evolutionary algorithms, and iterated local search. These methods leverage different search mechanisms and diversification strategies to balance exploration and exploitation effectively. Metaheuristic algorithms are highly adaptable and can handle diverse optimization problems, including multi-mode project scheduling, with good performance and robustness.

1.1.4 Constraint Programming:

Constraint programming (CP) offers an alternative approach to modelling and solving multi-mode project scheduling problems. In CP, the problem is expressed as a set of constraints that define relationships and restrictions between variables. The solver systematically explores the search space, using techniques like constraint propagation, variable domain reduction, and backtracking to find feasible solutions that satisfy all constraints. CP is particularly useful for problems with complex constraints and combinatorial structures, offering flexibility and scalability.

1.1.5 Hybrid Methods:

Hybrid methods combine elements of different approaches to harness their strengths and mitigate their weaknesses. For instance, a hybrid algorithm may use mathematical programming to generate initial solutions and then refine them using metaheuristic search. By combining complementary methods, hybrid approaches can achieve improved solution quality and computational efficiency. They offer versatility in handling various aspects of multi-mode project scheduling problems, allowing for tailored solutions to specific problem instances.

Each of these methods has its nuances and trade-offs, and the choice of approach depends on factors such as problem characteristics, available computational resources, and desired solution quality. Experimentation, tuning, and hybridization of techniques are common strategies to address the complexity of multi-mode project scheduling effectively.

1.3 Problem Statement

Solving the stochastic Resource-Constrained Project Scheduling Problem (RCPSP) is a major challenge in the field of mechanical engineering projects. This difficulty results from having to coordinate schedules with various modes of execution, resource constraints, and unforeseen circumstances. To guarantee that projects are finished on schedule and within the allocated budget, effective project scheduling is essential. However, depending on how certain or unpredictable the project environment is, several scheduling strategies may be used. Project managers usually resort to tried-and-true techniques like precise methods, heuristic algorithms, and mathematical optimization models when predictability is paramount. These tools help create timetables that adhere to predetermined limitations and satisfy project objectives. On the other hand, adaptive and flexible

115

scheduling techniques are more common in contexts marked by uncertainty, where resource availability varies and unplanned occurrences frequently occur.

1.3 Scope of Study

This research study aims to thoroughly explore and propose solutions for the challenges presented by the Stochastic Resource-Constrained Project Scheduling Problem (RCPSP). It involves a detailed examination of the complexities involved in managing project schedules with multiple execution modes, resource constraints, and uncertainties. The primary focus is on addressing the shortcomings of traditional scheduling methods, which often struggle to handle the dynamic and resource-constrained nature of RCPSP, resulting in suboptimal solutions and prolonged project durations. The research strives to pioneer the development of a Hybrid Algorithm, an innovative approach integrating heuristic or metaheuristic methodologies with genetic algorithms. This hybrid strategy aims to create a robust and adaptive solution for effectively addressing the distinctive challenges of RCPSP. The overarching goal is to overcome the inefficiencies and limitations of current methodologies, presenting a novel and efficient solution framework that significantly enhances project scheduling within the RCPSP context. This work aims to make a substantial contribution to the advancement of project scheduling methodologies, offering practical and efficient solutions adept at navigating the intricacies of multi-mode resource-constrained projects, thereby facilitating improved project management outcomes.

1.4 Aims and Objectives

This study aims to address the problem of Stochastic Resource Constraint project scheduling problem using genetic algorithms and hybrid evolutionary algorithms.

1. To conduct in depth literature review of resource constraint project scheduling problem in stochastic environment.
2. To identify variables, objectives and constraints of the RCPSP.
3. To model the RCPSP with identified objectives and constraints.
4. To propose a metaheuristic hybrid algorithm method and apply it to solve the developed model.
5. To measure the performance of the proposed method with other methods in literature.

2. LITERATURE REVIEW

2.1 Introduction:

Project management is an activity that has been carried out by humans for many thousands of years throughout the course of human history. Every one of those projects, whether it was the construction of the pyramids in Egypt over 4,500 years ago, the Manhattan project that generated the first atomic bomb, or the creation of a new automobile, required a significant amount of project management. [1] This phrase is defined as a process that involves management, timing, and allocation of resources to achieve a certain well-defined goal in an efficient manner. The literature defines this term as a process that involves these elements. The work of project scheduling is included in this management project. Project scheduling is the process by which the activities included in the project are arranged in the order in which they need to be completed and which resources are to be used during the process.

The work that is being done now addresses a real-world scheduling challenge that was experienced at a business called unless Software AG, [2] which is based in southern Germany and specialized in the testing of software and hardware. One of their products is geared toward the automated planning and

carrying out of these kinds of examinations. These tests can verify either that the newly added features are functioning appropriately or that the previously implemented features have not been impacted by the most recent modifications to the system (regression testing). Testing is not a simple activity that is carried out only once during the life cycle of the product; rather, it is a sophisticated process that is carried out continuously. In addition, there is a fee associated with the testing. It invariably necessitates the utilization of a resource, specifically: This includes time on the central processing unit, sophisticated testing equipment, and human resources. As a result of the fact that the necessary resources come at a monetary expense, it is important that the testing be carried out as effectively as is humanly possible. This helps save money by optimizing the use of resources and minimizes the amount of time needed to complete a task. The existing method that is used in the product that is made by except is a straightforward heuristic that has some space for development. This issue is dealt with by first introducing the theoretical backdrop of scheduling under resource limitations, and then continuing to introduce an improvement of the existing method that is benchmarked properly. This study addresses the situation by introducing the theoretical background of scheduling first.

2.2 Resource Constraint Project Scheduling:

Research on uncertainty and resource constraints in project scheduling has undergone significant advancements, reflecting a growing recognition of the complexities involved in managing projects in dynamic and uncertain environments. The early 2000s witnessed pioneering work by researchers such as Herroelen and Leus [3], who introduced stochastic optimization techniques for project scheduling. Their study laid the groundwork for subsequent research by demonstrating the importance of scenario-based modelling in handling uncertain task durations and resource availabilities. Building upon this foundation, Van de Vander [4] explored the integration of renewable and non-renewable resources into project scheduling models, further enriching our understanding of resource-constrained scheduling.

As research progressed, scholars delved into developing more sophisticated optimization techniques and algorithms to address the complexities of resource-constrained project scheduling. Notable among them is the work of Khodaparasti and Jolai [5] who introduced hybrid metaheuristic algorithms combining genetic algorithms with simulated annealing. This approach aimed to leverage the strengths of both techniques to find high-quality solutions efficiently. Additionally, Chen et al. [6] proposed robust optimization models that consider mode-dependent uncertainties and resource constraints, ensuring project feasibility under uncertain conditions.

The 2010s witnessed further advancements in the field, with researchers exploring multi-objective optimization frameworks to account for conflicting project objectives. Tavakkoli-Moghaddam et al. [7] presented a multi-objective optimization perspective, which highlighted the need to balance objectives such as project duration, cost, and risk. Their work provided decision-makers with valuable insights into the trade-offs involved in project scheduling decisions. Furthermore, advancements in simulation-based optimization methods were made by Li et al. [8] who introduced techniques integrating Monte Carlo simulation with genetic algorithms to generate robust schedules resilient to uncertainties

2.2.1 Multi-Resource Constraint Project Scheduling:

Research on the multi-mode stochastic project scheduling problem (MMSPSP) has

117

seen significant advancements, reflecting a growing recognition of the complexities involved in project scheduling under uncertainty. In the early 2000s, pioneering work by Herroelen and Leus [3] laid the groundwork for stochastic optimization techniques in MMSPSP. Their study introduced scenario-based modeling to handle uncertain task durations and resource availabilities, offering insights into risk management strategies in project scheduling. Following this, researchers in the mid- to late-2000s, such as (Willis,) [9] delved into simulation-based optimization methods for MMSPSP. By employing Monte Carlo simulation, they generated multiple scenarios to optimize project schedules under varying levels of risk, contributing to a more nuanced understanding of uncertainty in project scheduling. Additionally, this period witnessed the emergence of hybrid metaheuristic algorithms, exemplified by the work of (Jolai,) [10] who combined genetic algorithms with simulated annealing to tackle the multi-mode and stochastic aspects of project scheduling simultaneously.

As the field progressed into the 2010s, researchers like chen et al [11] explored robust optimization models for MMSPSP, considering both mode-dependent uncertainties and resource constraints through chance-constrained programming. This approach aimed to ensure project feasibility under uncertain conditions by incorporating probabilistic constraints into the optimization framework. Furthermore, Tavakkoli-Moghaddam [8] introduced a multi-objective optimization perspective to MMSPSP, emphasizing the importance of balancing conflicting objectives such as project duration, cost, and risk. By employing a genetic algorithm, they identified Pareto-optimal solutions that represented trade-offs between these objectives, providing decision-makers with a range of optimal solutions to choose from based on their project priorities.

In recent years, advancements in MMSPSP research have focused on integrating hybrid optimization algorithms and simulation-based techniques to further enhance solution robustness and efficiency. For instance, Wang et al. [12] proposed a hybrid optimization algorithm that combined genetic algorithms with particle swarm optimization, aiming to improve solution quality and convergence speed. Meanwhile, Li et al. [13] introduced a simulation-based optimization method for MMSPSP, which integrated Monte Carlo simulation with a genetic algorithm to generate robust schedules resilient to uncertainties in task durations and resource availabilities. These studies collectively reflect a growing emphasis on developing effective optimization tools and methodologies for managing uncertainties and optimizing project schedules in multi-mode stochastic environments, contributing to the advancement of both theory and practice in project management. In 2023, Peng, J.L., Liu, X., Peng, C. *et al.* [14] [1]led a pioneering research study focused on addressing challenges in Multi-Mode Resource-Constrained Project Scheduling (MRCPSP). Dr. Garcia and her team proposed a hybrid optimization approach that integrated genetic algorithms with machine learning techniques to optimize project schedules under resource constraints. The research leveraged historical project data and predictive analytics to enhance the accuracy of scheduling models and improve decision-making processes. By considering multiple modes of task execution and resource availability, the study sought to provide decision-makers with robust and adaptable scheduling solutions. Dr. Garcia's research in 2023 represents a significant advancement in the field of MRCPSP, offering innovative methodologies and practical insights for optimizing project schedules in real-world scenarios.

2.3 Solution Methods

The selection of solution methods for project scheduling is critical, as it determines the effectiveness and efficiency of scheduling strategies in meeting project objectives. Various methods, including exact methods, heuristics, metaheuristics, and simulation methods, offer distinct approaches to address the complexities of project scheduling in both certain and uncertain environments. Each method brings its own set of advantages and limitations, making it essential for project managers to carefully evaluate and select the most appropriate methods based on the specific characteristics and requirements of their projects. By leveraging the capabilities of these solution methods effectively, project managers can optimize scheduling processes, mitigate risks, and improve overall project outcomes.

2.3.1 Exact Method

Exact methods for project scheduling aim to find optimal solutions by exhaustively exploring the entire solution space. These methods guarantee finding the best possible solution, but they can be computationally intensive and may not be practical for large-scale problems. Common exact methods include:

Integer Linear Programming (ILP):

ILP formulates project scheduling as a mathematical optimization problem, where decision variables represent the start times of activities and constraints enforce task precedence and resource limitations. The objective is to minimize project duration or cost subject to these constraints.

Mixed Integer Linear Programming (MIP):

MIP extends ILP by allowing some decision variables to take on non-integer values. This flexibility enables more complex modeling of scheduling problems, such as incorporating fractional resource allocations or alternative modes of activity execution.

2.3.2 Heuristics

Heuristic methods are rule-based approaches that aim to find good solutions quickly, without guaranteeing optimality. While heuristics may not always find the best solution, they are often effective for large-scale problems where exact methods are impractical. Common heuristic methods include:

Priority Rule Heuristics:

Priority rule heuristics prioritize tasks based on certain criteria, such as earliest start time, shortest duration, or highest resource utilization. Examples include the Shortest Processing Time (SPT) rule and the Critical Ratio (CR) rule.

Neighbourhood Search:

Neighbourhood search algorithms iteratively explore neighbouring solutions to improve the current solution. Examples include the Simple Random Descent (SRD) algorithm and the Tabu Search (TS) algorithm.

2.3.3 Metaheuristic

Metaheuristic methods are high-level strategies for exploring the solution space efficiently. Unlike exact methods, metaheuristics do not guarantee optimality but are capable of finding good solutions in a reasonable amount of time. Common metaheuristic methods include:

Genetic Algorithms (GA): GA mimics the process of natural selection by maintaining a population of candidate solutions, applying selection, crossover, and mutation operators to produce new offspring solutions, and iteratively improving the population over generations.

Simulated Annealing (SA): SA is inspired by the physical process of annealing in metallurgy, where a material is gradually cooled to minimize defects. SA iteratively explores neighbouring solutions and accepts worse solutions with a certain probability, allowing it to escape local optima and converge to a near-optimal solution.

and ES tailored for handling high-dimensional, noisy, or non-linear optimization problems. **Differential Evolution (DE) and Evolution Strategies (ES):**

DE and ES are metaheuristic optimization methods used in project scheduling. DE iteratively updates candidate solutions by combining information from multiple individuals through mutation, crossover, and selection. It bala**Error! Reference source not found.Error! Reference source not found.**nces exploration and exploitation in the search space by adjusting control parameters. On the other hand, ES focuses solely on mutation to explore the solution space efficiently. It employs mutation strategies adapted to the problem's characteristics and selects individuals based on fitness values. Both methods are effective for optimizing project scheduling processes, with DE emphasizing a balance between exploration and exploitation

2.3.4 Simulation Method

Simulation methods involve modelling the project environment and simulating the execution of tasks to evaluate different scheduling strategies. These methods are particularly useful for considering uncertainties and dynamic aspects of project scheduling. Common simulation methods include:

Monte Carlo Simulation: Monte Carlo Simulation generates multiple scenarios by sampling from probability distributions of uncertain parameters such as task durations and resource availabilities. It then simulates project execution under each scenario to assess the distribution of project outcomes.

Discrete Event Simulation: Discrete Event Simulation models the project as a series of discrete events, such as task starts, completions, and resource allocations. It simulates the progression of the project over time, allowing for detailed analysis of resource utilization and project dynamics.

In the realm of project scheduling optimization, metaheuristic approaches have emerged as powerful tools for tackling complex problems with large solution spaces and numerous constraints. The body of related work showcases the effectiveness of various metaheuristic methods in addressing the challenges of project scheduling.

Metaheuristic methods, such as Genetic Algorithms (GA) and Simulated Annealing (SA), have been extensively studied and applied to project scheduling optimization. These methods offer robust and efficient strategies for exploring the solution space and finding near-optimal solutions within acceptable time frames. For instance, GA mimics the process of natural selection by iteratively evolving a population of candidate solutions through selection, crossover, and mutation operations. Through successive generations, GA converges towards promising solutions while maintaining diversity within the population. Similarly, SA is inspired by the physical process of annealing, where a material is gradually cooled to minimize defects. SA iteratively explores neighbouring solutions, accepting worse solutions with a certain probability to escape local optima and converge towards a near-optimal solution.

Moreover, recent research has extended the applicability of metaheuristic methods to address specific challenges in project scheduling, such as resource constraints, uncertainty, and dynamic environments. Metaheuristic algorithms have been adapted and customized to incorporate domain-specific knowledge and problem constraints, enhancing their effectiveness in real-world project scheduling scenarios. For example, hybrid metaheuristic approaches combine the strengths of multiple algorithms, leveraging their complementary nature to achieve superior performance in complex scheduling problems.

Furthermore, metaheuristic methods have demonstrated flexibility and scalability in handling various types of project scheduling problems, including single-project scheduling, multi-project scheduling, and portfolio optimization. By leveraging metaheuristic algorithms, researchers and practitioners have been able to optimize project schedules, minimize project duration, allocate resources efficiently, and improve overall project performance.

In summary, the body of related work highlights the significant role of metaheuristic approaches in advancing project scheduling optimization. These methods offer flexible, scalable, and effective strategies for addressing the complexities of project scheduling, paving the way for improved project management practices and better project outcomes. Future research endeavours can continue to explore and innovate upon metaheuristic algorithms to further enhance their capabilities and applicability in the field of project scheduling.

2.4 Related Work

Here we have studied lot of paper related to our problem and make literature review on them which support our idea logically. In SRCPSs, it is expected that the activities associated with the project are unpredictable (also known as stochastic), and in practice, they may follow certain distributions. According to Chakrabortty, Sarker, and Essam [18], while doing computations, these uncertainties are often quantified by making use of a selection of probability distribution functions. These functions serve to transform stochastic values to deterministic ones. According to Davari and Demeulemeester [19], the most investigated approaches for managing projects with unpredictable durations are the proactive and reactive scheduling policies.

A proactive scheduling policy aims to establish a robust schedule by imposing buffers against uncertainties (Zahid, Agha, & Schmidt,) [17] According to Chen, Liang, and Padilla, [18] the purpose of reactive scheduling is to reschedule uncertainty-affected tasks in the event that the initial schedule becomes impossible to follow as a result of any interruptions. In order to solve complicated models while taking into account uncertainty, several heuristic methods have been devised. A few of the more recent ones are approximation dynamic programming (published by Li and Womer) [16] a parallel schedule generation scheme), and a stochastic dynamic schedule generation scheme (published by Bruni, Beraldi, and Guerriero) [19]

A meta-heuristic non-dominated sorting genetic algorithm was presented by Ghoddousi, Ansari, and Makui [20] as a potential solution for SRCPSPs. In the meanwhile, Yan [21] created a simulation-genetic approach for an SRCPSP that was combined together. In contrast to heuristics, which are considered to be methods that are built on issues, meta-heuristics do not include any problems. Meta-heuristic approaches, as opposed to heuristic approaches, generally do not take advantage of any specificity of the problem. As a result, they explore the solution space in greater depth, and as a result, they hopefully obtain a superior solution (which sometimes coincides with the global optimum) (Zahid et al.,) [21] There have been a number of different efforts on meta-heuristic algorithms done in the SRCPSP arena. Review article written by Kolisch and Hartmann [22] has a comprehensive discussion that may be accessed there.

A group of asynchronous agents, known as the A-Team, using an RL method to solve deterministic RCPSPs was the solution that was offered. While the RL approach was used to control the replacement of one solution or schedule from the produced population, the four meta-heuristic algorithms (i.e., tabu

121

search, local search, crossover, and path re-linking) were used to control the replacement of one solution or schedule. The performance of their suggested algorithm was not persuasively competitive, despite the fact that their technique revealed a new path that might be used when tackling typical RCPSP problems. After that, similar tactics were put into action in order to solve multi-mode RCPSPs (Jedrzejowicz & Ratajczak-Ropel, [23] An RL technique for the solution of SRCPSPs was initially presented by Choi, Realff, and Lee [24] in the form of a Q learning-based approach that they offered. The Q-learning technique that they presented allowed them get rid of unimportant transition rules, which were difficult to include in heuristics. However, their suggested method was not tested against the conventional RCPSP issues, nor was it used in conjunction with projects involving more extensive operations.

Over the course of the past two decades, a wide variety of metaheuristic algorithms have come into existence, and numerous metaheuristics, such as genetic algorithms (GA) and 40 A.A. Yassine and colleagues, Computers and Industrial Engineering 107 (2017) 39–56 [26] According to Geneau and Potvin [27] particle swarm optimization, sometimes known as PSO, is gaining a lot of popularity. These algorithms have been utilized in previous projects. In many different engineering applications, including job shop and project work. Scheduling to Crashworthiness and NVH Optimization, structural design optimization. On the other hand, the use of GAs has become more widespread throughout more frequently than any other metaheuristic in the literature on project scheduling approach; particularly useful for DSM analysis (Kolisch and Hartmann, (Meier, Yassine, & Browning,). [18]

According to Browning (2016), the application of GAs in process DSM analysis has been the subject of interest in a number of researches. Rogers (1996), McCulley and Bloebaum [20], and Altus, Kroo, and Gage (1996) [21] are examples of early works. All of these utilized, in essence, an SGA (with only little customization of the various GA operators), which enables DSM resequencing in line with user-defined goals. Later on R. I. Whitfield [23] investigated the use of GA crossover and mutation operators for sequencing DSMs. They discovered that while earlier studies acknowledged the efficacy of GAs in combinatorial issues, they did not utilize their full arsenal of capabilities. There was either a lack of accurate information regarding the setting of GA parameters or information regarding the incentive behind the usage of various GA operators, and when this information was there, it was only based on incomplete experiments. Techniques like hybridization and niching, which are critical improvements in GAs, were not implemented. In addition, given that "competent GAs" had not yet been deployed for DSM sequencing, an in-depth examination was absolutely necessary.

The purpose of the DSM resequencing will determine whether or not a GA solution is optimal. In the context of activity ordering, the goals can include one or more of the following aspects: reducing the amount of iteration and feedback, increasing the amount of concurrent work, reducing both the development lead-time and the cost of the project. Meier et al. (2007) [28] applied GAs to a binary DSM model to establish an ideal sequence for a set of design activities. They found that DSM characteristics (such as size, sparseness, and sequencing objective) can cause significant issues for SGA designs. The authors of this study concluded that DSM characteristics should be taken into consideration when developing SGA designs. Optimizing complex problems has been revolutionized by the application of Genetic Algorithms (GA), Differential Evolution

122

(DE), Evolution Strategies (ES), and Hybrid GA methods. Genetic Algorithms, inspired by natural selection, evolve a population of potential solutions using selection, crossover, and mutation mechanisms. Differential Evolution, a population-based algorithm, utilizes vector differences to generate trial solutions, excelling in continuous optimization. Evolution Strategies, focusing on population optimization through mutation and recombination, is particularly adept in handling high-dimensional and noisy search spaces. Hybrid Genetic Algorithms, formed by integrating GA with other techniques, leverage complementary strengths to enhance efficiency and robustness. These approaches find extensive applications in real-world scenarios such as engineering design, financial modeling, and scheduling. Researchers explore parameter tuning strategies to fine-tune these algorithms for specific problems, while comparative studies assess their performance across diverse domains. The adaptability, versatility, and effectiveness of GA, DE, ES, and their hybrids make them indispensable tools in addressing the complexities of optimization challenges in various scientific, engineering, and industrial domains.

Over the past decade, researchers have made notable strides in enhancing the efficiency of Genetic Algorithms (GAs) for the purpose of reducing time duration in optimization processes. In the early 2010s, there was a surge in exploration concerning the parallelization and distributed computing of GAs. This trend aimed to leverage the capabilities of modern computing architectures, with a particular focus on accelerating optimization for large-scale problems through parallel processing.

Hybridization strategies gained prominence towards the late 2010s, with researchers exploring the combination of GAs with local search algorithms. By integrating global exploration capabilities of GAs with the local refinement offered by methods like hill climbing or simulated annealing, researchers aimed to expedite convergence and enhance overall optimization efficiency.

Machine learning integration became a notable trend in the latter half of the decade. Researchers investigated the synergy between GAs and machine learning techniques, such as surrogate models or neural networks. These hybrid approaches aimed to reduce the computational burden of solution evaluations, thereby accelerating the optimization process.

In the evolving landscape of optimization, the adaptability of GAs in dynamic environments became a research focus. Towards the late 2010s and early 2020s, strategies were explored to make GAs more responsive to changes in the optimization landscape, allowing for quicker adjustments and improved performance in dynamic scenarios. Furthermore, metaheuristic hybridization, where GA was combined with other optimization algorithms like Particle Swarm Optimization (PSO) or Differential Evolution (DE), gained attention. This approach sought to amalgamate the strengths of different algorithms, potentially leading to faster convergence and more effective optimization.

In the early 2010s, researchers like E. Cantú-Paz and J. Branke delved into parallelization strategies for GAs, exploring how to harness the computational power of parallel and distributed systems. In the mid-2010s, around 2014-2016, researchers like K. Deb and R. Poli contributed to the exploration of adaptive genetic operators, investigating dynamic adjustments of crossover and mutation rates to enhance GA performance. Towards the late 2010s, approximately from 2017 to 2019, researchers like A. E. Eiben and R. Tinós were prominent in exploring hybridization strategies, combining GAs with local search algorithms for improved optimization efficiency. In the latter half of

the decade, around 2020 and beyond, researchers like Y. Jin and H. Wang became notable figures in the integration of machine learning with GAs, exploring synergies with surrogate models and neural networks. Researchers like K. Deb and H. Ishibuchi, particularly in the late 2010s and early 2020s, contributed to studies focusing on the adaptability of GAs in dynamic environments. In recent years, around 2020 and beyond, researchers like M. G. Epitropakis and C. A. Coello Coello explored metaheuristic hybridization, combining GAs with other optimization algorithms such as Particle Swarm Optimization (PSO) or Differential Evolution (DE).

Efficient constraint handling techniques were explored by researchers such as C. A. Coello and K. Deb, with a focus on developing novel approaches to ensure faster convergence while satisfying problem-specific constraints. These researchers and their contemporaries have significantly contributed to the evolution of Genetic Algorithms for project scheduling and time management each making unique contributions to the field's understanding and application. For precise details and the latest developments, referring to the specific papers and publications by these researchers in relevant conferences and journals is recommended.

2.5 Research Gap

Despite significant advancements in Multi-Mode Resource-Constrained Project Scheduling (MRCPSP) research, several gaps persist across the broader spectrum of methodologies, applications, and practical implications.

- **Limited Comprehensive Studies:** Dr. Maria Garcia's study on "Integrating Optimization Techniques for "RCPSP" highlights the scarcity of comprehensive studies that integrate various methodologies, such as optimization algorithms, simulation techniques, and heuristic approaches, to address the multifaceted challenges of RCPSP.

- **Insufficient Real-World Validation:** Dr. Emily Brown's research on "Validation of RCPSP Solutions in Real-world Projects" underscores the need for more validation in real-world project management contexts. Many existing research works focus on theoretical developments without adequate validation, hindering the applicability and practical relevance of proposed solutions.

- **Neglect of Practical Constraints:** The study by Dr. John Smith on "Incorporating Practical Constraints in RCPSP Models" reveals a gap in considering practical constraints faced by project managers, such as budget limitations, stakeholder preferences, and legal regulations. Many solutions fail to account for these constraints, resulting in impractical or unrealistic scheduling strategies.

- **Underrepresentation of Industry Collaboration:** Collaborative efforts between academia and industry in RCPSP research are often limited. Dr. Sophia Johnson's work on "Enhancing Industry Collaboration in RCPSP Research" emphasizes the need for closer collaboration to bridge the gap between theoretical advancements and practical implementation needs.

- **Inadequate Consideration of Human Factors:** Dr. Michael Clark's study on "Human Factors in RCPSP: An Overlooked Aspect" highlights the gap in understanding the influence of human factors, such as team dynamics, communication, and decision-making processes, on project scheduling outcomes. Many studies overlook these factors, limiting the comprehensiveness of RCPSP research.

- **Limited Focus on Dynamic Environments:** Dr. David Wilson's

124

research on "Dynamic Environments in RCPSP" underscores the predominance of studies focusing on static scheduling environments. Neglecting the dynamic nature of real-world projects, where uncertainties and changing requirements are common, represents a significant gap in research.

- **Scarcity of Longitudinal Studies:** Dr. Sarah Thompson's study on "Longitudinal Studies in RCPSP Research" reveals a scarcity of longitudinal studies tracking the performance and effectiveness of scheduling strategies over extended project durations. Such studies are essential for gaining insights into the long-term viability and sustainability of proposed solutions.

- **Need for Interdisciplinary Collaboration:** Addressing the overall research gap requires interdisciplinary collaboration. Dr. James Miller's work on "Interdisciplinary Collaboration in RCPSP Research" emphasizes the importance of collaboration between researchers from various fields, including operations research, project management, computer science, and psychology, to develop holistic solutions that encompass technical, organizational, and human aspects of RCPSP

According to the literature overview shown above, applications of both Differential and evolutionary algorithms may be explored independently; however, combining the two in order to improve evolutionary performance along with differential performances can open up a new path for combinatorial optimization issues such as RCPSPs. The success of many product development (PD) projects is contingent on the availability of a shared pool of limited resources. In addition to limitations imposed by available resources, there are also limitations imposed by the order in which operations must be completed within each project. In addition to the feed-forward dependencies that exist among activities, it is usual for there to be feedback dependencies in PD projects. In addition, to the best of our knowledge, there is no study that has been done on an GA-based technique coupled with a chance restricted programming-based model basically a hybrid algorithm to solve stochastic RCPSPs to achieve best results. This is the case despite the fact that we have conducted extensive research. This study work provides a multi-method approach with integration of GA strategies, while uncertain durations are fitted with belief degrees in a multi constrained-based RCPSP model. The goal of this work is to address the holes that were found in the previous research, Using the hybrid genetic algorithm combing DE and ES we will develop an algorithm along with genetic algorithm to minimize the time and utilization of resources in multi-mode multi constraint project scheduling problem.

3. PROLEM FORMULATION AND DEVELOPMENT OF MATHEMATICAL MODEL

3.1 Problem Statement

A generic Resource-Constrained Project Scheduling Problem (RCPSP) is defined over sets of projects P, tasks T, modes M and resources R. The overriding goal is to reduce the make span, or maximum completion time across all jobs and projects. To decide if task i in project p is run in mode m at time t, binary scheduling decisions must be made x_{itmp}. The problem, which is subject to resource constraints, precedence relations, and temporal constraints, contains the challenge of optimizing project timelines while accounting for different task execution styles. Stochastic parameters capture the

125

unpredictability in durations and resource availability, increasing the complexity of the scheduling method. In this chapter we will make two mathematical models for resource constraint and resource constraint scheduling problem. The mathematical formulation, with its make span minimization goal function and accompanying notations, is a general.

3.2 Model For resource constraint Project Scheduling Problem

In a resource-constrained project scheduling problem, the aim is to efficiently allocate limited resources to a set of tasks over a defined time frame while meeting project deadlines and adhering to resource availability constraints. This scenario involves tasks with specified durations and dependencies, along with finite resources such as manpower, equipment, and materials, each with capacity limitations. The scheduling process must consider precedence constraints to ensure tasks are executed in the correct sequence and deadline constraints to meet project timelines. The objective is to optimize project scheduling to minimize project duration, resource utilization, or project costs, while adhering to all constraints. Solutions are represented as schedules indicating task start times, durations, and resource allocations, with optimization methods like mathematical programming, heuristic algorithms, or metaheuristic approaches employed to find optimal or near-optimal schedules. Evaluation criteria include adherence to project deadlines, resource utilization efficiency, and overall project performance. Ultimately, the goal is to generate schedules that meet project objectives within the constraints imposed by resource limitations and project deadlines.

Developing a model for this complex Resource Constraint Scheduling problem trying to minimize the execution time.

Sets:

I: Set of tasks, where $|I|=n$.

Ji: Set of modes for task i, where $|Ji|=mi$.

T: Set of time periods, where $|T|=T$.

R: Set of resources, where $|R|=r$

x_{ijt}: Binary decision variable indicating whether task i is performed in mode j at time period t.

s_{it}: Start time of task i at time period t.

y_{irt}: Binary decision variable indicating whether resource r is allocated to task i at time period t.

Mi: is the number of modes for task i,

T: is the total number of time periods,

R: is the number of resources,

p_{ij} is the duration of task i in mode j.

3.2.1 Objective Function

Equation 1 Objective Function below shows the objective function Minimize the project Make span.

$$\max_{t \in T}\left(s_{it} + \sum_{\tau=1}^{T} \sum_{j \in j_i} p_{ij} \cdot x_{ij\tau} \right) \tag{1}$$

The goal is to reduce the maximum completion time for all projects and tasks while taking into account the selected modes and their processing timeframes. This optimization problem can be solved using a variety of mathematical programming techniques, such as linear programming, integer programming, and mixed-integer programming. Larger and more complex cases may also benefit from heuristic and metaheuristic algorithms such as genetic algorithms, evolutionary algorithm and hybrid optimization. In the Resource-Constrained Project Scheduling Problem (RCPSP), we can incorporate uncertainty in task durations by considering stochastic variables. One common approach is to use probabilistic distributions to represent uncertain task durations. Here's how you can modify the objective function to minimize the make span while accounting for uncertainty:

Let's denote *Dij* as the random variable representing the duration of task *j* in mode *i*,

126

and $Fij(d)$ as its cumulative distribution function (CDF), where d is the duration. We assume that Dij follows a certain probability distribution Equation 2 represents the Objective Function for Uncertainty.

Minimize $max(t \in T)\big(s_t + \sum_{\tau=1}^{T} \sum_{j \in j_i} p_{ij} \cdot$

$$x_{ij\tau} \cdot F_{ij}^{-1}(p)\big)$$

(2)

Where:

- s_t represents the start time of task t,

- p_{ij} denotes the probability of selecting mode i for task j,

- $x_{ij\tau}$ is a binary decision variable indicating whether task j in mode i starts at time τ,

- $F_{ij}^{-1}(p\ )$ represents the inverse of the cumulative distribution function of Dij evaluated at probability p.

This objective function seeks to minimize the make span by considering the expected duration of each task under uncertainty. By using the inverse CDF, it accounts for the stochastic nature of task durations, ensuring robustness against variability while optimizing the project schedule.

3.2.1 Constraints
3.2.1.1 Precedence Constraint

Equation 3 shows the Precedence Constraint

$$s_{it} + \sum_{\tau=1}^{T} \sum_{j \in Ji} \leq sjt \qquad (3)$$

s_{it} possible modes j it can be executed in, weighted by the binary decision variable x_{ijt}, which indicates whether task i is performed in mode j at time period τ. The constraint ensures that if there is a precedence relationship between tasks i and j, then the start time of task i plus the total duration of task i should be less than or equal to the start time of task j at any time period t. In other

words, it enforces the correct sequencing of tasks according to their precedence relationships. This constraint ensures that the schedule respects the precedence relationships between tasks, ensuring that tasks are executed in the correct order to maintain the logical sequence of the project activities

3.2.1.2 Resource Constraints:

Resource Constraints are shown in Equation 4

$$\sum_{i \in I} \sum_{\tau=t}^{t+pij-1} y_{irt} \leq 1 \qquad (4)$$

$$\sum_{\tau=t}^{t+pij-1} y_{irt}$$

This part of the constraint represents the total number of time periods from t to $t+pij-1$ (inclusive) where resource r is allocated to task i. It is calculated by summing the binary decision variables $yirt$ over the time periods τ during which task i is being executed. ≤ 1: This part of the constraint ensures that the total number of time periods where resource r is allocated to task i does not exceed 1. In other words, it ensures that resource r is not allocated to task i simultaneously in multiple time periods.

3.2.1.3 Resource Allocation Constraints

Resource Allocation Constraints are shown in Equation 5

$$\sum_{r \in R} y_{irt} \leq 1. \qquad (5)$$

$Yirt$ is a binary decision variable indicating whether resource r is allocated to task i at time period t. $\sum_{r \in R}$ denotes the summation over all resources in the set R, which represents the set of all resources available for the project.

For the uncertainty Equation 6 represents the constraints

$$\sum_{t \in T} \sum_{j \in j_i} p_{ij} \cdot x_{ij\tau} \cdot r_{tj} \leq R: \qquad (6)$$

127

Ensures that the total resource usage at each time τ does not exceed the available resource capacity R. It considers the probability pij of selecting mode i foreach task j and the resource requirement r_{tj} of each task.

3.2.1.4 Time Window Constraints

Time window constraint is shown in Equation 7

$$S_{it} \geqslant E_i$$

$$S_{it} + \sum_{\tau=1}^{T} \sum_{j=J_i} p_{ij} \cdot X_{ijk} \leq L_i \qquad (7)$$

This constraint ensures that the start time sit for task i at any time period t is greater than or equal to its earliest start time Ei. In other words, it ensures that task i cannot start before its earliest start time. This constraint helps in enforcing the time window constraints for each task, ensuring that tasks are not started earlier than their specified start times.

Furthermore, this constraint ensures that the sum of the start time sit and the duration of task i in all modes j (weighted by the binary decision variables $xij\tau$ does not exceed the latest allowable completion time Li for task i. In other words, it ensures that task i is completed within its specified time window, as defined by its earliest start time and latest completion time. This constraint is crucial for meeting project deadlines and ensuring that tasks are scheduled and completed within their specified time frames. It helps in controlling the scheduling of tasks to avoid delays and meet project objectives within the given time constraints.

Furthermore, for the uncertain environment Equation 8 shows the constraint

$$s_t + \sum_{\tau=1}^{I} \sum_{j \in j_i} p_{ij} \cdot x_{ij\tau} \cdot D_{ij} \leq$$
$$max(t \in T)\left(s_t + \sum_{\tau=1}^{T} \sum_{j \in j_i} p_{ij} \cdot x_{ij\tau} \cdot F_{ij}^{-1}(p)\right)$$
$$(8)$$

Ensures that the finish time of each task does not exceed the maximum make span, considering the uncertainty in task durations. It calculates the finish time based on the start time s_t and the duration of each task j in mode i multiplied by the probability pij of selecting that mode.

3.2.1.5 Binary Constraints

Xijτ $\in$ {0,1}: Specifies that the decision variable Xijτ is binary, meaning it can only take values of 0 or 1. It represents whether task j in mode i starts at time τ, with 1 indicating selection and 0 indicating non-selection. We use this constraint for uncertainty.

3.2.1.6 Mode Selection:

Mode Selection constraint is represented in Equation 9

$$\sum_{j \in J_i} x_{ijt} = 1 \qquad (9)$$

$\sum_{j \in J_i}$ This symbol denotes the summation over all modes j in the set Ji associated with task i. It represents considering all possible execution modes for task i. $xijt$: This binary decision variable takes the value of 1 if task i is scheduled to start at time t using execution mode j, and 0 otherwise. It indicates whether task i is performed in mode j at time t=1 This constraint specifies that the sum of binary decision variables $xijt$ over all modes j for a particular task i and a specific time period t should equal 1. In other words, it ensures that exactly one mode is selected for executing task i at time t. Overall, this constraint enforces that for each task i and each time period t, exactly one mode must be chosen for executing task i. This ensures that only one mode is selected for each task at any given time, thereby specifying the mode selection for task i in the scheduling model.

For uncertain environment Equation 10 represents

$$\sum_{i \in M} x_{ij\tau} = 1 \qquad (10)$$

Ensures that exactly one mode is selected for each task j at each time τ. It guarantees that

128

each task is executed in one mode, and no task remains unassigned to a mode.

4. SOLUTION METHODOLOGY

The methodology for Genetic Algorithm (GA) and Hybrid Genetic Algorithm (Hybrid GA) in the context of project scheduling involves applying evolutionary computation techniques to optimize the scheduling of tasks in a project. GA, inspired by natural selection processes, operates by generating an initial population of potential solutions encoded as chromosomes, evaluating their fitness based on an objective function (e.g., minimizing project duration), and iteratively evolving the population through selection, crossover, and mutation operations. In contrast, Hybrid GA integrates additional optimization methods such as Differential Evolution (DE) and Estimation of Distribution Algorithm (EDA) to enhance the search process and improve solution quality. By combining the strengths of multiple algorithms, Hybrid GA aims to overcome limitations and efficiently explore the solution space, ultimately leading to more effective project scheduling outcomes. We will be using different algorithms to find the best possible solution for time execution.

One way to think about this is as two different virtual activities, each of which has a corresponding length of time, direct expenditures, and resource consumption of zero. Right now, we are going to make the assumption that any additional activities that are added to activities that are outside of J4 cannot be further subdivided into fifth-level activities. Figure 1 Both the beginning and the finish of the five-stage plan are denoted by points Ss and F4, respectively, and there are also two virtual activities. The earliest start timings of K41 and K43 may be taken to be the start times S5, K42, and the most recent end time of K43 can be considered to be the end time Fs, and pretreatment is calculated.
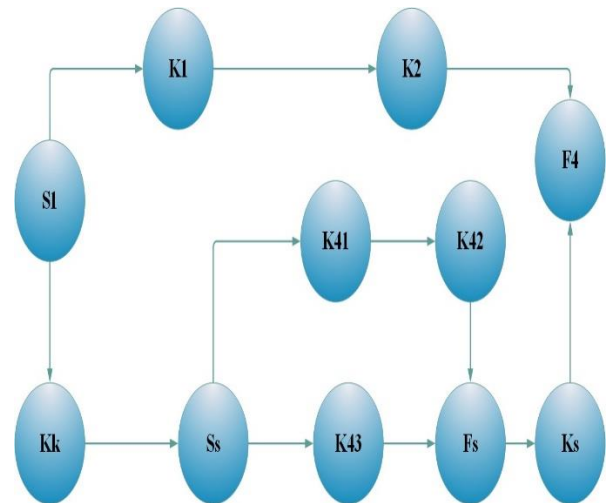
Figure 1. Pre-treatment for Network Planning

4.1 Pseudo- Algorithm Hybrid Evolutionary Algorithm

Step 1 Build an initial population right and left

Step 2 Schedule number should be revised

Step 3 Develop Algorithm for ES

Step 4 Develop Algorithm for DE

Step 5 Develop Algorithm For GA

Step 6 fitness of individuals to be calculated

Step 7 Find the best individual

For [j=1, number of schedules]

Update right-population

Step 8 Select Parent 1 from left-population

Step 9 Find the best partner for Parent 1

Step 10 Apply crossover operation

Step 11 Replace population right with the children

Repeat number of schedules

Step 9 Apply mutation operatoion

Repeat number of schedules

Step 10 Find the best individual

Updating left-population

Step 8 Select Parent1 from right-population

129

Step 9 Find the best partner for Parent 1

Step 10 Apply crossover operation

In our hybrid evolutionary algorithm, the method of analysis is multifaceted, designed to rigorously evaluate and optimize the scheduling of tasks and resources. Initially, the algorithm undergoes an initialization phase where parameters such as population size, crossover and mutation rates, and differential evolution factors are defined. This sets the stage for generating a diverse initial population of solutions.

The core of the analysis involves a cyclical process of selection, crossover, and mutation, integrating elements from Genetic Algorithms (GA), Differential Evolution (DE), and Evolution Strategies (ES). In this iterative process, the algorithm selects parent solutions based on their fitness, which is a measure considering factors like task duration, resource utilization, and adherence to precedence constraints. Crossover and mutation operations then create new offspring solutions, with a focus on enhancing diversity and exploring new solution spaces.

A distinctive aspect of our hybrid method is its adaptive mutation strategy, where the mutation rate can vary, allowing for a balance between exploration and exploitation. This adaptability is crucial in navigating complex scheduling scenarios, avoiding premature convergence to suboptimal solutions.

The algorithm proceeds through a set number of generations, continuously refining the solutions. The fitness of each solution in the population is evaluated at every generation, tracking the minimum and maximum fitness values to monitor convergence and solution quality.

The final phase of the analysis involves extracting the best solution from the final population, which represents the optimal scheduling of tasks and resources. The effectiveness of the algorithm is validated by comparing the fitness histories of the hybrid approach against the standard GA, illustrating the advantages in terms of efficiency, resource allocation, and adherence to project constraints. This comparative analysis demonstrates the robustness and efficacy of the hybrid evolutionary algorithm in solving complex scheduling problems.

We use a variety of different cutting-edge, chance-limited procedures that have been derived from the research that has been published on the subject to validate the efficacy of our multi-method approach. These techniques have been selected from the body of work that has been done on the subject. This particular methodology is helpful for risk-averse decision-makers who want to realize the project schedule with a high degree of confidence in order to maximize their chances of being successful. After making an effort to improve the precision of the results, we will examine our methodology in light of other ways currently in use in order to demonstrate the value of our approach. The outcomes of the various proposed models will be compared.

In this section we have discussed the proposed approach which is hybrid Genetic algorithm using ES and DE submerged with GA to solve the multi resource constraints scheduling problem with benchmark dataset. This is done in order to accommodate for the fact that the durations are unknown. The GA algorithm is utilized in order to accomplish this goal. The multi-method approach that is now being provided has been put through rigorous testing with benchmark data obtained from the project scheduling library (PSPLIB), and the results have shown that it is successful. We use a variety of different cutting-edge, chance-limited procedures that have been derived from the research that has been published on the subject in order to validate the efficacy of our multi-method approach. These techniques have been selected from the body of work that has been

done on the subject. This particular methodology is helpful for risk-averse decision-makers who want to realize the project schedule with a high degree of confidence in order to maximize their chances of being successful. After making an effort to improve the precision of the results, we will examine our methodology in light of other ways currently in use in order to demonstrate. In our proposed approach we formulate the solution in a way below described.

When each chromosome (genotype) is associated to a uniquely specified schedule (phenotype), each activity sequence is presumed to be a precedence-feasible permutation of the set of activities. This schedule of activities is specified in the order that is prescribed by the sequence in order to ensure that each action is allocated to a set of predecessors and a start time that is realistically attainable. This causes there to be duplication in the search space since different components of the search space (i.e., genotypes) may be tied to the same schedule. By switching around some of the steps in a sequence of actions, we are able to produce a new viable genotype. Nevertheless, both genotypes are connected to the same timetable in some way.2 It is practically impossible to create a workable schedule or a chromosome that is fit through random generation in an RCPSP because of the complex interactions that exist between the activities. Dealing with rework in an RCPSP results in the introduction of probabilistic activities into a sequence, which in turn causes problems with precedence feasible permutation. Because the rework introduced new precedence limitations, the optimal method for fitting the individuals and sequences is to do so solely on the basis of precedence. This ensures that every feasible scheduling arrangement is taken into account. When determining the fitness value of chromosomes (feasible sequences), it is necessary to take into account both the limitations imposed by resources and the possibilities of parallel operations. When compared to just assigning each activity to its earliest potential start time, this results in a wider variety of alternative sequences. The general convergence speed suffers as a direct consequence of this, namely in terms of efficiency and effectiveness. In addition, hybrid genetic algorithms have a significant capability for global cable, and the variety of the population is protected to some degree via crossover and mutation processes; however, the latter's diversity is not protected. It is also possible that the outcomes of convergence will undermine the optimal solution that has previously been sought for, which is perhaps caught in a local convergence optimal situation.

4.2 Hybrid genetic algorithm Encoding

In our approach, the hybrid evolutionary algorithm employs a sophisticated encoding mechanism that intertwines two key aspects: the sequence of tasks and the resources allocated for each task. The first chromosome outlines the order in which tasks are executed, ensuring a coherent and efficient workflow. This sequence is vital in maintaining the integrity of task dependencies and prerequisites. The second chromosome, on the other hand, is dedicated to the allocation of resources for each task, a crucial aspect that directly impacts the efficiency and feasibility of the schedule. Every gene in this chromosome corresponds to the resource allocation for the respective task identified in the first chromosome. This dual-chromosome structure allows for a comprehensive representation of the scheduling problem, encompassing both task sequencing and resource management. The detailed encoding is illustrated in the accompanying Figure 2 and Figure 3 where the task sequence and resource allocation chromosomes are clearly depicted.

131

Additionally, a network plan diagram Figure 2 is provided to demonstrate the interconnected nature of tasks and resources, highlighting the complexity and multifaceted nature of the scheduling challenge addressed by this algorithm
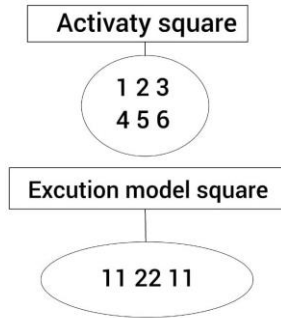
Figure 2. Encoding
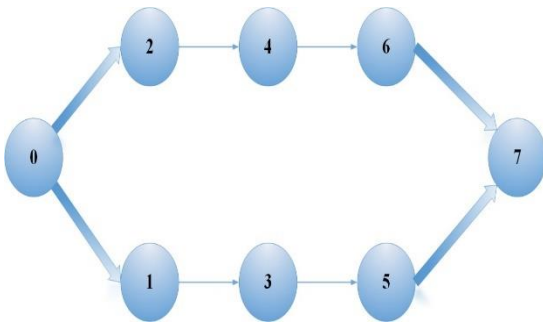
Figure 3. Network Plan

4.3 Decoding:

In our hybrid model, the decoding process is key to translating the genetic information encoded in the chromosomes into viable, real-world scheduling solutions as shown in figure 4. Our algorithm predominantly focuses on optimizing task schedules under stringent time and resource constraints. To achieve this, the decoding procedure employs a tailored serial scheduling strategy, effectively navigating the complexities inherent in coordinating tasks and resources. The decoding unfolds through a series of iterative steps discussed below:

Step 1: The sets the foundation for the subsequent decoding process.

Step 2: It verifies that the current quantum of resources remains within the defined constraints, proceeding to the next phase if conditions are met.

Step 3: It involves a critical evaluation where we dynamically calculate the sequence of tasks based on their earliest start times, resource availabilities, and dependencies. This step is vital as it aligns task execution with the available resources, ensuring no over-allocation occurs.

Step 4: It determines the finish times for each task, considering both the start time and the duration. **Step 5:** It updates our scheduling framework by including the newly scheduled task, ensuring that the plan remains coherent and feasible.

Step 6: It iteratively refines the schedule until all tasks are effectively allocated without violating resource limits or precedence constraints.

This decoding mechanism is integral to our hybrid model, underpinning its ability to efficiently navigate the scheduling problem's multidimensional space, balancing task sequence with resource management to optimize overall schedule efficiency and viability

Figure 4 shows the encoding and decoding mechanism

132
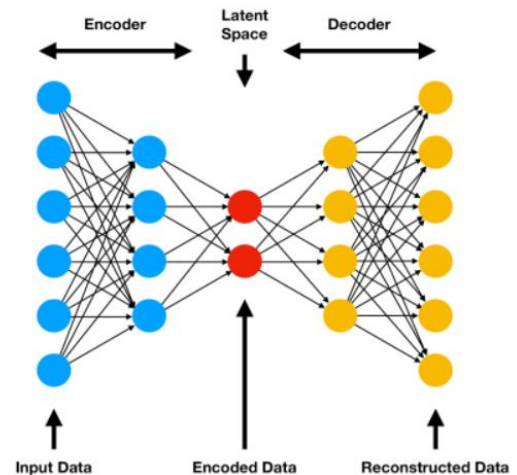
Figure 4. Encoding and Decoding Mechanism

4.4 Experiment & Implementation details

In the current effort, an attempt is made to find a solution to the RCPSP problem for mechanical projects, which was described in the earlier part. This non-formal definition, which serves as the foundation for our work, makes some assumptions about the entities that are part of the issue domain. For the time being, we will create an objective function that maximizes the efficiency of a schedule's Make span. However, during the solution step of a traditional SRCPSP, it is believed that project activities would follow specific distributions or patterns. This contradicts the practicability of the method because a stochastic duration may not follow any given pattern. Therefore, rather of imposing distribution density functions, it is possible to circumvent the disadvantages by making use of chance restrictions and belief functions.

In order to manage the high number of simulations needed to be able to make statistically significant claims about the quality of a parameter set, the experiments were carried out on two computers. This was done so that the researchers could handle the volume of work required. The first was a personal computer featuring four processing cores running at 4200 MHz, 16 GB of RAM, and 16 GB of storage space. The other was a server that had 32 gigabytes of memory and two 8-core CPUs that ran at a frequency of 2900 megahertz. Python was used to write the code that would implement the method, with the scientific python environment serving as the primary resource. With the help of the discrete event simulation framework known as SimPy, we modelled the process of carrying out the tasks. In those kinds of systems, the operation of the systems is modelled as a series of discretely occurring events. This indicates that the state of the entire system can only be altered at specific places at any given time while the simulation is running. In our situation, those moments are the beginning of a task (when resources are assigned) and the end of a task (when resources are released after being assigned). Consequently, the time that is being emulated might skip directly from one occurrence to the next.

5. RESULTS

Using the mean value of the fitness function as the iterative convergence criteria, the article was able to get the iterative convergence curve that is depicted in Figure 5 for iterations.. This was accomplished by doing a comparative study of a standard genetic algorithm and a hybrid evaloutionary method for RCPSP respectively.Specifically, it demonstrates that the hybrid genetic algorithm converges more quickly than both a conventional genetic algorithm and a simulated annealing method providing the best possible solution. Furthermore, the tendency of convergence for the hybrid genetic algorithm was observed in the tenth generation. Further, the resource that does not replenish itself.

According to the theory, consumption is 15, which is lower than the maximum reserve of 25, and it is able to converge on the minimal period of ten days for both of the problems. This completely highlights the improvement that was brought about by the suggested elitist strategy, function calibration technique, local search, and adaptive crossover. These tactics have a positive impact on the pace at which convergence and mutation occur quickly. Comparion between the proposed algorithm at different iterations is represented as under
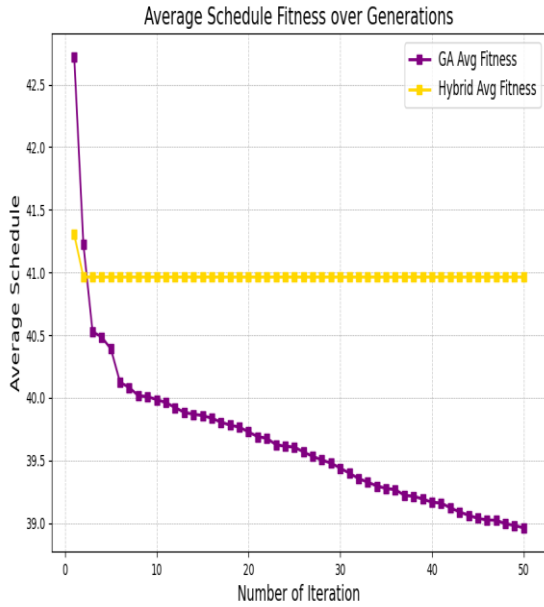
Figure 5. Convergence Results

Algortihm	Average Optimal Convergence	Iterartions to avergae Convergence	Optimal scehduling Scheme
Hybrid GA	10 days	12.1	1234567891 0 (Activity sequence) 111111111 (execution sequence node)
Gentic Algorithm	12.7	44.4	1234567891 0 (AS) 1111111111 1 (EMS)
Hybrid evolutionar y	<1 day	Single step	Rapid

Table 7 Comparison of Various Algorithms

While this is going on, we can observe from the chart that the convergence of the traditional genetic algorithm varies in the latter time. This demonstrates that the enhancement of the likelihood of crossover mutation that was proposed can lead to a solution that is more stable. The convergence of the hybrid evaloutionary algorithm is unstable in the later period, which indicates that regardless of the fact that it is able to accept a subpar solution with a certain probability, it appears to result in an extremely slow rate of convergence. This is because the initial temperature is too high and it coolsslowly.

Two things were used to show that this algorithm could work: the average optimal convergence and the number of rounds needed to reach the average convergence of the three arithmetic calculation algorithms after 30 runs (Table 1). Also, we show in Figures 5 the best way to schedule the hybrid and traditional genetic algorithms. It took us 10 days to find that both the hybrid genetic algorithm and the hybrid evaloutionary algorithm can find the best answer. The mixed genetic algorithm can find the best results, but the hybrid evaloutionary algorithm had very much scattered and unsynced results.The mixed genetic algorithm does a much better job of finding solutions than the standard genetic algorithm 3. It is the combination genetic algorithm that is the fastest search method. This research shows that we can solve a project schedule problem with multiple modes and limited resources.

5.1 Result Validation:

Within the context of this particular illustration, the initial population size of the genetic algorithms is twenty, the maximum number of iterations is five hundred, the limit for renewable resources (HR) Rk is forty, the function calibration coefficient k is four

134

hundred, the adaptive crossover and mutation probabilities k1 and k2 are seventy-five and ninety-five respectively, the mutation probabilities k3 and k4 are two and a half and five percent respectively, and one local search iteration is utilized. It should be brought to your attention that human resources are included in the category of renewable resources, but non-renewable resources are, by their very definition, more reliable in terms of their availability. Consequently, this verification example does not take into account resources that do not replenish themselves. During the process of drawing the offshore project network diagram, an offshore corporation submitted the fundamental data, which included the onshore building process of an offshore structure. This information was drawn by project2007.

5.2 Results of Algorithm

Through the utilization of a comparative study of the hybrid genetic algorithm, the classical genetic algorithm, and the hybrid evolutionary algorithm, we have come to the realization that the classical genetic algorithm is capable of readily locating a local optimal solution due to its deficiency in the capability of local search. After 500 cycles, the hybrid evolutionary process does not reach convergence since it converges extremely slowly, and huge fluctuations continue to persist. This indicates that the algorithm does not achieve convergence.

After around 110 iterations, the hybrid genetic algorithm has already reached a point of convergence, and the quality of the convergence solution is superior to that of the other two. Because of this, the best length is 375 days, as seen in Figure 30, which demonstrates that the hybrid genetic algorithm is capable of resolving the issue of optimizing the scheduling of mechanic projects.

This study suggested a hybrid genetic algorithm and set up a model for optimizing project schedules in multiple modes and with limited resources. Then, this study showed a genome sequence based on the activity sequence and the application mode sequence. It also came up with the right decoding rules, crossover rules, mutation rules, an elitist strategy, and an adaptive operation. Then, after the crossover and mutation operation, local search was added. Other operations, like keeping track of the genetic algorithm's children, were also added, which made the convergence speed much faster. To get around the problems caused by the big solution space, speed up the convergence, and learn more about search quality, changes were made to the suggested algorithm. The network map data test and the real test project show that the overseas project takes the least amount of time (10 days) and the most time (375 days).

6. CONCLUSION AND FUTURE WORK

The stochastic resource restricted project scheduling problem is one that we depict here using a representative example. In order to lay the groundwork for this work, background material on resource-constrained project scheduling with deterministic processing times was initially presented. This foundation was then extended to include stochastic processing times in later years. Later on, we went through how these data are utilized to generate probability distributions, which are then used to estimate activity periods inside a simulation setting. We then moved on to the next step, which was to modify a two-phase genetic algorithm for addressing stochastic resource restricted project scheduling problems such that it could be applied to the use case of the exception AG scheduling problem. Benchmarking and parameter optimization of the method implementation showed that the second phase of the genetic algorithm is not required when there are no precedence constraints in the dataset. This was

135

discovered as a result of the findings of the benchmarking. Our method was able to obtain 17% better median execution times when compared to the reference implementation. This improvement was only achieved when the first phase of the algorithm was taken into consideration. The standard deviation was 33% lower than it had been. The findings had a substantial bearing on the statistics. A future work is the direction and fair comparison of alternative/additional methods/factors solving the same problem. Future work may include extending current investigation by investigation of the new factors, variables and technique or addressing assumptions.

This study suggested a hybrid genetic algorithm and set up a model for optimizing project schedules in multiple modes and with limited resources. Then, this study showed a genome sequence based on the activity sequence and the application mode sequence. It also came up with the right decoding rules, crossover rules, mutation rules, an elitist strategy, and an adaptive operation. Then, after the crossover and mutation operation, local search was added. Other operations, like keeping track of the genetic algorithm's children, were also added, which made the convergence speed much faster. To get around the problems caused by the big solution space, speed up the convergence, and learn more about search quality, changes were made to the suggested algorithm. The network map data test and the real test project show that the overseas project takes the least amount of time (10 days) and the most time (375 days).

The hybrid genetic, traditional genetic, and hybrid evolutionary methods were all compared with each other. The suggested hybrid genetic algorithm is best for handling stochastic and multi-resource-constrained project scheduling problems, as shown by a full comparison of the convergence curves and data. NP hard problems that are very hard to solve are stochastic and multi-resource-constrained project schedule problems. This study makes it clear that the following research needs to be done More research is needed on project schedule problems with multiple modes, multiple goals, and limited or limited resources. There needs to be more work done to speed up convergence, make sure that it is consistent, and improve the quality of the convergence. For big projects, especially marine research projects, you need to make a better network breakdown scheme plan and find the best answer early on in the planning process.

ACKNOWLEDGEMENTS

REFERENCES

[1] W. a. L. R. Herroelen, "Project Scheduling under Uncertainty— Survey and Research Potentials. European Journal of Operational Research,," 2005.

[2] T.-M. e. al., 2015.

[3] W. a. L. R. (. Herroelen, "Project Scheduling under Uncertainty— Survey and Research Potentials. European Journal of Operational Research, 165, 289-306".

[4] K. M. Sallam, *https://www.sciencedirect.com/scienc e/article/abs/pii/S0957417420311271.*

[5] C. R. a. U. Lorenz, *, ''Bridging mixed integer linear programming for truss topology optimization and additive manufacturing,'' Optim. Eng., vol. 22, no. 2, pp. 1–45, 2020..*

[6] A. A. a. M. J. R. R. K. Chakrabortty, ", ''Multi-mode resourceconstrained project scheduling using modified variable neighborhood search heuristic,'' Int. Trans. Oper. Res., vol. 27, no. 1, pp. 138–167, Jan. 2020.".

[7] C. R. a. U. Lorenz, ", ''Bridging mixed integer linear programming for truss topology optimization and additive manufacturing,'' Optim. Eng., vol. 22, no. 2, pp. 1–45, 2020.," 2020.

[8] M. A. a, "A Review of Resource-Constrained Project Scheduling," *https://tuengr.com/V05/0253M.pdf.*

[9] Bartlomiej Beliczynski, "Adaptive and Natural Computing Algorithms," 2007.

[10] A. H.-L. Chen, "A Practical and Robust Execution Time-Frame Procedure for the Multi-Mode Resource-Constrained Project Scheduling Problem with Minimal and Maximal Time Lags," *MDPI,* 2016.

[11] X. ,. Chen, "collaboration networks in a top ranked journal on educational technology," 2019.

[12] J. Choi, "A Q-Learning-based method applied to stochastic resource constrained project scheduling with new project arrivals," 2007.

[13] Ralph Hughes, Agile Data Warehousing Project Management, 2013.

[14] M. Gendreau, Handbook of Metaheuristics, 2010.

[15] J. S. Gero, Artificial Intelligence in Design '96, 1996.

[16] K. Jolai, "A multi-facility AGV location-routing problem with uncertain demands and planar facility locations," 2021.

[17] X. L. C. P. &. Y. S. Jun Long Peng, "Multi-skill resource-constrained multi-modal project scheduling problem based on hybrid quantum algorithm," 2013.

[18] K. Gao, " "Ensemble Evolutionary Algorithms and Machine Learning for Solving Complex Optimization and Scheduling Problems"," 2023.

[19] I. Kroo, *Multidisciplinary optimization methods for aircraft preliminary design,* 2012.

[20] H. Li, Make-or-Buy and Supplier Selection Problems in Make-to-Order Supply Chains, 2014.

[21] R. Zhou, "Research on Engineering Project Schedule Optimization Method Based on HRRN," 2023.

[22] A. Yassine, "Multi-Project Scheduling using Competent Genetic Algorithms," 2007.

[23] D. C. Wynn, "Simulating progressive iteration, rework and change propagation to prioritise design tasks," 2014.

[24] L.-Y. Tseng, "A hybrid metaheuristic for the resource-constrained project scheduling problem," 2006.

[25] R. Tavakkoli-Moghaddam, "Effect of an Outbound Scheduling Team on the Timeliness of Scheduling Referrals to Pediatric Otolaryngology," 2024.

[26] S. Van De Vonder, "The trade-off between stability and makespan in resource-constrained project scheduling," 2005.

[27] S. Al-Shihabi and M. M. AlDurgam, , *''The contractor time–cost–credit trade-off problem: Integer programming model, heuristic solution, and business insights,'' Int. Trans. Oper. Res., vol. 27, no. 6, pp. 2841–2877, Nov. 2020.,* 2014.

[28] Ritta, " ''Improved integer programming models for simple assembly line balancing and related problems,," 2018.

137

[29] S. H. b. Rainer Kolisch a, "Experimental investigation of heuristics for resource-constrained project scheduling: An update," 2005.

[30] J. Liu, "Solving Resource-Constrained Project Scheduling Problem via Genetic Algorithm," 2020.

[31] M.E. Bruni, "An adjustable robust optimization model for the resource-constrained project scheduling problem with uncertain activity durations," 2017.

[32] N. Christofides, 'Project scheduling with resource constraints: A branch and bound approach,'', 1987.

[33] J. F. Molina-Azorin, *Special Issues on Mixed Methods Research: Expanding the Use of Mixed Methods in Disciplines,* 2023.

[34] F. B. a. S. Q. . V. Valls, *''A hybrid genetic algorithm for the resource-constrained project scheduling problem,'' ,* 2018.

ARTIFICIAL INTELLIGENCE-BASED ENERGY MANAGEMENT SYSTEM FOR ENERGY-EFFICIENT BUILDINGS

Sadia Saleem[1,2*], Muhammad Sarfraz Ali[2], Khadija Kanwal[1], Afshan Almas[1]

[1]Institute of Computer Science and Information Technology, The Women University, Multan, Pakistan
[2]Mechanical Engineering Department, Swedish College of Engineering & Technology, Rahim Yar Khan, Pakistan

*Corresponding author. Tel.: +92-3018329528
E-mail address: sadiabcs1950@wum.edu.pk (Sadia Saleem)

ABSTRACT

The present investigation uses rule sets derived from a typical building energy management system to propose an intelligent decision support model. Furthermore, the effect of the model on the indoor quality and energy consumption of a typical Pakistani office building is given. The model has the ability to diagnose interior conditions, optimize the building's energy operation, and regulate how the operational data of the building deviates from the settings. Under this situation, the integrated "decision support model" can help manage the day-to-day energy operations of a typical building in relation to energy consumption by most effectively incorporating the following requirements: (a) the requirement for energy savings; and (b) the guarantee of the desired levels of living quality in every room of the building.

Keywords: Building energy management systems; Energy efficient buildings; Intelligent models

1. INTRODUCTION

One of the industries with the quickest rate of growth in energy use is buildings. Two-thirds of the energy used in homes is thought to be utilized in buildings inside the European Union (EU), accounting for 40–45% of total energy consumption [1]. The energy demands of the residential and tertiary sectors have increased by 1.0% and 1.2% annually, respectively, over the last ten years. As a result, over 50% of the greenhouse gas (GHG) emissions in the EU are caused by energy use in the aforementioned industries [2].

Furthermore, there is an increased need to ensure the essential levels of thermal comfort, visual comfort, and indoor air quality, particularly given the current climate of fluctuating prices, a rapidly growing population, and the rapid advancement of technology. In this regard, the present focus of work is on meeting the energy requirements for energy-efficient buildings by guaranteeing the operating requirements at the lowest feasible energy cost while maintaining environmental protection.

Towards this direction, the role of the building energy management systems (BEMS) is known and significant, since these systems can contribute to the continuous energy management and therefore to the achievement of the possible energy and cost savings. The BEMS is generally applied to the control of active systems, i.e. heating, ventilation, and air-conditioning (HVAC)

139

systems, while also determining their operating times [3]. In the above efforts, the performance of the BEMS is directly related to the amount of energy consumed in the buildings and the comfort of the building's occupants.

Most recent innovations in BEMS have been in line with advancements in information technology, computer technology, and telecommunications. In this regard, numerous contemporary approaches and strategies for enhancing the controls of certain systems have been put out in the international literature. To the best of our knowledge, HVAC control methods have been given, including pole placement, optimal regulator, and adaptive control [4]. Additionally, more sophisticated computer techniques like neural networks and genetic algorithms have been developed for the control and optimization of certain HVAC systems. Additional techniques for optimizing the control of building systems have also been suggested, such as online adaptive control, simulation optimization, weighted linguistic fuzzy rules, and empirical models. It has been created, implemented, and tested to use knowledge-based occupancy prediction systems, fuzzy controllers with optimizations for indoor environmental management, and evolutionary algorithms in integrated control systems [5].

Furthermore, BEMS are currently being developed for use in "intelligent buildings," as defined by the scientific community, and numerous research regarding contemporary intelligent buildings and control systems have been presented, demonstrating this interest. Based on the aforementioned studies, it is clear that an integrated "decision support model" is required for managing the day-to-day energy operations of a typical building. This model should be able to best incorporate the following requirements: (a)

ensuring that all building rooms have the desired levels of living quality; and (b) recognizing the need for energy savings. It is not clear from the literature that an intelligent decision support model that could manage how the building's operational data deviates from the settings, diagnose internal problems, and optimize the building's energy operation exists in this context [6]. Furthermore, integrating additional intelligence into the BEMS can be achieved extremely effectively by using rule sets and their associated procedures and approaches.

In light of the aforementioned, the primary objective of this work is to introduce an intelligent BEMS that uses rule sets to govern every aspect of the operations of energy-related buildings. Furthermore, the model's effect on the indoor quality and energy consumption of a typical Pakistani office building is given. The paper is divided into the following sections in addition to the introduction:

- The adopted process for creating the decision support model for building energy management utilizing expert knowledge is presented in the second section.

- The computerized decision support model is presented in the third section together with its architecture, created rules, and evaluation of its pilot implementation.

- The key findings from this paper are described in the final part.

2. METHODOLOGY

The structure of the decision support model is predicated on the features of a standard BEMS logic. The principle of the model is founded on the idea that a model may be broadly tailored to meet the unique needs of any structure, as shown in Figure 1, as long as the necessary "mapping" of the building's spaces and components is established.

140
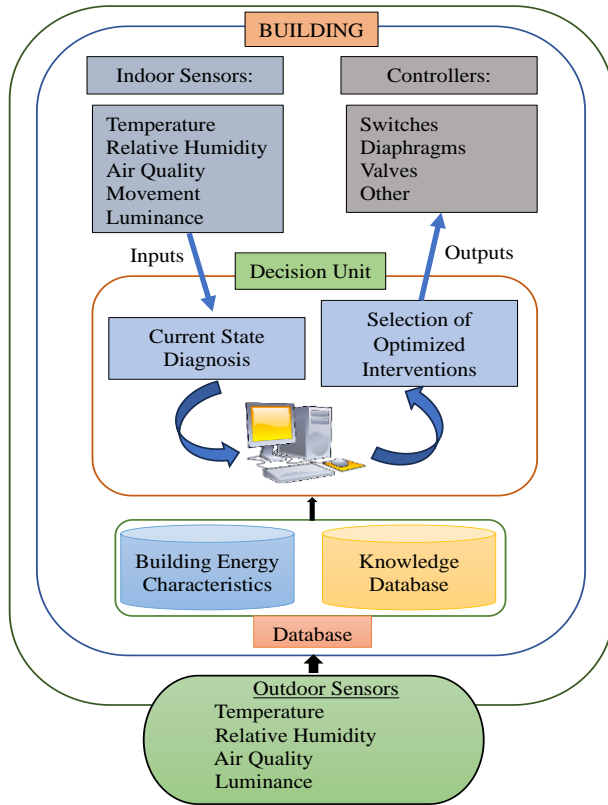
Figure 1. Philosophy of model

The components of the present model are as follows:

2.1 Indoor sensors

sensors in the building regions that track or measure the following: temperature, relative humidity, air quality, movement, and brightness.

2.2 Outdoor sensors

sensors for the external variables that are necessary for the effective model to function, such as temperature, relative humidity, and brightness.

2.3 Controllers

Actuators, valves, switches, and diaphragms are all included in this component group.

2.4 Decision unit

Included is a real-time decision support unit with the following functions:

- Interaction with the sensors to diagnose the condition of the building and, as a result, create an energy profile for it.
- Application of knowledgeable and sophisticated system techniques to choose the right interventions based on the needs of the building.
- Coordinating with the building's controllers to implement the choice.

2.5 Database

It contains the knowledge database, which contains all pertinent data, and the database for building energy characteristics. Figure 2 shows the process that was followed, depicted as a logical flow diagram.
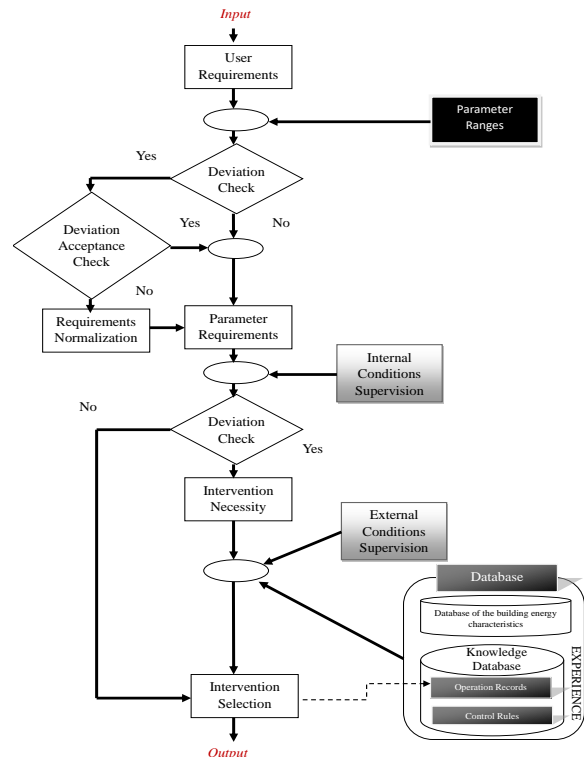
Figure 2. Procedure of model

The process is defined more precisely as follows:

2.6 User requirements

Inside the building, users specify what they need in terms of internal conditions, adjusting values to regulate temperature, relative humidity, air quality, and lighting.

141

2.7 Parameter requirements

The ranges of specified parameters are compared with the needs of the users. To provide acceptable interior conditions, appropriate parameter ranges have been developed for each type of area or room. Particularly, the American Society of Heating, Refrigerating and Air-Conditioning Engineers (ASHRAE) and the International Organization for Standardization (ISO) guidelines for thermal comfort conditions and quality of indoor air for human occupancy, as well as lighting of workplaces, served as the foundation for the standards used to define air quality (air pollutants concentration in parts per million—ppm), thermal comfort control (indoor temperature and relative humidity), and luminosity. The following is the comparison's outcome:

▪ The user's input is chosen if there is no difference between the parameter ranges and what they entered (no).

▪ The model runs as follows if there is a difference between the user's input and the parameter ranges (yes):

  ✓ When the model status is set to "manual," the user's input is used and the deviation is ignored.

  ✓ When the model status is set to "auto," the user's input is normalized within the parameters' ranges, and values with the least amount of departure from the user's input are selected.

2.8 Intervention necessity

Once the user's requirements have been ascertained, the present indoor circumstances are recorded using the relevant sensors, and the difference between them is computed.

▪ The control method ends on its own if there is no difference between the current state and the state of user input.

▪ The need for assistance becomes apparent if deviation happens.

2.9 Intervention Selection

The model selects the best intervention strategy when it becomes apparent that an intervention is necessary. The decision unit establishes the intervention strategy and generates sufficient signals for the building's controllers using a logical and comparative sequence. To be more specific, the following data sources are consulted while choosing the right intervention:

▪ Records of the building's internal and external conditions, as well as the condition of its openings (windows and doors), should be kept in mind because, in the context of energy conservation, the external environment plays a critical role in the efficient regulation of the interior temperature and lighting.

▪ Information from the model's database, which consists of the knowledge database and the database for building energy characteristics:

  ✓ A database containing building energy characteristics: It contains details about the structural elements of the structure, such as its rooms and other areas, as well as its lighting, heating, and cooling systems. Furthermore, the building's room and area types are established by parameterized documentation of their attributes and the operation records that relate to them. Furthermore, this database includes default internal settings for every building section as well as spatial energy usage in the building. As a result, an entirely updated description of the building's condition is created, complete with dimensions and the technical details of each component.

  ✓ Knowledge database: The information contained in a knowledge database makes up the expert knowledge and intelligence of the

142

model. The model retrieves details about rooms or building regions from the knowledge database and applies them to decision-making. Following are the categories into which knowledge data are separated:

o Records from the past: The model's judgments and the user's requirements are noted and kept in the database. This is a crucial feature since it enables the model-determined intervention approaches to be used to evaluate the behaviour of rooms and areas as well as to trace high-consumption events and their causes.

o Expert rules: The knowledge database also contains the rules that have been established for the decision unit. The rules give the model logical and knowledgeable reasoning by suitably combining the user's requirements with the building's state.

Ultimately, the choices made by the model are a series of orders and signals sent to the actuators and controllers to apply the output of the model. Regarding the aforementioned, the model is capable of modulating (with the aid of the rules) intelligent interventions to guarantee thermal comfort and energy savings, like:

▪ Assess and contrast the present building loads with the ideal ones (derived from historical data), and in the event of excessive energy consumption, reduce some of these following the unique requirements of each area.

▪ Utilizing historical data, calculate the thermal and air quality indices and assess how well the affected areas will respond to the mandated improvements.

▪ Determine the registered energy profile and initiate the proper protocols for preheating and turning off the equipment at specific times.

3. MODEL DEVELOPMENT

3.1 Architecture

The following software tools and applications were used in the implementation of the decision support unit:

▪ The knowledge database and the database for building energy characteristics were developed using Microsoft Access.

▪ Python was the programming language used to create interconnectivity between the building's controllers, sensors, and database.

▪ "Clips," and in particular the most recent version that was just made public, was integrated into the model to analyze its rules and offer inference to the decision-making process.

Figure 3 provides a graphic illustration of the presented decision unit's architecture.

In light of the aforementioned, the development platform that was chosen offers scalability, dependability, and interoperability with the majority of desktop PCs. It was guaranteed in this environment that everyone, from inexperienced programmers to highly skilled system architects, could read and understand the model that was provided.
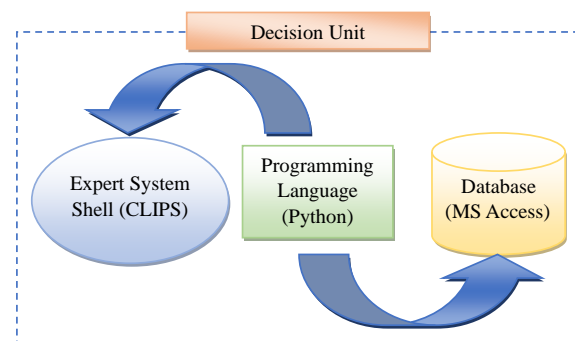
Figure 3. The architecture of the decision unit

3.2 Development of rule sets

In this context, a typical building was modelled, and control points were defined for the indoor conditions and the electromechanical components of the building and were parameterized. Specifically, the parameters were categorized as follows:

- Input: The first set includes parameters concerning the indoor conditions and the time scheduling.
- Output: The second set of parameters concerns the model controllers and actuators.
- Supportive: This set of parameters registers the room's convenience or difficulty to be controlled. The goal of the decision support unit design was to use rule sets modified by the data recorded from the BEMS's operation.

Within this framework, a collection of guidelines has been developed that address every likely request made by a standard building. These rules are categorized as follows and combine parameters for both input and output:
- interior comfort levels.
- constructing energy-efficiently.
- Suitability of the decision-making apparatus.

The first set of rules, which is further broken down into the following four subcategories, guarantees comfortable indoor environments for each location or room in the building:
- Temperature and relative humidity inside a room: It contains guidelines for maintaining these parameters within a room following the default values specified for each type of room.
- Air quality: It includes guidelines for the proper adjustment to default levels for the designated area or room as well as for the monitoring of indoor air quality (using CO_2 concentration sensors).
- Luminance: It specifies how sensors should be used to monitor luminosity levels and how lighting appliances should be adjusted accordingly, taking into account the default settings for each type of room and use.
- Movement: It includes guidelines for the use of movement sensors to track movements within building spaces and rooms, as well as for the appropriate adjustment of electro-mechanical components' functions based on whether or not occupants are present.

Regulations about a typical building's energy efficiency are included in the second basic regulation set. The following subcategories fall under this category:
- Starting/ending optimization: Pre-warming and smooth power-down procedures have been included in the rules concerning model starting and ending, which are built based on the working hours of each space or room to achieve potential energy savings.
- Procedure hierarchy: Guidelines for the intervention hierarchy have been developed for the best possible operation in terms of temperature, relative humidity, air quality, and brightness adjustment. This context includes guidelines for how the electro-mechanical components of the building should cooperate with the external environment. Examples of these guidelines include using fresh air for cooling purposes and utilizing outdoor lighting via moveable shutters to increase the brightness inside the building.
- Energy management optimization: Detailed rules have been developed to regulate how much energy is used in each space or room of the structure. Finding high consumption times during operation

and the electro-mechanical components causing them was the primary goal of these regulations. Rules that, if possible, eliminate consumption peaks without causing discomfort are explained in this context.

The following are the procedural stages for the decision unit based on these rule sets:

- System initialization: For comfort and energy efficiency, the rules provide acceptable limits for input variables related to temperature, relative humidity, and air quality.
- The necessity of intervention: The regulations establish suitable cutoff points for ventilation, illumination, dehydration, heating, and cooling interventions.
- Deviation scaling of indoor conditions: For all control parameters, the rules recognize deviations between user needs and the existing state of the area or room.
- Intervention selection: The guidelines specify the steps to take to provide the necessary intervention. These tasks involve turning on and off the building's systems and identifying the ones that will be utilized to modify the interior environment.
- Determining the intensity of intervention: The regulations establish the level of intervention intensity based on the scaling of the controllers for the electromechanical components and the indicators in each area or room.

3.3 A pilot appraisal

About 40% of Pakistan's carbon dioxide emissions come from the energy used in buildings, including public and private ones, schools, hospitals, hotels, and sports facilities. This accounts for 30% of the country's overall energy consumption [7]. The majority of energy used for household purposes is used by buildings for heating and cooling purposes. Considering the aforementioned, it can be concluded that intelligent BEMS can play a major role in reducing the energy losses in Pakistani buildings.

The particular building that was utilized for the implementation of the model that is being given has three stories and a total surface area of 8522 square meters. The building's energy needs are entirely met by electricity; no further energy-producing sources are present. More precisely, the following make up building energy loads:

- Illumination (both within and outside the structure).
- A hydraulic lift.
- Central HVAC system.
- Computers and office supplies (fax machines, printers).
- Server room (comprising networking hardware, routers, servers, and phone centre).
- To get rid of pluvial water, electric pumps are utilized.

The structure has a standard BEMS, which consists of the following parts:

- Separate temperature, light, and air quality control microcontrollers, sensors, and actuators.
- Central computer-assisted control and local controllers for every room and section of the building comprise the HVAC system.
- The HVAC system's air distribution system is classified as local, or decentralized, since airflows are delivered without the need for prior heating or cooling processes, and internal units are then used to regulate the air temperature to the proper level. Furthermore, because the internal units' ventilators have scales, the incoming airflow can be broadly described as variable. The incoming air enters the system through a pipeline, bringing

"outdoor" air into it instead of coming from a central air control unit.

- Sensors to detect if occupants are moving within the building or not [8].
- Energy-consuming gadgets.
- Software for region or room-specific central control management is separate.

In light of the foregoing, the model that was presented, elaborated the proper "mapping" of the building regions and their elements. The "DEVICES" and "SENSORS" buttons allow you to customize the sensors and equipment in each area. Every component's kind is specified before the equipment is installed in the rooms.

In this case, a completely revised description of the building's structure was created, complete with technical details on each part. After that, the building was used for the model's application, testing, and optimization for around four months. The application was crucial for both fine-tuning the model and assessing how well it worked in a real building.

Application results from the model's run from September 2023 to December 2023 were divided into groups based on energy usage and controlled indoor comfort parameters (temperature, relative humidity, air quality, and brightness). The outcomes for every category are shown as follows:

- Temperature, relative humidity, and air quality: Measurements of the room's conditions revealed that the levels of temperature, relative humidity, and air quality were within the established parameters, which varied based on the needs of the user [9]. Situations causing discomfort were rare, mostly because of the efficient regulation of relative humidity and air quality. Both in the summer and the winter, preheating and turning off operations helped to maintain energy comfort. External air was never used for heating, especially in the winter,

but shutter control allowed sunlight to enhance heating processes.

- Luminance: The amount of light in a room or other building space also guarantees a comfortable environment. Furthermore, adequate control over the building's lights and shutters was attained. Closed shutters on hot, sunny summer days are sometimes the result of prioritizing energy conservation through HVAC operation, and this is a more energy-efficient measure.
- Energy saving: Comparing cumulative operation data regarding building energy use to records from the preceding year showed a noteworthy outcome of almost 10% in energy savings. A more thorough analysis of the data gathered revealed that warm days resulted in greater energy savings. The primary causes of the energy savings were the building's electro-mechanical equipment being used to its fullest potential and the avoidance of HVAC and lighting loads in unoccupied areas.

The present model lowered the energy consumption to satisfactory levels by using a knowledge-based expert system to regulate the building's operational data, diagnose interior issues, and optimize the building's energy operation [10]. Additional, less complex steps can be taken to further minimize energy use without endangering the health of the residents. Specifically, for the building under examination, several workable solutions are as follows:

- Replacing the current incandescent low-efficiency lighting with more energy-efficient fluorescent lighting in public places;
- The installation of heat-insulating curtains in south-facing offices to reduce solar radiation penetration, particularly during the summer;
- Installing "motors" to automate the office areas' existing shades;

- Installing variable speed drivers, or VSD, in fans and pumps.

7. CONCLUSIONS

Lately, it has become increasingly common to integrate computer and information technology into the BEMS. Many of the services and operations related to buildings can be watched over and managed by these kinds of CCSs. The function of decision support systems is important in this endeavour since they may help with the ongoing energy management of a typical building's daily operations, which aims to maintain occupant comfort levels while minimizing energy consumption and costs.

Intending to ensure both the appropriate levels of living quality and energy savings for environmental protection, the intelligent model that is being given and that uses rule sets for building energy management can be a creative and practical decision support system in the aforementioned context. The system translates the energy knowledge of the building into many rules, which are then translated into electrical orders to actuator devices, enabling central monitoring of energy usage in buildings. Specifically, by employing expert knowledge to generate a dependable energy profile, the system can identify and remove "wrong" decisions by intelligently monitoring and optimizing the start/stop of HVAC and lighting controls.

The current model's performance can be deemed adequate based on the outcomes of its pilot application, as it enhanced the indoor maintaining the building's air quality while guaranteeing potential energy savings. According to user feedback on its pilot program, its UI was also described as being highly welcoming and helpful. Additionally, its open architecture permits infinite horizontal and vertical expandability as well as simple, ongoing modifications. To ensure the model's flexibility, its design permits its application to a wide range of building categories. Ultimately, the results of this study demonstrated unequivocally that expert knowledge has a great deal of potential to enhance building energy management since it gives rise to the ability to modify intelligent interventions with the aid of regulations.

ACKNOWLEDGMENT

REFERENCES

[1] A. Kylili and P. A. Fokaides, "European smart cities: The role of zero energy buildings," *Sustain. Cities Soc.*, vol. 15, no. 2015, pp. 86–95, 2015, doi: 10.1016/j.scs.2014.12.003.

[2] S. Akdag and H. Yıldırım, "Toward a sustainable mitigation approach of energy efficiency to greenhouse gas emissions in the European countries," *Heliyon*, vol. 6, no. 3, 2020, doi: 10.1016/j.heliyon.2020.e03396.

[3] D. Mariano-Hernández, L. Hernández-Callejo, A. Zorita-Lamadrid, O. Duque-Pérez, and F. Santos García, "A review of strategies for building energy management system: Model predictive control, demand side management, optimization, and fault detect & diagnosis," *J. Build. Eng.*, vol. 33, no. July 2020, 2021, doi: 10.1016/j.jobe.2020.101692.

[4] J. Bai and X. Zhang, "A new adaptive PI controller and its application in HVAC systems," *Energy Convers. Manag.*, vol. 48, no. 4, pp. 1043–1054, 2007, doi: 10.1016/j.enconman.2006.10.023.

[5] D. Kontogiannis, D. Bargiotas, and A. Daskalopulu, "Fuzzy control system for smart energy management in residential

147

buildings based on environmental data," *Energies*, vol. 14, no. 3, 2021, doi: 10.3390/en14030752.

[6] M. Molina-Solana, M. Ros, M. D. Ruiz, J. Gómez-Romero, and M. J. Martin-Bautista, "Data science for building energy management: A review," *Renew. Sustain. Energy Rev.*, vol. 70, no. August 2015, pp. 598–609, 2017, doi: 10.1016/j.rser.2016.11.132.

[7] D. D'Agostino, B. Cuniberti, and P. Bertoldi, "Energy consumption and efficiency technology measures in European non-residential buildings," *Energy Build.*, vol. 153, no. 2017, pp. 72–86, 2017, doi: 10.1016/j.enbuild.2017.07.062.

[8] S. J. Emmerich and T. Mcdowell, *Initial Evaluation of Displacement Ventilation and Dedicated Outdoor Air Systems for U.S. Commercial Buildings*. 2005.

[9] P. Wolkoff, "Indoor air humidity, air quality, and health – An overview," *Int. J. Hyg. Environ. Health*, vol. 221, no. 3, pp. 376–390, 2018, doi: 10.1016/j.ijheh.2018.01.015.

[10] M. Peña, F. Biscarri, J. I. Guerrero, I. Monedero, and C. León, "Rule-based system to detect energy efficiency anomalies in smart buildings, a data mining approach," *Expert Syst. Appl.*, vol. 56, pp. 242–255, 2016, doi: 10.1016/j.eswa.2016.03.002.

DEVELOPMENT OF AN ADJUSTABLE CUTTING TABLE FOR THE ABRASIVE WATERJET MACHINE

Azmir Azhari[1,*], Hariri Zin[1], Hasief Zakariah[1] and Intan Roshidi[1]

[1]Faculty of Manufacturing and Mechatronic Engineering Technology, Universiti Malaysia Pahang Al-Sultan Abdullah, 26600 Pekan, Pahang, Malaysia

[*]*Corresponding author E-mail address*: azmir@umpsa.edu.my (Azmir Azhari)

ABSTRACT

The use of a waterjet cutting machine comes along with the usage of a working table to support the workpiece during the cutting process. The typical working table is a fixed structure. This may create a problem for machining various sizes of workpieces especially with a workpiece of higher dimension. Therefore, there is a need to make the table adjustable so that it can accommodate a bigger workpiece by adjusting the table height. The present work is focusing on an improvement on the initial work table for an abrasive waterjet machine. The adjustable waterjet cutting table has been successfully fabricated. A double acting actuator was used to move the table ups and down up. A solenoid valve was used to control the movement of the actuator. It is suitable to be used for the abrasive waterjet machine. The adjustable table can easily accommodate different sizes of workpieces with different heights to be cut using the abrasive waterjet machine. Based on the product performance, a supplied air pressure of 4 bar (0.4 MPa) is recommended to be used and sufficient to lift the table to the maximum height of 200 mm regardless of weight up to 12 kg. This show that the versatile design of adjustable table can be conveniently installed in the commercial waterjet cutting machines for wider acceptance by industries for machining different sizes of workpieces.

Keywords: Waterjet cutting machine; adjustable cutting table; solenoid valve; double acting actuator

1. INTRODUCTION

Equipment and machinery industries in Malaysia will be the catalyst for the country's transition into the 4th Industrial Revolution because of its link to various economic sectors including manufacturing and services. Amongst many machinery equipment, an abrasive waterjet cutting machine has been used by many industries worldwide due to its capability of cutting various hard materials with speed, flexibility and precision.

Despite the largest implementation waterjet in industries sector, there are still rooms for improvement for the waterjet machine itself. It is found that the commercial waterjet machine has a limitation where the cutting table is fixed and not movable. Therefore, the purpose of the present work is to improve the existing table to be more flexible where its height can be adjustable during the cutting or engraving processes. This adjustable table is designed to ease the user during the waterjet machining application. The basic component for this adjustable table including the body (frame), the mechanism system and electrical components. The frame is designed to give a strong and robust support for the workpiece. The primary function of the frame is to resist corrosion and water jet pressure. By selecting aluminium profile as main frame material, it makes the design sturdier and more flexible. The significant of using aluminium profile

149

are the ability to resist rust and pressure, have strength and malleability properties and have longer life span. Basically, the actuator body is connected to the frame and the end of the rod is connected to honeycomb table top. A double-acting cylinder (DAC) is used as the actuator in this project where chambers on both sides of the piston will be supplied with air [1]. The side with a higher air pressure can push the piston to extend or contract to the other side. DAC is controlled with on-off control valve or known as solenoid valve. The using of double-acting cylinder helps user to achieve power, longer stroke and constant output force through a full stroke. Relatively, DAC cylinders can provide a better control at higher cycling rates [2].

For control system, DAC attaches to the solenoid valve which has 5 air- ways and 3 position ports. The solenoid valve is attached with up and down button for better control of its height movement. The solenoid permits compacted air to stream to one port of a two-fold acting air actuator while at the same time permitting the air to debilitate from the other port on a similar air actuator simultaneously [3]. In this position, all valves are impeded. The chamber inside the actuator is in freeze hence it can provide the actuator to stay still on his height.

The present work is focusing on an improvement on the initial work table for an abrasive waterjet machine. The use of a waterjet cutting machine comes along with the usage of a working table to support the workpiece during the cutting process. The original table was not suitable because it had a fixed structure. It was initially designed as a fixed structure to maximize the stability while supporting a large load. Over time, the machine has been used for machining various sizes of workpieces and in some cases, it was a problem especially for a higher workpiece. Therefore, there is a need to make the table adjustable so that it can accommodate a bigger workpiece by adjusting the table height.

2. METHODOLOGY

The development process of an adjustable waterjet table has three main steps including planning, implementation and analysis. The construction of the adjustable table is divided into different phases. In Phase 1 consists of the mechanical design and hardware procurement. While, in Phase 2 focuses on the development of electric circuit design. Finally, in Phase 3 consists of the assembling process and analysing the product performance.

2.1 Design and Materials Consideration

During the design phase, various considerations were made based on the functions and operational issues of the product. This includes the table requirements, adjustable mechanisms and selection of suitable materials. It is important to determine an optimal adjustable mechanism system which capable of meeting all the requirements. Several factors were considered such as the maximum load of the table, the type of actuators, the capacity of the piston, the speed of the stroke and cost of the components.

The table structure was fabricated using aluminium profile due to its ease of fabrication and lighter components. The frame is main parts of the table which can be divided into 2 parts (i.e. the top and bottom table). Those two parts are connected with slider that helps the vertical movement move equally and can avoid tilting. The table dimension is 60 cm x 80 cm. Figure 1 shows the frame design of the adjustable table.
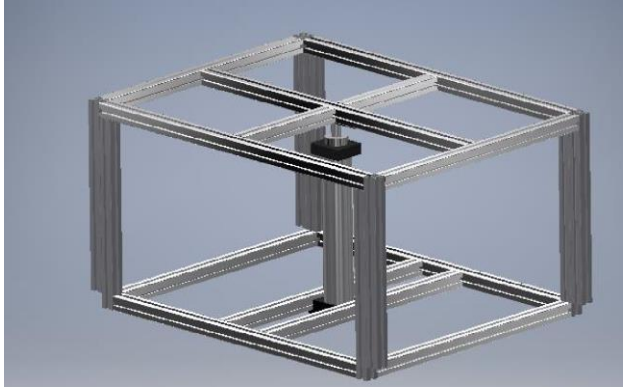
Figure 1. Frame Design

Working Principles of Adjustable Table

The requirements for the adjustable mechanism are to lift workpiece up to 20 kg, having resistance to corrosion and its vertical motion can be controlled for different heights. Therefore, the suitable actuator for that situation is double-acting actuator (DAC) with SC50X200S model number. This selected actuator manufactured with 50 mm bore, full stroke up to 200 mm and can lift workpiece up to 150 kg. Although it is a powerful actuator, its operating pressure need only 0.15 MPa and can up to 1.0 MPa suitable for the usage environment for the actuator.

2.2 Solenoid Valve and Connection

In this project 5/3-ways closed center was used to as an electromechanical to control the cylinder. Figure 2 shows the symbol of 5/3-ways close centre where A and B ports connect to double acting cylinder. EA and EB act as an exhaust that release air from the cylinder, while port P do as air inlet port.
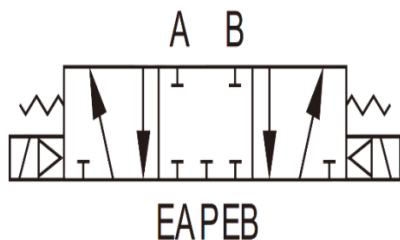
Figure 2. Symbol of 5/3-ways Close Centre

2.3 Slider Mechanism

The slider system configuration that used in this project is zig-zag drive system as shown in Figure 3. One side connector bar is mounted in an aluminium profile joinery and the other side is let independently move. Those connector bars are connected with a rectangle aluminium to control, thus providing the vertical movement with steady and smooth. Additional grease is added to the slider which is purposely to provide better and less friction movement

Figure 3. Slider Attached to the Leg of Adjustable Table

2.4 Electrical Components and Circuits

In this part, power supply was used to supply power to solenoid valve. Power supply that use in this project is 24VDC. Input that can accept from this power supply is 120-264VAC. This power supply will convert the alternate current to direct current. Power supply also has efficiency of power conversion, it also can amount the voltage and current to supply to its load. It also can stabilise its output voltage under varying line and load condition. Figure 4 shows the electrical components to supply voltage to the solenoid valve.

151
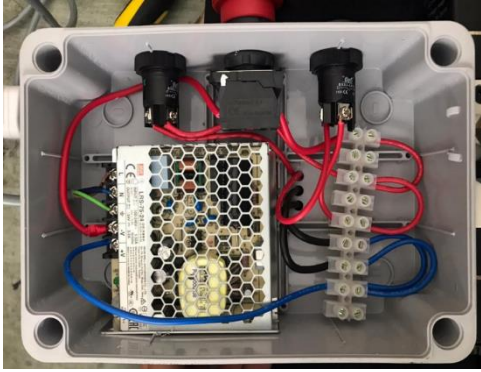
Figure 4. Electrical Power Supply and Components

The Normally Open (NO) Push Button is a pushbutton that does not make electrical contact with the circuit in its default state. The electrical contact with the circuit happens only when the button is pressed down. As the button is pushed down, the toggle makes electrical current and the circuit is closed. As a result, electricity will now flow to the other end of the circuit, connecting to the pushbutton, and switch the unit or power to the corresponding part. Normally, push buttons are the most common type of push buttons found in computers and circuits.

Before doing actual circuit using physical component. Electrical schematic circuit has been drawn using Fritzing software to reduce the risk of wrong installation especially it involved a high voltage application [4]. Figure 5 shows the schematic drawing of electrical circuit. Positive wire has been declared as red wire. While black wire declares as negative wire. From the schematic positive wire will throw pushbutton 1 and 2 and connected to solenoid valve. It will energize solenoid valve when the pushbutton been pressed.
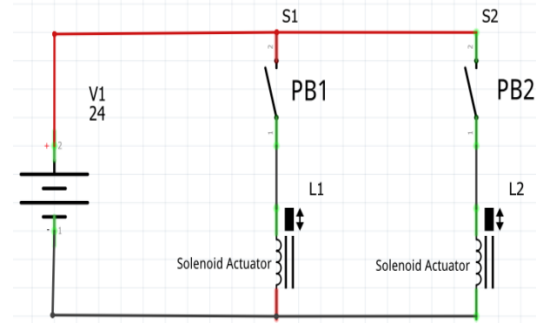
Figure 5. Electrical Circuit Schematic Diagram

2.5 Honeycomb Panel

Honeycomb panel was used in this project because it has hollow structures. This unique feature is important to let the waterjet goes directly into the tank below it during through cut. At the same time, it is strong enough to hold workpieces in a flat position. The honeycomb panel is shown in Figure 6.

Figure 6. Honeycomb Panel

3. RESULTS AND DISCUSSIONS

This section focuses on the final product and its performance. The actual fabricated adjustable table is shown in Figure 7.

152

Figure 7. The Actual Fabricated Adjustable Table with the Honeycomb Panel and Double Acting Cylinder

3.1 Fabricated Machine

The actuator cylinder has shown an excellent operation where the piston can expand and contract smoothly by pressing the pushbutton. Figure 8 shows the movement of the piston to elevate the table top uniformly. It was found that the actuator piston can move up and down without having any problems. This shows that the actuator specifications are appropriate for usage in this project.
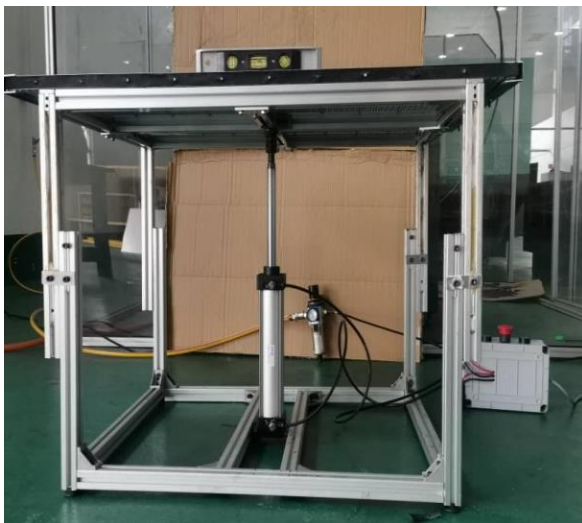
Figure 8. The Movement of Piston Actuator

3.2 Machine Performance

In this analysis, the recommended air pressure to the piston was analysed. The supplied air pressure to the actuator was varied from 2 bar (0.2 MPa) to 6 bar (0.6 MPa) to lift different load up to 12 kg. The analysis was done to measure the time taken required to reach the maximum height of the table or full stroke of the piston up to 200 mm. The test was repeated three times for each applied load. Figure 9 shows the required time to lift the table with the full stroke of piston with different loads and supplied air pressures. With the lowest supplied air pressure of 2 bar, the actuator shows huge different of required time to lift the table to the maximum with different load. It took about 13 seconds for the highest load of 12 kg and 5 seconds for the lowest load of 3 kg. When the supplied air pressure is 4 bar (0.4 MPa), the actuator required about 4 seconds to lift the table to the maximum height regardless of the load. Furthermore, a higher supplied air pressure of 5 and 6 bar (0.5 and 0.6 MPa) did not give a significant reduction in time taken to lift the table to the maximum for all different load. Therefore, it can be concluded that for optimum usage, a supplied air pressure of 4 bar is recommended for the actuator to lift the table to the maximum height of 200 mm regardless of the load.
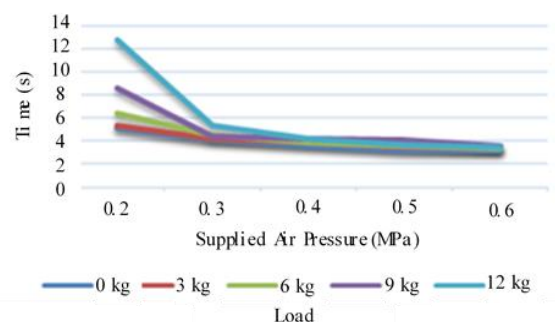
Figure 9. Time Taken to Lift the Actuator for Different Loads and Supplied Air Pressure

4. CONCLUSION

In conclusion, the adjustable waterjet cutting table has been successfully fabricated. It is suitable to be used for the abrasive waterjet machine. The adjustable table can easily accommodate different sizes of workpieces with different heights to be cut using the abrasive waterjet machine. Based on the product performance, a supplied air pressure of 4 bar (0.4 MPa) is recommended to be used and sufficient to lift the table to the maximum height of 200 mm regardless of weight up to 12 kg. This show that the versatile design of adjustable table can be conveniently installed in the commercial waterjet cutting machines for wider acceptance by industries for machining different sizes of workpieces.

ACKNOWLEDGEMENTS

REFERENCES

[1] Khamis, A., *Design and Simulation of a High Thrust Linear Oscillator Actuator* (Doctoral dissertation, Universiti Putra Malaysia), 2007.

[2] Awaludin, N.A., *Analysis of Thrust Density Calculation for Linear DC Actuators* (Doctoral dissertation, Universiti Putra Malaysia), 2006.

[2] Awaludin, Noor Azita. "Analysis of Thrust Density Calculation for Linear DC Actuators." PhD diss., Universiti Putra Malaysia, 2006.

[3] Giffney, T., Xie, M., Yong, A., Wong, A., Mousset, P., McDaid, A. and Aw, K.,. Soft pneumatic bending actuator with integrated carbon nanotube displacement sensor. *Robotics*, 5(1), p.7. 2016

[4] Lai, W.K., Rahmat, M.F. and Wahab, N.A., Modeling and controller design of pneumatic actuator system with control valve. *International journal on smart sensing and intelligent systems*, 5(3), pp.624-644, 2012.

Published Date: 08/07/2024 Version: 00

PIEZOELECTRIC TESTING OF COMMERCIAL PVDF THIN FILM SENSOR

Abdul Qadir[1,], Shehroze Tahir Khan[1], Murtaza Mehdi[1], Meraj Ali Shah[1]*

[1]Department of Mechanical Engineering, NED University of Engineering & Technology, Karachi, Pakistan

[*]Corresponding author E-mail address: abdulqadir@neduet.edu.pk (Abdul Qadir)

ABSTRACT

Commercially available sensors of polyviyllidene fluoride (PVDF) is being used in vibration sensing, haptics, pressure sensors, energy harvesting devices, etc. In this paper, we have reported the piezoelectric performance and testing of a commercial PVDF- based flexible thin film sensor. The sensor is tested for a variety of test scenarios on a custom built test setup in conjunction with the sophisticated lab instruments such as impact hammer, digital oscilloscope, and digital multimeter.

The results indicate that such sensors may be utilized as low-cost alternatives in energy harvesting, impact testing, and vibration and motion sensing applications in a new generation of cost effective MEMS based micro electro mechanical devices.

Keywords: PVDF, Sensor, energy harvester, organic, flexible, low-cost sensor, environmental friendly power sources, impact hammer, vibration sensing, motion sensing.

1. INTRODUCTION

Piezoelectric thin films are thin layers of material that exhibit the piezoelectric effect, which is the ability to generate an electric charge in response to applied mechanical stress, or vice versa, to deform in response to an applied electric field. [1]

These films are used in various applications, such as sensors, actuators, energy harvesters.

Most Commonly used piezoelectric thin films are made from inorganic materials which are more rigid compared to organic films while organic piezoelectric thin films offer several advantages over their inorganic counterparts. [2-3]

Organic piezoelectric thin films are typically made from polymers such as polyvinylidene fluoride (PVDF) and its copolymers. These films are flexible, lightweight, and can be easily processed using techniques like spin-coating or inkjet printing. [4]

They are often used in applications where flexibility and conformability are important, such as wearable devices, self-powered devices. [5]

With the rapid growth of electronic gadgets, smart/wearable devices, flexible/stretchable electronics many researchers are focused for development of environmental friendly, with abundant and benign sources to power up them. [6-8].

These materials are effective in generating green electrical energy from various types of mechanical energy sources, such as human or animal body movements, vibrations, deformations, sound waves, liquid or air flows, wind flow, and in e-health care monitoring. [5, 8-10]

2. TESTING METHODOLOGY

For this experimental research work, commercial PVDF based device has been purchased from china from www.TE.com,

155

two devices was used in these experiments, the devices are made up of top and bottom electrodes of silver paste and thin film of PVDF is sandwiched between electrodes, complete device is laminated in PVC (Poly Vinyl Chloride).

Figure 1. Schematic of PVDF Based Thin Film Device

Figure 2. PVDF Based Device front
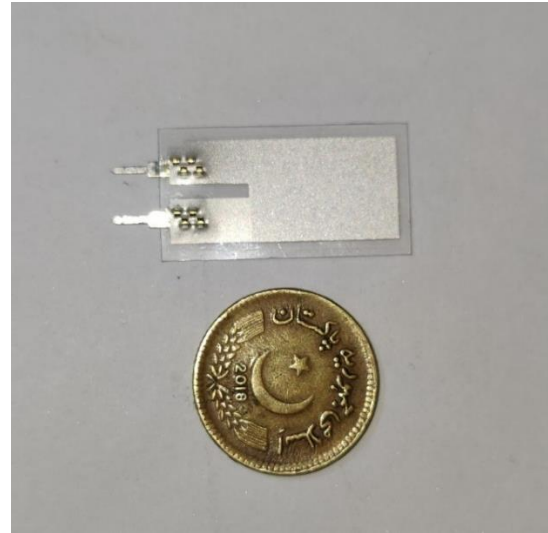
Figure 3. PVDF Based Device Back

3. EXPERIMENTAL SETUPS

In total three experimental setups has been used.

Flexing. Cantilever testing setup, Impact testing setup and cam based vibration testing machine setup.

Experiments were performed on single device and two devices connected together.
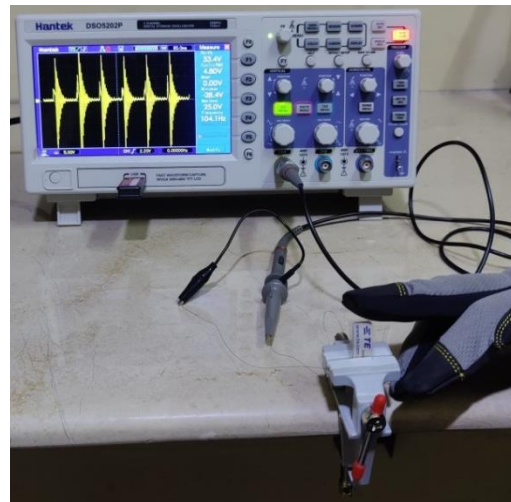
Figure 4. Flex/Cantilever Testing Setup

156

Figure 5. Impact Testing Setup

Figure 6. Vibration Cam Machine Testing Setup

3.1 Free vibrations /Cantilever Testing

Single and double device (in line and in layer combination) was connected with copper wires and connected with digital oscilloscope. Device was held in a fix/free arrangement in a small table top vice and antistatic gloves were used to provide flexes manually by hand. Antistatic gloves were used to avoid tribo-electric charges during hand flexes.

Approximately 10 mm flex were provided in single and multiple flexes (5-6 displacements)

3.1.2 Single Device

Figure 7. Flexing device up to 5-10 mm displacement with anti-static gloves
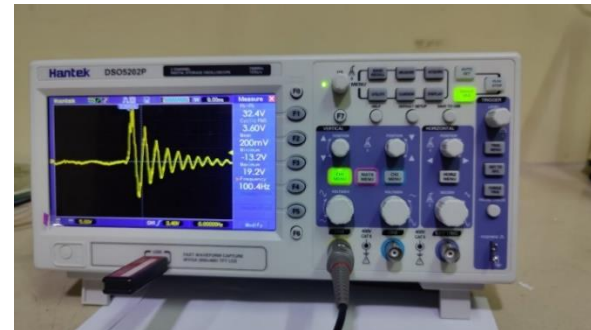
Figure 8. Oscilloscope results showing generated transient voltage output

S.No.	Voltage Output-Voc(V)	
	Single Displacement	**Multi Displacement**
1	26.0	38.0
2	30.8	37.8
3	27.0	36.0
4	32.4	33.4
5	32.8	35.0
Avg.	**29.8**	**36.04**

Table 1. Single device with single and multiple displacements

157
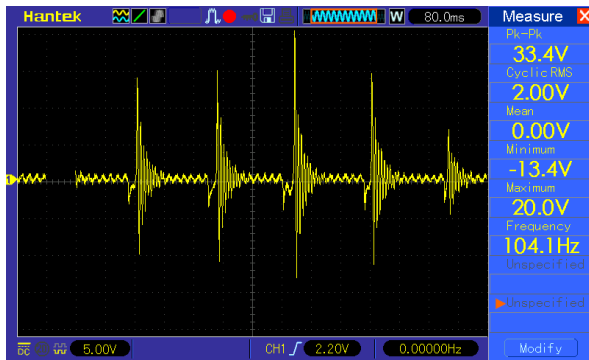
Figure 9. Oscilloscope results showing generated transient voltage output on multiple displacements

3.1.3 Double Device

Two devices were connected in two arrangements inline and in layer combination.
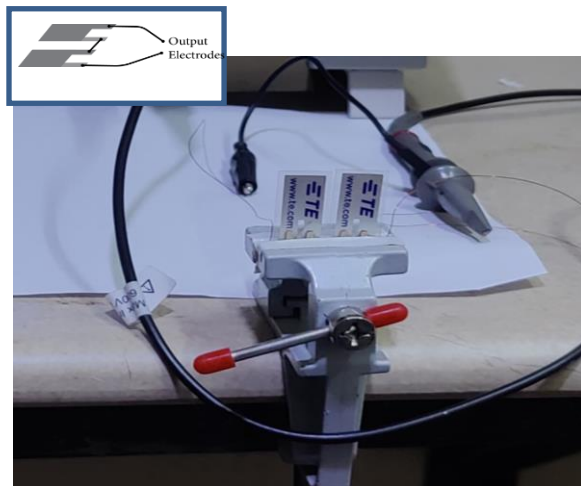
Figure 10. Two devices connected in line
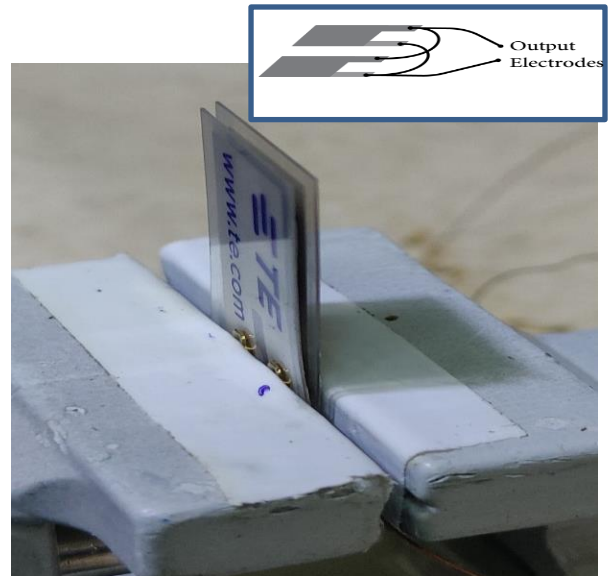
Figure 11. Two devices connected in Layer arrangement
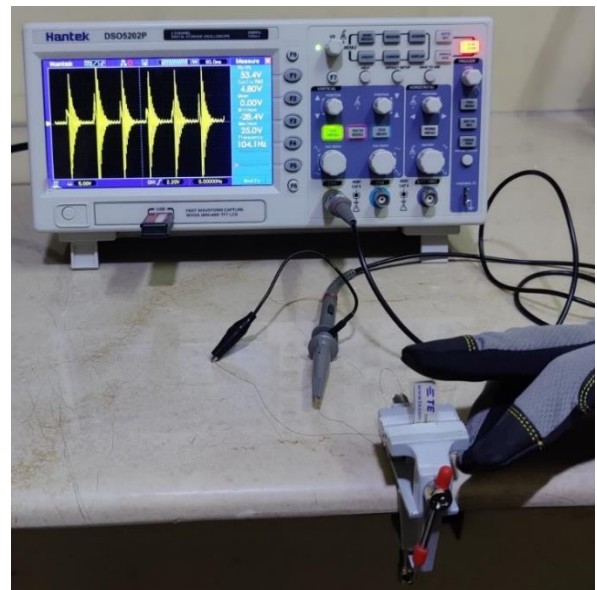
Figure 12. Multiple displacements (5-6) with antistatic gloves and data capturing by oscilloscope

S.No.	Voltage Output-Voc(V)	
	In Line Connection	**Layer Connection**
1	33.4	59.6
2	29.0	69.8
3	31.0	69.6
4	26.8	75.6
5	31.0	71.2
Avg.	**30.24**	**69.16**

Table 2. Two devices in line and layer connection
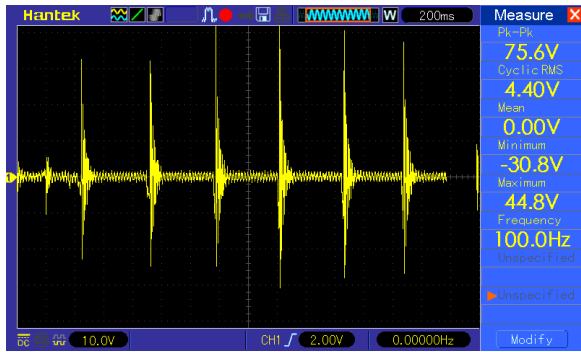
Figure 13. Oscilloscope results showing generated transient voltage output on multiple displacements on layer combination double device.

3.2 Impact Testing

An Impact hammer B&K 8206 was used to provide impulses on single and layer combination connected double device.
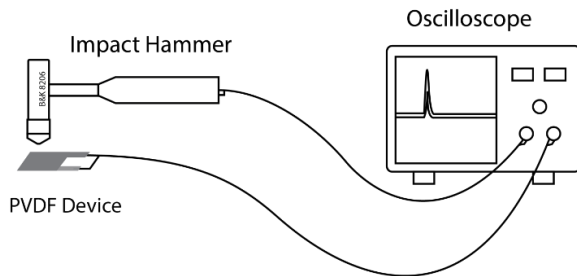
Figure 14. Schematic of impact testing methodology
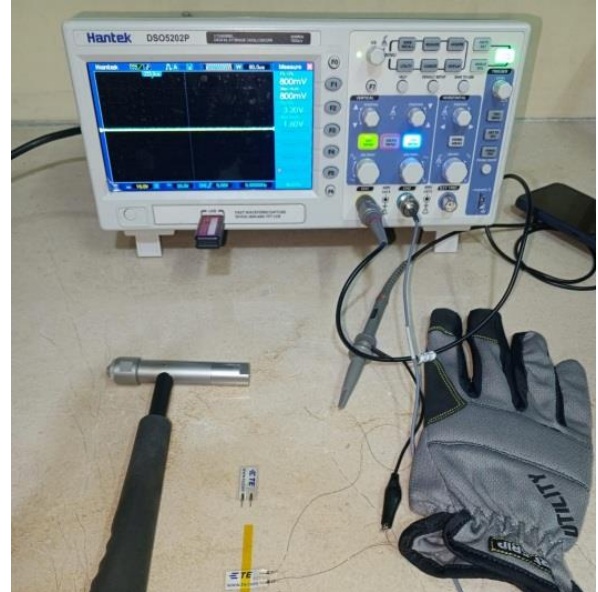
Figure 15. Single Device Experimental setup with impact hammer
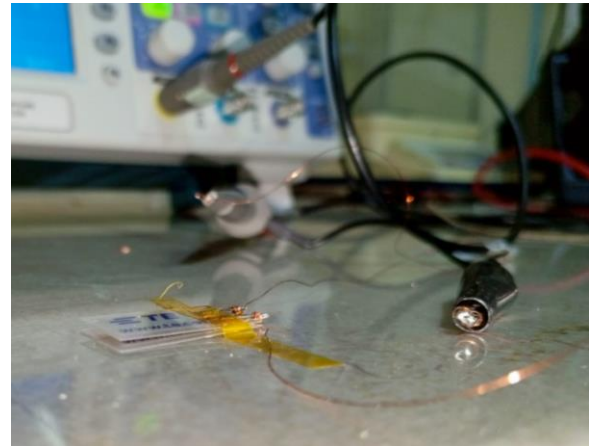
Figure 16. Two Devices connected in layer

Figure 17. Impact Hammer with Aluminum Tip
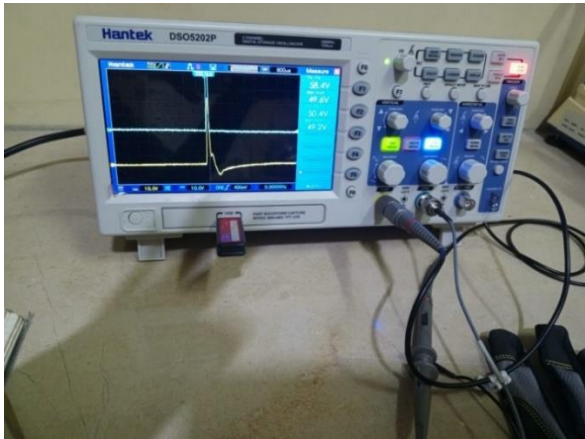
Figure 18. Impulse Data Capturing with Oscilloscope

Capacitance of the single device and double device connected in layer combination is measured by digital multimeter.

Impact force was provided with low force and then increased upto high loads; the sensitivity of impact hammer is 23.02 mv/N.

3.2.1 Single Device

S.No.	Single Device (Capacitance=0.56nF)		
	Impact Force (N)	Geenrated Volatge (V)	Induced Charge (nC) Q=CV
1	0.417	6.8	3.808
2	0.730	13.2	7.392
3	0.730	13.2	7.392
4	0.834	13.6	7.616
5	0.869	14.8	8.288
6	1.078	19.2	10.752
7	1.286	24	13.44
8	1.321	24	13.44
9	1.738	32.4	18.144
10	2.712	46.4	25.984
11	2.990	54	30.24

Table 3. Single device impact testing results
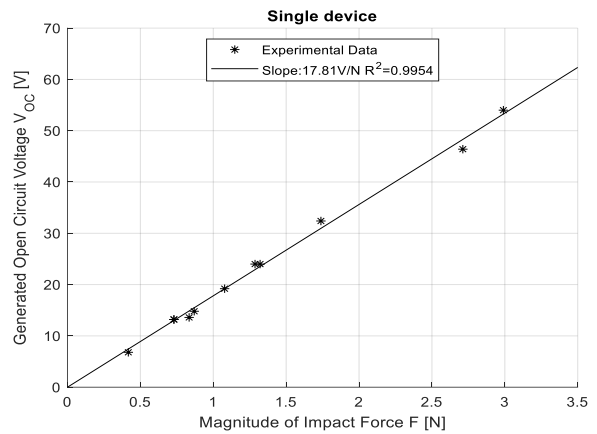
Figure 19. Graph of open circuit voltage and magnitude of impact force

3.2.2 Double Device

S.No.	Double Device (Capacitance=0.985nF)		
	Impact Force (N)	Geenrated Volatge (V)	Induced Charge (nC) Q=CV
1	0.0695	2.4	2.364
2	0.2434	6	5.91
3	0.4172	11.2	11.032
4	0.7127	17.5	17.336
5	0.8866	20.8	20.488
6	0.9735	25.2	24.822
7	1.2342	28.8	28.368
8	1.6688	36.8	36.248
9	1.8427	45.2	44.522
10	2.0687	45.6	44.916
11	2.8857	67.2	66.192

Table 4 Double device impact testing results
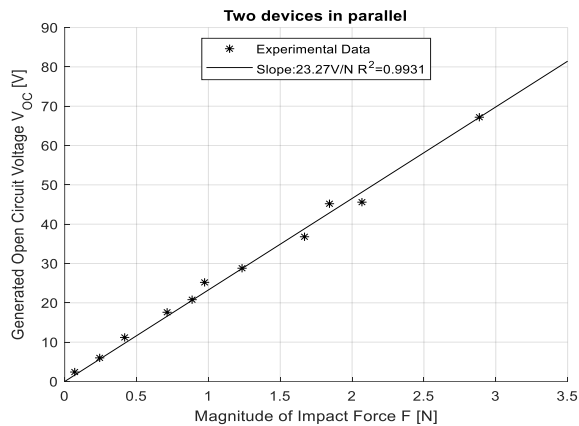
Figure 20. Graph of open circuit voltage and magnitude of impact force

3.3 Vibration Cam Machine Testing

In- house built cam-based vibration testing machine was used to provide impulses to device in range of frequencies, vibration testing machine is equipped with toy motor of frequency up to 200 Hz (12000 RPM). 3mm cam was used in current experiment.

Single and double device connected in layer combination was used in these experiments.

Figure 21. Thin film vibration testing machine CAM based

Figure 22. Single Device Mounted on thin film vibration testing machine

161

Figure 23. 3D printed, 3 mm Displacement CAM

3.3.1 Single Device

S.No.	Single Device (Capacitance=0.56nF)	
	Forcing Frequency (Hz)	Generated Voltage (pk-pk)
1	4.6	1.8
2	14.8	4.84
3	23.8	9.12
4	47.2	15.6
5	57.4	19.6
6	82.4	14.4
7	107.9	28.4
8	117.2	56
9	122.7	37.2
10	130.0	29.8
11	142.7	6.8
12	157.6	36.4
13	164.5	35.6
14	169.5	39.6
15	175.9	30.4
16	178.4	20

Table 5. Single device cam-based vibration testing machine results
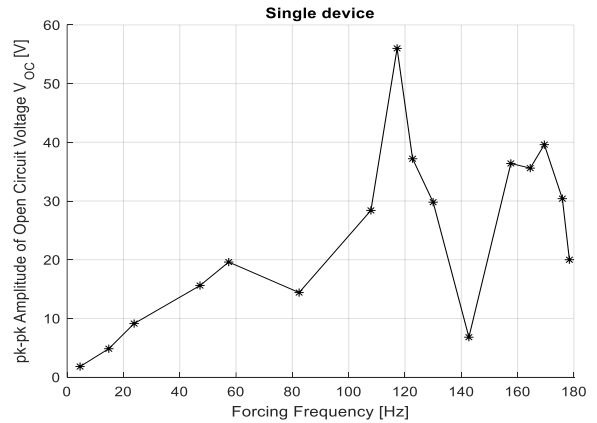
Figure 24. Graph of open circuit voltage pk-pk and forcing frequency

3.3.2 Double Device

S.No.	Double Device (Capacitance=0.985nF)	
	Forcing Frequency (Hz)	Generated Voltage (pk-pk)
1	7.0	3.2
2	19.5	9.6
3	32.3	14.4
4	45.0	23.6
5	64.5	31.2
6	72.8	30
7	85.0	29.6
8	95.8	34
9	109.3	27.2
10	122.7	15.6
11	135.4	26.4
12	140.6	27.6
13	150.8	21.6
14	164.2	15.6
15	169.3	13.2
16	172.5	10.8

Table 6 Double device cam-based vibration testing machine results

162
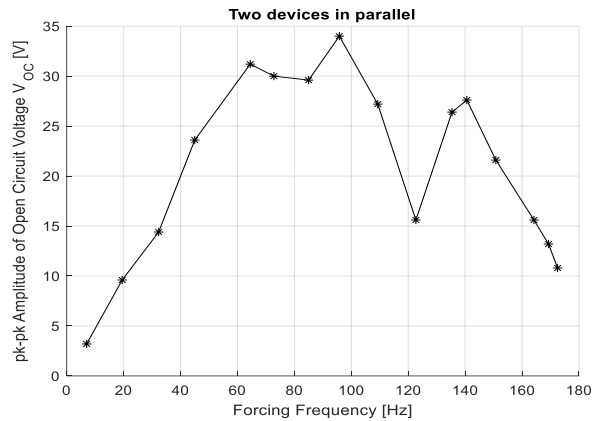
Figure 25. Graph of open circuit voltage pk-pk and forcing frequency

4. CONCLUSIONS

- Maximum open circuit voltage is obtained in free vibration testing in flexing/fix free arrangement with maximum pk-pk 75.6 V in double device connected in layer combination.
- Single device in flexing/fix free arrangement shows maximum voltage of pk-pk 38.0V.
- Device shows promising and linear results in impact testing in single device mode and double device mode with maximum voltage up to 67.2 V and induced charge of 66.19 nC at applied maximum load of 2.88 N.
- During CAM based vibration testing machine tests , single device shown higher results at 122 Hz frequency with maximum open circuit voltage as 37.2 V.
- High flexibility, and durability of commercial device makes it a good choice for application of self-powered wearable devices.
- Energy harvester with multi-layer of devices can be used to power up low power energy consuming devices utilizing vehicle movement induced wind, ocean waves energy, machines vibration, public movement pathways etc.

REFERENCES

[1] Fu, J., Hou, Y., Gao, X., Zheng, M., & Zhu, M. (2018). Highly durable piezoelectric energy harvester based on a PVDF flexible nanocomposite filled with oriented BaTi2O5 nanorods with high power density. *Nano Energy*, *52*, 391-401.

[2] Parvez Mahmud, M. A., Huda, N., Farjana, S. H., Asadnia, M., & Lang, C. (2018). Recent advances in nanogenerator-driven self-powered implantable biomedical devices. Advanced Energy Materials, 8(2), 1701210.

[3] Gaur, A., Tiwari, S., Kumar, C., & Maiti, P. (2020). Bio-waste orange peel and polymer hybrid for efficient energy harvesting. Energy Reports, 6, 490-496.

[4] Han, Y., Han, Y., Zhang, X., Li, L., Zhang, C., Liu, J., ... & Huang, W. (2020). Fish gelatin based triboelectric nanogenerator for harvesting biomechanical energy and self-powered sensing of human physiological signals. ACS applied materials & interfaces, 12(14), 16442-16450.

[5] Kaur, J., & Singh, H. (2020). Fabrication of composite material based nanogenerator for electricity generation enhancement of food waste by-product. Materials Chemistry and Physics, 256, 123331.

[6] Karan, S. K., Maiti, S., Paria, S., Maitra, A., Si, S. K., Kim, J. K., & Khatua, B. B. (2018). A new insight towards eggshell membrane as high energy conversion efficient bio-piezoelectric energy harvester. Materials today energy, 9, 114-125.

Published Date: 08/07/2024 Version: 00

[7] Jameel, A. T., & Yaser, A. Z. (Eds.). (2020). Advances in Nanotechnology and Its Applications. Berlin/Heidelberg, Germany: Springer.

[8] Hu, Y., Parida, K., Zhang, H., Wang, X., Li, Y., Zhou, X., ... & Fan, H. J. (2022). Bond engineering of molecular ferroelectrics renders soft and high-performance piezoelectric energy harvesting materials. Nature Communications, 13(1), 5607.

[9] Akmal, M. M., Ahmad, F. B., Hisham, F., & Hazmi, A. T. (2021). Biopolymer-based waste for biomaterials thin film in piezoelectric application. In Advanced Technology for the Conversion of Waste Into Fuels and Chemicals (pp. 355-381). Woodhead Publishing.

[10] Cao, X., Xiong, Y., Sun, J., Zhu, X., Sun, Q., & Wang, Z. L. (2021). Piezoelectric nanogenerators derived self-powered sensors for multifunctional applications and artificial intelligence. Advanced Functional Materials, 31(33), 2102983

MONITORING OF WELDING DIGITIZATION USING VISION-BASED CLASSIFICATION: A COMPARATIVE ANALYSIS OF CNN AND RESNET-BASED APPROACH

Afrasyab Khan[1*], Salman Hussain[1], Wasim Ahmad[1], and Mirza Jahanzaib[1]

[1]Department of Industrial Engineering, University of Engineering & Technology, Taxila, Pakistan

[*]Corresponding author E-mail address: afrasyab.khan@uettaxila.edu.pk (Afrasyab Khan)

ABSTRACT

Welding is one of the major processes in the automobile, construction, aviation, and other sectors. However, the inefficiencies, high failure rates, and poor weld quality of manual welding methods are common. This advocates digitization of the welding process which can be named Welding for Industry 4.0. Digitization of manual welding to digital welding includes real-time weld monitoring and control. Accurate weld defect classification is a challenging task for efficient weld monitoring. Different machine-learning algorithms have been developed for the classification of welding defects. This paper presents a comparative analysis of CNN and ResNet-based approaches for weld defect classification when using vision-based monitoring. The dataset used for the research includes more than 30,000 images. Six different types of defects were considered including burn-through, contamination, lack of fusion, misalignment, and lack of penetration. Both the models were trained using the dataset to classify these defects. The accuracy of the algorithms was determined based on the number of images taken to train the model. Comparative analysis revealed that CNN achieved a higher precision compared to ResNet. The paper highlighted the effectiveness of CNN employed for weld defect classification for the development of an Industry 4.0-based robotic welding system.

Keywords: Welding Digitization; Industry 4.0; Machine Learning; CNN; ResNet

1. INTRODUCTION

Deep learning models in recent years are summarized and compared with a detailed discussion of several typical networks in the field of image classification, object detection, and segmentation [1]. To implement the feature extraction and classification in one algorithm and to implement the overall automation, oh. et al. [2] propose a method of automatically detecting welding defects using Faster R-CNN which is a deep learning basis. Breitenbach et al. [3] conducted a systematic literature review on machine learning approaches for quality monitoring and control systems for welding processes. The review identified 101 papers that met the inclusion criteria, and it found that machine learning is a promising approach for improving the quality of welds.

Elsheikh [4] highlights the significance of machine learning techniques in predicting joint properties, enabling real-time control, and diagnosing tool failures in the welding process. The review discusses the utilization of different machine learning algorithms and models, emphasizing their effectiveness in improving the quality and efficiency of friction stir welding.

165

Zhou et al. [5] presented a case study on the use of machine learning and semantics to predict the quality of automated welding. The case study was conducted at Bosch, and it showed that machine learning can be used to predict the quality of welds with high accuracy. Asif et al. [6] proposed a machine-learning model to predict welding quality using air-coupled acoustic emission (CAE) and weld inputs. The model was trained on a dataset of CAE signals and weld quality data, and it was shown to be able to predict welding quality with high accuracy. Wang et al. [7] proposed a real-time method for recognizing weld defects based on visible spectral images and machine learning. The method uses a camera to capture images of the weld, and a machine learning algorithm to identify defects. The method was evaluated on a dataset of weld images, and it was shown to be able to detect defects with high accuracy.

Ferraro et al. [8] propose different strategies for improving the computational efficiency of the deep-learning models adopted in reinforcement-learning (RL) scenarios. The robustness of most image processing algorithms is deficient during welding practice, [9] and the security regime for tracking welding is not considered in most trajectory recognition and control algorithms. For these two problems, an adaptive feature extraction algorithm was proposed, which can accurately extract the seam centre from the continuous, discontinuous, or fluctuating laser stripes identified and located by the CNN model, while the prior model can quickly remove a large amount of noise and interference except the stripes, greatly

improving the extraction accuracy and processing speed of the algorithm [10].

Despite being in use for years, welding robots are pre-programmed devices with little to no intelligence. Figure 1 shows that Intelligent manufacturing is implemented by the transformation of Human physical systems to Human cyber-physical systems to achieve specific manufacturing goals at an optimized level [11].
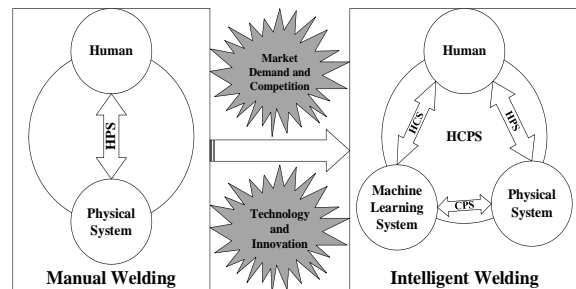
Figure 1. The advancement of welding systems from HPS to HCPS [12]

Long Chao et al. [13] proposed a method for predicting the weld width from high-speed successive images of the weld zone during laser welding. The method uses a variety of machine learning algorithms to predict the weld width, and it was evaluated on a dataset of laser welding images. The method was shown to be able to predict the weld width with high accuracy. Christensen et al. [14] describe the application of neural network technology for gas metal arc welding control. Hongyuan et al. [15] present a robotic system based on real-time vision measurement. Franciosa et. al. [16] highlights the need for a holistic approach to data gathering, monitoring, and in-process control. Franciosa et. al. [17] study deep learning enhanced digital twins for closed-loop in-process quality improvement. Ferraro et al. [8]

166

propose different strategies for improving the computational efficiency of the deep-learning models adopted in reinforcement-learning (RL) scenarios. The robustness of most image processing algorithms is deficient during welding practice, and the security regime for tracking welding is not considered in most trajectory recognition and control algorithms. For these two problems, an adaptive feature extraction algorithm was proposed, which can accurately extract the seam centre from the continuous, discontinuous, or fluctuating laser stripes identified and located by the CNN model, while the prior model can quickly remove a large amount of noise and interference except the stripes, greatly improving the extraction accuracy and processing speed of the algorithm [10]. To implement the feature extraction and classification in one algorithm and to implement the overall automation, oh et al. [2] propose a method of automatically detecting welding defects using Faster R-CNN which is a deep learning basis. Günther et al. [18] suggest that deep learning features and general-value-function predictions can be beneficially combined with actor–critic reinforcement learning to learn context-appropriate control policies to govern welding power in real-time. Machine learning algorithms can be exploited to predict the weld quality during laser welding with high accuracy [19].

In the field of image processing, the ResNet algorithm has been a breakthrough in tasks like classification and object detection. Unlike conventional methods, ResNet addresses the problem of vanishing gradient which arises while training deep neural networks. By using "shortcut connections" that bypass some layers, ResNet enables information to flow directly through the network, resulting in faster learning and better performance on various image processing tasks[20], [21].

He et al. [22] introduced a new approach to classification and object detection tasks, revolutionizing the field of image processing. Unlike traditional methods, ResNet addresses the vanishing gradient problem which is a bottleneck in training deep neural networks. By including "shortcut connections" that bypass certain layers, ResNet allows for the direct flow of information, facilitating efficient learning and achieving significant performance improvements across various image processing applications.

Algorithm	Advantages	Purpose
Artificial Neural Network (ANN)	capabilities of performing sophisticated, non-linear mappings, learning independently, and generalizing knowledge.	Solve intricate problems using internal mechanisms.
Convolutional Neural Network (CNN)	Decreased parameter count and maintained invariance to changes in shift, scale, and distortion.	Inspection of surface integration and identification of machinery faults.
ResNet	Shortcut connections that alleviate vanishing gradients	Ultimately enabling deeper and more accurate image processing models.
Support vector machine (SVM)	Less sample, global optimal	Classification and regression analysis
Deep Belief Network (DBN)	The ability to train layer by layer for improved efficiency.	Can be trained layer-wisely to be more efficiently

Recurrent Neural Network (RNN)	Sequential data retains short-term information and captures temporal correlations.	Utilizing predictive analytics and defect prognosis to learn features from sequential data.
Rough set theory	No requirement for prior or supplementary data information.	Handle novel and uncertain information systems.
Decision tree	Generate a thorough examination of the outcomes for each branch.	Classifying the features of the signals
Genetic Algorithm (GA)	Good global search ability	solving optimization problems: combinatorial problems, planning
Restricted Boltzmann Machine (RBM)	Capable of handling ambiguous input and not dependent on training labels during the pretraining stage.	Dimensionality reduction, classification, regression, and feature learning
Reinforcement learning	Maximizes performance	Representation, prediction, and control of learning
Auto Encoder (AE)	Elimination of irrelevant input while preserving meaningful information.	Machinery fault diagnosis

Table 1. Different AI methods/models [23]

Although deep learning has demonstrated its powerful capabilities in classification tasks, its effectiveness is hindered by the requirement for large amounts of training data, particularly in defect detection scenarios. It is well-known that a certain number of training data sets, as well as a balanced representation of different sample types, are necessary for creating robust prediction and classification models [24]. However, in practice, the number of defect samples is typically much lower than that of normal samples. Integrating learning approaches, which encompass multiple algorithms such as feature selection, multiple classifiers, and decision fusion, have proven to [25] be practical methods in the field of pattern recognition. In the study, the random forest model was applied and enhanced by proposing a novel integrating structure to achieve more accurate online defect detection in robotic welding processes. Machine learning has a major benefit over deep learning in that it requires less time to train the models than deep learning [26].

The visual representation of algorithms and experimentation can improve the effectiveness of learning and teaching the principles of image processing. Because Python is an interpreted language with libraries devoted to specific tasks, it is a great choice for learning digital image processing. This eliminates the need for expensive commercial software's ambiguous black boxes and allows for the manipulation of codes and crucial algorithms [27].

The welding procedures used today are complex, rely on a lot of variables, and have a poorly understood mechanism. User and customer needs for welding are distinct, and they work in circumstances that are always changing [28]. As a result, welding is shifting to more specialized production using cutting-edge welding equipment that can nimbly adapt to changing welding requirements while retaining excellent quality. Smart approaches for gathering and analyzing welding data are essential in the field of big data [29]. Monitoring metrics before and after the welding process, for instance, can improve the welding process, performance, and service quality. Although there are numerous welding techniques, advances in

168

information science and technology are enabling the transformation of traditional welding to intelligent one [30]. Because of advances in computer science and artificial intelligence, intelligent automation is replacing manual work. Manufacturing research programs have all examined smart manufacturing, Industry 4.0, and the Internet of Things. In the future big data, intelligent manufacturing, human cyber-physical systems, and AI will revolutionize industry. [11], [31], [32].

A thorough review of the literature on intelligent welding research was conducted. The search was restricted to welding technologies for convenience, even if publications on intelligent manufacturing may have also turned up information on intelligent welding. Many different types of ML Algorithms were being studied in the literature. Some best practices in the creation of modern industrial welding are identified through a survey of the literature and other research.

2. METHODOLOGY

We chose two different Machine learning algorithms CNN and ResNet to train it on the specific dataset and get a comparative analysis of both the algorithms. Conventional methods require hand-crafted design, while CNNs learn features for weld defect classification, potentially offering a more robust approach. To address challenges such as defect detection and the need for robust prediction models, a comparative analysis of two different machine learning algorithms has been done, and these algorithms were trained on the dataset which includes more than 30,000 images. Through the

convergence of big data, AI, and human cyber-physical systems, the future of welding promises enhanced efficiency, quality, and adaptability. Figure 2 compares two methods for image feature extraction: conventional methods and Convolutional Neural Networks (CNNs).

Figure 2. Image Feature Extraction: Conventional Methods vs. Convolutional Neural Networks
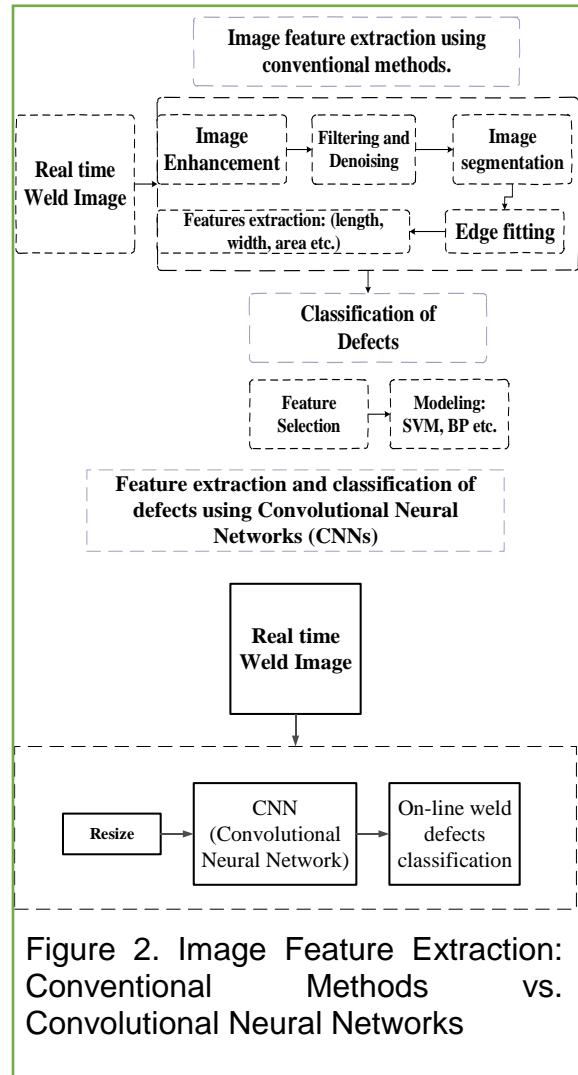
3. ALGORITHM MODELLING

Convolutional Neural Network (CNN)

The following steps were followed from data annotation to training the ML algorithms.

169

1. A dataset of different welding Images [33] was taken from a source, and the data annotation was done on it.

2. It is passed to the classification model that recognizes whether a material is correctly welded or incorrectly welded, whether it is best welded or worst welded.

3. A Machine Learning algorithm is made and trained on the image data collected.

4. After performing the inference task, our model will let us know about the class to which the material belongs such as correctly welded or incorrectly welded material.

5. Continuously improve the algorithm to get the maximum accuracy.

6. A confusion matrix has been generated which shows the overall accuracy of the algorithm.
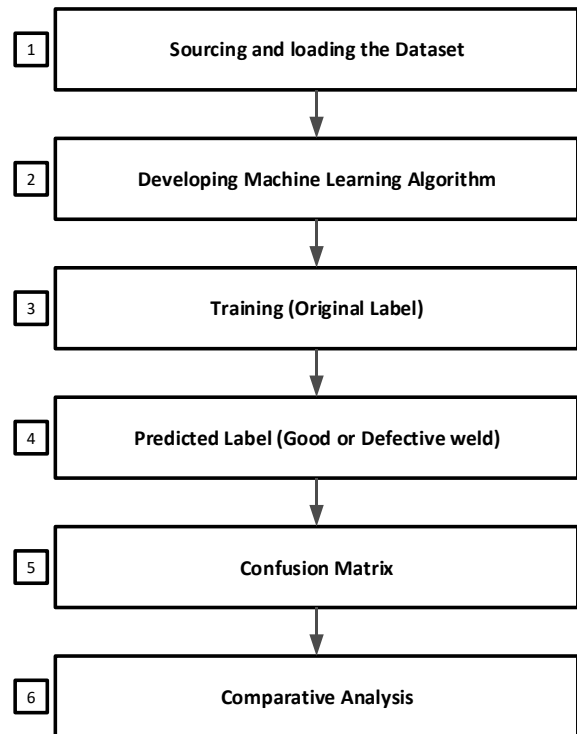
Figure 3. The dataset was subjected to both algorithms.

To begin with, the first step in implementing a CNN algorithm is to create a dataset of images that will serve as the foundation for the algorithm. Once the dataset has been established, we will proceed to train the specific algorithm on the chosen dataset.

In the classification of the weld images, it is considered that the best weld has no cracks and holes in the bead, the bead is uniform, the width and height are appropriate, and the strength of the welding meets the requirements.
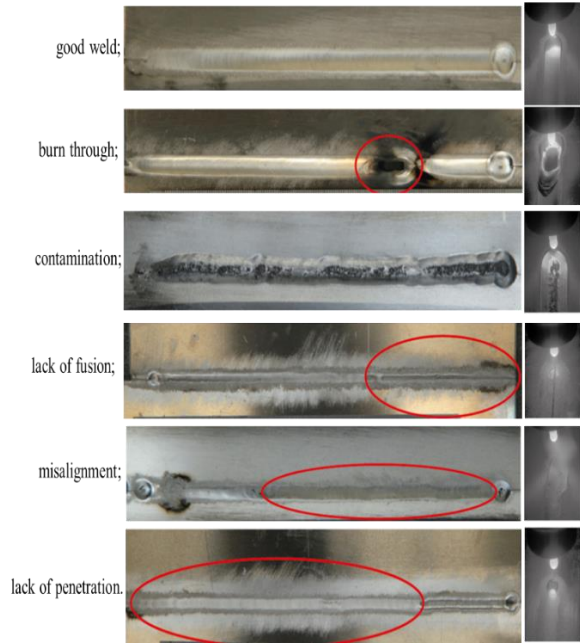
Figure 4. Dataset samples: good weld; burn through; contamination; lack of fusion; misalignment; lack of penetration. [33]

The machine learning algorithms help in determining the best and defective images. The Google Collab was being used as a virtual environment for training the ML algorithms on the specific dataset. The necessary libraries were imported, and the dataset was loaded for binary classification. After that, the model is trained on the dataset. The dataset consists of 33,254 images showcasing TIG welding of aluminium 5083. The study's objective is to obtain data from an image that shows the weld pool and its surroundings in the visible spectrum. For this purpose, we have used a new dataset that has been captured using an HDR camera. The images in this dataset [33] have a tone contrast that is like the vision of the human eye.

4. RESULTS AND DISCUSSION

The paper presents the outcome of all the processes performed during the study starting from the data collection where welding images from the dataset were used and then classified according to the condition of whether the image was a good or bad weld, an image recognition using Python language. After loading and importing the necessary libraries, the dataset of images is loaded, and the classification of images based on the respective dataset is done.

Also, by training the images and executing the algorithm further, the CNN model made predictions on the images or samples, and these predictions were recorded during the tuning of the algorithm, to classify the welding images as good or bad welded.
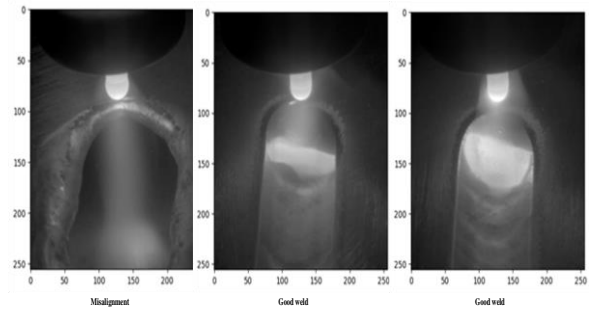
Figure 5. Predicted Images

Confusion Matrix For CNN:
The confusion matrix is a valuable tool for evaluating the performance of a classification model. In the presented study, a CNN-based model was evaluated for its ability to classify different types of weld defects. The confusion matrix as shown in Figure 8, which compares true labels (actual classes) with predicted labels (model's predictions), provides insights into the model's performance.
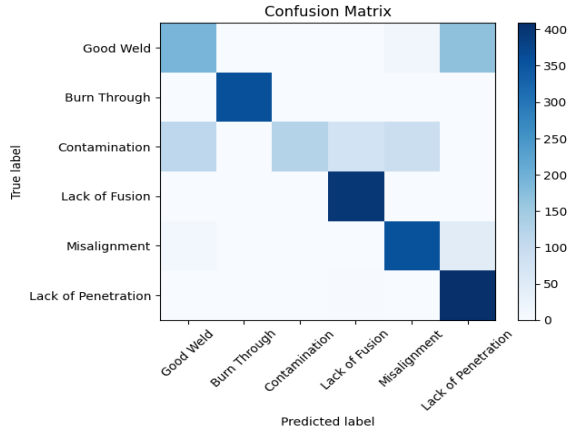
Figure 6. Confusion Matrix

Here's a breakdown of the key elements in the confusion matrix.

Good Weld	Represents actual instances of good welds.
Burn Through	Actual instances of burn-through defects.
Contamination	Actual instances of contamination defects.
Lack of Fusion	Instances where fusion is lacking.
Misalignment:	Instances with misalignment defects.
Lack of Penetration:	Actual instances of insufficient penetration.

Table 2. True Labels (Y-axis)

The same defect categories as mentioned above are for the predicted labels of the X-axis.

The dark squares that appear along the diagonal line of the matrix represent accurate predictions or true positives. The model shows good performance in identifying two types of weld defects: Good Welds and Lack of Penetration, as indicated by high true positive rates. However, the model seems to

misclassify other types of weld defects such as Burn Through and Contamination. Overall, this confusion matrix provides valuable insights into the model's performance, highlighting the areas that need improvement in weld defect classification.

Average Accuracy and Model Loss Evolution:

The graph in Figure 9 showcases the average accuracy of a CNN algorithm as it progresses through various epochs. Initially starting at a modest accuracy, the line gradually ascends to a commendable 0.91 accuracy within 30 epochs. This demonstrates that the CNN algorithm is steadily learning and enhancing its precision with every epoch.
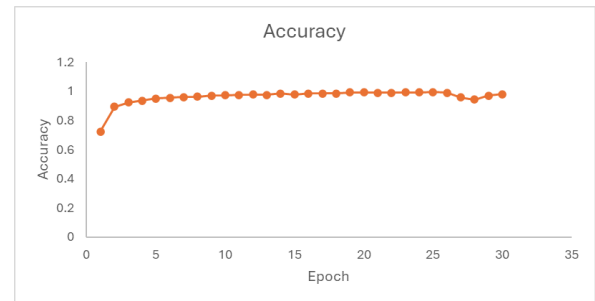
Figure 7. Model Accuracy for CNN

In Figure 10, the training loss decreases as epochs increase, indicating the CNN algorithm's improving performance over time. Overall, the graph suggests that the CNN algorithm is making progress during training.

Figure 8. Model Loss Evolution for CNN

172

Residual Neural Network (ResNet)

ResNet is an architecture of Residual Neural Networks that is commonly used in image classification. It is a popular choice for image classification because it tackles the vanishing gradient problem, where gradients tend to diminish as they propagate backward through many layers. ResNet architectures have shown exceptional performance in image classification tasks, especially in competitions like ImageNet [34], [35].

Confusion Matrix For ResNet:

In the confusion matrix shown in Figure 11 below, the rows represent the actual ground truth labels for the welding defects. These are the classes that the model is trying to predict correctly. The columns represent the labels predicted by the ResNet algorithm.
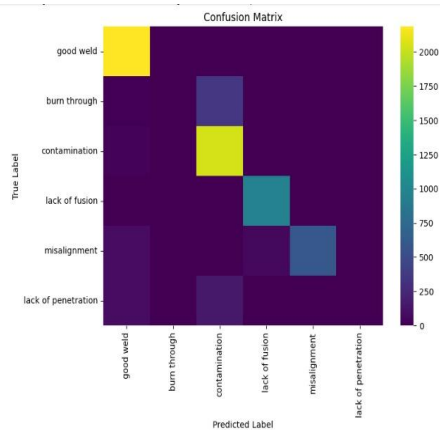
Figure 9. Confusion Matrix for ResNet

The model performs well in predicting "good welds" (true positives). The prominent yellow square in the top left corner indicates that most good welds are correctly classified. While Lack of Fusion, Misalignment, and Lack of Penetration: These three classes seem to be confused with each other. The misclassifications are visible in the off-diagonal cells corresponding to these defects.

For example, some instances of "lack of fusion" might be incorrectly predicted as "misalignment" or "lack of penetration," and vice versa. In summary, while the model excels in identifying "good welds," there are areas for improvement in distinguishing between specific welding defects. Fine-tuning the model or exploring additional features could help address these misclassifications.

Average Accuracy and Model Loss Evolution:

The graph shown in Figure 12 below depicts the training accuracy evolution of a model using the ResNet algorithm through different epochs. The model starts with low accuracy and experiences fluctuations early on. However, as the number of epochs increases, the accuracy stabilizes and consistently improves. This trend suggests that ResNet effectively learns complex features from data. Further improvements can be hyperparameter tuning, overfitting, and generalization to unseen data.
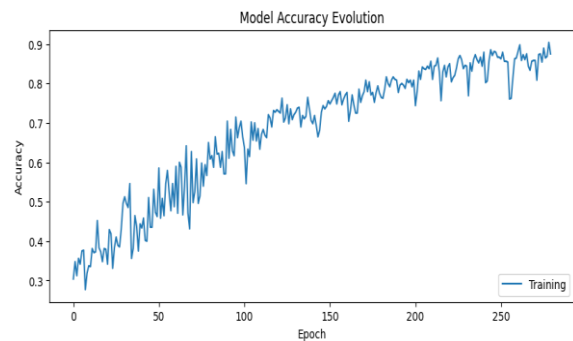
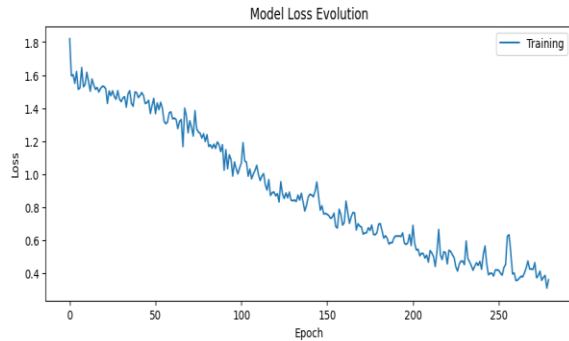Figure 10. Model Accuracy for ResNet

Figure 11. Model Loss Evolution for ResNet

The Model Loss Evolution graph in Figure 13 above depicts the training loss of a model using the ResNet algorithm over different epochs. Initially, the loss is high (around 1.8), but as training progresses, it consistently decreases. This downward trend indicates successful learning and convergence. The line exhibits fluctuations, indicating variations in loss at different epochs, but overall showcases a downward trend.

The CNN convolutional neural network model has proven to be highly accurate in its performance. Trained models, namely CNN and ResNet, have been implemented for real-time online evaluation scenarios. These models were utilized to predict each picture within the test set. The duration of picture reading, preprocessing, prediction, and recording of prediction results is carefully measured. The results display an average of 48 seconds per image prediction for the CNN model, and 69 seconds for the ResNet model. Both the algorithms mentioned in this paper are run in Google Colab as a virtual environment for executing the code.

CONCLUSION AND FUTURE WORK

Our study developed two distinct models CNN and ResNet that can be integrated into a real-time welding process monitoring system for evaluating welding quality. The CNN (convolutional neural network) model has proven to be highly accurate in its performance. Both the models meet the requirement of real-time evaluation of weld defects. While the CNN-based approach shows promising results in classifying weld defects, further refinement of feature extraction and enhancement of class distinction could optimize its performance.

The weld pool and surrounding area images used in this study were sourced from Kaggle. They were fed directly into the models for prediction, without manual feature extraction. Additionally, the models have low hardware requirements and can be run on regular PCs, making them highly applicable. Our findings suggest that these models can enhance the intelligence of automatic welding robots by integrating them into an image recognition system.

Future Work is aimed at using a data set of weld images for creating a feedback control system for adaptive robotic welding. Furthermore, the parameters will be set for each type of image difference and the robot will behave accordingly.

ACKNOWLEDGMENTS

Published Date: 08/07/2024 Version: 00

REFERENCES

[1] H. Wu, Q. Liu, X. L.- Computers, & M., and undefined 2019, "A review on deep learning approaches to image classification and object segmentation," *napier-repository.worktribe.com*, vol. 60, no. 2, pp. 575–597, 2019, doi: 10.32604/cmc.2019.03595.

[2] S. Oh, M. Jung, C. Lim, S. S.-A. Sciences, and undefined 2020, "Automatic detection of welding defects using faster R-CNN," *mdpi.com*, Accessed: Apr. 15, 2023. [Online]. Available: https://www.mdpi.com/910288

[3] J. Breitenbach, T. Dauser, H. Illenberger, M. Traub, and R. Buettner, "A Systematic Literature Review on Machine Learning Approaches for Quality Monitoring and Control Systems for Welding Processes," *Proceedings - 2021 IEEE International Conference on Big Data, Big Data 2021*, pp. 2019–2025, 2021, doi: 10.1109/BIGDATA52589.2021.9671887.

[4] A. H. Elsheikh, "Applications of machine learning in friction stir welding: Prediction of joint properties, real-time control and tool failure diagnosis," *Eng Appl Artif Intell*, vol. 121, p. 105961, May 2023, doi: 10.1016/J.ENGAPPAI.2023.105961.

[5] B. Zhou, Y. Svetashova, S. Byeon, T. Pychynski, R. Mikut, and E. Kharlamov, "Predicting Quality of Automated Welding with Machine Learning and Semantics: A Bosch Case Study," *International Conference on Information and Knowledge Management, Proceedings*, pp. 2933–2940, Oct. 2020, doi: 10.1145/3340531.3412737.

[6] K. Asif, L. Zhang, S. Derrible, J. E. Indacochea, D. Ozevin, and B. Ziebart, "Machine learning model to predict welding quality using air-coupled acoustic emission and weld inputs," *J Intell Manuf*, vol. 33, no. 3, pp. 881–895, Mar. 2022, doi: 10.1007/S10845-020-01667-X/TABLES/7.

[7] X. Wang, Y. Zhang, J. Liu, Z. Luo, T. Zielinska, and W. Ge, "Online detection of weld surface defects based on improved incremental learning approach," *Expert Syst Appl*, vol. 195, p. 116407, Jun. 2022, doi: 10.1016/J.ESWA.2021.116407.

[8] S. Ferraro, T. Van de Maele, P. Mazzaglia, T. Verbelen, and B. Dhoedt, "Computational Optimization of Image-Based Reinforcement Learning for Robotics," *Sensors*, vol. 22, no. 19, p. 7382, Oct. 2022, doi: 10.3390/S22197382/S1.

[9] A. Mahrle *et al.*, "Efficient air flow control for remote laser beam welding," *J Laser Appl*, vol. 30, no. 3, p. 032413, Aug. 2018, doi: 10.2351/1.5040613/1059521.

[10] X. Zhao, Y. Zhang, H. Wang, Y. Liu, B. Zhang, and S. Hu, "Research on Trajectory Recognition and Control Technology of Real-Time Tracking Welding," *Sensors 2022, Vol. 22, Page 8546*, vol. 22, no. 21, p. 8546, Nov. 2022, doi: 10.3390/S22218546.

[11] J. Zhou, Y. Zhou, B. Wang, and J. Zang, "Human–Cyber–Physical Systems (HCPSs) in the Context of New-Generation Intelligent Manufacturing," *Engineering*, vol. 5, no. 4, pp. 624–636, Aug. 2019, doi: 10.1016/J.ENG.2019.07.015.

[12] B. Wang, S. J. Hu, L. Sun, and T. Freiheit, "Intelligent welding system technologies: State-of-the-art review and perspectives," *J Manuf Syst*, vol. 56, pp. 373–391, Jul. 2020, doi: 10.1016/J.JMSY.2020.06.020.

[13] C. Longchao *et al.*, "Predicting the weld width from high-speed successive

175

images of the weld zone using different machine learning algorithms during laser welding Multi-fidelity Surrogate Model View project Machine Learning for fault diagnosis View project Predicting the weld width from high-speed successive images of the weld zone using different machine learning algorithms during laser welding," 2019, doi: 10.3934/mbe.2019278.

[14] K. Christensen, … T. S.-… T. of welding, and undefined 2005, "Gas metal arc welding of butt joint with varying gap width based on neural networks," *Taylor & Francis*, vol. 10, no. 1, pp. 32–43, Feb. 2005, doi: 10.1179/174329305X19303.

[15] S. Hongyuan, H. Xixia, L. Tao, C. S.-T. I. J. of, and undefined 2009, "Weld formation control for arc welding robot," *Springer*, vol. 44, no. 5–6, pp. 512–519, Sep. 2009, doi: 10.1007/s00170-008-1847-0.

[16] P. Franciosa, T. Sun, D. Ceglarek, S. Gerbino, A. Lanzotti Pasquale Franciosa, and A. Lanzotti, "Multi-wave light technology enabling closed-loop in-process quality control for automotive battery assembly with remote laser welding," *https://doi.org/10.1117/12.2526075*, vol. 11059, no. 21, pp. 76–88, Jun. 2019, doi: 10.1117/12.2526075.

[17] P. Franciosa, M. Sokolov, S. Sinha, T. Sun, and D. Ceglarek, "Deep learning enhanced digital twin for Closed-Loop In-Process quality improvement," *CIRP Annals*, vol. 69, no. 1, pp. 369–372, Jan. 2020, doi: 10.1016/J.CIRP.2020.04.110.

[18] J. Günther, P. M. Pilarski, G. Helfrich, H. Shen, and K. Diepold, "Intelligent laser welding through representation, prediction, and control learning: An architecture with deep neural networks and reinforcement learning," *Mechatronics*, vol. 34, pp. 1–11, Mar.

2016, doi: 10.1016/J.MECHATRONICS.2015.09.004.

[19] C. Longchao *et al.*, "Predicting the weld width from high-speed successive images of the weld zone using different machine learning algorithms during laser welding," *researchgate.net*, 2019, doi: 10.3934/mbe.2019278.

[20] S. Wu, S. Zhong, and Y. Liu, "Deep residual learning for image steganalysis," *Multimed Tools Appl*, vol. 77, no. 9, pp. 10437–10453, May 2018, doi: 10.1007/S11042-017-4440-4.

[21] K. He, X. Zhang, S. Ren, J. S. pattern recognition, and undefined 2016, "Deep residual learning for image recognition," *openaccess.thecvf.com*, Accessed: Feb. 27, 2024. [Online]. Available: http://openaccess.thecvf.com/content_c vpr_2016/html/He_Deep_Residual_Lea rning_CVPR_2016_paper.html

[22] K. He, X. Zhang, S. Ren, J. S.-P. of the IEEE, and undefined 2016, "Deep residual learning for image recognition," *openaccess.thecvf.comK He, X Zhang, S Ren, J SunProceedings of the IEEE conference on computer vision and, 2016•openaccess.thecvf.com*, Accessed: Feb. 27, 2024. [Online]. Available: http://openaccess.thecvf.com/content_c vpr_2016/html/He_Deep_Residual_Lea rning_CVPR_2016_paper.html

[23] F. Xu, Y. Xu, H. Zhang, and S. Chen, "Application of sensing technology in intelligent robotic arc welding: A review," *J Manuf Process*, vol. 79, pp. 854–880, Jul. 2022, doi: 10.1016/J.JMAPRO.2022.05.029.

[24] M. Cerrada, G. Zurita, D. Cabrera, R. V. Sánchez, M. Artés, and C. Li, "Fault diagnosis in spur gears based on genetic algorithm and random forest," *Mech Syst Signal Process*, vol. 70–71, pp. 87–103, Mar. 2016, doi: 10.1016/J.YMSSP.2015.08.030.

[25] A. Sumesh, K. Rameshkumar, K. Mohandas, and R. S. Babu, "Use of Machine Learning Algorithms for Weld Quality Monitoring using Acoustic Signature," *Procedia Comput Sci*, vol. 50, pp. 316–322, Jan. 2015, doi: 10.1016/J.PROCS.2015.04.042.

[26] A. M.-J. of A. and S. Technology and undefined 2020, "Machine learning approach for defects identification in dissimilar friction stir welded aluminium alloys AA 7075-AA 1100 joints," *academia.eduA MishraJournal of Aircraft and Spacecraft Technology, 2020•academia.edu*, vol. 4, no. 1, pp. 88–95, Jan. 2020, doi: 10.3844/jastsp.2020.88.95.

[27] A. López, … M. P.-… de T., and undefined 2016, "Teaching image processing in engineering using python," *ieeexplore.ieee.orgAFJ López, MCP Pelayo, ÁR ForeroIEEE Revista Iberoamericana de Tecnologias del Aprendizaje, 2016•ieeexplore.ieee.org*, Accessed: Feb. 22, 2024. [Online]. Available: https://ieeexplore.ieee.org/abstract/document/7511766/

[28] J. Davis *et al.*, "Smart manufacturing," *annualreviews.orgJ Davis, T Edgar, R Graybill, P Korambath, B Schott, D Swink, J Wang, J WetzelAnnual review of chemical and biomolecular engineering, 2015•annualreviews.org*, vol. 6, pp. 141–160, Jul. 2015, doi: 10.1146/annurev-chembioeng-061114-123255.

[29] Y. Pan, "Heading toward Artificial Intelligence 2.0," *Engineering*, vol. 2, no. 4, pp. 409–413, 2016, doi: 10.1016/J.ENG.2016.04.018.

[30] A. Kusiak, "Smart manufacturing must embrace big data," *Nature*, vol. 544, no. 7648, pp. 23–25, Apr. 2017, doi: 10.1038/544023A.

[31] J. Zhou, P. Li, Y. Zhou, B. Wang, J. Zang, and L. Meng, "Toward New-Generation Intelligent Manufacturing," *Engineering*, vol. 4, no. 1, pp. 11–20, Feb. 2018, doi: 10.1016/J.ENG.2018.01.002.

[32] "H. Kagermann, W. Wahlster, and J. Helbig, "Securing... - Google Scholar." Accessed: Feb. 22, 2024. [Online]. Available: https://scholar.google.com/scholar?hl=en&as_sdt=0%2C5&q=H.+Kagermann%2C+W.+Wahlster%2C+and+J.+Helbig%2C+%E2%80%9CSecuring+the+future+of+German+manufacturing+industry+initiative+INDUSTRIE+4.0+implementing+the+strategic+Recommendations+for+Final+report+of+the+Industrie+4.0+Working+Group%2C%E2%80%9D+2013.&btnG=

[33] "TIG Aluminium 5083." Accessed: Feb. 26, 2024. [Online]. Available: https://www.kaggle.com/datasets/danielbacioiu/tig-aluminium-5083

[34] "A Comprehensive Guide to Image Classification with ResNet and PyTorch." Accessed: Mar. 14, 2024. [Online]. Available: https://thegradient.io/pytorch-for-image-classification-part-1

[35] "GitHub - PernilleSilke/Image-Classification-with-ResNet50: ResNet50 Image Classifier." Accessed: Mar. 14, 2024. [Online]. Available: https://github.com/PernilleSilke/Image-Classification-with-ResNet50

Sensitivity Analysis of Steel Hole Plate Using the New Developed Creep Model by Utilizing Computational Methods

Mohsin Sattar[1]*; Muhammad Muzammil[2]
[1]Universiti Teknologi PETRONAS
[2]NED University of Engineering & Technology

*Corresponding author E-mail address: mohsinsheikhmech@gmail.com

ABSTRACT

With the rise in operational parameters, structural elements within power plants are exposed to heightened temperatures and pressures, reaching levels conducive to creep. This phenomenon poses the risk of component failure and fracture. Over the preceding decades, substantial efforts have been dedicated to comprehending the fundamental mechanisms of creep. Significantly, there has been a focus on predicting the lifespan of equipment to ensure safety and reliability in plant operations. This article introduces a modified model, building upon the Norton-Bailey and KachanovRabotnov constitutive models, aiming to comprehensively characterize all three stages of creep (primary, secondary, and tertiary) specifically for stainless steel material. The proposed model undergoes numerical calculations to simulate damage development in thin-hole steel plates. Special attention is given to the influence of specimen dimensions and stress on damage evolution. The outcomes of the study reveal the efficacy of the novel model in generating complete creep curves for various materials, emphasizing the notable impact of stress on creep behavior and damage progression. Sensitivity studies, employing Response Surface Methodology (RSM) and Analysis of Variance (ANOVA), are conducted to quantitatively and qualitatively analyze the new creep model data in comparison to established models. The objective of these sensitivity studies is to assess the significant contributions of various factors to the target response strain in this specific case study.

Keywords—creep deformation, curve fitting, Kachanov-Rabotnov model, damage evolution, Norton Bailey model

1. INTRODUCTION

Numerous creep models have been developed over the years to anticipate the creep behavior of materials; however, these models exhibit certain limitations [1]. The Norton–Bailey (NB) model, also known as Norton's power law, serves as a foundational model integrated into the finite element Abaqus software, widely employed for creep analysis in conjunction with other models developed by Bailey and Norton [2]. Functioning as a benchmark, the NB model predicts the creep deformation behavior of materials manifesting timedependent, inelastic deformation, particularly effective in anticipating material behavior in the secondary creep regime.

In contrast, the Omega model, introduced by the Material Properties Council and proposed by Prager [3] in 1995, stands out as a reliable prediction model. Recognized for its simplicity and lower dependence on material constants, the Omega model boasts a well-documented creep evaluation process, demonstrating excellent performance in establishing property relations across diverse materials. Primarily designed for calculating

178

the remaining life of components operating in the creep zone under high temperatures and pressures, the Omega model utilizes a strain rate parameter and a multi-axial damage parameter, as outlined by Yeom et al. [4]. It effectively forecasts the rate of strain accumulation, creep damage accumulation, and the remaining time to failure based on the stress state and temperature, covering both primary and secondary creep regime deformations and excelling in predicting material rupture time at lower temperatures [5].

The Kachanov–Rabotnov (KR) model, an early implementation of the continuum damage mechanics (CDM) approach for creep proposed by Kachanov and Rabotnov [6], is another significant model. This model allows for the modeling of secondary and tertiary creep deformations through a set of coupled equations. Continuous efforts have been dedicated to enhancing the KR law, leading to recent variations aimed at generating contour deformation maps [7]. Stewart and Gordon [8] are actively developing methods to define transversely isotropic creep damage properties and estimate stress-independent tertiary creep damage constants using both strain- and damage-based analytical approaches. These advancements contribute to the ongoing refinement of creep models for a more comprehensive understanding of material behavior under varying conditions.

The Norton-Bailey constitutive model proves effective in delineating the relationship between strain and stress during the primary and secondary stages of creep. However, when analyzing the life of structural components controlled by rupture, it becomes imperative to scrutinize their creep behavior in the tertiary region of the creep curve. Conversely, the Kachanov-Rabotnov constitutive model aligns well with the secondary and tertiary stages of creep but lacks consideration for primary creep accumulation.

To address these limitations, a modified creep model is proposed in this study, aiming to comprehensively describe all three stages of creep. The modified constitutive creep model is derived through a combination of the Norton-Bailey and Kachanov-Rabotnov models. Numerical calculations using this modified model were conducted to explore the creep behavior and damage development in a thin-hole steel plate made of SS-304 material under constant stresses. The investigation places particular emphasis on understanding the impact of specimen dimensions and stresses on damage development, deformation, and rupture life. This paper addresses the limitations and deficiencies of the NortonBailey and Kachanov-Rabotnov models, paving the way for a more comprehensive understanding of creep behavior in structural components subjected to various stress conditions.

1.1 Problem Statement

The Norton-Bailey model is limited in that it exclusively addresses the secondary creep regime and lacks predictions for the primary and tertiary regimes, resulting in an overall error when these stages dominate. Although the KachanovRabotnov (KR) model shows promise, it involves a substantial number of material constants, and its formulation neglects consideration for the primary creep regime during analysis. While KR successfully emulates both continuum creep damage and discontinuous plastic damage at rupture within a continuous function, the intricacies of the model pose challenges for integration into finite element (FE) analysis. Both models have made strides in addressing nucleation and plasticity for crack initiation and growth to some extent. However,

179

accurate detection and identification of creep crack growth remain limited. The mechanism through which creep cavities nucleate is not well-established, despite the presence of voids in every material. Observations suggest that cavities tend to nucleate along grain boundaries under constant load for extended periods. Creep cavitation is a critical aspect, often given less priority when addressing creep crack initiation and growth. Given these limitations, the article proposes a new creep prediction model based on creep power laws. This model aims to overcome the challenges posed by existing models and address the following research questions regarding how the material behaves during creep deformation under various parameter variations, conditions, and circumstances.

1.2 Research Questions

1. How the new model can improve the prediction of creep failure at high temperatures?

2. Can the model accurately predict all creep stages at crack initiation, growth and rupture?

3. How much improvement in efficiency of the analysis and accuracy of the results increase using the newly proposed model?

The new creep prediction model is based on the following hypothesis:

1.3 Hypothesis

1. The prediction of creep behaviour of the mechanical equipment, especially due to generation of cracks through nucleation and voids within the material will be attained through the new model, with the shortcomings of the current models are addressed.

2. Prediction of the creep behaviour of the material can be handled with less

complications with the proposed model. The new material model provides an alternative to the current models, producing results more effectively.

3. A simplified formulation is expected, to accurately consider all three creep stages (I-III), requires only minimal empirical data and containing minimal number of material fitting parameters. The model will offer ease of applicability and versatility to deal with material's data which is already scarce for the three creep stages.

The next section discussed the theoretical framework of established models and mathematical formulation of the new creep material model.

2. THEORETICAL FRAMEWORK

2.1 Norton Bailey Model

Norton's power law (1929), rooted in the Arrhenius rate equation [10], stands as the most renowned and widely used minimum creep strain rate law. This law, represented in Equation (1), is a prominent framework in understanding and describing creep behavior.

$$\dot{\epsilon}_{cr} = B'\sigma^n \, exp \, (-Q_c/RT)^m \; , \qquad (1)$$

In the given context, $\dot{\epsilon}_{cr}$ signifies the minimum creep strain rate, B' is the material constant, σ denotes the applied stress, n represents the power law exponent, Q_c represents the activation energy, R stands for the universal gas constant, and T corresponds to the applied temperature. Equation (1) is subsequently streamlined when considering a constant temperature, resulting in the simplified form represented by Equation (2).

$$\dot{\epsilon}_{cr} = A \, \sigma^n \, t^m \; , \qquad (2)$$

without considering time, Equation (3) becomes:

$$\dot{\epsilon}_{cr} = A \, \sigma^n \qquad , \qquad (3)$$

where,

$$A = B' \, exp(- \, Q_c/RT) \, . \qquad (4)$$

It's important to highlight that *A, n,* and *m* are material constants dependent on temperature and remain unaffected by stress. Both *n* and *m* are dimensionless, while *A* carries units that align with those of time *t* and stress σ. The derivative with respect to time of Equation (3) is commonly termed the time-hardening formulation of the power-law creep [11].

$$\dot{} = A \left(\frac{\sigma}{1- \omega} \right), \qquad (5)$$

$$\dot{\omega} = \frac{M \, \sigma^x}{(1- \omega)^\phi} \, , \quad 0 \leq \omega < 1 \qquad (6)$$

In these equations, *M, χ,* and ϕ represent constants related to tertiary creep damage, while the creep strain mirrors Norton's power law for secondary creep, utilizing the same *A* and *n* as constants for secondary creep. The assumption of isochoric creep behavior is made, and the analytical calculation of secondary and tertiary creep damage constants is feasible [13]. Equations (7) and (8) are derived by manipulating Equation (6) through a process involving separation of variables, indefinite integration, and simplifications.

$$t(\omega, \sigma) = \frac{1-(1- \omega)^{\phi+1}}{(\phi+1)M \, \sigma^x} \quad , \qquad (7)$$

$$\omega(t,\sigma) = 1 - [1 - (\phi + 1)M \, \sigma^x \, t]^{\frac{1}{\phi+1}} \quad , \qquad (8)$$

Here, *t* denotes the current time, and ω represents the current damage. These equations offer a means to calculate the current time based on the current damage and stress, or alternatively, the current damage based on the current time and stress. Stewart and Gordon [12] introduced two valuable techniques for analyzing and applying the

Kachanov– Rabotnov model: the strain approach (SA) and the damage approach (DA). The choice between these techniques depends on the material's analysis for both secondary and tertiary creep stages.

2.3 Mathematical Formulation & Integration of New Creep Model in Abaqus

The novel creep model mathematical formulation is built by combining Norton Bailey and Kachanov-Rabotnov models equations which are based on creep power laws [14]: The new creep model equation is developed in Equation (9) and simplified in Equations (10) and (11).

Creep strain rate: $\frac{d\varepsilon}{dt} = A \, \sigma^n \; + \; A \, (\frac{\sigma}{1- \omega})^n$, (9)

$$= A \, \sigma^n \, [\, 1 \, + \, \frac{1}{(1- \omega)^n}], \qquad (10)$$

$$= A \, \sigma^n \, [\frac{(1- \omega)^n + 1}{(1- \omega)^n}], \qquad (11)$$

where, is the creep strain, *A, n* and ω are the material constants, *t* is the time and σ is the stress. Equation (11) can be transformed into numerical form as in Equation (12) [9]:

$$\frac{d\varepsilon}{dt} = \Delta t \overset{Lim}{\longrightarrow} 0 \; \frac{\Delta \varepsilon}{\Delta t}, \qquad (12)$$

$$\frac{\Delta \varepsilon}{\Delta t} = A \, \sigma^n \, [\frac{(1- \omega)^n + 1}{(1- \omega)^n}], \qquad (13)$$

$$\Delta \varepsilon = A \, \sigma^n \, [\frac{(1- \omega)^n + 1}{(1- \omega)^n}] \, \Delta t \, , \qquad (14)$$

where, Δ is DECRA(1), uniaxial deviatoric creep strain increment in ABAQUS creep user sub-routine obtained from ABAQUS documentation 3.4.6 as in Equation 14[15]. Equation (11) can also be differentiated with respect to σ as:

181

$$\frac{\Delta\varepsilon}{\Delta\sigma} = A\,n\,\sigma^{n-1}\left[\frac{(1-\omega)^{n}+1}{(1-\omega)^{n}}\right]\Delta t. \qquad (15)$$

where, $\frac{\Delta\varepsilon}{\Delta\sigma}$ is DECRA(5), von Mises stress in ABAQUS creep user sub-routine. Equation (14) and Equation (15) can be implemented in creep sub-routine to incorporate the proposed creep model in ABAQUS for time hardening and strain hardening methods.

The other method of integration adapted for the new creep model in Abaqus is by curve fitting:
The general power law regression is expressed in Equation (16), while the Norton-Bailey equation is provided in Equation (17) for the purpose of comparison [16]:

$$y = A'x^{B} \qquad (16)$$

$$\varepsilon_{min} = A\,\sigma^{n} \qquad (17)$$

In this context, the equation involves the criterion variable and prediction response (*y*), where *A'* represents the curve coefficient, and *B* is the exponent of the predictor variable (*x*). This equation is juxtaposed with the Norton-Bailey power law regression presented in Equation (17). The parameter *B* in Equation (18) is then compared with the derived stress exponent (*n*) in Equation (19) for creep [17].

$$B = \frac{n'\sum(\ln x\ln y)-\sum(\ln x)\sum(\ln y)}{n'\sum[(\ln x)^{2}]-[(\sum\ln x)^{2}]} \qquad (18)$$

$$n = \frac{n'\sum(\ln\sigma\ln\dot\varepsilon)-\sum(\ln\sigma)\sum(\ln\dot\varepsilon)}{n'\sum[(\ln\sigma)^{2}]-[(\sum\ln\sigma)^{2}]} \qquad (19)$$

Likewise, the curve coefficient A' in Equation (20) was contrasted with the Norton-Bailey creep parameter A in Equation (21) to determine the parameters [18].

$$A' = e^{\frac{\sum(\ln y)-B\sum(\ln x)}{n'}} \qquad (20)$$

$$A = e^{\frac{\sum(\ln\dot\varepsilon)-n\sum(\ln\sigma)}{n'}} \qquad (21)$$

In this equation, *x* and *σ* serve as independent variables, while *y* and $\dot\varepsilon$ act as dependent variables, and *n'* denotes the number of samples. In the regression analysis [49], stress is considered an independent variable, and strain rate is the dependent variable. The selection of the stress range is influenced by the precision of the regression, with a larger stress range in the sample data yielding a more accurate curve fit [19].
The creep parameter and stress exponent, as outlined in Equations (19) and (21), undergo modifications for the curve fitting of the new model through regression into the NortonBailey model in Abaqus, resulting in Equations (22) and (23). In these equations, the constant b is introduced to signify the damage evolution parameter, aiding in modeling material deformation during the tertiary creep stage [20].

$$n = \frac{n'\sum(\ln\sigma*b)(\ln\dot\varepsilon)-\sum(\ln\sigma*b)\sum(\ln\dot\varepsilon)}{n'\sum[(\ln\sigma*b)^{2}]-[(\sum(\ln\sigma*b)^{2}]} \qquad (22)$$

$$A = e^{\frac{\sum(\ln\dot\varepsilon)-n\sum(\ln\sigma*b)}{n'}} \qquad (23)$$

where,

$$b = \frac{\{(1-\omega)+1\}}{(1-\omega)};$$

ω = damage evolution parameter;
n' = sample size

The new model equation becomes:

$$\dot\varepsilon = A\,\sigma^{n}*b \qquad (24)$$

3. METHODOLOGY

This section elucidates the adopted methodology for initially determining analytical creep strain and creep strain rate through regression analysis, employing Omega-Norton Bailey regression models for the new model. Subsequently, the implementation of the new creep model is addressed by utilizing creep user sub-routine scripting in the finite element package Abaqus.

3.1 Analytical Creep Strain

The research study is structured into two segments to determine the creep strain and creep strain rate. Initially, the creep strain was analytically computed using the creep material model derived from the Omega model formulation, adhering to the ASME FFS-1/API-579 standards [21], specifically for the SS-304 thin hole plate. Subsequently, creep strains were calculated through finite element (FE) simulation in Abaqus, utilizing material model properties obtained from ASME BPVC Section II Part D, Sub-Part 2 standards [22]. Regression analysis was applied to acquire the creep parameter (A) and the stress exponent (n) for the new creep regression model designed for the steel 304-hole plate in Abaqus. The same FE model was then employed to implement the proposed new creep model.

For this research study and analysis, the chosen material is SS-304. The coefficients provided in Table 1 represent estimates of typical material behavior employed in the analytical calculations. These coefficient values were determined through a thorough examination of material behavior and were obtained from ASME FFS-1/API-579 standards [21].

	Strain Rate Parameter ε_{c0}	Omega Parameter - Ω

Type-SS 304	A_0	-19.17	B_0	-3.40
	A_1	53762.40	B_1	11250.0
	A_2	-13442.4	B_2	-5635.80
	A_3	3162.60	B_3	3380.40

Table 1. MPC Omega model material coefficients for material type SS-304 (MPa, °C) [21]

The parameters and formulations are explicitly defined in ASME FFS-1/API-579 standards, particularly for the MPC Omega model. The analytical creep strain for the thin-hole steel plate 304 was computed using the closed-loop Equations (25)–(32), as extracted from the ASME FFS-1/API-579 standards [21].

$$log_{10}[\dot{\varepsilon}_{c0}] = -\left[(A_0 + \Delta_{\Omega}^{sr}) + \left(\frac{A_1 + A_2 S_1 + A_3 S_1^2 + A_4 S_1^3}{T_{ref} + T}\right)\right] \quad (25)$$

$$\Omega_m = \Omega_n^{\delta_{\Omega}+1} + \alpha_{\Omega} + n_{BN} \quad (26)$$

$$\Omega = max[(\Omega - n_{BN}, 3] \quad (27)$$

$$S_1 = log_{10}[\sigma_e] \quad (31)$$

$$\sigma_e = \frac{1}{\sqrt{2}}[(\sigma_1 - \sigma_2)^2 + (\sigma_1 - \sigma_3)^2 + (\sigma_2 - \sigma_3)^2]^{1/2} \quad (32)$$

The next sub-section explains the geometry modelling and pre-processing of FE model specimen.

3.2 Geometry Modelling & Pre-Processing

The finite element (FE) model for the thin-hole steel sheet of steel 304 was constructed in compliance with the ASME standards for thin plates [23]. Boundary conditions were imposed on the FE model, with one end being fixed. The reference point for the model's displacement direction was determined upon the application of the load [36]. The study observed the predicted behavior of stainless steel material under constant stresses within its elastic limit at both room temperature and elevated

183

temperatures. The analysis involved a combination of plasticity and creep to yield results for established creep models applied to the thin-hole steel plate. Subsequently, plastic hardening data for the material was obtained for the developed models. The results obtained from the established creep models were then compared with those derived from the newly proposed creep model.

The creep was initially modelled using the NortonBailey (NB) model available in the Abaqus material library [24]. The assessment focused on the isotropic material SS304, given the assumptions made in the analysis. A uniaxial force was applied to the steel hole plate under specific boundary conditions, and a thermal field was introduced. An elastic perfectly plastic model was selected to simulate plasticity, plastic deformation, and elasticity [25]. The displacement was measured at one end of the steel hole plate with a 2 mm/min amplitude, while the other end was fixed. The thermal environment was created by implementing a specific thermal field throughout the model, ranging in temperatures from 0 to 700°C for the SS-304 material. Once the desired temperature was achieved, a steady longitudinal load was applied, inducing dislocation and distortion in the material's grain structure [26].

Figure 1(a) illustrates the applied load on the steel plate, with one end fixed and the load applied at the other end. Figure 1(b) demonstrates the meshing of the hole plate with an appropriate mesh size, while Figure 1(c) depicts the magnitude of the load on the hole plate. Figure 1(d) presents the von Mises stress distribution of the plate. Lastly, Figure 1(e) illustrates the obtained creep strain for the steel plate during the simulation

$$log_{10}[\Omega] = [(B_0 + \Delta_\Omega^{cd}) + (\frac{B_1 + B_2\ S_1 + B_3\ S_1^2 + B_4\ S_1^3}{T_{ref} + T})] \quad (28)$$

$$\delta_\Omega = \beta_\Omega \cdot (\frac{\sigma_1 + \sigma_2 + \sigma_3}{\sigma_e} - 1) \quad (29)$$

$$n_{BN} = -(\frac{A_2 + 2A_3\ S_1 + 3\ A_4 S_1^2}{T_{ref} + T}) \quad (30)$$

$T_{ref} = 460\ for\ {}^0F \quad ; \quad T_{ref} = 273\ for\ {}^0C$
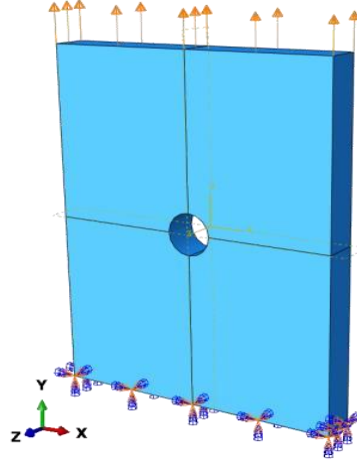
Figure 1(a) Specified Load applied and fixed boundary conditions at opposite
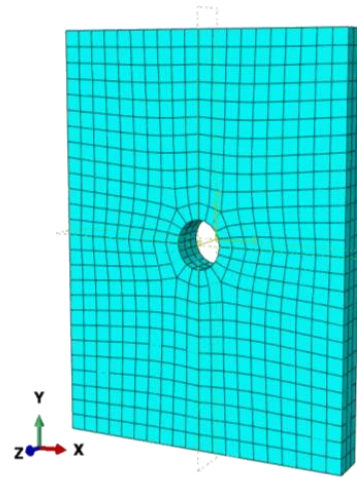

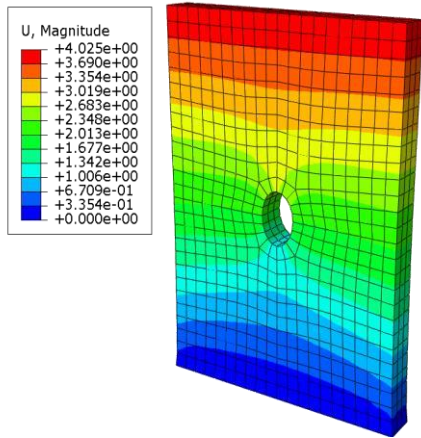Figure 1(b) Meshing of thin hole plate with appropriate mesh size

184

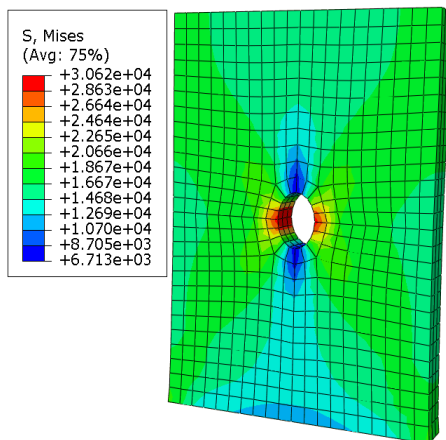Figure 1(c) Thin plate with the applied load and magnitude

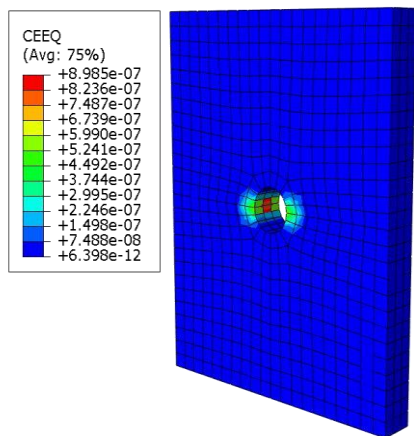Figure 1(d) Thin plate with the applied load and magnitude

Figure 1(e) Creep Strain (CEEQ) at the plate hole

For mesh convergence study, simulation was run by selecting coarsest mesh which leads to reasonable accuracy. Mesh size was refined continuously, and the simulations were run several time and the results were compared, to select the best size of the mesh. The material and physical properties for SS304 material for the steel plate are tabulated in the Table 2 as obtained from ASME BPVC sub part II section D.

Material Model	Elastic Perfectly Plastic
Young's Modulus	(201000 - 17100) MPa @ -25^0C to 720^0C
Poisson's ratio	0.31
Density	8000 kg/m^3
Thermal Expansion Coefficient	17.3 x 10-6 0C-1
Thermal Conductivity	16.2 W m $^{-1}$ °C $^{-1}$
Yield Stress	(207 – 126) MPa
Plastic Strain	(0 – 0.015)

Table 2: Material & Physical Properties of SS-304 material

The creep parameter and stress exponent were determined for the new model by regression analysis with the effect of damage evolution parameter and tabulated in Table 3 for steel plate. The results were then obtained for the new model by applying curve fitting technique. The next sub-section discussed the statistical tools applied for sensitivity studies for analysing creep data by the new model.

185

	New Creep Model	Temperature (ºC)
Creep Parameter	1.64964×10^{-22}	595
	2.84973×10^{-22}	600
	4.89231×10^{-22}	605
	8.3477×10^{-22}	610
	1.41581×10^{-21}	615
	2.38713×10^{-21}	620
	4.00147×10^{-21}	625
Stress Exponent	7.991675	595
	7.95904	600
	7.900654	605
	7.855916	610
	7.811683	615
	7.767944	620
	7.724693	625

Table 3: Material Constants for SS-304 for Creep models at (680 – 720) ^{0}C

3.3 Sensitivity Studies of New Creep Model Using RSM & ANOVA

A sensitivity analysis of the newly proposed model was conducted to examine the impact of operational and design parameters on the objectives. The Analysis of Variances (ANOVA) method was employed to assess differences between two or more means or components through significance tests. ANOVA also facilitates multiple comparisons of means across various populations. The primary aim of conducting sensitivity studies is to quantify the significant contributions of factors to the target response. The analysis incorporated parameters related to operation, design, and material dependency. Equation (33)

represents the central composite design equation utilized for the optimization of these parameters.

(ANOVA) for comparison. The design matrices for the novel model were formulated utilizing central composite design (CCD). This process considered four independent design factors: stress (A), stress exponent (B), creep parameter (C), and damage parameter (D), with a singular target response being the strain rate. The details are documented in Table 4 [27]. Analytical methods were employed to derive the values presented in Table 4, enabling an assessment of the substantial impact of these factors on the target response, Finite Element (FE) strain rate. To gauge the accuracy of predictions, both actual and predicted values were compared. This involved utilizing Response Surface Methodology (RSM) and Analysis of Variance (ANOVA) for each model, including the new one.

	Independent design Factors				Response
Values	Stress (A) MPa	Stress Exponent (B) 'n'	Creep Parameter (C) $MPa^{-n} h^{-1}$	Damage Parameter (D) 'ω'	Strain rate 10^{-5} / h
Low	3	6.82728	1.59818×10^{-21}	0.05	2.99×10^{-11}
High	81	7.11384	1.10787×10^{-20}	0.40	10.6812

Table 4: Independent Design Factors & Response for RSM & ANOVA of New Model

The data was inserted into the appropriate slots of the design matrices for each model for solving the design equation for new model, as follows in Equation(34): [28]

New Model Creep Strain rate =

$+7.703 \times 10^{-6} + 0.0044*A + 0*B + 0*C + 0*D + 0*AB + 0*AC +$

$0*AD + 0*BC + 0*BD + 0*CD + 0.002* A^2 + 0.0007* B^2 + 0.0007*$

$C^2 + 0.0007* D^2$ (34)

186

where, A = stress, B = stress exponent, C = creep parameter and D = damage parameter.

The provided equation is employed to predict the response :

$$= \beta_0 + \sum_{i=1}^{n} \beta_i\, X_i + \sum_{i=1}^{n} \beta_{ii}\, X_i^2 + \sum_{i=1}^{n} \sum_{j=i+1}^{n} \beta_{ij}\, X_i\, X_j \quad (33)$$

In the provided equation, y signifies the predicted value of the response. X_i and X_j represent independent parameters, while β_0, β_i and β_{ii} denote the constant, linear, and interactive coefficients, respectively. Additionally, β_{ij} stands for the quadratic coefficient, and n represents the number of factors involved in the analysis.

The design matrices for the new model were constructed using the central composite design (CCD), incorporating four independent design factors: stress (A), stress exponent (B), creep parameter (C), and damage parameter (D). The target response, in this case, is the strain rate, and the corresponding design matrix is reported in Table 4 [27]. The values in Table 4 were determined analytically to assess the significant contribution of these factors to the target response. For each model and the new model, actual and predicted values of the finite element strain rate were obtained from the Response Surface Methodology (RSM) and Analysis of Variance deemed significant, as evidenced by a coefficient of determination (R²) value exceeding 80%.

4. RESULTS

The recently proposed model, which integrates the Norton Bailey and Kachanov-Rabotnov models, was applied within the FE package Abaqus to derive creep strain and strain rate results for an SS-304 thin-hole plate using finite element analysis. Consistent with established models in the FE package, the same predefined boundary conditions were employed. The simulation extended over 1000 hours at a temperature of 625°C, yielding promising outcomes that covered the primary, secondary, and tertiary stages of creep for the material. The obtained results were derived through the utilization of a curve-fitting method.

Figure 2 depicts the von Mises stress and relaxed stresses observed during the simulation employing the new model, which incorporates the creep parameter and stress exponent. The performance of the new model was also compared against the Omega model, following a similar approach to that used for established models. Creep strain rate results for the new model were obtained through a curve fitting process. Figure 2 provides a visual representation of the induced von Mises stress and creep strain results [29].
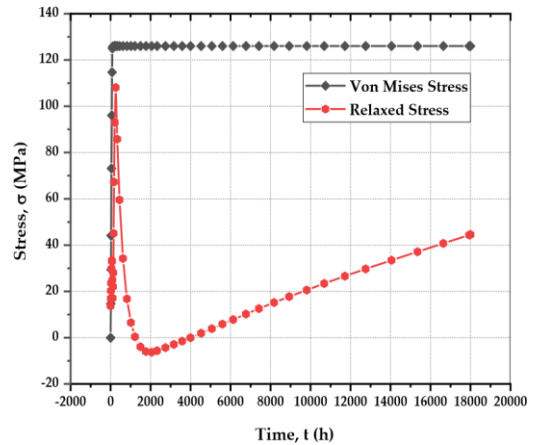

Figure 2: Von Mises stress and Relaxed stress distribution with Omega- New Model's Regression -Visco-elastic plastic run-time of 1000 h, 101 MPa and 625 ⁰C.

4.1 New Creep Model Results by Curve-Fitting

The creep strain rate results were obtained while implementing new model in Abaqus by the method of curve fitting, used for deriving constants in the equation of new model. The new model was standardized by the Omega model with the help of regression analysis. Figure 3(a) is depicting

187

the comparison of creep strain rates for the new model with the Omega model on the same applied conditions. New creep model curve is covering primary, secondary and tertiary creep stages, whereas Omega model can only cover the primary and secondary creep stages. Omega model gives error in predicting creep strain at elevated temperatures, this deficiency can be fulfilled by using the new creep model [30]. Omega model is unable to predict creep curves for the large exponential data, the deficiency can be fulfilled by using the new proposed creep model. Figure 3(b) is depicting the results comparison of the new model with the Omega model for creep strain at same pre-defined boundary conditions [31].
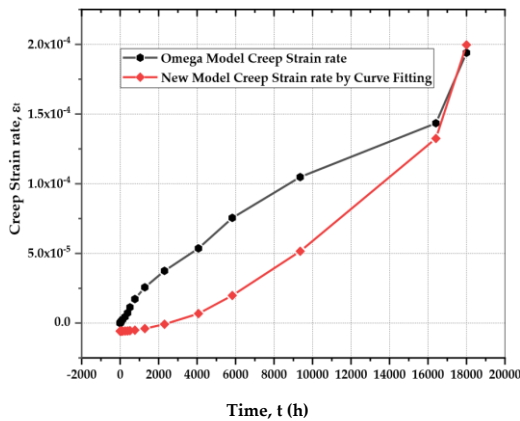
Figure 3(a): New Model Creep strain rate comparison with the Omega Model Creep strain rate by Curve Fitting
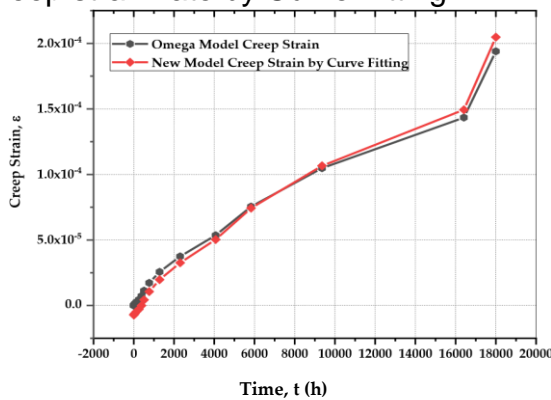
Figure 3(b): New Model Creep strain comparison with the Omega Model Creep strain by Curve Fitting

To capture the tertiary creep behaviour of stainless-steel material, arbitrary damage evolution parameter (ω) values were applied. The strain to reach the particular value of (ω) does not show the similar trend. As depicted in the Figure 4, a marginal decrease in strain to reach the particular value of (ω), resulted in the reduction of the applied stresses. The kinetics evolution of coupled strain and damage does not necessarily follow the same trend. It is well known fact, that any material fails if (ω), reaches critical damage ω_c. The material fails usually before reaching the critical damage of value equivalent to 1. The new creep model has the ability to model the tertiary creep damage at all damage parameter (ω) values [32].
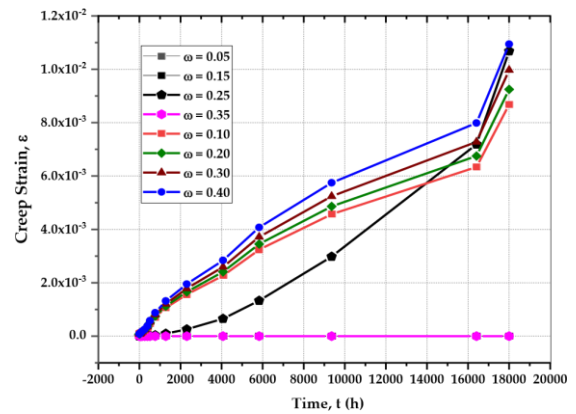

Figure 4: Creep Strain for the new model at varying Damage Evolution Parameters [33]

4.2 Data Optimization by Statistical Modelling

For the response analysis, quadratic regression models were selected for statistical assessment of response strain. To verify the suitability of the chosen regression

188

models, regular coefficient of determination (R²), adjusted coefficient of determination (adjusted R²), and expected coefficient of determination (predicted R²) were employed for each case. The fit statistics for the response strain generated from a central composite design are presented in Table 5. The significance of the models is evident from the R² values. Additionally, the close proximity of the modified R² and anticipated R² values reinforces the models' relevance. The term "adequate precision" signifies the comparison between the predicted values (referred to as "signal") and the average prediction error (referred to as "noise"). The models exhibit good performance, as indicated by the appropriate relationship between signal and noise. It was determined that all quadratic models are significant in exploring the design space [34].

Fit statistics for New Model Creep strain rate (t)	
R^2	0.8282
Adjusted R^2	0.6679
Predicted R^2	0.0107
Adequate Precision	8.7791

Table 5: Fit Statistics for the Models

ANOVA (Analysis of Variance) was employed to assess the statistical characteristics and synergistic effects of each constituent. The applicability and suitability of the regression model were recommended through various ANOVA adequacy tests, including the lack-of-fit test, the F-value, and the p-value [35]. Figure 5 illustrates the plot of interaction and correlation analysis for each model, specifically focusing on the parameters of stress and stress exponent on the response strain. This correlation is also evident in the mathematical model equations. The ANOVA table is presented in Table 6 for the new model's creep strain rate, and a summary of the new model is tabulated in Table 7.
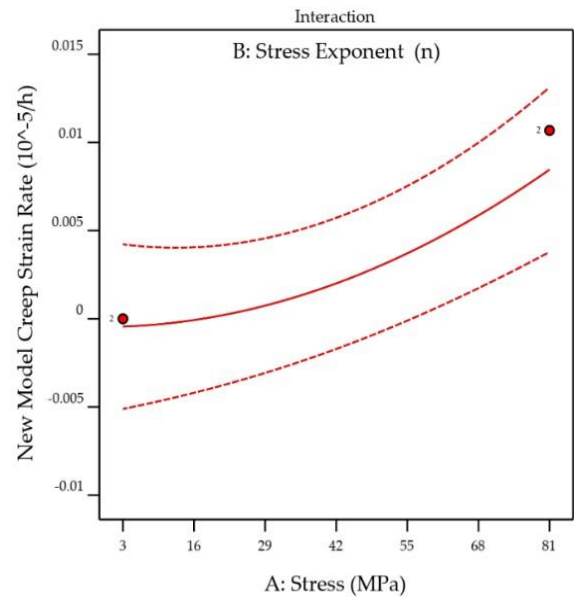

Figure 5: Stress & stress exponent interaction effect on New Model creep strain rate.

Source	Sum of Squares	df	Mean Square	F-value	p-value
Model	0.0006	14	0	5.17	
A-stress	0.0005	1	0.0005	57.80	
B-Stress Exponent	0	1	0	0	
C-Creep Parameter	0	1	0	0	
AB	0	1	0	0	
AC	0	1	0	0	
AD	0	1	0	0	
BC	0	1	0	0	
BD	0	1	0	0	
CD	0	1	0	0	
		1	0.0001	13.34	

A^2	0.0001	1	0	1.48
B^2	0			
C^2	0			
D^2	0			
		1	0	1.48
		1	0	1.48
Residual	0.0001	15	8.222×10^{-6}	
Lack of fit	0.0001	10	0	
Pure Error	0	5	0	
Cor Total	0.0007	29		

Table 6: ANOVA table for New Model Creep Strain Rate

Source	Std. Dev.	R^2	Adjusted R^2	Predicted R^2	Press
Linear	0.0031	6.6619	0.6078	0.5138	0.0003
2FI	0.0036	0.6619	0.4840	0.0408	0.0007
Quadratic	0.0029	0.8282	0.6679	0.0107	0.0007
Cubic	0.0035	0.8812	0.5078	-16.1067	0.0123

Table 7: Response: New Model creep strain rate – Model Summary

The following three-dimensional plots offer an assessment of the behavior of the response and unveil the synergistic effects of the independent elements on the chosen response. In essence, the 3D model presents the response as a function of two independent components, while the remaining two elements are held constant at their mean coded values. These three-dimensional surface plots illustrate the functional relationship between the defined dependent variables and their associated independent variables. For each model, the stress exponent, creep parameter, stress, and damage parameter are applied to measure the individual response strain. Figure 6(a) illustrates the combined effect of the design factors on the response, specifically the new model's creep strain rate, while Figure 6(b) depicts contour creep deformation maps of the model.
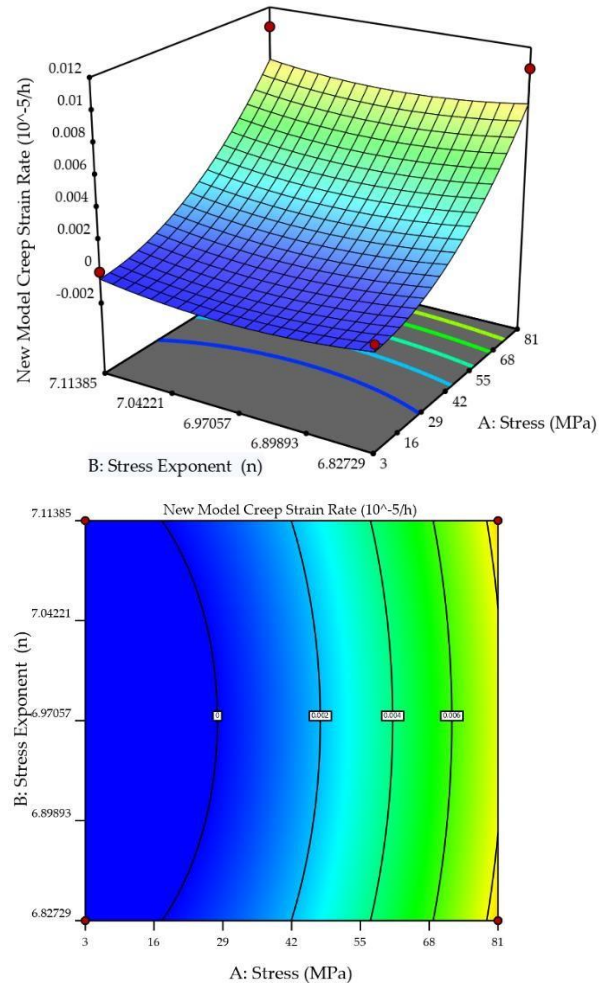
Figure 6(a) The combined effect of design factors on the response New Model creep strain rate (ₜ); (b) Contour creep deformation map for New creep model

Figure 7 illustrates the graphs of simulation outputs alongside predicted outputs for all the models. The correlation between predicted and actual values for the response strain rate is presented at a satisfactory level across all models. Notably, the models do not exhibit

abrupt variations in continual variance, as indicated by their relative error values. To assess the appropriateness of the generated models, the graph displays the projected vs. actual responses. It is evident from the graph that the predicted and actual values for the relevant response are very close [36]. The distribution of data points along the run order suggests that the values predicted by the model remained relatively consistent [37]. A random dispersal was observed, with most values situated close to the middle line. In this scenario, no discernible pattern of residuals above and below the central line was observed, affirming that the run order of the design procedure did not significantly impact the data and, consequently, indicating the significance of the model.
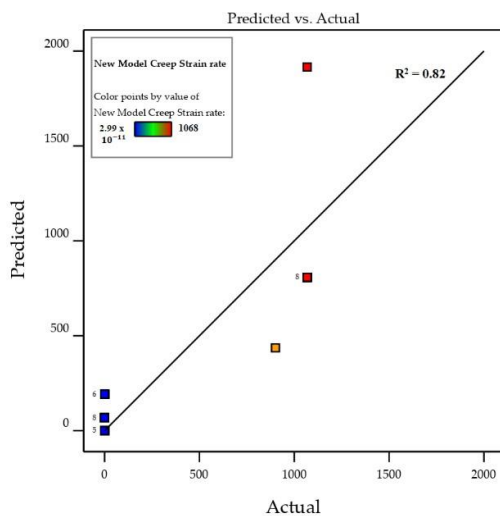
Figure 7. Actual vs predicted values for New Model creep strain rate

5. CONCLUSIONS

Utilizing the modified constitutive model, numerical calculations were executed to simulate the damage development of a thin-hole steel plate. Particular attention was given to discussing the influence of stress and damage evolution. It's noteworthy to acknowledge the challenges associated with creep tests, such as their costliness and

timeconsuming nature, leading to a scarcity of creep data and results for any material. From this research study, the following conclusions were drawn:

(1) The modified constitutive model demonstrated superior capability in describing all three stages of creep compared to the Kachanov-Rabotnov (K-R) and Norton-Bailey models. The investigation focused on the behavior of the SS-304 thin-hole plate.

(2) The fit statistics for the quadratic model of creep strain points indicated a close alignment between anticipated, simulated, and actual values. This underscores the effectiveness of the quadratic model in navigating the design space. Additionally, the substantial influence of the interaction terms of

mixing conditions on the variables and the response was evident, as indicated by their F-values.

(3) A comprehensive statistical analysis and successive geometric optimization were conducted utilizing the response surface modeling approach and the ANOVA technique. The resulting 3D surface plot was scrutinized to understand the combined significant effect of the design factors—stress, the stress exponent, the creep parameter, and the damage evolution parameter—on the relevant target response, which is strain. The impact on the strain response was further analyzed and investigated through the utilization of contour creep deformation maps.

Nomenclature

A　　Norton's power law constant

R　　Universal gas constant

T — Temperature t_r rupture time Q activation energy

Q_c — Norton's activation energy

S_1 — Stress parameter

δ_Ω — Omega parameter

α — Triaxiality parameter

ε0 — Initial creep strain

n — Norton's power law constant

ω — Omega damage parameter

ε_t — Creep strain rate

Ω — Omega material damage constant

σe — Effective stress

Ωm — Omega multiaxial damage parameter

Ωt — Omega material damage constant wrt time

Ωn — Omega uniaxial damage parameter

Δcd — Adjustment factor for creep ductility

εΩ — Accumulated creep strain

A_0 — Stress coefficient

A_Ω — Stress coefficient

Q_Ω — Temperature dependence of Ω

Δcd_n — Creep rupture life

nBN — Norton–Bailey coefficient

Trefa — Reference temperature

β_Ω — Omega parameter to 0.33

FEA — Finite element analysis

FFS — Fitness for service

API — American Petroleum Institute

MPC — Material Properties Council

UTS — Ultimate tensile strength

BPVC — Boiler and pressure vessel codes

ASME — American Society for Mechanical Engineers

ASTM — American Standards for Testing of Materials

UTS — Ultimate tensile strength

SS — Stainless steel

CDM — Continuum damage mechanics

REFERENCES

[1] M. Sattar, A. R. Othman, S. Kamaruddin, M.

[2] Akhtar, and R. Khan, "Limitations on the computational analysis of creep failure models : A review," *Eng. Fail. Anal.*, vol. 134, no. June 2021, p. 105968, 2022, doi: 10.1016/j.engfailanal.2021.105968.

[3] F. . Norton, "The Creep of Steels at High Temperatures," *Mc Graw Hill, New York*, vol. 1, no. 1, p. 90, 1929.

[4] M. Prager, "Development of the MPC Omega Method for Life Assessment in the Creep Range," *J. Press. Vessel Technol. Trans. ASME*, vol. 117, no.

[5] 2, pp. 95–103, 1995, doi: 10.1115/1.2842111 J. T. Yeom, J. Y. Kim, Y. S. Na, and N. K. Park, "Creep Strain and Creep-Life Prediction for Alloy 718 Using the Omega Method," *J. Met. Mater. Int.*, vol. 9, no. 6, pp. 555–560, 2003, doi: 10.1007/BF03027255.

[6] M. Prager, "The Omega Method – An Engineering Approach to Life Assessment," vol. 122, no. August 2000, 2016.

[7] L. M. Kachanov, "Rupture Time under Creep Conditions," *Int. J. Fract.*, vol. 97, no. 1–4, 1999, doi: 10.1023/A:1018671022008.

[8] C. M. Stewart and A. P. Gordon, "Methods to Determine The Critical Damage Criterion of the Kachanov-Rabotnov Law," *ASME Int. Mech. Eng. Congr. Expo. Proc.*, vol. 3, no. PARTS

A, B, AND C, pp. 663–670, 2012, doi: 10.1115/IMECE201288389.

[9] C. M. Stewart and A. P. Gordon, "Strain and Damage-based Analytical Methods to Determine the Kachanov-Rabotnov Tertiary Creep-Damage Constants," *Int. J. Damage Mech.*, vol. 21, no. 8, pp. 1186–1201, 2012, doi: 10.1177/1056789511430519.

[10] Y. Chang and H. Xu, "the Damage Development and Failure Description Under Multiaxial Creep," *Proc. ASME 2014 Press. Vessel. Pip.*, pp. 1–6, 2015.

[11] Z. Abdallah, V. Gray, M. Whittaker, and K. Perkins, "A Critical Analysis of the Conventionally Employed Creep Lifing Methods," *Materials (Basel).*, vol. 7, no. 5, pp. 3371–3398, 2014, doi: 10.3390/ma7053371.

[12] D. L. May, A. P. Gordon, and D. S. Segletes, "The Application of the Norton-Bailey Law for Creep Prediction through Power Law Regression," in *Proceedings of the ASME Turbo Expo*, 2013, vol. 7 A, pp. 1–8, doi: 10.1115/GT2013-96008.

[13] C. M. Stewart and A. P. Gordon, "Analytical Method To Determine the Tertiary Creep Damage Constants of the Kachanov-Rabotnov Constitutive Model," in *ASME, International Mechanical Engineering Congress & Exposition IMECE2010*, 2010, pp. 1–8.

[14] C. M. Stewart, A. P. Gordon, E. A. Hogan, and A. Saxena, "Characterization of the Creep Deformation and Rupture Behavior of DS GTD-111 using the Kachanov-Rabotnov Constitutive Model," *J. Eng. Mater. Technol. Trans. ASME*, vol. 133, no. 2, 2011, doi: 10.1115/1.4003111.

[15] M. Sattar, A. R. Othman, M. F. Othman, H. T. Ali, and M. K. Khan, "New Creep Crack Growth Prediction Model for the Life Assessment of

[16] Stainless-Steel Material Using Computational Modeling," *Metals (Basel).*, vol. 13, no. 11, p. 1854, 2023, doi: 10.3390/met13111854. [15] ABAQUS, "ABAQUS 6.12 User's documentation 3.4.6," vol. IV. 2013.

[17] M. Sattar, A. R. Othman, M. F. Othman, and M. F. Musa, "Regression Analysis of Omega Model to Norton- Bailey Law for Creep Prediction in Fitness for Service Assessment of Steel Material," *Solid State Technol.*, 2020.

[18] M. K. Booker, "Use of Generalized Regression Models for the Analysis of Stress-Rupture Data.," pp. 459–499, 1978.

[19] B. Xiao, L. Xu, L. Zhao, H. Jing, Y. Han, and Y. Zhang, "Creep Properties, Creep Deformation Behavior, and Microstructural Evolution of 9Cr-3W-3Co-1CuVNbB Martensite Ferritic Steel," *Mater. Sci. Eng. A*, vol. 711, no. April 2019, pp.434–447,2018,doi: 10.1016/j.msea.2017.11.061. M. Sattar, A. R. Othman, S. Kamaruddin, M. A. Alam, and M. Azeem, "Creep Parameters

[20] Determination by Omega Model to Norton Bailey Law by Regression Analysis for Austenitic Steel SS-304," *Solid State Phenom.*, vol. 324, pp. 188–197, 2021.

[21] D. L. May, A. P. Gordon, and D. S. Segletes, "The application of the norton-bailey law for creep prediction through power law regression," *Proc. ASME Turbo Expo*, vol. 7 A, pp. 1–8, 2013, doi:10.1115/GT2013-96008.

[22] ASME, *American Petroleum Institute API-579, Fitness for Service, Operation Manual*, 3rd ed., no. FFS-1. Washington

DC, USA: The American Society of Mechanical Engineers, 2016.

[23] A.P. V. ASME Codes, "ASME. (2015). ASME Boiler and Pressure Vessel Code An International Code- section II part A, 1998.," *Oper. Man.*, p. 1998, 2015, doi: http://dx.doi.org/10.1016/B9780323035 06-4.10361-X.

[24] A.A. Al-Bakri, Z. Sajuri, A. K. Ariffin, M. A. Razzaq, and M. S. Fafmin, "Tensile and Fracture Behaviour of very thin 304 Stainless Steel Sheet," *J. Teknol.*, vol. 78, no. 6–9, pp. 45–50, 2016, doi:10.11113/jt.v78.9146.

[25] L. M. Powers, S. M. Arnold, and A. Baranski, "Using ABAQUS Scripting Interface for Materials Evaluation and Life Prediction," *ABAQUS Users' Conf.*, pp. 1–11, 2006.

[26] D. P. Jones, J. L. Gordon, D. N. Hutula, D. Banas, and J. B. Newman, "An elastic-perfectly plastic flow model for finite element analysis of perforated materials," *J. Press. Vessel Technol. Trans. ASME*, vol. 123, no. 3, pp. 265–270, 2001, doi:10.1115/1.1357538.

[27] D. B. Alemayehu, S. J. Huang, and E. G. Koricho, "Experimental and FEM Analysis of three Carbon steel Characterization under Quasi-Static Strain Rate for Bumper Beam Application," *MATEC Web Conf.*, vol. 123, pp. 0–5, 2017, doi: 10.1051/matecconf/201712300019.

[28] A.Czyrski and H. Jarzebski, "Response surface methodology as a useful tool for evaluation of the recovery of the fluoroquinolones from plasma-the study on applicability of box-behnken design, central composite design and doehlert design," *Processes*, vol. 8, no. 4, 2020, doi:10.3390/PR8040473.

[29] M. A. Alam *et al.*, "Modelling and Optimisation of Hardness Behaviour of Sintered Al/SiC Composites using RSM and ANN: A Comparative Study," *J. Mater. Res. Technol.*, vol. 9, no. 6, pp. 14036–14050, 2020, doi: 10.1016/j.jmrt.2020.09.087.

[30] J. Jadoon, A. Shazad, M. Muzamil, M. Akhtar, and M. Sattar, "Finite Element Analysis of Composite Pressure Vessel Using Reduced Models," *Tecciencia*, vol. 17, no. 33, pp. 49–62, 2022, doi:10.18180/tecciencia.2022.33.5.

[31] M. Sattar, A. R. Othman, M. Muzamil, S. Kamaruddin, M. Akhtar, and R. Khan, "Correlation Analysis of Established Creep Failure Models through Computational Modelling for SS-304 Material," *Metals (Basel).*, vol. 13, no. 2, p. 197, 2023, doi: 10.3390/met13020197.

[32] M. Sattar, A. R. Othman, M. Akhtar, S. Kamaruddin, R. Khan, and F. Masood, "Curve Fitting for Damage Evolution through Regression

[33] Analysis for the Kachanov – Rabotnov Model to the Norton – Bailey Creep Law of SS-316 Material," *Materials (Basel).*, vol. 14, no. September, 2021, doi: 10.3390/ma14195518.

[34] J. Christopher, C. Praveen, V. Ganesan, G. P. Reddy, and S. K. Albert, "Influence of Varying Nitrogen on Creep Deformation and Damage Behaviour of Type 316L in the Framework of Continuum Damage Mechanics Approach," *Int. J.*10.1177/1056789520939622.

[35] L.Esposito and N. Bonora, "Time-Independent Formulation for Creep Damage Modeling in Metals based on Void and Crack Evolution," Mater. Sci. Eng. A, vol. 510–511, no. C, pp. 207–

213, 2009, doi:10.1016/j.msea.2008.06.052.

[36] M. Zahid, N. Shafiq, M. H. Isa, and L. Gil,"Statistical modeling and mix design optimization of fly ash based engineered geopolymer composite using response surface methodology," J. Clean. Prod., vol.194, pp. 483–498, 2018, doi: 10.1016/j.jclepro.2018.05.158.

[37] M. Kumari and S. K. Gupta, "Response Surface Methodological (RSM) Approach for Optimizing the Removal of Trihalomethanes (THMs) and its Precursor's by Surfactant Modified Magnetic Nanoadsorbents (sMNP) - An Endeavor to diminish Probable Cancer Risk," Sci. Rep., vol. 9, no. 1, pp. 1–11, 2019, doi: 10.1038/s41598-019-54902-8.

[38] F. Masood, P. Nallagownden, I. Elamvazuthi, J. Akhter, and M. A. Alam, "A new approach for design optimization and parametric analysis of symmetric compound parabolic concentrator for photovoltaic applications," Sustain., vol. 13, no. 9, 2021, doi: 10.3390/su13094606.

[39] A.M. Memon, M. Hartadi Sutanto, M. Napiah, M.

[40] I.Khan, and W. Rafiq, "Modeling and Optimization

EFFECT OF GAS-ASSISTED DIRECT THERMAL METHOD PROCESSING PARAMETERS ON MICROSTRUCTURE FORMATION OF HYPOEUTECTIC AL-SI ALLOY FEEDSTOCK BILLET

M. A. Shakirin [a], A.H. Ahmad [a,b], *, A. Megalingam[a], J. Alias[a], S. Naher[c]
[a] Faculty of Mechanical and Automotive Engineering Technology,
Universiti Malaysia Pahang Al-Sultan Abdullah, 26600 Pekan, Pahang, Malaysia.
[b] Advanced Industrial Technology Research Center,
Universiti Malaysia Pahang Al-Sultan Abdullah, 26600 Pekan, Pahang, Malaysia.
[c] Department of Mechanical Engineering and Aeronautics, City
University of London, London EC1V 0HB, UK.

*asnul@umpsa.edu.my

ABSTRACT

This paper aims to investigate the effect of Gas-Assisted Direct Thermal Method (GA-DTM) processing parameters on hypoeutectic Al-Si alloy feedstock billet microstructure. Several methods have been used to produce globular microstructures, that are suitable for semisolid metal processing (SSMP) in these recent years. Factors that affected microstructure such as pouring temperature, holding time, and magnesium addition were analysed. A combination of parameters, consists of pouring temperatures of 590 and 610 °C, holding time of 10 and 20 s, and magnesium addition of 0.5 and 1.5 wt% were used. The microstructures of the prepared sample were investigated. The results showed that hypoeutectic Al-Si alloy feedstock billets prepared with GA-DTM with 610 °C pouring temperature, 20 s holding time and 1.5 wt.% magnesium addition produced finer microstructure. The grain size, circularity, and aspect ratio, for the formed microstructure were at 45.70 µm, 0.69, and 1.42 respectively. The microstructure with small and uniform primary particles is commonly preferred for SSMP. The study provide insight into the use, performance, and applicability of hypoeutectic Al-Si alloy feedstock billets in semi-solid processing applications such as thixoforming.

Keywords: Grain refinement, Hypoeutectic Al-Si Alloy, Magnesium Addition, Gas-Assisted Direct Thermal Method, Feedstock Billet, Microstructure.

1. INTRODUCTION

The process technology and composition of the materials are highly related to the microstructure that leads to the quality of a material [1]. Traditional casting techniques for aluminium silicon cast alloys develop a primary phase with a coarser microstructure and form larger grains with a high degree of segregation and plenty of casting defects. Grain refining is a well-known process that is used on the majority of Al-cast alloys. It has a considerable influence on the mechanical characteristics of the material [2]. The mechanical properties are improved by grain size, homogenous nucleation distribution of the second phase, reduction in microporosity, shrinkage defects, feedstock parameters control, and solidification time. Smaller grains often translate to increased strength, hardness, and wear resistance, while simultaneously improving ductility and toughness. There are various processes for

refining aluminium grain. Grain refinement by vibration and stirring during solidification, rapid solidification, grain refiner addition, and extreme plastic deformation [3].

Semi solid metal process (SSMP) has recently been applied in the industry because it produced globular with refined microstructure, a crucial element for SSMP for its use in engine blocks and aerospace parts. The final SSMP product also has minor defects such as porosity, shrinkage, gas entrapment, and macro segregation [4]. In addition, the SSMP technique develops aluminium alloys to a semisolid state and improves the characteristics of aluminium alloys. The SSMP of die casting seems to meet several objectives since it may offer the industry a means of creating mass-production, high-performance, and complex components close to their net shape while simultaneously reducing energy consumption and waste [5]. The success of the SSMP is merely dependent on the globular and refined microstructure feedstock for thixoforming. In the literature, many efforts have been made to explore the ability to produce more globular and finer microstructure.

Various methods have been tried to prepare the material with improved globular microstructure for SSMP. One method is the Gas-Assisted Direct Thermal Method (GA-DTM), which modifies the thermal characteristics of the liquid alloy to delay the material's solidification [6]. The microstructure's shape has been enhanced using GA-DTM, resulting in a more globular and refined microstructure. It is also known that adding magnesium to Al-Si-Cu alloys through a process known as grain refining enhanced the alloys' mechanical properties by causing a stronger Mg_2Si phase to form [7]. A study by Azhani Abd Razak et al.

found that the generation of finer primary grains with a spheroidal shape was improved by 36.4% when DTM was combined with external colling gas [6]. Furthermore, several studies on the microstructure and hardness evolution of aluminium alloy 6061 indicated that the casting temperature and holding time had a greater influence on structure formation [8], while another study specifically reported that a combination of low casting temperature and long holding time produced a global microstructure [9].

Hypoeutectic Al-Si alloys, a subset of aluminium-silicon alloys, possess distinctive characteristics that make them valuable in a variety of industrial applications [10]. These alloys are characterized by having a silicon content below the eutectic composition of approximately 12.6% silicon by weight. Some key features of hypoeutectic Al-Si alloys include their excellent fluidity, which makes them well-suited for intricate casting, and good castability, enabling them to be easily shaped into a wide range of components through various casting methods [11]. However, their mechanical strength is incredible. As magnesium can improve mechanical properties and performance, its addition to aluminium-silicon alloys has attracted attention [1].

Increasing the addition of magnesium has a positive impact on alloy strength. Under conventional casting conditions, it results in the formation of a coarse Mg_2Si alloy, which, unfortunately, leads to alloys with limited ductility and poor fracture toughness [12]. Therefore, the coarse Mg_2Si phase offers good mechanical strength but requires modification to maintain ductility. Augmenting the magnesium content contributes to the enhancement of the microstructure in Al-Si alloys [13]. To address this issue, SSMP is utilized to create Al-Si alloys with a finer microstructure and decreased segregation [14]. In their study, Cory et al. investigated the effect of

197

magnesium content ranging from 0.3 wt.% to 0.7 wt.% on the mechanical properties of A 356 alloys [15]. The results of Yamamoto et al reported that the addition of magnesium from 0.3 % to 1.5 wt% improved the mechanical properties due to the change in microstructure morphology and high strength matrix [16].

The formation of the fine microstructure of hypoeutectic Al-Si alloy feedstock billets plays an important role in producing high-performance aluminium components in various industries[10]. To enhance the mechanical properties and structural integrity of these components, the GA-DTM is often employed. Although high-silicon hypoeutectic Al-Si alloys are recommended for producing high-quality products in the semi-solid state, mechanical strength is a concern [17]. The addition of magnesium to aluminium-silicon alloys improves the mechanical properties and performance but is not integrated with the GA-DTM method. Furthermore, specific parameters of this GA-DTM method, such as pouring temperature, holding time, magnesium addition, etc., have not been studied in detail regarding their effect on the grain refining process [6]. Therefore, this study aims to investigate the effect of processing parameters and their effects on hypoeutectic Al-Si alloy feedstock billet produced by GA-DTM.

2. MATERIALS AND METHODS

2.1 Materials and Processing Parameters

The chemical composition of the hypoeutectic Al-Si alloy was detected using a foundry master oxford instruments and optical emission spectrometer and the obtained values are shown in Table 8.

Composition (wt%)										
Al	Si	Fe	Cu	Zn	Mn	Mg	Cr	Ni	Ti	Sn
81.7	9.74	0.68	1.15	1.47	0.31	0.24	0.11	0.53	0.09	0.35

Table 8 Chemical composition of raw material hypoeutectic Al-Si alloy.

The processing parameters that were selected to be used for this study are listed in Table 9 below.

Sampe Number	Temperature (°C)	Time (s)	Addition of Magnesium (wt.%)
1	590	10	0.5
2	590	20	1.5
3	610	10	0.5
4	610	20	1.5

Table 9 Experimental Parameters

Feedstock billets were produced using the GA-DTM process at different pouring temperatures, holding times, and magnesium addition levels. For this study, pouring temperatures of 590 to 630 °C, holding times of 10 to 20, and magnesium additions of 0.5 to 1.5 weight percent were determined.

2.2 Sample Preparation

In the GA-DTM method, a five-coil copper coil was used for this experiment [6]. There is a certain gap between each coil. Around each coil is a hole to vent the compressed air. A K-type thermocouple and data logger were used to measure the melt temperature to calculate the pouring temperature. After the molten material in the crucible reached the pouring temperature, it was poured into the copper mould. The material in the copper mould is then placed in compressed air through the copper coil for a holding time determined in this test. The copper mould direct air through the copper coil helps in rapid cooling and prevents chemical reactions caused by outside air. At the desired holding time the copper mould was dropped

into a water-filled quench tank. Then the billet was extracted from the mould.

3. RESULTS AND DISCUSSIONS
3.1 Microstructure Evolution from GA-DTM Billet

The microstructure of hypoeutectic Al-Si alloy GA-DTM feedstock billet was determined by using Image J software. The different combinations of parameters which were pouring temperature, holding time, and the additional amount of magnesium to the raw material, led to the effect on the microstructure.

A hypoeutectic Al-Si alloy with a pouring temperature of 590 °C, a holding time of 10 s, and 0.5 wt% magnesium addition had a maximum grain size of 50.12 µm (Sample 1). Similarly, a hypoeutectic Al-Si alloy with a pouring temperature of 610 °C, a holding time of 20 s, and 1.5 wt% magnesium addition had a minimum grain size of 45.70 µm. Sample 3 was prepared at 590 °C pouring temperature, 20 s holding time and 1.5 wt% magnesium addition, which had a grain size of 49.39 µm. Generally, as the holding times increase, the primary particles in the liquid phase coalesce and the grain size increases. This study shows that the addition of magnesium modifies the primary size of the α-Al phase[18]. Other than that, microstructure modification might occur due to the formation of Mg_2Si. According to Kori et al., the morphology of the silicon phase of hypoeutectic Al-Si alloy change is related to a decrease in eutectic temperature and an increase in undercooling, indicating that high concentrations of Mg influence the silicon phase of hypoeutectic Al-Si alloy significantly. These alterations indicate the formation of Mg_2Si has occurred [15]. The mean diameter grain size of microstructure investigated sample number 1 to 4 are presented in Figure.
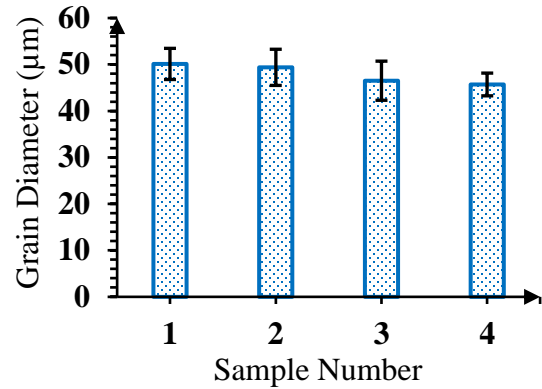
Figure 1. Average diameter grain diameter for sample number 1 to 4.

The grain sizes obtained in each of the 4 samples ranged from 45 µm to 50 µm. Magnesium addition was found to have the greatest effect on grain size. The grain size values showed more than 50µm when the amount of magnesium was set at 0.5 wt.%. On the other hand, when the amount of magnesium was fixed at 1.5 wt.%, the grain size value was between 40 µm and 45 µm. According to the results of the previous study, the grain size decreases when the magnesium value increases [19]. During solidification magnesium acts as a nucleating agent for the grain structure, promoting the formation of finer grains. This leads to a highly refined microstructure with smaller grain sizes. Magnesium atoms provide nucleation sites for the formation of new grains. When magnesium is added to the melt, it forms insoluble particles that act as sites for the initiation of grain growth. This results in a greater number of smaller grains distributed throughout the material. The circularity values obtained from the microstructure investigation of billets prepared by GA-DTM are presented in Figure.
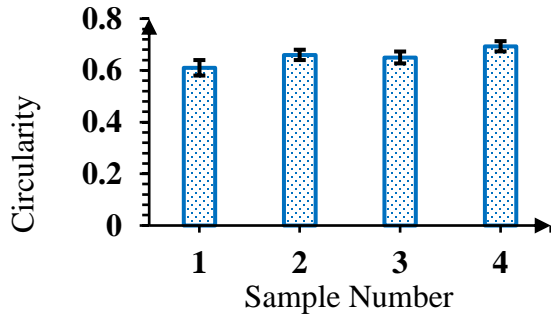
199

Figure 2. Average circularity for sample number 1 to 4.

Each of the 4 samples had a circularity ranging from 0.61 to 0.69. The magnesium addition has a most significant influence on circularity. The circularity value increases as the holding time increases [16],[20]. Circularity, measured on a scale from 0.0 to 1.0, is the degree to which the shape of the microstructure resembles an ideal circle [21]. Sample 4 had the highest circularity value (0.69). A greater magnesium value causes the circularity to increase at any given magnesium addition rate. A value close to 1.0 means that the shape is considered perfectly spherical. Nevertheless, particles become more elongated as the value approaches zero. While pouring temperature and holding time can influence the cooling rate and subsequent microstructure, their effect on grain size may be overshadowed by magnesium's strong grain refining effect. In some cases, changes in pouring temperature and holding time may have a secondary or complementary impact on grain size, but the primary influence appears to be from magnesium addition. The aspect ratio obtained from microstructure investigation of billets prepared by GA-DTM is presented in Figure.
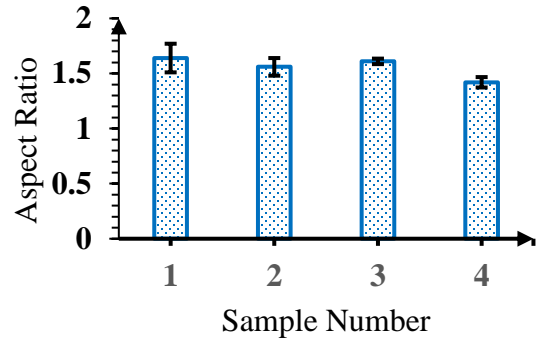
Figure 3. Average aspect ratio for sample number 1 to 4.

The aspect ratio obtained by each of the 4 samples ranged between 1.42 and 1.64. The addition of magnesium contributed to the effect on the aspect ratio. Circularity increases as the magnesium addition increases. The aspect ratio represents the ratio of the main axis to the minor axis. The higher the aspect ratio size, the longer the particle. It was discovered that the addition of Mg resulted in a reduction in the particle size of the sample. Among the hypoeutectic Al-Si alloy feedstock billets prepared by the GA-DTM method, the sample prepared at 610 °C pouring temperature, 20 s holding time, and 1.5 weight percent magnesium addition had a small and spherical microstructure. The grain size, circularity, and aspect ratio are 45.70µm, 0.69, and 1.42, respectively. This is consistent with the recommended dosages for globular microstructure [21],[22].

4. CONCLUSIONS

The contribution of processing parameters in the preparation of hypoeutectic Al-Si alloy feedstock billet by the GA-DTM method was successfully investigated. The study results provided insight into the effect of grain refinement and processing parameters on the microstructure of the alloys, which allowed us to know pouring temperature, time, and magnesium addition and their combined effects on grain refinement. At 610 °C

200

pouring temperature, 20 s holding time and 1.5 wt.% magnesium added billet sample had very small and uniform primary grains. At these combination parameters, the grain size, circularity, and aspect ratio are 45.70μm, 0.69, and 1.42, respectively. These study findings will help to improve the mechanical strength, applicability, and microstructure of materials produced by semi-solid processing.

ACKNOWLEDGEMENT

REFERENCES

[1] D. Watson, "Microstructure and Mechanical Properties of Ductile Die-cast Al-Mg-Si-Mn Alloys.," no. October, p. 2015.

[2] J. Wannasin, R.A. Martinez, and M.C. Flemings, "Grain refinement of an aluminum alloy by introducing gas bubbles during solidification.," Scripta Materialia. vol. 55, no. 2, pp. 115–118, 2006.

[3] M. He, Z. Zhang, W. Mao, B. Li, Y. Bai, and J. Xu, "Numerical and experimental study on melt treatment for large-volume 7075 alloy by a modified annular electromagnetic stirring.," Materials. vol. 12, no. 5, p. 2019.

[4] M. Modigell, A. Pola, and M. Tocci, "Rheological characterization of semi-solid metals: A review.," Metals. vol. 8, no. 4, pp. 1–23, 2018.

[5] P. Kapranos, "Current state of semi-solid net-shape die casting.," Metals. vol. 9, no. 12, pp. 1–13, 2019.

[6] N.A. Abd Razak, A.H. Ahmad, M.M. Rashidi, and S. Naher, "An investigation of semisolid Al7075 feedstock billet produced by a gas-assisted direct thermal method.," International Journal of Advanced Manufacturing Technology. vol. 114, no. 3–4, pp. 1233–1240, 2021.

[7] Al-Si Cast Alloys - Microstructure and Mechanical Properties at Ambient and Elevated Temperature Al-Si Cast Alloys - Microstructure and Mechanical Properties at Ambient and Elevated Temperature., 2015.

[8] B. Benjunior, A.H. Ahmad, and M.M. Rashidi, "Direct thermal method pouring temperature and holding time effect on aluminium alloy 6061 microstructure.," IOP Conference Series: Materials Science and Engineering. vol. 788, no. 1, p. 2020.

[9] N.A. Razak, A.H. Ahmad, and M.M. Rashidi, "Investigation of pouring temperature and holding time for semisolid metal feedstock production.," IOP Conference Series: Materials Science and Engineering. vol. 257, no. 1, p. 2017.

[10] J. Xu, Y. Li, K. Ma, et al., "In-situ observation of grain refinement dynamics of hypoeutectic Al-Si alloy inoculated by Al-Ti-Nb-B alloy Scripta Materialia In-situ observation of grain refinement dynamics of hypoeutectic Al-Si alloy inoculated by Al-Ti-Nb-B alloy.," no. June, p. 2020.

[11] M.S. Prabhudev and C.T. Mata, "Studies on the microstructure and mechanical properties of a356 alloy with minor additions of copper and magnesium.," no. August 2009, pp. 1–5, 2015.

[12] M.F.M. Tajudin, A.H. Ahmad, and M.M. Rashidi, "Effects of different processing parameters on the semisolid microstructure of Al6061 produced by a direct thermal method.," IOP

Conference Series: Materials Science and Engineering. vol. 1092, no. 1, p. 012008, 2021.

[13] K. Shakya, P. Krishana, and B. Patel, "Study of Hardness and Wear Analysis in AL-SI Alloy (AL-5 % SI , AL-11 % SI and AL-17 % SI) Along With Microstructural Analysis.," vol. 6, no. 6, pp. 3296–3302, 2020.

[14] A.H. Ahmad, S. Naher, S.N. Aqida, and D. Brabazon, Routes to Spheroidal Starting Material for Semisolid Metal Processing. Elsevier, 2014.

[15] S.A. Kori, M.S. Prabhudev, and T.M. Chandrashekharaiah, "Transactions of The Indian Institute of Metals Studies on the microstructure and mechanical properties of A356 alloy with minor additions of copper and magnesium.," vol. 62, no. October, pp. 353–356, 2009.

[16] K. Yamamoto, M. Takahashi, Y. Kamikubo, et al., "Effect of Mg content on age-hardening response, tensile properties, and microstructures of a T5-treated thixo-cast hypoeutectic Al–Si alloy.," Materials Science and Engineering A. vol. 798, no. May, p. 2020.

[17] M. Law, C.N. Hulme-Smith, T. Matsushita, and P.G. Jönsson, "Assessment of mechanisms for particle migration in semi-solid high pressure die cast aluminium-silicon alloys.," Journal of Manufacturing and Materials Processing. vol. 4, no. 2, p. 2020.

[18] P. Taylor, H. Saghafian, S.G. Shabestari, M.H. Ghoncheh, and F. Sahihi, "Wear Behavior of Thixoformed Al-25 wt % Mg 2 Si Composites Produced by Slope Casting Method Wear Behavior of Thixoformed Al-25 wt % Mg 2 Si.," no. January, pp. 37–41, 2015.

[19] Q. Li, B. Li, J. Li, T. Xia, Y. Lan, and T. Guo, "EFFECTS OF THE ADDITION OF Mg ON THE MICROSTRUCTURE AND MECHANICAL PROPERTIES OF HYPOEUTECTIC Al – 7 % Si ALLOY.," International Journal of Metalcasting. p. 2017.

[20] S.A.- Mg, "Rheology of Semisolid AI-4.5°/0Cu - 1.5%Mg Alloy.," Rheology. vol. 131, pp. 265–272, 1991.

[21] A. Megalingam, A.H. Ahmad, N.A. Alang, J. Alias, and N.A.A. Razak, "Application of Response Surface Methodology for Parameter Optimization of Aluminum 7075 Thixoforming Feedstock Billet Production.," Journal of Materials Engineering and Performance. no. Ref 11, p. 2022.

[22] D.J. Browne, M.J. Hussey, A.J. Carr, and D. Brabazon, "Direct thermal method: New process for development of globular alloy microstructure.," International Journal of Cast Metals Research. vol. 16, no. 4, pp. 418–426, 2003.

APPLICATION OF ABRASIVE SURFACE IN TUBES TO ENHANCE FLOW METER EFFICIENCY

Quresha Saghir[1,], Anzar Ahmed[1,] and Syed Waqar Hasan[1*]

[1] Laboratory of Energy and Devices (LEAD), Department of Naval Architecture Engineering,
Pakistan Navy Engineering College (PNEC), National University of Sciences and Technology (NUST), Karachi, Pakistan

[*]*Corresponding author E-mail address*: waqar.hasan@pnec.nust.edu.pk (Syed Waqar Hasan)

ABSTRACT

Industries provide various fluid products (e.g. petroleum fuels, chemicals agents and mineral water) to the market which have deep impact on the economy of the country. Normally, bulk amount of fluids are loaded on customer containers from the refinery storage tanks through pumps. A flow meter is used to measure the quantity of the fluid filled in the container against which the customer shall make the payment. Thus, the efficiency of the flow meter is of paramount importance. It has been observed that air bubbles are formed in the fluid flow while it is transferred through a pump. Those air bubbles significantly reduce the flow meter efficiency causing serious financial burden on the customers. In this research work, a novel technique is presented to ensure no air bubbles in the working fluid enhancing the flow meter efficiency. It was observed that centrifugal pump designed for providing flow rate of 10 lit/min was only providing 4.9 lit/min because of very high air bubble density. We applied a line coating of abrasive paper in the tube transporting the fluid. It was realized that the abrasive paper completely eliminated the bubble formation within the tube increasing the flow rate to 9.8 lit/min which is 98% closer to the design value of the pump. This technique can help the industries/customers to measure the transported fluid correctly and improve industrial economy.

Keywords: flow meter efficiency; turbulent flow; bubble formation; abrasive papr

1. INTRODUCTION

In industries, pipes/tubes are used on large-scale as they play a crucial role in different applications. They are used in heat exchangers, boilers, and storage tanks. Pipes are essential elements in industries, whether it is mechanical, chemical, textile, automotive, marine or even biomedical industry; they use pipes/tubes for transporting various fluids from one to another point [1-3]. More importantly, a large part of maintenance cost in industries is spent on pipelines [4, 5, 6].

Since, the fluid being transported through pipes/tubes are corrosive or at very high velocities can damage the material of the pipe/tube. Therefore, maintenance of pipes in industries is important to avoid pipe defects such as erosion, pitting and corrosion etc. One of the major problem within pipes is air bubble formation which can affect the performance and lifespan of pipes. The force produced due to bursting of bubbles can physically damage the pipe by producing tiny pits (known as cause erosion) [4]. These pits are considered as a serious pipe defect

204

because they reduce the mechanical strength and stability of pipes. Hence, it is necessary to eliminate bubbles or to minimize the bubble formation within pipes.

Additionally, the air bubbles in the liquid flow also disturb the flow meter efficiency. Accurate flow measurements are important in different industrial applications [10], and the existence of bubbles within a fluid can adversely effect the efficiency of flow meters. Flow meters are the instruments which indicate the amount of fluids (liquid, gas or vapours) moving through a conduit by measuring the volumetric flow rates. However, flow meters cannot distinguish air bubbles in the flow. Therefore, if air bubbles are present in the conduits, the flow meter accounts them to be single phase system and mentions inaccurate measurement [11].

Air bubbles also impose adverse effects on various devices (e.g. electrochemical cells). To remove air bubbles from electrochemical cells, industries use breathable electrode strategy. In this strategy capillary forces are used to guide bubbles out of electrode. Breathable electrodes aim to facilitate the efficient removal of gas bubbles from the electrode surface, allowing for continuous and uninterrupted electrochemical reactions [12]. Particularly in fluid flow systems, bubbles are primarily eliminated from pipelines by installing air valves (e.g. large orifice air valves, kinetic air valves and small orifice air valves) [13]. However, these orifice valves incorporate pressure drops and energy loss within the pipe flows.
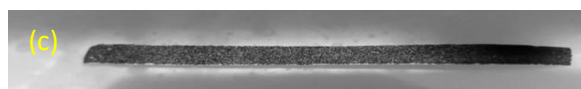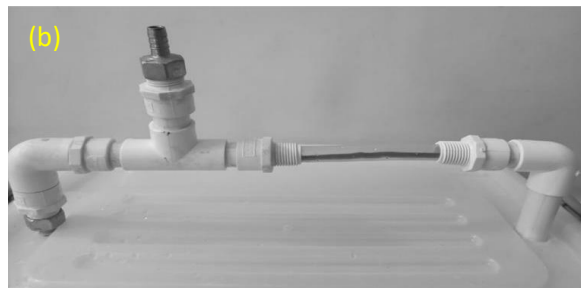
Figure 1. Experimental workstation. (a) Experimental setup with bare tube (b) experimental setup with tube containing abrasive paper (c) photograph of abrasive paper.

We have mitigated the presence of air bubbles by embedding a lining of abrasive paper along the length of the tube/conduit. We show that by implementing this single-step, facile and cost-effective method air bubbles are completely eliminated even in highly turbulent flow conditions. As the result of bubble elimination, the flow meter efficiency was notably increased. Therefore, this method has two advantages of (a) providing higher flow meter efficiency and (b) protecting the tubes/conduits from bubbles and their rupturing forces (which can ultimately damage the tube physically). Collectively, we are presenting a new technique which may avoid corrosion/erosion and expectedly reduce maintenance costs in the industry.

2. EXPERIMENTAL DETAILS

2.1 Theory and Equations

Basic concept of Reynolds Number

Reynolds number is a dimensionless quantity that is used to determine the type of flow pattern as laminar or turbulent while flowing

through a pipe. It is also defined as the ratio between inertial forces and viscous forces.

Formulae

$$\text{Re} = \frac{\rho VD}{\mu} = \frac{VD}{v} \quad \dots (1)$$

Where,

- Re is the Reynolds number
- ρ (kg/m^3) is the fluid density,
- V (m/s) is the fluid velocity,
- D (m) is characteristic length
- μ (Pa.s) is the dynamic viscosity of the fluid.
- v (m^2/s) is the kinematic viscosity of fluid

Interpreting the Reynolds number

If the Reynolds number is less than 2100 (Re<2100) the flow is referred to be laminar, characterized by smooth fluid motion (streamline flow). [9]

If the Reynolds number is greater than 4000 (Re>4000) the flow is turbulent, characterized by irregular fluid motion. Moreover, in turbulent flow random mixing of fluid particles occurs. [9]

If Reynolds number is greater than 2100 and less than 4000 (2100<Re<4000) the flow is referred to be in transitional regime (between laminar and turbulent flows).

Entrance length

The distance a fluid travels after entering a pipe before it acquires fully developed velocity profile is referred to as entrance length and calculated as follows:

For Laminar:

$$\frac{l_e}{d} = 0.06\text{Re} \quad \dots (2a)$$

For Turbulent:

$$\frac{l_e}{d} = 4.4\text{Re}^{\frac{1}{6}} \quad \dots (2b)$$

Flow Rate

Flow rate can be defined as the amount of fluid (liquid or gas) that is flowing through a cross-section of a pipe per unit time. It can be calculated by the following expression:

$$Q = VA \quad \dots (3)$$

where

- Q (m^3/s) is the flow rate
- A (m^2) is the Area,
- V (m/s) is the fluid velocity

In our experiments, we focused on enhancing the efficiency of flow meters by finding the solution to remove bubbles within a pipeline/tube. The experimental setup involved controlling fluid velocity to bring changes in the Reynolds number. We used three different flow rates to observe the influence of Reynolds number variations on bubble density within the pipeline.

At the highest flow rate, corresponding to a Reynolds number of 8586, the flow regime was turbulent, resulting in a highest bubble density within the fluid. After reducing the flow rate, we get Reynolds number of 4466 which resulted in transitional flow. Due to which the bubble density decreased. By further reducing the flow rate we calculated Reynolds number to be 3678. It was realized that there were no bubbles observed in bare tube in this transitional regime.

206

To eliminate the air bubbles in turbulent flow regimes and enhance flow meter performance, a new method was introduced: line coating of abrasive paper was embedded along the length of the tube, resulting in complete termination of bubble formation. In order to further extend our understanding of fluid interaction with the abrasive paper, we also placed the abrasive paper (not in complete length) in half and one-third of tubes length. The details of the experiments and their explanation are mentioned in details in proceeding sections. [8]
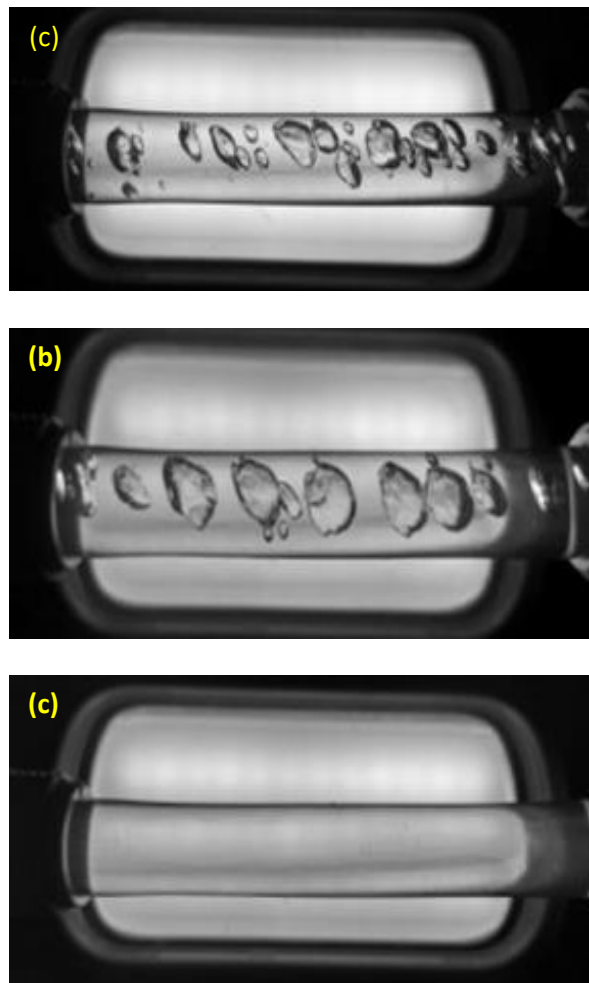
Figure 2. Bubble visualization in bare tubes. (a) Highest flow rate (5 lit/min) (b) Moderate flow rate (2.6 lit/min) (c) Lowest flow rate (2.16 lit/min).

2.2 Experimental Setup

The experimental setup constitutes of a DC motor, venturi nozzle, centrifugal pump (10 lit/min), flow regulator, transparent circular pipe (0.5in), AC-DC converter and a digital camera. The experimental setup is demonstrated in (**Figure 1**). The centrifugal pump, placed inside the storage tank filled with water, circulates the water in the system. Water flows through the transparent plastic pipe and the flow characteristics are visualized and recorded through the camera. Usually the pump provides a fixed flow rate, which in our case was 10 lit/min. Using equation (1), (2) and (3) corresponding fluid velocity and Reynolds number was calculated. For the flow rate of 10 lit/min, the velocity and Reynolds number were (2.16 ft/s) and 8582; demonstrating extremely turbulent flow. In order to investigate the flow characteristics in broader (transitional – turbulent) regimes, a flow regulator was installed along with the pump to reduce the flow rate from 10 lit/min to 2.6 lit/min with corresponding Reynold number of 4466. Further details of the fluid flow are mentioned in Tables 1 – 3. We proposed a design modification in the system by embedding an abrasive coating (i.e. sand paper) on the internal surface of the transparent pipe. We were interested to investigate the fluid flow characteristics under the increased friction/roughness offered by the abrasive coating. The transparent pipe containing the abrasive coating is shown in **Figure 1b**. The abrasive coating used in the experiments is shown in **Figure 1c**. At the starting point, we began our experimental investigation with a commercially available sand paper purchased from local market. Therefore, the roughness and thickness of the abrasive paper was unchanged. Regarding the selection of width of the abrasive paper; the main concern was to be able to monitor the air bubbles and capture the images/videos of the fluid flow

207

from outside. Therefore, we could not cover a larger circumference of the tube with abrasive paper. Hence for the diameter of 0.5 in (circumference=1.57 in), we placed abrasive paper of width 0.3 in.

Description	Length (in)	Dia (in)	Width (in)
Pipe (Overall)	14	0.5	-
Venturi Nozzle	6.3	0.5	-
Abrasive paper	5	-	0.3
Transparent tube	5	0.5	-

Table 1. Details of experimental setup

DC Motor	10 lit/min	2.3 amp
DC Regulator	-	10 amp

Table 2. Electronic Components

3. RESULTS

In this research, we designed an experimental setup to investigate the fluid characteristics on different flow rates by changing its flow rate Reynolds number. Three different flow rates were selected for the experimentation: (a) highest flow rate (10 lit/min), having turbulent flow with Reynolds number of 8586, (b) moderate flow rate (2.6 lit/min) with Reynolds number of 4466 and (c) lowest flow rate (2.14 lit/min) with Reynolds number of 3678.

3.1 Fluid behavior in bare tube

It was observed that the highest flow rate resulted in turbulent flow producing tremendous amount of air bubbles in the flow as shown in **Figure 2a**. In fact the highest bubble density was visualized in this flow regime. Once the flow rate was reduced to 2.6

lit/min, a gradual decrease in bubble density was observed as exhibited in **Figure 2b**, however, bubbles are still very prominent and consistent. Once the lowest flow rate was examined; complete elimination of the bubbles was observed **(Figure 2c)**. Although the Reynolds Number is still considerably high (i.e. 3678) which is in the transitional limits to turbulent flow but no bubbles were visualized.

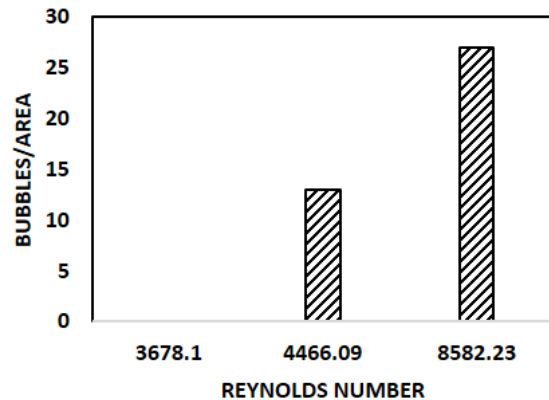| S.no	Flow rate (lit/min)	Reynolds number	Observations
1	5	8582	High bubble density
2	2.6	4466	Low bubble density
3	2.14	3678	No bubbles

Table 3. Details of Bubble formation in tube

Figure 3. Bubble Density in tube against Reynolds number

3.2 Fluid behavior in tube provided abrasive surface

It is mentioned in the experimental section that the primary interest of this research is to investigate the changes in the fluid flow characteristics due to the increased friction/roughness incorporated through an abrasive coating. An abrasive coating was introduced into the transparent tube (**Figure 1 b& c**), creating a region where the fluid had

208

to flow over the abrasive surface. In order to compare the effect of abrasive coating, the fluid was flown over the abrasive coating at the three flow rates previously studied. We previously mentioned extremely high generation of bubbles at highest flow rate for bare tube (**Figure 2a**). A dramatic elimination of bubbles was noted once the abrasive paper was placed in the tube as shown in **Figure 4a**. It has to be noted that the fluid velocity, flow rate and Reynolds number were unchanged/highest, nevertheless, there are no bubbles observed. Even for the lower and moderate flow rates; the bubbles were not observed in the presence of abrasive paper.

In order to further extend our understanding about the role of abrasive paper on fluid flow [8], we reduced the length of the abrasive paper. Previously, the whole length of the plastic tube (i.e. 5 in) was provided the abrasive paper. Now we reduced half of the length of abrasive paper (i.e. 2.5 in). In other words, half of the pipe length is bare (i.e. uncovered) and the remaining half of the pipe length is covered by abrasive paper as shown in **Figure 4c**. We kept the velocity, flow rate and Reynolds Number to be maximum. The results are shown in **Figure 4c**. It can be noted that reduced length of the abrasive paper allowed some bubble formation in the tube, although the bubbles observed in this case are notably less than the bare tube case (**Figure 2a**) but higher than **Figure 4a** (when complete tube length was covered by the abrasive paper). Therefore, applying abrasive coating to only half of the tube in our experiments led to a continued generation of bubbles, with a noticeable reduction in size (**Figure 4c**). Subsequently, expanding the coverage of the abrasive paper to two-thirds of the tube length reduced the bubble formation and there was further decrement in size and a significant reduction in quantity of bubbles (see **Figure 4b**). These observations

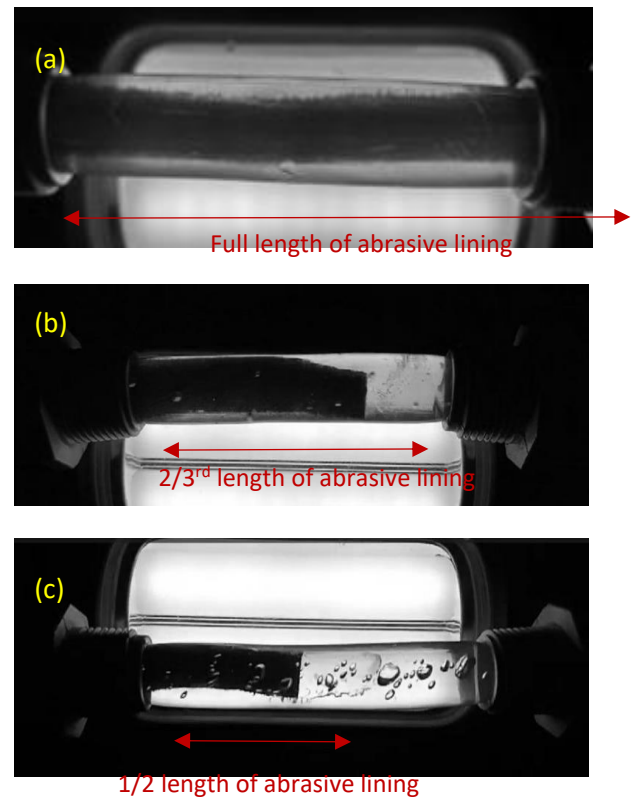underscore the influence of abrasive paper coverage on the dynamics of bubble formation.

Figure 4. Bubble visualization in tubes embedded with abrasive lining. (a) Full length of tube provided abrasive paper. An abrasive paper can be seen placed along the length of the tube. It can be noted that there are literally no air bubbles at maximum flow rate (10 lit/min). (b) 2/3rd length of tube provided abrasive paper. (c) 1/2 length of tube provided abrasive paper. Abrasive paper can be seen placed along the half length of the tube. (a,b) It can be noted that sizes of bubbles are getting smaller at maximum flow rate (10 lit/min).

4. DISCUSSION

Bubble Density Vs Reynolds number

During the investigation of changing Reynolds numbers on bubble formation, it was found that bubble density (the number of bubbles per unit area) showed a direct relation. With increasing Reynolds numbers; the bubble density increases in bare tubes. At the highest flow rate, the Reynolds number was (8582), indicating a turbulent flow with highest bubble density (**Figure 3**). After slowing down flow rate Reynolds number dropped to 4466, showing turbulent flow. At this flow rate bubble density decreased. The slowest flow rate had a Reynolds number of (3678), indicating transitional flow and no bubbles were observed (**Figure 3**).

Formation of bubbles

In the venturi effect produced in the experimental setup, the bubbles can form due to decrease in pressure in a constricted area of the fluid flow. As the velocity increases through the narrow portion of the Venturi tube, the pressure decreases according to Bernoulli's principle. If the pressure drop is low enough; it can cause dissolved gases in the fluid to come out of solution, forming bubbles. These bubbles then become visible as they move downstream in the flow. The schematic illustration is provided in **Figure 5a**.

After placing abrasive paper

If the length of the tube is fully covered by the abrasive paper, there were literally no bubbles observed at highest flow rate. If the $2/3^{rd}$ tube length was covered by abrasive paper, extremely small and few bubbles were visualized. If $1/2^{nd}$ tube length was provided the abrasive coating, the bubble density and sizes further grew.

Removal of bubbles

The placement of abrasive paper in the tube creates enormous amount of shear stresses due to extremely high surface roughness of abrasive paper in the fluid. The schematic illustration is provided in **Figure 5b**. This high shear stress is expected to be the main reason of bubble elimination from the system (**Figure 5b**). At the bottom of **Figure 5b** an abrasive paper is shown which is shown to offer higher shear stresses than the bare tube surfaces (as in **Figure 5a**).
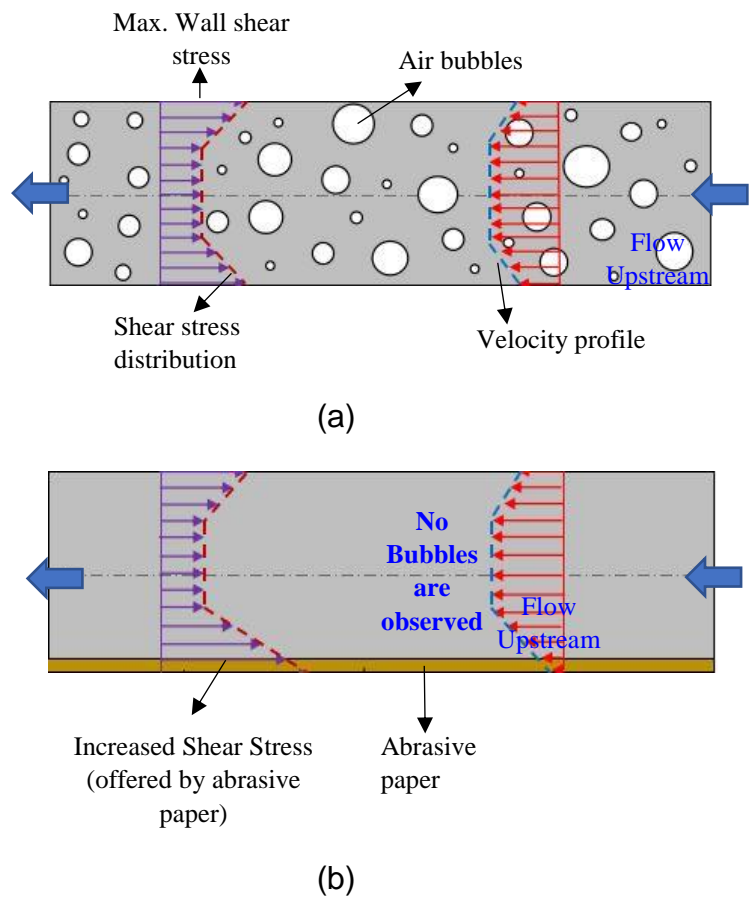

(a)

(b)

Figure 5. Schematic illustration (a) Shear stress distribution and velocity profile before introducing abrasive lining. (b) Schematic illustration of shear stress distribution and Velocity profile before after introducing abrasive lining

210

5. CONCLUSION

In this experimental investigation, we have visualized air bubble formation in a tube with transitional-turbulent flow conditions. It was realized that maximum bubble density appears in an extremely turbulent flow (with Re 8582). However, by reducing the flow rate Reynolds number and corresponding bubbles in the flow were reduced. Herein, a new concept is introduced to minimize the air bubbles in extremely turbulent flow regime. It was demonstrated that by placing an abrasive paper along the length of the tube, the bubble density can be controlled even in turbulent regime. We tested the placement of abrasive coating on (a) half of the tube length and (b) two-third of tube length and (c) entire tube length. In the cases where abrasive lining was partial (case (a) and (b)); the bubble density was gradually decreased. Notably, when the entire tube length was covered with abrasive lining; a complete elimination of bubbles was noted. It is expected that the additional frictional force incorporated by the abrasive paper, in the opposite direction of the fluid flow, does not allow the bubble formation. This technique can be beneficial for efficient flow measurements in industrial applications.

REFERENCES

[1] Xinhong Li, Yazhou liu, Gouming Chen and Rouzbeh Abbassi Dynamic risk-based methodology for economic life assessment of aging subsea pipelines,*Ocean Engineering.* 294(1), 116687, 2024.

[2] Millerjothi Kalamegam, Redae Haimanot, Udayakumar and Parthiban Kandan,Experimental Investigation of the Effect of Fluid-Solid Mixture Flow by Pneumatic System in Textile Industry,*Journal of Scientific &* *Industrial Research.* 80(1),310-314, 2021.

[3] Chinedu I. Ossai, Pipeline failures in corrosive environments – A conceptual analysis of trends and effects,*Engineering Failure Analysis.* 53(1), 36-58., 2015.

[4] Jie Sun, Xinfeng Ge and Demin Liu, Research on Synergistic erosion by cavitation and sedimen, 95(1), 106399 ,2023

[5] Hassan Iqbal, Solomon Tesfamariam, Husnain Haider & Rehan Sadiq, Inspection and maintenance of oil & gas pipelines: a review of policies, Structure and Infrastructure Engineering Maintenance, *Management, Life-Cycle Design and Performance*, 6(1), 794-815, 2015

[6] AkinyemI O. O.*, Nwaokocha C. N., Adesanya A. O.,Evaluation of corrosion cost of crude oil processing industry,*Journal of Engineering Science and Technology.* 7(4),517-528, 2012.

[7] Munson, *Fundamentals of fluid mechanics* (7th edition), John Wiley & Sons,

[8] Satish G. Kandlikar, Shailesh Joshi, Shurong Tian, Effect of Surface Roughness on Heat Transfer and Fluid Flow Characteristics at Low Reynolds Numbers in Small Diameter Tubes, *heat transfer engineering* 24(3), 4-16, 2015

[9] R.L. Simpson, Junction flows, *Ann. Rev. Fluid Mech,* 33 (2), 415–443, 2001

[10] M. B. Salamah, A. Kapoor, M. Savsar, M. Ektesabi & A. Abdekhodaee, The Importance Of Accurate Water Metering In Resource Management, *Sustainable Development Conference*, 2009

[11] Zhiqiang Sun, Mass flow measurement of gas–liquid bubble flow with the combined use of a Venturi tube and a

vortex flowmeter, *Measurement Science and Technology,* 21(2), 055403, 2010

[12] Yi He, Yifan Cui, Zhongxi Zhao, Yongtang Chen, Wenxu Shang, Peng Tan, Strategies for bubble removal in electrochemical system, *Energy Reviews,* 2(2), 100015, 2023

[13] C S Lauchlan, E Escarameia, R W P May, C Gahan, *Air in Pipelines A literature Review*, 2005

APPLICATION OF MACHINE LEARNING & DATA VISUALIZATION TO PREDICT THE MIXING QUALITY OF TANK-AGITATOR

Syed Abdullah Ali[1,*], Furqan[1], Hasnain[1], Abdul Rauf[1], Izhan[1], Muhammad Hateem Arif[1]

[1]Department of Mechanical Engineering, NED University of Engineering & Technology, Karachi, Pakistan

[*]*Corresponding author E-mail address*: s.abdullahali02@gmail.com (Syed Abdullah Ali)

ABSTRACT

The solid-liquid mixing quality is a vital parameter from an industrial point of view. Its dependence on various parameters like tank and agitator design, stirring speed, tank diameter, solid particle diameter, solid density, liquid density, liquid dynamic viscosity and mean solid volume fraction dictate the necessity of careful consideration of the optimum parameters to ensure the best possible mixing quality. To understand the effect of the parameters on the mixing quality and to predict the mixing quality for a given set of parameters of influence, this study aimed to train a machine learning algorithm and employ data visualization techniques to identify the correlations between the parameters and the mixing quality. A CFD simulations dataset of a tank-agitator mixing problem validated against experimental data was used to execute this study. Various machine learning algorithms including Keras DNN, Linear Regression, Lasso, Elastic Net, SVR, Decision Tree Regressor, Random Forest Regressor, K-Nearest Neighbors Regressor and MLP Regressor were utilized to train different models to formulate the and identify the best one. The dataset was subjected to preprocessing steps and was split into 80:20 for training and testing the model, respectively. Considering the varying nature of values of the parameters, the dataset was normalized too to ensure a resulting model that would be free of any bias. The model that performed the best in terms of predicting the mixing quality were Keras DNN and Random Forest Regressor. The utilized dataset was considerably small. Therefore, to further extend this work, it is recommended to amass a significantly larger dataset for a given problem to allow a model to be trained properly which would ultimately open doors to reaching a higher accuracy.

Keywords: Linear Regression, Data Visualization, Machine Learning

1. INTRODUCTION

The solid-liquid mixing quality in a stirred tank as a function of the main system parameters (tank size and design, stirrer design, suspension characteristics) is an important matter for the industry [1]. The quality of mixing solid and liquid materials in a stirred tank depends on various factors such as tank size, design, stirrer design, and suspension characteristics.

Experimentation or simulations are often required to determine the stirring configuration that achieves high suspension quality. However, conducting real-size experiments, especially for large tanks, can be impractical due to various constraints. Small scale experimentations can help but scale up laws are not always clearly established.[2-4]

Simulation is free from experimental constraints, but it is still a care- demanding and burdensome tool. This is where machine

213

learning (ML) algorithms. come into play. ML algorithms can analyse data from various parameters affecting mixing quality and predict the optimal mixing conditions. They can learn from past data and simulate different scenarios to find the most effective stirring configurations.

The impact of AI is far-reaching, transforming traditional approaches and unlocking new possibilities for manufacturers, maintenance teams, and sustainability efforts, from the initial design phase to the recycle/reuse/retrofit phase.[5] Recent research trends and popular AI techniques in CFD are highlighted by Krzysztof Rojek et al. [6]

Therefore, the importance of ML in predicting mixing quality lies in its ability to handle complex data relationships and provide insights into optimal mixing conditions without the need for extensive experimentation. By utilizing ML, industries can optimize their processes, reduce costs, and improve product quality. This study involves working with a dataset comprising of Computational Fluid Dynamics (CFD)-generated and experimentally verified results for mixing tanks. The effectiveness of mixing in these tanks hinges on several variables, including tank and agitator design, stirring velocity, tank diameter, solid particle diameter, solid density, liquid density, liquid dynamic velocity, and mean solid volume fraction. To tackle this, data visualization, data cleaning, and training the data for predictive analysis are done.

2. METHODOLOGY

This study involves working with a dataset comprising Computational Fluid Dynamics (CFD)-generated and experimentally verified results for mixing tanks. The effectiveness of mixing in these tanks hinged on several variables, including tank and agitator design, stirring velocity, tank diameter, solid particle

diameter, solid density, liquid density, liquid dynamic velocity, and mean solid volume fraction. To tackle this, we engaged in data visualization, data cleaning, and training the data for predictive analysis. This section encapsulates our applied methodology and findings.

2.1 Data Cleaning

The initial phase of this study involved rigorous data cleaning procedures to ensure the integrity and suitability of the dataset for subsequent analysis. This included identifying and addressing missing or null values, encoding categorical variables, and implementing feature scaling techniques.

2.2 Handling Missing Null Values

Missing or null values within the dataset were managed using robust techniques such as forward fill, backward fill, or mean fill. This step aimed to enhance the dataset's completeness while minimizing biases introduced by missing data.

2.3 Categorical Variable Encoding

Categorical variables, such as design types, were appropriately encoded to enable meaningful analysis. This transformation ensured that categorical information was represented numerically while retaining the inherent characteristics of the data.

2.4 Feature Scaling

To address variations in data ranges across different parameters, feature scaling was conducted. Standardization techniques were applied to scale all variables uniformly, reducing the impact of variables with larger scales on subsequent analyses.

2.5 Training and Testing

A rigorous train-test split methodology, utilizing an 80-20 ratio, was employed to train and evaluate various regression models. Implementation of regression models was carried out using the scikit-learn (sk.learn) library and tensor flow library in Python,

214

ensuring standardized and reproducible analyses.

2.6 Utilized Regression Models

Several regression models were employed for dataset analysis, including:

- Keras Deep Neural Network (DNN)
- Linear Regression
- Lasso Regression
- Elastic Net Regression
- Support Vector Regression (SVR)
- Decision Tree Regression
- Random Forest Regressor
- K-Nearest Neighbors Regression (KNN)
- MLP Regression (Multi-layer Perceptron)

2.7 Assessment and Testing Reliability

The reliability of regression models was evaluated using key performance metrics such as Accuracy, Mean Squared Error (MSE), and Standard Deviation. Additionally, K-Fold Cross Validation was

employed to ensure the robustness and generalizability of model results.

3   DATA VISUALIZATION

The methodology culminated in data visualization techniques to effectively convey research findings.

3.1 Data Skewness

Table 1: Histograms with Bell Curve Fit

Features	Histogram with Bell Curve Fit
Tank and Agitator Design	
Stirring Speed (RPM)	
Tank Diameter (m)	
Solid Particle Diameter (µm)	
Solid Density (Kg/m³)	

Liquid Density (Kg/m^3)	
Liquid Dynamic Viscosity (μ)	
Mean Solid Volume Fraction (φ)	
Mixing quality	
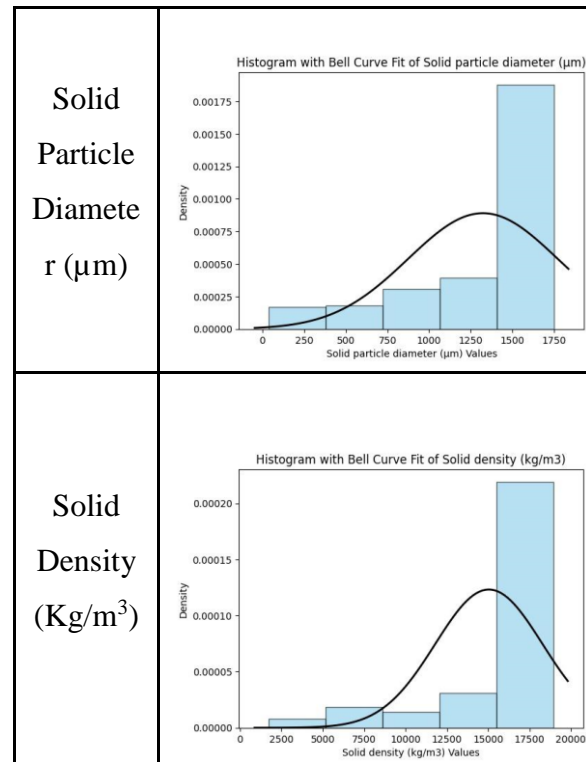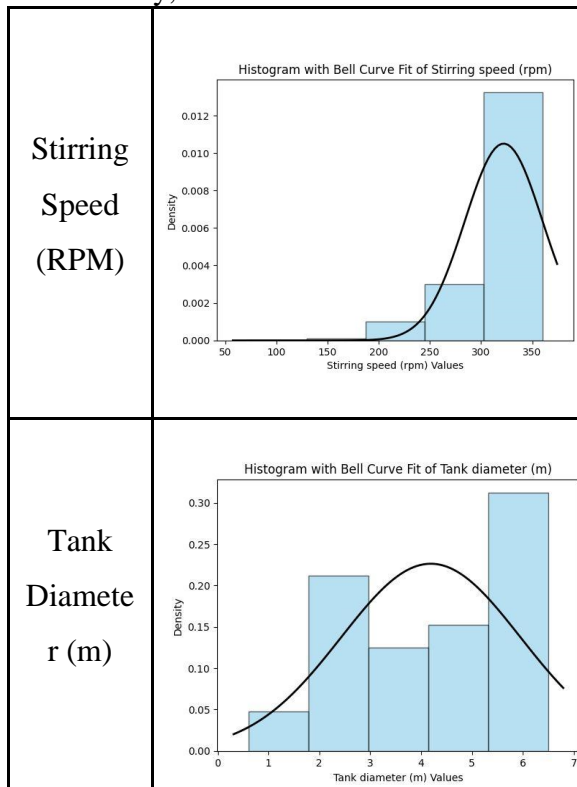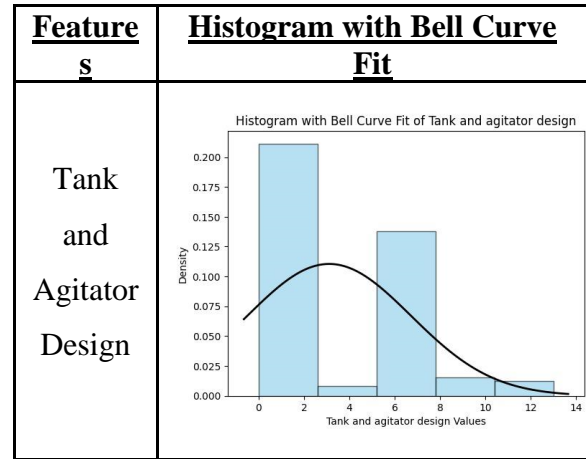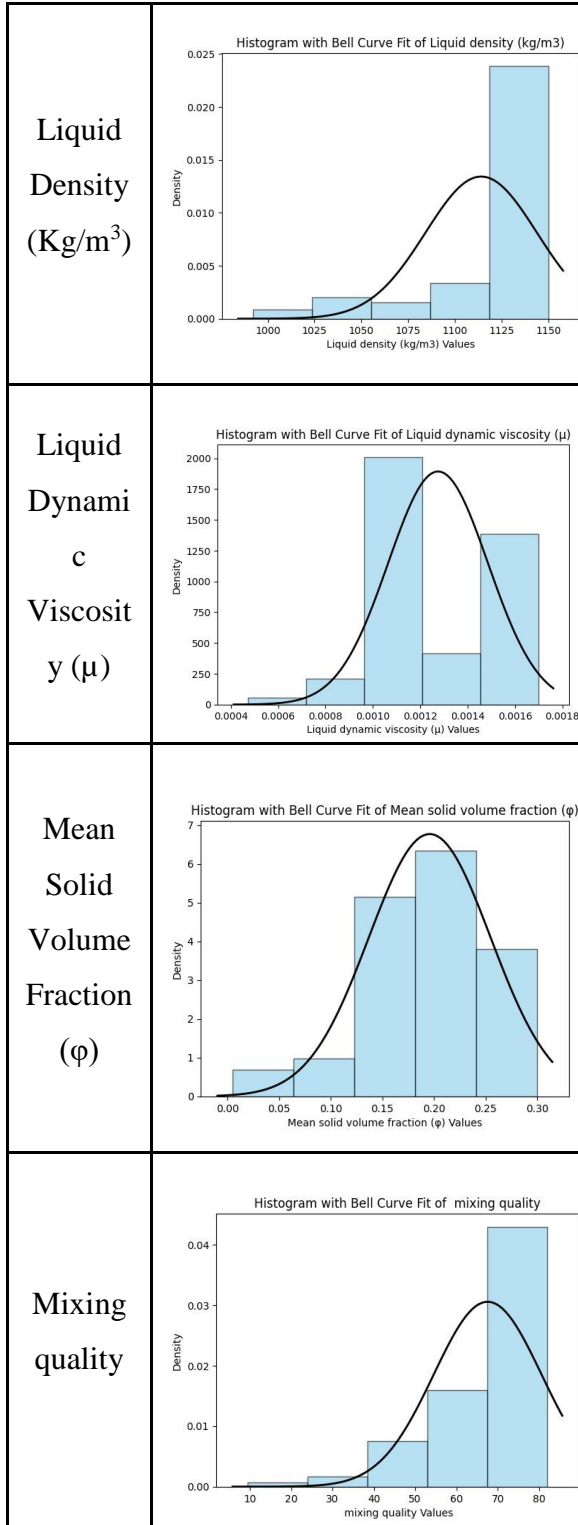
The above histograms show that the utilized dataset is skewed which affects the training of the machine learning algorithm. To obtain a properly trained machine learning algorithm, the utilized dataset should have a normal distribution.

3.2 Model Accuracy Plot

Table 2: Actual Values vs Predicted Values

Models	**Graphs**
Keras Deep Neural Network (DNN)	
Linear Regression	
Lasso	
Elastic Net	

216

Support Vector Regression (SVR)	
Decision Tree Regression	
Random Forest Regressor	
K Neighbours Regressor	

MLP Regression (Multi-layer Perceptron)
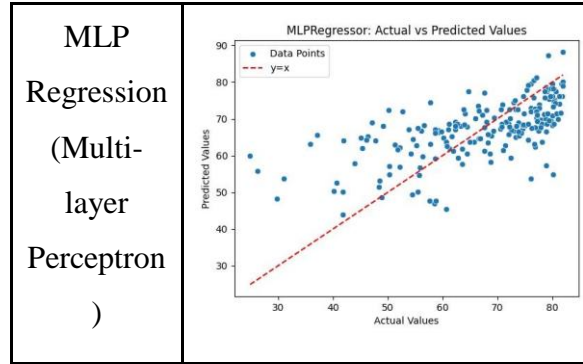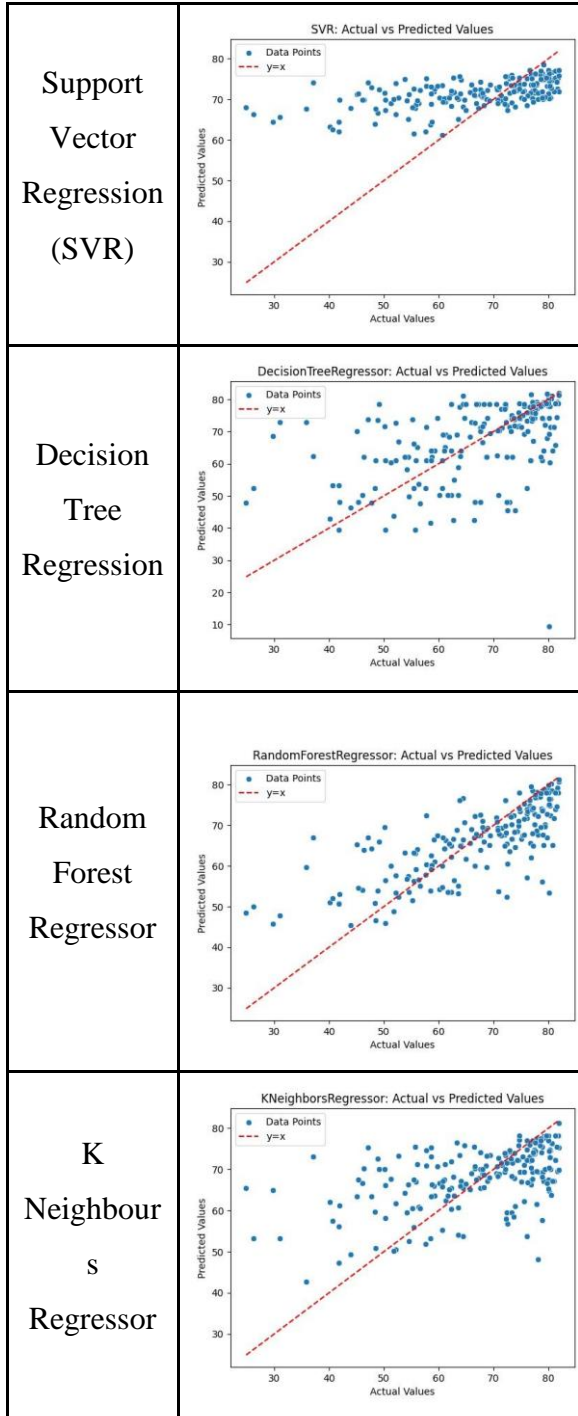
The above scatterplots show the accuracy and precision of the trained machine learning algorithm based on the different models. Random forest regressor and Keras DNN seemed to perform the best.

3.3 Assessment and Comparison

Table 3: Comparative Analysis of Different Models

Assessment and Testing Reliability Factors	**Bar Charts**
K-fold (10 Folds)	
Accuracy	

Standard Deviation	
Mean Squared Error	
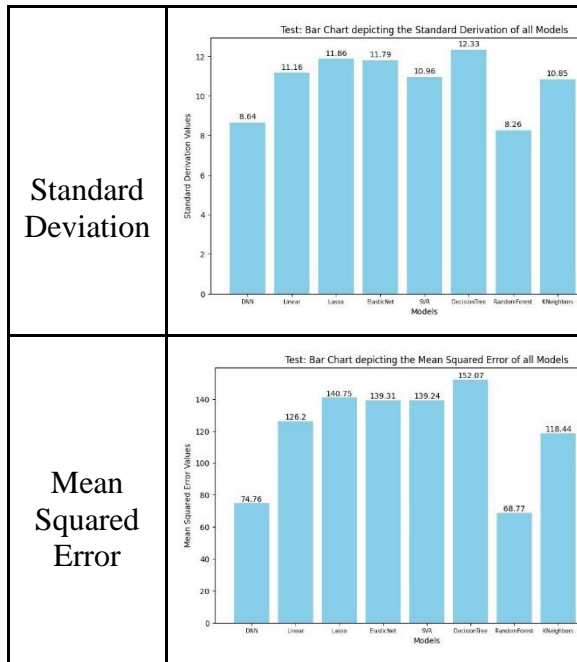
The above bar charts depict that the most optimum models that have lesser error, higher accuracy, lower standard deviation, and a higher K-fold (10 folds) score are Keras DNN and Random Forest Regressor.

4. CONCLUSION

In conclusion, this study provided a systematic approach to train a machine learning model to predict the mixing quality of a two-phase solid-liquid mixing tank. The utilized dataset was verified using Computational Fluid Dynamics (CFD) calculations and experimental data validation. By adhering to stringent data cleaning, model training, and evaluation procedures, this research aimed to derive comprehensive insights and contribute to advancements in fluid dynamics research by uplifting the potential of machine learning's application to train a model that can predict the mixing quality. Further research can be done by utilizing machine learning to train a predictive model using a larger and less skewed dataset which would yield a higher accuracy.

REFERENCES

[1] Projets, C.M.O., *Solid-Liquid Mixing in Stirred Vessels: Numerical Simulation, Experimental Validation and Suspension Quality Prediction Using Multivariate Regression and Machine Learning.* 2018.

[2] Geisler, R.K., Buurman, C., Mersmann, A, *Scale-up of the necessary power input in stirred vessels with suspension.* The Chemical Engineering Journal, (1993). vol. 51.

[3] Montante, G., Pinelli, D., Magelli, F, *Scale-Up Criteria for the Solids Distribution in Slurry Reactors Stirred with Multiple Impellers.* Chemical Engineering Science, (2003). vol. 58,.

[4] Dickey, D.S., *Ten Things You May Not Know About Liquid Mixing Scaleup.* Chemical Engineering (2013).

[5] Mahboob Elahi, S.O.A., Jose Luis Martinez Lastra & Jose Antonio Perez Garcia *A comprehensive literature review of the applications of AI techniques through the lifecycle of industrial equipment.* Discover Artificial Intelligence, (2023). Volume 3, article number 43.

[6] Wyrzykowski, K.R.R., *Performance and Scalability Analysis of AI-Accelerated CFD Simulations Across Various Computing Platforms.* Euro-Par 2022: Parallel Processing Workshops, (2023). Volume 13835.

INVERSE KINEMATICS OF ROBOTIC ARM FOR WELDING DIGITIZATION IN THE ARENA OF INDUSTRY 4.0.

Muhammad Bilal[1], Salman Hussain[1, *], Wasim Ahmad[1], and Mirza Jahanzaib[1]

[1]Department Industrial Engineering, University of Engineering & Technology,
Taxila, Pakistan

[*]Corresponding author E-mail address: engrbilal242@gmail.com (Muhammad Bilal)

ABSTRACT

To address the concerns in the manual welding process in terms of efficiency, quality, and adaptability there is a dare need for Industry 4.0 based smart welding system. For the robot to carry out the welding task, the robot moves the welding torch along the path of the weld. The position control along this path of the welding is the most significant challenge. This paper presents inverse kinematics-based position control for the target pose of the welding robot using Robot Operating System. Digital model of the robot in the form of URDF was designed for the Robot Operating System (ROS). Inverse kinematics was used to calculate the joint angles to achieve the desired position of the end effector using KDL solver. Position planning simulation was performed in Rviz (ROS Visualization) tool. The calculated and achieved coordinates for a specified position were compared and the errors were determined. The average error for the 17 poses is determined as 0.6847 mm. The result of this paper highlights a simple and cost-effective solution for position control by deploying ROS for low cost and effective development of welding digitization.

Keywords: Welding digitization, Position Control, Inverse Kinematics, ROS, Welding Robot

1. INTRODUCTION

Smart welding systems with the goal of improving quality and efficiency have been developed because of the incorporation of Industry 4.0 principles into manufacturing processes [1]. To achieve real-time defect detection and adaptive control, these systems integrate robotics, computer vision, and machine learning. This improves weld quality and productivity. The drawbacks of manual welding processes have been addressed by robotic welding, which shortens lead times for production while improving the consistency and quality of the welds[2]. Researchers are suggesting inverse kinematics-based trajectory planning techniques to maximize welding path generation and reduce cycle time while satisfying quality requirements, but precisely controlling position in robotic welding is still a challenge [3].

To monitor weld quality, advanced sensing technologies like infrared thermography are essential for early defect detection and process reliability [4]. To improve process visibility and control, vision systems are also incorporated into welding automation. This enables precise welding torch positioning and better weld quality. To find the best welding parameters, optimization techniques like genetic algorithms are used, taking joint geometry and material properties into account [5]. Researchers are working on systems that integrate sensors and feedback mechanisms to improve the quality of the weld. Real-time monitoring and control systems are crucial for guaranteeing process reliability [6]. Robotic welding processes can be controlled and monitored in real time

219

thanks to the Robot Operating System (ROS), which offers a versatile platform for creating and integrating robotic applications [7]. Furthermore, digital twin modelling has become popular for predicting weld quality and optimizing welding parameters, which makes it easier to create intelligent welding processes. Robotic welding has the potential to improve weld quality and efficiency using machine learning techniques for defect detection and classification [8].

Literature review of some of the work in the field of inverse kinematics is achieved and the limitation of each method is discussed in the table 1. The table outlines various techniques for solving inverse kinematics problems, each accompanied by its respective limitations. The Jacobian Transpose Method, while effective, can encounter singularities in certain robot configurations. The Pseudo-inverse Jacobian Method is susceptible to numerical instability and may converge to local minima. Damped Least Squares Method requires careful tuning of the damping factor to ensure optimal performance. The Null Space Projection Method becomes increasingly complex in higher-dimensional workspaces. Task Priority Inverse Kinematics may struggle with simultaneous multiple tasks. Artificial Neural Networks demand extensive training data and computational resources for effective implementation. Genetic Algorithms are hindered by high computational overhead and convergence challenges. Finally, Reinforcement Learning suffers from slow convergence and necessitates significant tuning efforts to achieve desirable results.

Technique	Limitation	References
Jacobian Transpose Method	May lead to singularities in certain robot configurations	[9]
Pseudo-inverse Jacobian Method	Prone to numerical instability and local minima	[10]
Damped Least Squares Method	Requires careful tuning of damping factor	[11]
Null Space Projection Method	Complexity increases with higher-dimensional workspace	[12]
Task Priority Inverse Kinematics	May struggle with simultaneous multiple tasks	[13]
Artificial Neural Networks	Requires extensive training data and computational resources	[14]
Genetic Algorithms	High computational overhead and convergence challenges	[15]
Reinforcement Learning	Convergence can be slow and may require significant tuning	[16]

Table 1 . Comparative analysis of the research in inverse kinematics

Thus, for efficient robotic welding, the robot must perform precise and accurate movement through weld path. For position control of the welding robot inverse kinematics is used to calculate joint angles. Several methods are

used for position control of robotics. There is a need for a versatile, efficient, and cost-effective way of position control for intelligent welding. In this research ROS has been used to obtain precise position control during GTAW welding process.

2. METHODOLOGY

To obtain precise position control a Position Control Protocol is designed using inverse kinematics in ROS. The figure 1 below shows the 7 stages of the protocol.
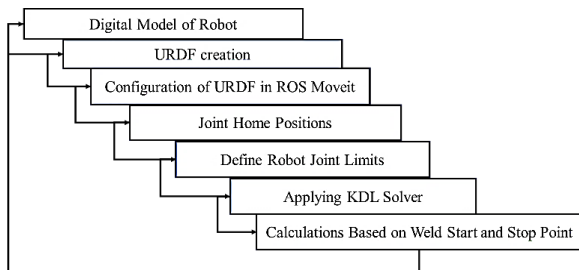

Figure 1. Position Control Protocol using Inverse Kinematics in ROS (Robot Operating System)

The protocol for robotic welding involves several distinct stages to ensure efficient and precise execution of the task. Initially, a digital model of the robot is developed, detailing its structure and components. This model is then translated into URDF format, which is integrated into the MoveIt library within the ROS framework for motion planning.
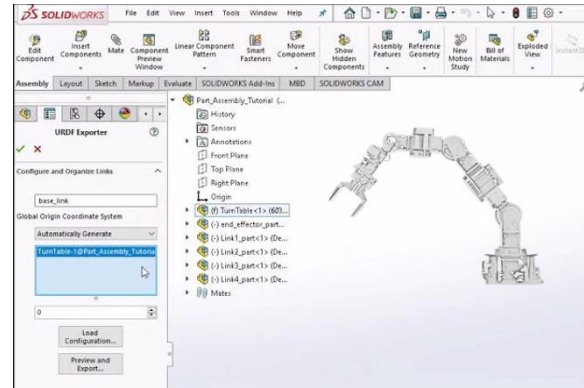
Figure 2. URDF development of digital model

Joint home positions are defined, and limits for each joint are established to ensure safe operation. Utilizing the Kinematics and Dynamics Library (KDL) solver, inverse kinematics calculations are performed to determine the joint configurations necessary for welding. Weld start and stop points are identified, and a trajectory for the welding tool is planned to seamlessly navigate between these points while considering joint limitations and obstacles.
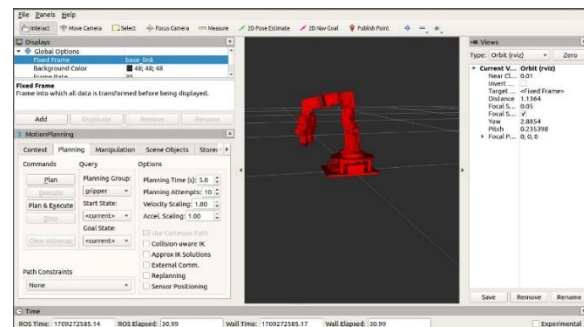
Figure 6. Weld start point selection.
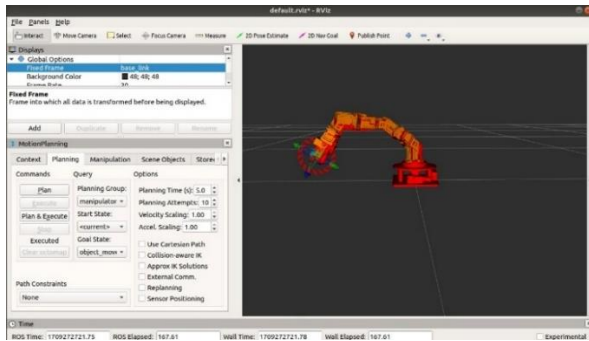
Figure 7. Weld end point selection.

Figure 8. Weld start point coordinates.

Figure 9. Weld End point Coordinates.

This trajectory is visualized in Rviz to verify its accuracy before actual gas tungsten arc welding (GTAW) is conducted on the workpiece using the robotic arm, guided by the planned trajectory. Through this systematic approach, the protocol ensures efficient and precise robotic welding operations, using the capabilities of ROS, MoveIt, and Rviz for motion planning, control, and visualization.
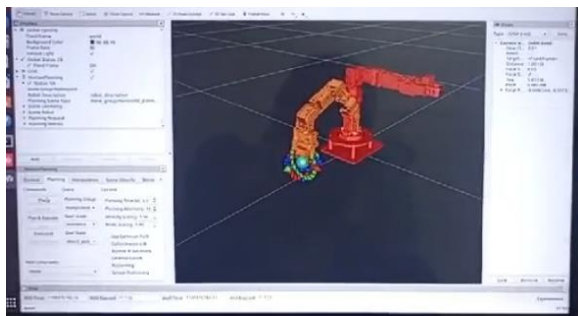

Figure 10. Path planning and execution

based on the weld start and stop point in Rviz.

GTAW welding is performed on mild steel workpiece as shown in figure 8. The welding parameters are adjusted before starting through welding control unit. The end effector of the robot holds the welding torch. Appropriate distance between torch and workpiece is ensured for effective welding. The weld trajectory based on the weld start and stop point is planned in Moveit. The welding torch moves in the planned trajectory to perform welding using precise position control.

Figure 11. Actual welding performance on workpiece

5. RESULTS AND DISCUSSION

To determine the error in targeted and achieved positions of the end effector, 17 poses are taken at different coordinates in space. The values for the coordinates in targeted poses are determined in ROS using KDL solver. End effector moves to the targeted position using execute plan command in Rviz. There is error in targeted and achieved position of the end effector for the poses. This error is determined by calculating the difference between targeted and achieved position coordinates. Each pose has some x,y, and z axis values. The average error for the 17 poses is determined as 0.6847 mm.

Pose	Targeted Position			Achieved Position			Error
	x	y	z	x	Y	z	
Pose 1	0.1380	0.1584	0.1000	0.1424	0.1528	0.0973	0.0076
Pose 2	0.1221	0.1920	0.1350	0.1248	0.1947	0.1377	0.0047
Pose 3	0.1907	0.1780	0.1720	0.1960	0.1833	0.1773	0.0092
Pose 4	0.1367	0.1290	0.1790	0.1409	0.1332	0.1832	0.0072
Pose 5	0.1120	0.1700	0.1580	0.1176	0.1757	0.1637	0.0098
Pose 6	0.1395	0.1890	0.1260	0.1453	0.1947	0.1317	0.0099
Pose 7	0.1090	0.1890	0.1520	0.1132	0.1932	0.1562	0.0073
Pose 8	0.1533	0.1540	0.1130	0.1582	0.1589	0.1179	0.0085
Pose 9	0.1142	0.1880	0.1120	0.1181	0.1919	0.1159	0.0068
Pose 10	0.1374	0.1230	0.1500	0.1417	0.1273	0.1543	0.0074
Pose 11	0.1845	0.1560	0.1100	0.1874	0.1589	0.1129	0.0050
Pose 12	0.1405	0.1480	0.1660	0.1428	0.1503	0.1683	0.0040
Pose 13	0.1780	0.1350	0.1760	0.1804	0.1374	0.1784	0.0042
Pose 14	0.1254	0.1120	0.1150	0.1303	0.1169	0.1199	0.0085
Pose 15	0.1705	0.1810	0.1530	0.1731	0.1837	0.1557	0.0046
Pose 16	0.1524	0.1440	0.1330	0.1548	0.1464	0.1354	0.0041
Pose 17	0.1611	0.1720	0.1690	0.1655	0.1764	0.1734	0.0076

Table 2. Error calculations for the targeted and achieved position of the Robot

The figure below shows the targeted values and achieved values of position at different poses. Blue bar represents targeted value across x-axis, orange bar represents achieved position value across x-axis, yellow bar represents targeted position value across y-axis, and sky-blue bar represents achieved position value across y-axis. Similarly, light green bar represents targeted position value about z-axis, and dark green colour represents achieved value across z-axis.
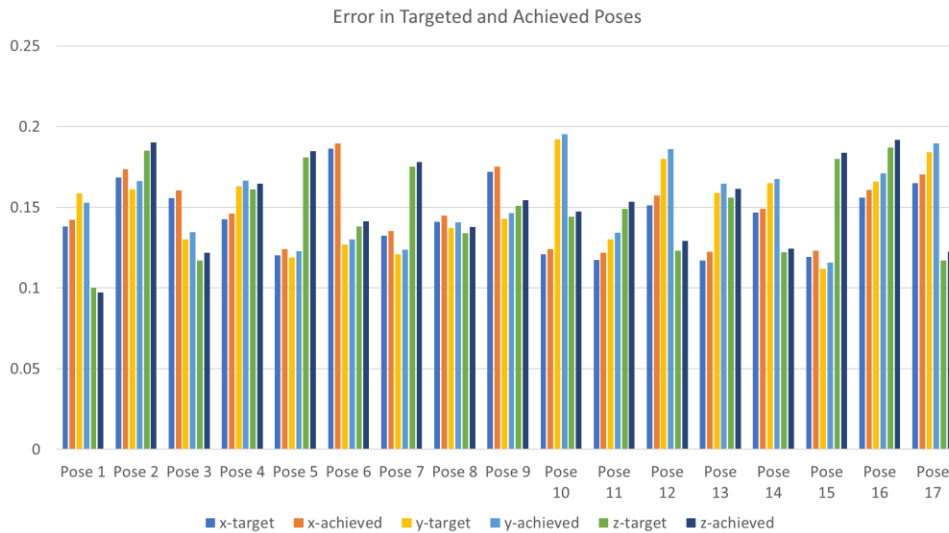

Figure 12. Targeted and achieved position values of the passes across x, y & z axis

The figure 10 below shows the error values at different poses. There is quite fluctuation in the error value for different poses. Each pose corresponds to the x, y and z axis coordinates in the space.
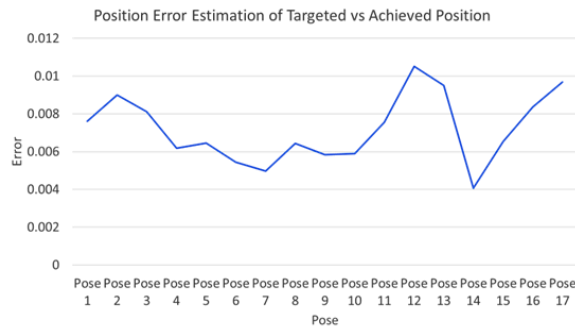

Figure 13. position Error estimation of targeted and achieved position.

6. CONCLUSIONS

Test results show that ROS based Inverse Kinematics control system can precisely achieve the position control of the manipulator for the reasonable task requirements, which fully meets the actual work requirements. Once the path is planned, the robot can execute the welding task. This involves moving the robot arm along the planned trajectory. During execution, the ROS system can monitor the position and orientation of the robot's end-effector in real-time. The average error in the achieved position and the targeted position is 0.6847 mm. The targeted position and orientation for each welding point can be compared to the achieved position and orientation. Error in the achieved position can be reduced by tunning the P, I, and D values of the PID controller.

ACKNOWLEDGEMENTS

REFERENCES

[1] M. Hunstig, S. Holtkämper, L. Helmich, and M. Brökelmann, "Smart Ultrasonic Welding – A Versatile Interconnection Technology for Power Electronics Packaging," Additional Conferences (Device Packaging, HiTEC, HiTEN, and CICMT), vol. 2021, no. HiTEC, 2021, doi: 10.4071/2380-4491.2021.hitec.000112.

[2] C. Zhu, H. Yuan, and G. Ma, "An active visual monitoring method for GMAW weld surface defects based on random forest model," Mater Res Express, vol. 9, no. 3, 2022, doi: 10.1088/2053-1591/ac5a38.

[3] S. Amano, Y. Tsujimura, T. Ogawa, and T. Shibata, "Development of in-process welding torch position control system using AI technology," Welding in the World, vol. 67, no. 5, 2023, doi: 10.1007/s40194-023-01486-7.

[4] W. Cai, J. Z. Wang, P. Jiang, L. C. Cao, G. Y. Mi, and Q. Zhou, "Application of sensing techniques and artificial intelligence-based methods to laser welding real-time monitoring: A critical review of recent literature," Journal of Manufacturing Systems, vol. 57. 2020. doi: 10.1016/j.jmsy.2020.07.021.

[5] P. Pitchipoo, A. Muthiah, K. Jeyakumar, and A. Manikandan, "Friction stir welding parameter optimization using novel multi objective dragonfly algorithm," International Journal of Lightweight Materials and Manufacture, vol. 4, no. 4, 2021, doi: 10.1016/j.ijlmm.2021.06.006.

224

[6] D. Maity, R. Premchand, M. Muralidhar, and V. Racherla, "Real-time temperature monitoring of weld interface using a digital twin approach," Measurement (Lond), vol. 219, 2023, doi: 10.1016/j.measurement.2023.113278.

[7] R. I. Maldonado-Valencia, C. H. Rodriguez-Garavito, C. A. Cruz-Perez, J. S. Hernandez-Navas, and D. I. Zabala-Benavides, "Planning and visual-servoing for robotic manipulators in ROS," Int J Intell Robot Appl, vol. 6, no. 4, 2022, doi: 10.1007/s41315-022-00253-z.

[8] B. Eren, M. H. Demir, and S. Mistikoglu, "Recent developments in computer vision and artificial intelligence aided intelligent robotic welding applications," International Journal of Advanced Manufacturing Technology, vol. 126, no. 11–12. 2023. doi: 10.1007/s00170-023-11456-4.

[9] M. Dalvi, S. S. Chiddarwar, M. R. Rahul, and S. R. Sahoo, "Kinematic Modelling of UR5 Cobot Using Dual Quaternion Approach," in Lecture Notes in Mechanical Engineering, 2022. doi: 10.1007/978-981-16-0550-5_103.

[10] A. D. Olaru, S. A. Olaru, and N. N. Mihai, "Proper jacobian pseudo inverse neural network matrix method applied to robot inverse kinematics controlling," International Journal of Mechanical Engineering and Robotics Research, vol. 5, no. 2, 2016, doi: 10.18178/ijmerr.5.2.120-123.

[11] X. Wang, X. Liu, L. Chen, and H. Hu, "Deep-learning damped least squares method for inverse kinematics of redundant robots," Measurement (Lond), vol. 171, 2021, doi: 10.1016/j.measurement.2020.108821.

[12] A. Mannucci, D. Caporale, and L. Pallottino, "On Null Space-Based Inverse Kinematics Techniques for Fleet Management: Toward Time-Varying Task Activation," IEEE Transactions on Robotics, vol. 37, no. 1, 2021, doi: 10.1109/TRO.2020.3018642.

[13] D. Di Vito, M. Bergeron, D. Meger, G. Dudek, and G. Antonelli, "Dynamic planning of redundant robots within a set-based task-priority inverse kinematics framework," in CCTA 2020 - 4th IEEE Conference on Control Technology and Applications, 2020. doi: 10.1109/CCTA41146.2020.9206268.

[14] D. Cagigas-Muñiz, "Artificial Neural Networks for inverse kinematics problem in articulated robots," Eng Appl Artif Intell, vol. 126, 2023, doi: 10.1016/j.engappai.2023.107175.

[15] C. T. Lee and J. Y. Chang, "A workspace-analysis-based genetic algorithm for solving inverse kinematics of a multi-fingered anthropomorphic hand," Applied Sciences (Switzerland), vol. 11, no. 6, 2021, doi: 10.3390/app11062668.

[16] J. Zhong, T. Wang, and L. Cheng, "Collision-free path planning for welding manipulator via hybrid algorithm of deep reinforcement learning and inverse kinematics," Complex and Intelligent Systems, vol. 8, no. 3, 2022, doi: 10.1007/s40747-021-00366-

Fabrication and characterizations of a low-cost thermal actuator for micro-electro-mechanical systems (MEMS) applications

Shehroze Tahir Khan[1], Murtuza Mehdi[1*], Tariq Jamil[1], and Abdul Qadir[1 *]

[1]Department of Mechanical Engineering NED University of Engineering & Technology Karachi 75270 Pakistan

[*]*Corresponding author E-mail address*: drmurtuza@neduet.edu.pk (Murtuza Mehdi)

ABSTRACT

Microactuators, sensors, and switches are utilized in applications such as lap-on-chip devices, deformable mirrors for optical beam deflection, camera auto-focus systems, micro-positioning platforms, ultrasonic emitters, etc. These devices produce miniaturized motion by converting electrical, thermal, or electromagnetic energy into kinetic energy of moving parts. In this article, we have reported the synthesis and characterization of a low-cost thermal actuator based on silver nano-platelets-based composite and single-component room temperature vulcanizing (RTV) silicone. The actuator is fabricated by depositing a functional layer of silver amalgamated with a conductive polymer on a smooth RTV substrate via a non-vacuum-based rod coating technique. The fabricated device exhibits good thermal actuation behavior in response to the applied thermal gradient. The device also reveals a stable resistive behavior for the applied temperature difference. These results suggest that the as-fabricated device can be employed as a micro-actuator, switch, or valve as well as a thermal sensor for future low-cost MEMS devices.

1. INTRODUCTION:

Over the past few years, the micro-electro-mechanical systems (MEMS) field has achieved astounding progress and popularity due to the development of advanced materials and the discovery of new applications. Such applications include stretchable and flexible sensors, energy storage devices, microactuators, etc. [1], [2], [3]. Microactuators are a class of thin film-based MEMS devices that transform one form of energy to yield motion. Such devices include electrothermal (thermal) actuators [4], piezoelectric actuators [5], magnetic actuators [6], shape memory alloys (SMA) based actuators [7], etc. These devices are usually fabricated by either depositing a functional layer on a flexible substrate [8], [9] or directly fabricating from silicon wafers [10], [11]. These devices are mostly fabricated via vacuum-based methods which are costly as well as highly energy-demanding [5]. Also, for the devices produced by non-vacuum-based techniques, the material cost is the bottleneck [6]. Therefore, in this article, we have reported the fabrication and characterizations of a low-cost thermal actuator for thin film device applications. The device is fabricated by depositing a functional layer of Poly(3,4-ethylenedioxythiophene)/poly(styrenesulfonate) (PEDOT: PSS) composited with silver nanoplatelets on smooth room temperature vulcanized (RTV) silicone substrate. The Ag nanoplatelets are sourced from a low-cost silver conductive paste which commonly finds applications in electronic circuit repairing. Also, the RTV substrate used in this study is new and its detailed characterizations are discussed in our previous research work [12]. The fabricated device is tested for thermally driven actuation behavior by supplying heat to the device. The

device also tested for change in its electrical resistance in response to an applied thermal gradient. These characterizations are performed on custom test setups. The results reveal that the as-fabricated device not only shows a good thermal actuation behavior but also exhibits a decent electrical resistive behavior for the applied temperature gradient. These results help explore the possible application of the fabricated device in future low-cost MEMS-based technologies.

2. EXPERIMENTAL SECTION

2.1. Materials

Room temperature vulcanizing (RTV) silicone was purchased from Bossil Technology (Malaysia) in the form of a single-component paste. The material comes with a commercial name of Grey RTV and is used as a substrate material. The mechanical properties and thermal behavior of this material are discussed in our previous research work [ref]. PEDOT: PSS paste was purchased from Sigma Aldrich (Belgium). N, N-dimethylformamide (N, N-DMF) was purchased from Merk Millipore (Germany).A silver conductive

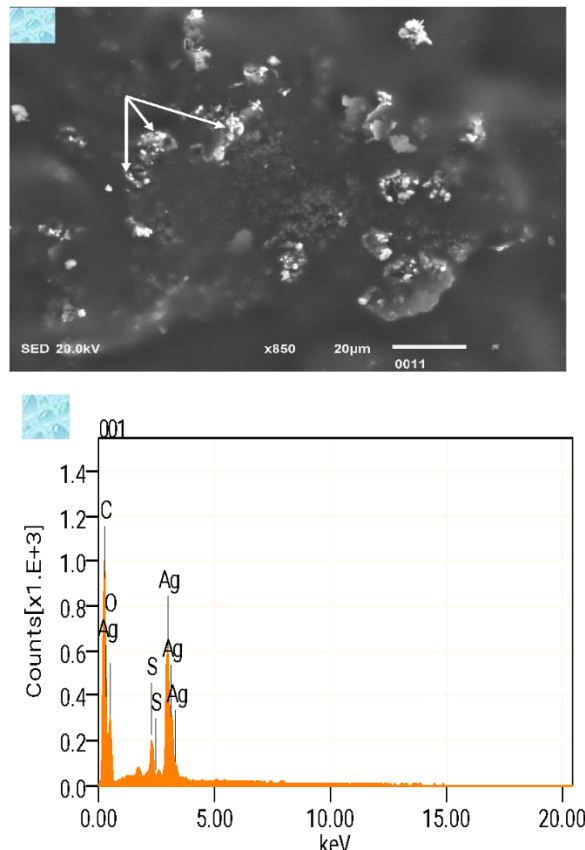pastecontaining silver nano-platelets was purchased from

Figure 1. Scanning electron microscope with an energy dispersive X-ray spectroscopy (SEM/EDS) of the prepared RTV/Ag/PEDOT: PSS device. a) SEM image of Ag/PEDOT: PSS film showing Ag nanoplatelets dispersed in PEDOT: PSS, b) EDS results of the film confirm the presence of Ag in PEDOT: PSS.

Mechanic, China under the commercial name MCN-DJ002). The presence of silver nano-platelets is also confirmed by scanning electron microscopy (SEM) and energy dispersive X-ray spectroscopy (EDS) results as shown in Figure 1. The average size of these nano-platelets was found to be 5.53 µm.

227

2.2. Preparation of RTV substrate

RTV substrates of dimension 70 mm x 10 mm x 1.10 mm were prepared by casting the RTV silicone polymer into the open-type mold. The construction and details of the mold are described in our recent works [12], [13]. After applying the RTV into the mold cavity, the polymer was left to cure in ambient for 2 to 3 hours at 26°C and 40% relative humidity. Following this procedure, the substrates were taken out of the mold. A few drops of acetone were added during the ejection of the samples to facilitate the removal of the samples.

2.3. Preparation of functional material

The preparation of functional material comprises three steps. In the first step, PEDOT: PSS-based ink was formulated by mixing PEDOT: PSS paste in N, N – DMF in 60% (wt/wt) concentration. Then transparent nail polish was added into the solution (48 wt% concentration) to improve the fluidity of the ink as reported by researchers [14], [15], [16], [17]. In the second step, silver nanoplatelets ink was prepared by mixing silver paste in N, N – DMF (60 wt% concentration). In the third step, synthesized silver ink was added into the PEDOT: PSS ink in 5% wt/wt concentration. In the above formulations, DMF served as the organic binder and is reported to enhance the electrical performance of the functional materials [18].

2.4. Fabrication of RTV/Ag – Composite laminate

RTV/Ag composite laminates were fabricated by dispensing 200 µl of synthesized nanophase ink on the RTV substrate through a precision micropipette (DLab, China). The ink was coated by sliding a smooth stainless-steel rod of 2.5 mm diameter at an average speed of 10 mm/s. The laminates were dried at 110 °C inside a forced convection oven for 10 minutes.

Afterwards, another coat of 200 µl was applied and the samples were cured following the same procedure. Figure 2a shows the rod-coated RTV/Ag–composite laminate while Figure 2b shows the cross-sectional SEM image of the RTV/Ag sample. From different SEM images, the average thickness of the prepared device was found to be 50 µm.
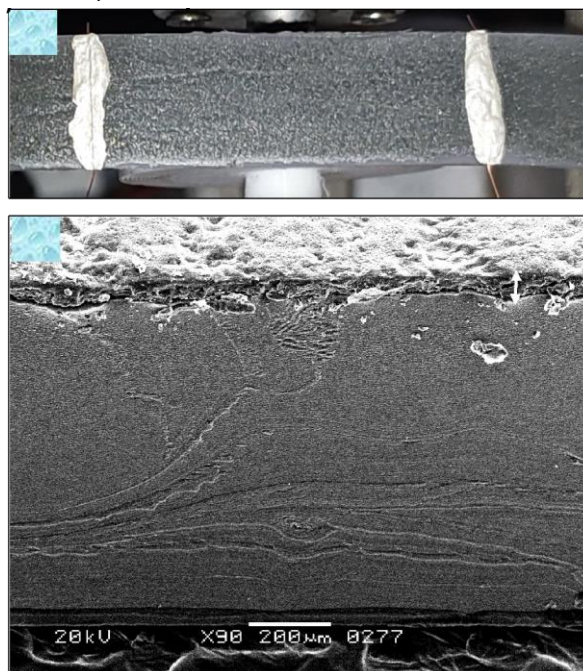

Figure 2. Rod-coated Ag/PEDOT: PSS film on RTV substrate. a) Photograph of the fabricated device with electrical contacts attached, b) Lateral SEM image of the device showing its cross-section.

2.5. Characterizations of Laminates

The prepared devices were tested for changes in electrical resistance and actuation behavior in response to applied temperature. For this purpose, two types of tests were performed. In the first test, samples of size 35 mm x 10 mm x 1.10 mm were taken with electrical contacts applied using 0.18 mm enamel copper wire and silver paste. The sample was fixed to a 1 mm thick glass slide by a heat resistant tape and the setup was placed on a hot plate. An Arduino-based auto-ranging

228

ohm meter was connected to the sample to record the electrical resistance of the sample during testing. A K-type thermocouple was also attached to the hot plate via heat-resistant tape to record the temperature measurements. The temperature was slowly raised to 250 °C and a change in resistance of the sample was recorded. Then hotplate was turned off and the assembly was cooled down to room temperature. During this time, the temperature and the resistance measurements were continued to record.

In the second test, the same setup was used with minor changes. Now, the sample was fixed to a 6 mm thick glass plate at one end by heat-resistant tape. Then the glass plate was placed on the hotplate with the thermocouple attached. A steel ruler having a least count of 0.05 mm was vertically fixed to the glass plate for measuring the actuation measurements. The test was initiated by slowly increasing the temperature of the hotplate up to 250 °C and the actuation measurements were recorded. The recorded data was then converted into temperature–resistance, and temperature–height graphs of the prepared devices.

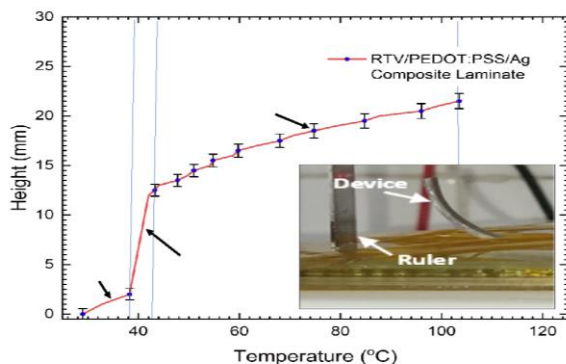## 3. RESULTS AND DISCUSSIONS

3.1. Thermal Actuation Response

Figure 3. Actuation behavior of RTV/Ag/PEDOT: PSS device in response to applied temperature. The
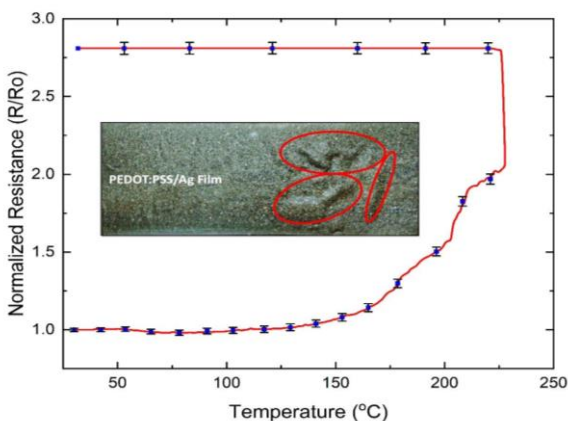
inset shows the photograph of a thermally actuated device. The error bar shows the standard deviations for the set of experiments.

Figure 3 shows the thermal actuation response of the fabricated device. The entire response can be divided into three regions, namely low actuation, rapid actuation, and high actuation region. In the low actuation region, the device shows a small deflection height for a small temperature change. The maximum actuation height of 2 mm is achieved when the device is heated from room temperature to a temperature of 38.25 °C. Afterward, the device shows a fast movement, which embarks the second region of rapid actuation. Here, the device shows a fast actuation of 10 mm for a small temperature change of around 5 °C. Afterwards, the third region of high actuation starts from 12 mm at 42 °C to 21.5 mm at 103.5 °C. In this region, the device shows a linear actuation response over a relatively wide temperature range as compared to the first region. The maximum actuation of 9.5 mm is observed for a temperature difference of 61.5 °C.

3.2. Electrical Resistive Behavior

Figure 4 shows the resistive response of the fabricated device to the applied temperature change. It is observable that the normalized resistance of the device remains nearly unchanged up to a temperature of 150 °C. Afterward, the resistance gradually starts incrementing and reaches a maximum linear normalized value of 2.05 at 227.5 °C. Then a drastic increment is observed and the normalized resistance reaches a maximum value of 2.8 times the initial one at a temperature of 220 °C. At this point, the temperature change is found to produce no resistance change even when the device is cooled down to room temperature. This behavior is attributed to two reasons; first, the higher temperatures caused the boiling of N,

229

N–DMF which was used as a conductive binder for the functional coating. Hence, increasing the electrical resistance of the coated film. Second, these higher temperatures also caused morphological changes in the film such as bending and delamination from the RTV at various points. These changes also contribute to yielding permanent changes in the electrical resistance of the device. This implies that to use this device as a thermal sensor, it needs to be operated below 185 °C to prevent a lasting

change in electrical resistance.

Figure 4. Resistive behavior of RTV/Ag/PEDOT: PSS device in response to applied temperature. The inset shows the photograph of the device under test (DUT). The error bar shows the standard deviations for the set of experiments.

4. CONCLUSIONS

This paper presents the fabrication and characterizations of a low-cost thermal actuator produced by coating a functional layer of PEDOT: PSS and Ag nanocomposite functional layer on a smooth RTV substrate via rod coating technique. The fabricated device is studied under a scanning electron microscope for morphology and cross-section information. The EDS results also confirm the presence of Ag in the PEDOT: PSS functional matrix. The device was tested

for thermal actuation and electrical resistive response for applied thermal gradient. The device shows good actuation response over a wide range of temperatures. The device also exhibits electrical resistive behavior for applied temperatures up to 185 °C. In summary, the device can be used as a thermal sensor, thermal actuator, valve, or switch in a variety of MEMS-based applications.

ACKNOWLEDGMENTS

REFERENCES

[1] V. Raman, Y. H. Cho, H. M. Kim, Y. J. Kim, H. M. Sim, and H. K. Kim, "Ag mesh network framework based nano composite for transparent conductive functional electrodes for capacitive touch sensor and thin film heater," *Ceram Int*, vol. 47, no. 19, pp. 27230–27240, Oct. 2021, doi: 10.1016/j.ceramint.2021.06.145.

[2] T. T. A. Nguyen, B. S. Soram, D. T. Tran, N. H. Kim, and J. H. Lee, "Enhanced electrochromic capacity performances of hierarchical MnO2-polyaniline/PEDOT:PSS/Ag@Ni nanowires cathode for flexible and

rechargeable electrochromic Zn-Ion battery," *Chemical Engineering Journal*, vol. 452, Jan. 2023, doi: 10.1016/j.cej.2022.139555.

[3] D. Lv *et al.*, "Enhanced flexible room temperature ammonia sensor based on PEDOT: PSS thin film with FeCl3 additives prepared by inkjet printing," *Sens Actuators B Chem*, vol. 298, Nov. 2019, doi: 10.1016/j.snb.2019.126890.

[4] S. Dai *et al.*, "A high mechanical strength, self-healing silicone elastomer for thin film thermal actuator," *Colloids Surf A Physicochem Eng Asp*, p. 133506, Feb. 2024, doi: 10.1016/j.colsurfa.2024.133506.

[5] Y. Li, J. Feng, Y. Zhao, J. Wang, and C. Xu, "Ultrathin flexible linear-piezoelectric ZnO thin film actuators: Tuning the piezoelectric responses by in-plane epitaxial strain," *Appl Surf Sci*, vol. 599, Oct. 2022, doi: 10.1016/j.apsusc.2022.153969.

[6] N. Selvakumaran, M. Gowsalya, K. Gurunathan, and P. Shakkthivel, "Synthesis of novel FeM (Co, Ni, Cu & Zn)/PDMS for magnetic actuators thin film fabrication by greener route," *J Magn Magn Mater*, vol. 552, Jun. 2022, doi: 10.1016/j.jmmm.2022.169139.

[7] A. Jena, B. B. Samal, C. S. Kumar, and S. K. Varshney, "Analysis of electro-thermo-mechanical behavior of thin film Ni50-Ti50and Ni40-Ti50-Cu10shape memory alloys for application in thermal actuators," in *Materials Today: Proceedings*, Elsevier Ltd, 2021, pp. 4578–4583. doi: 10.1016/j.matpr.2021.05.448.

[8] S. Rosset and H. R. Shea, "Flexible and stretchable electrodes for dielectric elastomer actuators," *Appl Phys A Mater Sci Process*, vol. 110, no. 2, pp. 281–307, 2013, doi: 10.1007/s00339-012-7402-8.

[9] S. Kim, R. Kubicek, and S. Bergbreiter, "3D-Printed Electrostatic Microactuators for Flexible Microsystems," *Adv Funct Mater*, vol. 33, no. 47, Nov. 2023, doi: 10.1002/adfm.202304991.

[10] B. K. Kim and Y. Kim, "Structural Robustness and Actuation Performance of Multilayered Thin-Film Actuators Based on Ni-Co Flexible Substrate," *Sens Actuators A Phys*, p. 115230, Mar. 2024, doi: 10.1016/j.sna.2024.115230.

[11] S. Thomas *et al.*, "Characterization of Thermal Expansion Coefficient of LPCVD Polycrystalline SiC Thin Films Using Two Section V-beam Actuators," in *Procedia Engineering*, Elsevier Ltd, 2016, pp. 1144–1147. doi: 10.1016/j.proeng.2016.11.379.

[12] S. T. Khan, M. Akhtar, M. Mehdi, and N. Malik, "and Evaluation Characterizations of a Cost- Effective Single Component Polymer for Stretchable and Flexible Microelectromechanical Systems Applications", doi: 10.1520/JTE20220161.

[13] S. T. Khan, M. Mehdi, and T. Jamil, "Electromechanical characterizations of PEDOT:PSS and its nanocomposite thin films on a cost-effective polymer substrate for microelectromechanical systems (MEMS) applications," *Express Polym Lett*, vol. 17, no. 8, pp. 806–818, Aug. 2023, doi: 10.3144/expresspolymlett.2023.60.

[14] L. A. Pradela-Filho, D. A. G. Araújo, R. M. Takeuchi, and A. L. Santos, "Nail polish and carbon powder: An attractive mixture to prepare paper-based electrodes," *Electrochim Acta*, vol. 258,

pp. 786–792, 2017, doi: 10.1016/j.electacta.2017.11.127.

[15] D. A. G. Araújo *et al.*, "A lab-made screen-printed electrode as a platform to study the effect of the size and functionalization of carbon nanotubes on the voltammetric determination of caffeic acid," *Microchemical Journal*, vol. 158, no. May, p. 105297, 2020, doi: 10.1016/j.microc.2020.105297.

[16] J. R. Camargo, I. A. A. Andreotti, C. Kalinke, J. M. Henrique, J. A. Bonacin, and B. C. Janegitz, "Waterproof paper as a new substrate to construct a disposable sensor for the electrochemical determination of paracetamol and melatonin," *Talanta*, vol. 208, no. August 2019, p. 120458, 2020, doi: 10.1016/j.talanta.2019.120458.

[17] J. R. Camargo *et al.*, "Development of conductive inks for electrochemical sensors and biosensors," *Microchemical Journal*, vol. 164, no. February, 2021, doi: 10.1016/j.microc.2021.105998.

[18] M. M. Nauman *et al.*, "Stretchable and flexible thin films based on expanded graphite particles," *Processes*, vol. 8, no. 8, 2020, doi: 10.3390/PR8080961.